

UNIVERSITY OF BIRMINGHAM

EVALUATION OF FUEL ADDITIVES AND ENGINE CONDITIONS ON FUEL DEPOSIT FORMATION AND PREVENTION IN GDI AND PFI ENGINES: AN ACCELERATED APPROACH

by

ANDREW JAMES NORMAN

A thesis submitted to the University of Birmingham for the degree of

DOCTOR OF PHILOSOPHY

Department of Mechanical Engineering

The University of Birmingham

25th September 2024

UNIVERSITY OF
BIRMINGHAM

University of Birmingham Research Archive

e-theses repository

This unpublished thesis/dissertation is copyright of the author and/or third parties. The intellectual property rights of the author or third parties in respect of this work are as defined by The Copyright Designs and Patents Act 1988 or as modified by any successor legislation.

Any use made of information contained in this thesis/dissertation must be in accordance with that legislation and must be properly acknowledged. Further distribution or reproduction in any format is prohibited without the permission of the copyright holder.

ABSTRACT

Modern engines require precise control of variables to optimise drivability, power, emissions and efficiency. Fuel deposits disrupt this balance by affecting components such as fuel injectors, Exhaust Gas Recirculation (EGR) coolers, and intake valves. To mitigate this, an understanding of conditions that promote deposits, their impact on performance and prevention methods are essential. This study uses accelerated deposit growth cycles to evaluate how fuel and additives as well as engine and fuel parameters influence deposit growth, prevention, and removal on Gasoline Direct Injection (GDI) injectors, GDI EGR coolers and Port Fuel Injection (PFI) intake valves.

An iterative method was established to create an effective accelerated GDI injector deposit growth cycle, which alternated a sequence of high and low loads, with sequence timing critical to deposit growth and additive effectiveness. Additives reduced injection duration increase from 6.8 - 2.1 %, and to 1 % with a renewable fuel. Another method, with an EGR cooler, showed that additives maintained exhaust Total Hydrocarbon (THC) and soot levels, preventing EGR cooler deposits, decreasing pressure loss and intake manifold temperature, with a predicted 1.2 % reduction in Brake Specific Fuel Consumption (BSFC) compared to a base fuel. A deposit formation cycle on PFI intake valves used an experimental rig with a novel design which can control parameters such as valve and cylinder head temperature, air and fuel flow rates, and valve speed. 34.3 mg of deposits were generated in a 5 hr test whilst identifying a critical temperature of 210 ^{o}C for deposit formation, replicating real engine trends. This study provides a detailed account of the rig's design for future experimentation of a similar nature.

ACKNOWLEDGEMENTS

I would like to thank my main supervisor, Dr. Jose Martin Herreros, for his continuous support, guidance, and dedication to ensuring I had the best opportunities throughout my PhD. I also extend my gratitude to Prof. Athanasios Tsolakis, Dr. Soheil Zeraati Rezaei, and Dr. Omid Doustdar for their assistance and commitment to fostering a supportive research group. None of this would have been possible without the support of two excellent technicians Jack Garrod and Kevan Charlesworth who's experience, expertise and hard work was essential for the design and construction the experimental setup and to my own personal development. I would also like to say a huge thank you to Mengda Wu, George Brinklow and Nikhil Khedkar, for their fantastic efforts in assisting the procurement, manufacture and running of experimental setups.

This PhD would also not have been possible without the support of my friends and family who helped me to continue through some difficult times. I'd like to give a big thank you to my amazing girlfriend Sashini Iddawela, who has been such a great supporter throughout this journey. I am very grateful to my Aunt Sarah and Uncle Martyn as well as my friends Diego Perez and Angharad Davies who gave me a home during the latter stages of my PhD, without whom I would not have been able to complete my studies.

I too am incredibly grateful for my contacts in Spain, from Repsol and la Universidad de Castilla la Mancha who gave me fantastic experiences and support. A huge thanks goes to Fermín Oliva Miñana, David Donoso Malagón and Rafa Pitarch Berná from Repsol and Luis Augusto from AVL for their work and collaboration throughout my study. Without your hard work and expertise none of this would have been possible.

TABLE OF CONTENTS

1. INTRODUCTION 1

1.1 Background 1

1.2 Research Focus 6

1.2.1 Aims and Objectives 7

1.2.2 Novelty of Research 9

1.3 Thesis Outline 11

2. LITERATURE REVIEW 14

2.1 Gasoline Injection Technologies 14

2.1.1 Overview 14

2.1.2 Mechanism of Action 15

2.1.3 Injector Design 16

2.1.4 GDI vs PFI 19

2.2 Injector Fouling 25

2.2.1 Overview 25

2.2.2 Formation Mechanisms/ Processes 26

2.2.3 Parameters Impacting Injector Deposits 26

2.2.4 The Impact of Fuel Deposits on Injection, Engine Performance and Emissions 32

2.3 EGR Cooler Fouling 35

2.3.1 Overview 35

2.3.2 Fouling Mechanism 35

2.3.3 Impact on Engine Performance 36

2.3.4 Summary 39

2.4 Intake Valve Deposits 40

2.4.1 Overview 40

2.4.2 Formation Mechanisms/ Processes 41

2.4.3 Parameters Impacting Intake Valve Deposition 44

2.4.4 Impact of Intake Valve Deposits on Engine Performance and Emissions 49

2.5 Deposit Control Additives 52

2.5.1 Mechanisms 52

2.5.2 Types of Additives 53

2.5.3 DCA in GDI Engines 54

2.5.4 Impact on Exhaust 55

2.5.5 DCA in PFI Engines 56

2.5.6 Impact of Alcoholic Fuels on DCA Composition 57

2.5.7 Summary 57

2.6 Accelerated Fouling Test Methods 58

2.6.1 Overview 58

2.6.2 Injector Fouling 58

2.6.3 EGR Fouling 64

2.6.4 Intake Valve Fouling 65

3. METHODOLOGY 70

3.1 Engine Setup and Facilities. 70

3.1.1 Engine 70

3.1.2 Fuel Properties 72

3.1.3 Emissions and Instrumentation 74

3.1.4 Engine Instrumentation and Data Acquisition 76

3.1.5 Fuel Injector Cleaning 78

3.2 Intake Valve Deposit Experimental Rig 78

3.2.1 Proof of Concept Testing 78

4. GDI INJECTOR FUEL DEPOSITS 82

4.1 Introduction 82

4.2 Methodology 83

4.2.1 Development Procedure for Discovery of an Accelerated Injector Deposit Formation Cycle 83

4.2.2 Analysis Techniques 90

4.3 Results and Discussion 93

4.3.1 Development Procedure for Discovery of an Accelerated Injector Deposit Formation *Cycle* 93

4.3.2 Effect of Fuel on Injector Deposits, Fuel Consumption and Emissions..... 113

4.4 Conclusion..... 130

5. GDI ENGINE EGR COOLER FOULING..... 133

5.1 Introduction..... 133

5.2 Methodology..... 134

5.2.1 Analysis of EGR Cooler Effectiveness and Impact on Engine Performance . 135

5.3 Results and Discussions..... 141

5.3.1 Impact of Fuel on Engine Operation Parameters and Carbonaceous Emissions 141

5.3.2 Impact of Fuel on EGR Cooler Performance..... 146

5.3.3 Impact of Fuel-Derived EGR Deposits on EGR Cooler and Engine Performance for Various EGR Scenarios..... 149

5.4 Conclusions..... 155

6. DEVELOPMENT OF AN EXPERIMENTAL METHOD TO INVESTIGATE FUEL DERIVED DEPOSITS ON ENGINE INTAKE VALVES..... 157

6.1 Introduction..... 157

6.2 Design and Manufacture..... 158

6.2.1 Product Design Specification..... 158

6.2.2 Design and Manufacture of the System to Modify Cylinder Head Temperature 161

6.2.3 Design and Manufacturing of the System to Modify Valve Temperature... 177

6.2.4 Design and Manufacturing of the System to Actuate Intake Valves 188

6.2.5 Design and Manufacturing of the Fuel Injection System 199

6.2.6 Design and Manufacturing of the Air Intake and Extraction Systems 202

6.3 Results and Discussion of Proof of Concept Testing 205

6.3.1 Impact of Temperature 206

6.3.2 Distribution of Deposits 209

6.3.3 Control Variables 217

6.4 Conclusions 221

7. CONCLUSIONS AND FUTURE WORK 222

7.1 Conclusions 222

7.2 Future Work 225

8. LIST OF REFERENCES 228

9. APPENDICES 247

LIST OF FIGURES

Figure 1-1: Published Articles with a) Engine Fuel Deposits, b) GDI Injector Deposits, c) EGR Cooler Fouling, d) Intake Valve Deposits in the title or abstract. 7

Figure 2-1: PFI and GDI injector location (48). 14

Figure 2-2: Types of stratified change (46). 18

Figure 2-3: Mechanism of DDA (152). 53

Figure 3-1: a) Exhaust layout, b) Photographs of the exhaust layout. 72

Figure 3-2: Emissions probe. 76

Figure 3-3: Ohaus Pioneer scale being used to weigh a valve. 81

Figure 4-1: Flowchart of process used to develop accelerated fouling Cycle. 85

Figure 4-2: Definition of Cycle Parameters. 86

Figure 4-3: Definition of Phases of injection duration change throughout a Sequence at a) 1250 rpm 6 bar IMEP b) 1500 rpm 16 bar IMEP. 92

Figure 4-4: Soot emissions contour map. 94

Figure 4-5: Photos taken after Cycle 7 a) no Additive, b) with Additive. 105

Figure 4-6: Average increase in injection duration of all Sequences used in Cycles 4 and 6, averaged over a whole Cycle a) Initial Change, b) Post Start Change, c) Total Change. Error bars represent 90 % confidence intervals. 109

Figure 4-7: Injection Duration Percentage Increase of Cycle 12 a) Evolution of Injection Duration of both Setpoints combined, b) Percentage increase of Injection Duration, from the start to the end, combined average of both Setpoints. 115

Figure 4-8: Average increase in injection duration of both Setpoints of a Sequence and their sum, averaged over a whole Cycle (including repeats) a) Cycle 7, b) Cycle 10, c) Cycle 11, d) Cycle 12. Error bars represent 90 % confidence intervals. 117

Figure 4-9: Photos of the three injectors, clean, pre-test. 125

Figure 4-10: Photos of external deposits and nozzle deposits from a) Gasoline Base Fuel, b) Gasoline with Additive, c) Renewable Base, d) Renewable with Additive. 125

Figure 4-11: Fuel consumption change throughout Cycle 12 (averaged across Setpoints). 126

Figure 4-12: THC change throughout Cycle 12 (averaged across Setpoints). 127

Figure 4-13: CO change throughout Cycle 12 (averaged across Setpoints). 127

Figure 4-14: Change in FSN at the end of the Cycle compared to the beginning. 129

Figure 4-15: Evolution of soot at 1500 rpm 16 bar IMEP. 129

Figure 4-16: Soot Results (FSN) from the end of each Cycle with GPF. 130

Figure 5-1: Graph showing how speed and BMEP change for the first 2 Loops of the Cycle. 134

Figure 5-2: Schematic showing the different scenarios used in analysis. 137

Figure 5-3: Evolution of injection duration throughout test. 142

Figure 5-4: Fuel mass flow rate. 143

Figure 5-5: THC measured at EGR Cooler out. 144

Figure 5-6: Soot measured at engine out. 145

Figure 5-7: EGR Cooler dP change with time. 147

Figure 5-8: EGR Cooler Effectiveness change with time, all fuels. 148

Figure 6-1: Intake Valve Fuel Deposits Rig. 160

Figure 6-2: Fuel injector location..... 161

Figure 6-3: Cylinder Head gasket plate design a) oil channels, b) gasket plate, c) 3D scan and CADD model..... 164

Figure 6-4: Extraction box..... 165

Figure 6-5: Heat Exchanger CADD a) 2D plates, b) Isometric view, c) Photograph with Insulation. 167

Figure 6-6: Oil system design..... 170

Figure 6-7: PID electronics: Controller Box a) Internal wiring, b) User interface c) Electrical schematic. 172

Figure 6-8: Valve heater and holder final design. 178

Figure 6-9: Valve heater CADD model a) 3D scan, b) imported model of heaters and holder, c) checking for collisions between holder and gasket plate, d) aligning upper bracket with valves, e) cross section view. 179

Figure 6-10: Cartridge heater bracket design a) jaws, b) upper bracket front view, c) base plate, d) bolt holes and thermocouple placement, e) valve, f) valve attachment and thermocouple, g) thermocouple bracket. 183

Figure 6-11: 3d print of upper bracket. 184

Figure 6-12: CNC machining process a) upper bracket on the clamping face of the pocket NC after the underside had been cut, b) Pocket NC machine. 185

Figure 6-13: Valve temperature controller box a) user interface, b) internal wiring c) Electrical Schematic. 187

Figure 6-14: Camshaft control system..... 189

Figure 6-15: Cylinder Head extension a) base and side plates, b) camshaft extension, c) assembled extension (side), d) assembled extension. 191
Figure 6-16: 2D design of Cylinder Head extension. 192
Figure 6-17: Drawing for seal to face plate adapter. 193
Figure 6-18: Camshaft extension. 194
Figure 6-19: Valve cover. 196
Figure 6-20: 3d print design. 196
Figure 6-21: Camshaft lubrication system. 198
Figure 6-22: Fuel injection system. 200
Figure 6-23: Fuel rail adapter a) full assembly, b) adapter, c) fuel rail inlet. 201
Figure 6-24: Intake air diagram. 203
Figure 6-25: Intake plate a) pipe connections and thermocouple placement, b) fittings to other intake ports. 204
Figure 6-26: Extraction pipe and fittings. 205
Figure 6-27: Impact of Valve Temperature on IVD mass: a) All results, b) Sum of valve mass against mean temperature (deposit mass is measured immediately after the tests and normalised against duration). 208
Figure 6-28: 170 ^{o}C static test images. 214
Figure 6-29: 210 ^{o}C static test images. 214
Figure 6-30: 250 ^{o}C static test images. 214
Figure 6-31: 330 ^{o}C static test images. 215
Figure 6-32: 370 ^{o}C static test images. 215
Figure 6-33: 270 ^{o}C 9 hr dynamic test images (Valve 1). 215

Figure 6-34: 290^{o}C 9 hr dynamic test images (Valve 2). 216

Figure 6-35: 250^{o}C 2 hr dynamic test images (Valve 2). 216

Figure 6-36: 230 ^{o}C 2 hr dynamic test images (Valve 1). 216

Figure 6-37: Control of temperatures a) Valve, b) Cylinder Head..... 219

LIST OF TABLES

Table 2-1: Summary of standard valve deposition tests (138). 66

Table 3-1: Engine specifications. 70

Table 3-2: Fuel properties (* approximate value for confidentiality, ** range of values used for confidentiality). 73

Table 3-3: Emissions measurement equipment accuracy. 75

Table 3-4: IVD proof of concept test conditions. 80

Table 4-1: Variables that were adjusted throughout accelerated fouling Cycle development process. 86

Table 4-2: Summary of stability (1 hr) test results. The shade of red indicates how high a value is comapred to the average. Setpoints in yellow were chosen for the next section. 97

Table 4-3: Summary of short Cycle test results (* first 9h continuously at 1500 rpm 16 bar IMEP, followed by cycling between 1500 rpm 16 bar IMEP (60 min) and 4000 rpm 7bar IMEP (30 min). 100

Table 4-4: SOI at high load Setpoints. 103

Table 4-5: Adaptive testing with additive cycle results. 105

Table 5-1: Engine operating Setpoints. 134

Table 5-2: The impact of fuel, scenario and Setpoint on predicted intake manifold temperature and the predicted impact on BSFC and MFB50. 150

Table 5-3: The impact of increased EGR Cooler dP due to fouling in the context of the total dP found across 3 typical EGR setups. 154

Table 6-1: System to modify Cylinder Head temperature: Specification. 162

Table 6-2: PID Calculations Symbols. 176

Table 6-3: System to modify valve temperature specification. 177

Table 6-4: System to actuate valve specification. 188

Table 6-5: Fuel injection system specification. 199

Table 6-6: Air intake and extraction systems specifications. 202

LIST OF ABBREVIATIONS

ΔT_{LMTD} - *Log Mean Temperature Difference*

h_g - *Forced Heat Transfer Coefficient of Gas*

P_{in} - *compressor in Pressure*

P_{out} - *compressor out Pressure*

$R_{conv,g}$ - *thermal resistance due to the forced convective heat transfer for the coolant*

$R_{conv,c}$ - *thermal resistance due to the forced convective heat transfer for the gas*

R_f - *Thermal resistance due to fouling*

R_w - *Thermal resistance of wall*

T_g - *bulk gas Temperature*

T_{in} - *Compressor in Temperature*

T_{out} - *Compressor out Temperature*

T_w - *wall Temperature*

k_g - *Thermal Conductivity of Gas*

$\dot{m}$ - *Gas Mass Flow Rate*

r_c - *Compression ratio*

η_I - *Indicated Efficiency*

η_{comp} - *Adiabatic Compressor Efficiency*

A - cooling surface Area

AIGN – Angle of Ignition

aTDC - after Top Dead Centre

BMEP - Brake Mean Effective Pressure

BSFC- Brake Specific Fuel Consumption

bTDC - before Top Dead Centre

CAD - Crank Angle Degree

CADD - Computer Aided Design Drafting

CCD – Combustion Chamber Deposits

CNC – Computer Numerical Control

CO – Carbon Monoxide

CO_2 – Carbon Dioxide

C_p - Specific heat capacity, constant pressure

C_s - Local soot concentration

d - Pipe Diameter

DCA – Deposit Control Additive

DDA – Deposit Dispersant Additive

DI – Direct Injection

dP - Pressure Difference

E100 - Evaporated Fuel 100 ^oC

E150 – Evaporated Fuel 150 ^oC

E70 - Evaporated Fuel 70 ^oC

ECU – Engine Control Unit

EDA – Exploratory Data Analysis

EGR - Exhaust Gas Recirculation

EGR% - EGR percentage of intake by mass

FSN – Filter Smoke Number

GDI - Gasoline Direct Injection

GDPI – Gasoline Direct/Port Injection

GPF - Gasoline Particulate Filter

H - Enthalpy

HC - Hydrocarbons

HP - High Pressure

ICE – Internal Combustion Engine

IMEP - Indicated Mean Effective Pressure

IVD – Intake Valve Deposits

K_1 *- Cooler shape coefficient 1*

K_2 *- Cooler shape coefficient 2*

K_d *- Thermal conductivity of soot*

K_{th} *- Thermophoretic coefficient*

L - Hydraulic Length

LED – Light Emitting Diode

LOESS - Locally Estimated Scatterplot Smoothing

LP - Low Pressure

MFB50 - 50% of Mass Fraction Burned

NA – Not Applicable

NO – Nitric Oxide

NO_2 *– Nitrogen Dioxide*

NO_X *– Nitrogen Oxides*

Nu - Nusselt Number

OLED – Organic Light Emitting Diode

PDS – Product Design Specification

PFI – Port Fuel Injection

PID – Proportional – Integral - Derivative

PM - Particulate Mass

Pr - Prandtl Number

PWM – Pulse Width Modulation

Q - Heat Transfer

Re - Reynolds number

SOF - Soluble Organic Fraction

SOI – Start of Injection

SPI – Serial Peripheral Interface

SSR – Solid State Relay

St - Stanton Number

T - Temperature

THC - Total Hydrocarbons

T_0 *- EGR inlet temperature*

T90 – 90% distillation temperature

T_{c1} *- Temperature of cold fluid, inlet*

T_{c2} *- temperature of cold fluid, outlet*

T_{h1} *- Temperature of hot fluid, inlet*

T_{h2} *- Temperature of hot fluid, outlet*

THC – Total HydroCarbons

TWC - Three Way Catalyst

u - Fluid velocity

U - Local overall heat transfer coefficient

v - Volume

γ - Ratio of Specific Heats

1. INTRODUCTION

1.1 Background

Climate change and pollution are urgent global challenges that necessitate significant advancements in vehicle manufacturing, particularly with regards to efficiency and emissions. The transportation sector accounts for approximately 15 % of total greenhouse gas emissions predominantly from road vehicles (1). Additionally, urban air quality has deteriorated due to pollutants such as NO_X and PM, largely emitted by conventional ICE vehicles using fossil fuels (2). Consequently, regulatory bodies worldwide have implemented stringent emissions standards and fuel efficiency requirements, compelling manufacturers to innovate and adopt cleaner technologies. These advancements have led to significant improvements in ICE technologies, such as turbocharged engines (3), direct fuel injection (4) and advanced exhaust after-treatment systems (5). These innovations aim to enhance fuel efficiency, reduce emissions, and meet the evolving demands of an environmentally conscious consumer base while utilising the existing infrastructure for ICE vehicles (6).

One of these improvements is the GDI engine, which has improved the fuel efficiency and performance of gasoline ICE by injecting fuel directly into the combustion chamber, allowing for more precise control over the air-fuel mixture and combustion process. This technology enhances thermal efficiency and power output while reducing fuel consumption compared to its predecessor the PFI engine. However, GDI engines face challenges with PM emissions. Despite the advancements in GDI technology, PFI engines

remain relevant due to their lower emissions of CO, HC, and PM, reduced frictional losses, and lower costs (7) (8).

Fuel deposits present a significant issue for the efficiency and longevity of ICE in both PFI and GDI configurations. These deposits accumulate on critical engine components such as fuel injectors and intake valves in PFI engines, adversely affecting engine performance, fuel economy, and emissions (9) (10) (11). In GDI engines the exposure of the injector to the combustion chamber can result in deposits forming inside the injectors. This process occurs when fuel evaporates within the nozzle, leaving behind residual substances. It is primarily caused by the high-temperature environment in which GDI engines operate. As fuel evaporates inside the injector, it leaves behind carbonaceous deposits through mechanisms such as auto-oxidation and pyrolysis (12). These deposits obstruct the injector nozzle, leading to distorted fuel spray patterns and delayed injection timings, leading to poor combustion that results in reduced fuel efficiency and increased PM emissions (13). Furthermore, delayed injection timing can cause misfires and increased emissions of unburned HC and CO (14). The accumulation of deposits also leads to higher injector tip temperatures, further exacerbating the problem by creating a self-reinforcing cycle of deposit formation (15). This cycle of inefficiency and increased emissions underscores the importance of maintaining clean injectors by utilising technologies such as fuel additives for optimal engine performance and compliance with emission standards (16). Addressing these issues is crucial for optimising the environmental and operational benefits of GDI technology.

Another component that is impacted by deposits is the EGR Cooler. Deposits here cause fouling which occurs due to the high-temperature gradient between the exhaust gas and the Cooler walls, causing soot particles to be driven towards the wall through thermophoresis. This is particularly pronounced in engines with high soot and hydrocarbon emissions, as seen in GDI engines, especially those with high amounts of injector deposits (17) (18). The soot accumulates on the Cooler walls, reducing its effectiveness and increasing the pressure drop across the system. This deposition can reach an equilibrium where the rate of soot deposit formation equals the rate of removal, influenced by factors such as transient engine behaviour, soot concentration, and EGR inlet temperature (19) (20). Additionally, hydrocarbon condensation affects the soot packing structure and removal mechanisms, further complicating the fouling process (20).

The consequences of EGR Cooler fouling include a reduced EGR rate and increased EGR outlet temperatures and hence intake manifold temperatures, impacting engine efficiency and emissions. A lower EGR rate diminishes the system's ability to lower combustion temperatures, increasing the knock propensity and reducing the engine's efficiency (21). Increased EGR outlet temperatures due to fouling can also increase combustion temperatures, sometimes to the point where the hot EGR can increase knock propensity more than the inert nature of EGR is capable of reducing it (22). This can lead to higher PM and NO_X emissions due to less effective temperature control in the combustion chamber (23). Ultimately, the increased intake temperatures and reduced EGR efficiency result in higher emissions and lower overall engine performance,

highlighting the need for effective management of EGR Cooler fouling to maintain engine efficiency and meet emission regulations (24).

Deposit problems are not limited to GDI engines, as PFI engines encounter similar issues. In particular, these engines exhibit increased susceptibility to IVD, which can negatively impact engine performance and lead to engine malfunction (25) (26). IVD in PFI engines form primarily due to the evaporation of fuel that leaves behind heavy fractions of hydrocarbons (27). Near constant contact between the fuel and the intake valve in PFI engines leads to the accumulation of these deposits. This process is influenced by valve temperature and boiling points of the fuel components. IVD contribute to poor cold start performance due to impaired combustion and reduced valve temperature, which can affect the valve's operation and engine efficiency (28). The deposits can also result in increased frictional losses and a higher likelihood of engine knock, further compromising the engine's performance (29).

Fuels and their additives play a crucial role in the formation of deposits on all engine components. Components such as olefins, sulphur and heavy aromatics, can lead to increased deposits due to their tendency to remain on surfaces (30) (10). Alcohol content in fuels, particularly ethanol and methanol, has also been found to increase IVD significantly (31) (32). The relationship between the evaporation points of fuel components and the operating temperatures of intake valves and injectors has been demonstrated to have a significant impact on intake valve and injector deposit formation (30) (12).

Additives such as detergents can be employed to reduce deposit formation. These additives, which typically consist of long-chain hydrocarbons with polar head groups, attach to metal surfaces, preventing deposit formation and dispersing deposit precursors (12). They also clean existing deposits by bonding to them and removing them, and have been found to effectively clean dirty injectors to near original performance (33) (16). Effective additives can reduce the mass of deposits to negligible amounts at optimal dosages and operating temperatures, though they may become unstable at higher temperatures (34) (35). Therefore, the appropriate selection and dosing of fuel additives are critical in minimising IVD and maintaining engine performance.

It can take years for deposits to form in regular engine conditions. Therefore, the long-term fouling process needs to be accelerated under controlled conditions in order to observe the performance of fuels and additives. Developing accelerated testing methods for fuel additives is essential to reduce test time, costs, and fuel usage, making the research process more efficient (35). These methods allow manufacturers to rapidly evaluate the effectiveness of additives in preventing and cleaning deposits, as traditional testing over the lifetime of a vehicle is impractically time consuming and expensive (36). Physical simulations can replicate years of deposit buildup in a short time, whilst significantly reducing the resources needed (37) (38). These tests demonstrate the possibility of testing without running a full engine, which can allow for more control of isolated variables and precise control of conditions (38). This approach provides a controlled environment to test the efficiency of additives under specific, repeatable conditions, in addition to enhancing understanding of the deposition processes (39).

1.2 Research Focus

Research on engine deposits has been increasing (Figure 1-1a), especially since the early 2000s with the rising popularity of GDI engines (currently representing 73 % of new vehicles in the US and an ever-increasing global market share (40) (41)). Since the early 2000s legislative bodies worldwide have introduced low emissions zones in major cities, which continue to increase in number as well as enforcing strict efficiency criteria on manufacturers (42). To reach efficiency standards, GDI engines are a popular choice, but with much emphasis being put on PM emissions in low emissions zones the importance of studying technologies that are impacted by PM emissions and deposits such as GDI injector deposits and EGR Cooler Fouling has increased (Figure 1-1b,c).

This study builds upon the current understanding of this field to equip future researchers with knowledge to develop fuels and additives that can combat this ever increasing problem. Although GDI engines are being developed at a higher rate than its counterpart, PFI engines are still popular due to their relatively low cost and simplicity. Therefore, it is important to represent PFI deposits in this study. IVD have been studied for decades and are well understood (Figure 1-1d), therefore this study focuses more on improving the efficiency of methods used to test for IVD when developing fuels.

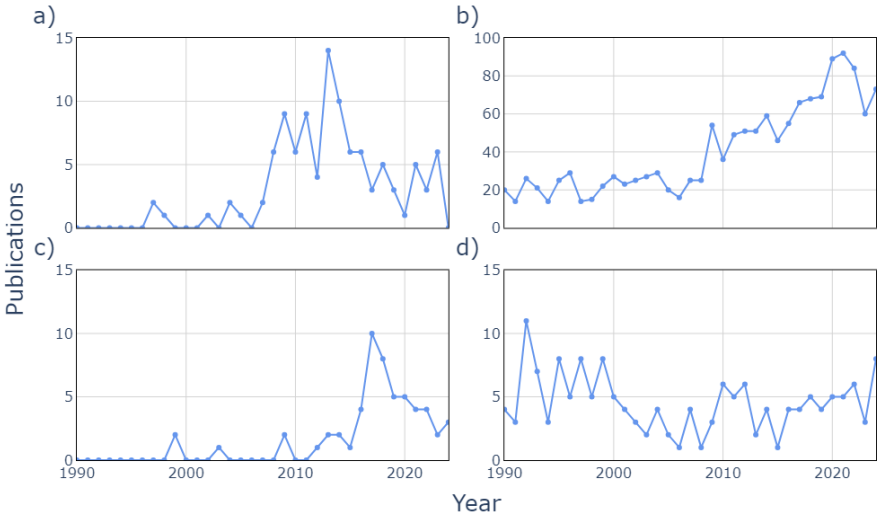


Figure 1-1: Published Articles with a) Engine Fuel Deposits, b) GDI Injector Deposits, c) EGR Cooler Fouling, d) Intake Valve Deposits in the title or abstract.

1.2.1 Aims and Objectives

Aim 1:

The key aims of the research are to examine the factors that influence formation of fuel deposits on critical engine components, including fuel injectors, EGR Coolers, and intake valves, in both GDI and PFI engines.

Aim 2:

To gain insight into the influence of fuel composition and additives as well as various engine parameters (e.g. temperature, mass flow rates, and fuel properties) on the formation of these deposits.

Aim 3:

Investigate various methods for simulating the real-world, long-term formation of these deposits in an accelerated manner, with the aim of improving fuel and additive

development for cleaner, more efficient engines. The creation of these accelerated deposit growth cycles is documented in this study with the aim of providing a framework for future researchers to follow, thus reducing the time required to create accelerated cycles and thus saving on fuel consumption and costs.

To achieve these aims, the research is divided into the following objectives:

Objective 1:

Investigate the impact of different fuels and additives on the formation of GDI injector deposits and how they impact the function of the fuel injector and thus understanding the impact on engine performance and emissions. To do that, the development and assessment of an accelerated fouling procedure that can both generate GDI injector deposits rapidly and allow for the function of fuels and additives to be analysed has been pursued. To create the procedure the impact of various testing techniques and engine parameters on the formation of GDI injector deposits were detailed to create a framework for the process.

Objective 2:

Study the impacts of different exhaust conditions on deposit formation in the EGR Cooler, and the subsequent effect the deposits have on its own functioning. Furthermore, the study will relate the impact of GDI Injector deposits to EGR Cooler fouling and predicted effect of EGR Cooler fouling on engine performance. An accelerated method to quickly generate EGR Cooler deposits has been developed, allowing for the long-term impacts of using different fuel additives to be seen in a short amount of time.

Objective 3:

Design, manufacture and evaluate an experimental rig and methodology that can emulate the formation process of fuel-derived deposits on intake valves in an ICE across a range of conditions. The system should allow different elements to be controlled independently (e.g. valve temperature, intake air temperature, fuel injection parameters, valve actuation) to study the impacts of various parameters on intake valve properties and deposit formation. The system and method should create sufficient deposits to allow the impacts of fuels and additives to be seen in a cost effective and timely manner.

1.2.2 Novelty of Research

This study presents several innovative aspects, particularly its focus on the methodology for creating fuel-derived deposits and their effects on various engine parameters including engine performance and emissions. This approach allows future researchers to understand the strengths and limitations of the techniques described, offering a thorough account of the development strategies employed in accelerated fouling procedures for both operational engines and physical simulations.

The Injector Deposits chapter presents several original elements, including a comprehensive account of the methodology employed in the development of an accelerated injector deposit growth cycle. This cycle is capable of generating GDI injector deposits and evaluating the efficacy of an additive. Section 4.2 provides a detailed description of the testing techniques, along with the analytical techniques used at each stage of the cycle development. Much research has been conducted on the results from

accelerated deposit growth cycles but documenting the process of creating them is novel and can assist future researchers with the arduous task of developing new cycles. The increase in injection duration throughout various phases and transition points over multiple engine conditions is analysed for the first time. This analysis technique allows the assessment of the influence of different parameters on the formation of injector deposits throughout different phases of a cycle, thereby facilitating the rapid development of the accelerated fouling procedure. Once developed, this analysis technique enables the behaviour of how GDI injector deposits are formed and removed with different fuels and additives to be investigated.

The novelty in the EGR Cooler section lies in the contextualisation of the results and by directly comparing how different additives impact EGR Cooler Fouling. Multiple studies have independently assessed how fuel additives can impact engine exhaust composition and how EGR Cooler fouling is generated, but none have done these two things in the same experiment. Another novelty is that this study contextualises the effect of the additives on EGR Cooler fouling on overall engine performance, by calculating the predicted impact of the fouling on engine intake manifold temperature and EGR pressure drop. Furthermore, these predictions help assess the trade-off between the costs (out of the scope of this thesis) and energy expended in additive development and the potential impacts on engine performance.

The PFI IVD experimental rig is an innovative design that, enables the simultaneous and independent operation of various parameters: valve temperature, cylinder head temperature, valve actuation speed, fuel injection parameters (pressure, pulse width,

injection frequency), and intake air parameters (temperature, pressure, and flow rate) in an authentic ICE cylinder head. Additionally, the detailed description of the design and manufacturing process aims to facilitate the replication of similar constructions in future studies, addressing the issues identified in this study and allowing for improved experimental rigs to be built in less time and at less cost.

1.3 Thesis Outline

Chapter 1: Introduction

The introduction aims to provide an overview of the work carried out and to give it context within the current state of research. The focus, aim and objectives of the thesis are also established along with the novelty of the research.

Chapter 2: Literature Review

This chapter provides relevant background knowledge allowing the reader to understand the research itself, why it is important and to give it context with respect to other relevant work. It also aims to identify a gap in the current literature.

Chapter 3: Methodology

The experimental setup and specifics of the utilised equipment are covered in this section. In-depth explanations of experimental techniques specific to a certain section are covered in their corresponding chapters.

Chapter 4: GDI Injector Fuel Deposits

This section starts by describing the process taken to develop a test cycle designed to accelerate the formation of GDI fuel injector deposits in its own methodology section. The section: Development Procedure for Discovery of an Accelerated Injector Deposit Formation *Cycle* then proceeds to explain and discuss the results from the various sections of the Development Procedure. Analysis is carried out using these results to explain how engine and cycle parameters were changed in real-time based off of the results. This analysis is then continued after the whole Development Procedure has been explained in order to discuss the final impacts of various engine and cycle parameters both on how the Cycle generated Injector deposits and how the Cycle allowed a Fuel Additive to perform. The chapter then explores the potential mechanisms underlying the different behaviours of the deposits when using a standard Gasoline fuel and a Renewable fuel along with additives, and their influence on deposit growth. Additionally, it examines the impact of injector deposits on injector performance and the consequent effects on overall engine performance and emissions. The experimental results of this chapter address Objective 1.

Chapter 5: GDI Engine EGR Cooler Fouling

This chapter builds on Chapter 4 by investigating the impacts of how injector deposits can impact the exhaust makeup and how this in-turn impacts the EGR Cooler, located downstream of the cylinder. The EGR Cooler experiences fouling, and to investigate the impact of this another accelerated fouling method was developed. Analysis was conducted on the results of the accelerated fouling procedures to observe the impacts

of soot on EGR Cooler performance and predictions were made using similar experiments from literature to estimate the potential impacts of this on engine performance. The results of this analysis were done with a Reference Fuel and fuel additives to compare the difference, and to allow the potential of fuel additives on EGR Cooler fouling and engine performance to be judged. The experimental results of this chapter address Objective 2.

Chapter 6: Development of an Experimental Method to Investigate Fuel Derived Deposits on Engine Intake Valves

This chapter details the design and manufacture process of an experimental method built to simulate intake valve fuel deposition. The final design and manufacturing decisions are broken down for the overall product and its subsystems. The results of a proof of concept test are then discussed to show how the experimental rig allowed for the variation of multiple variables that were predicted to impact IVD, and how well this simulates real deposits found in an engine. The final product described in this chapter addresses Objective 3.

Chapter 7: Conclusions and Future Work

The main conclusions of the study are outlined and compiled in this chapter. Based on the findings, recommendations are also given, and future directions for the work are also covered.

2. LITERATURE REVIEW

2.1 Gasoline Injection Technologies

2.1.1 Overview

PFI is a method whereby fuel is injected within the intake system before the combustion cylinder, in comparison to GDI where the fuel is delivered directly into the combustion cylinder. PFI was first introduced in the 1980s to improve upon carburettor technology (43). GDI has been increasing in popularity since the 1990s to help engine manufacturers reduce fuel consumption in an effort to meet emissions regulations (44) (45) (46) and by 2018 over 50 % of new light duty vehicles in the US were powered by GDI engines (40). However PFI injection engines are still popular worldwide as they are simpler, easier to maintain (43), and more resistant to low quality fuels (7) thereby making them popular in cost sensitive markets (47). Hybrids between GDI and PFI (GDPI) which have multiple injectors and inject fuel in both the port and cylinder in varying quantities are increasing in popularity, with most manufacturers using either GDI or GDPI in over 80 % of their new vehicles as of 2023 (40).

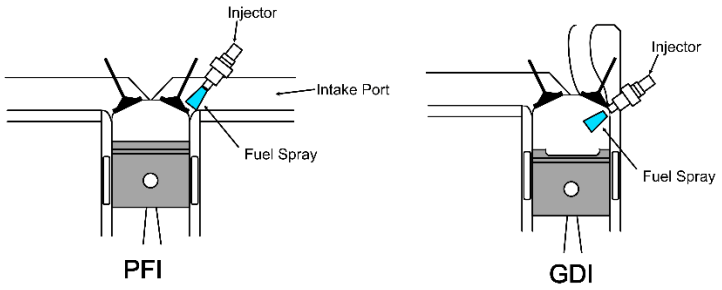


Figure 2-1: PFI and GDI injector location (48).

2.1.2 Mechanism of Action

The requirements of most fuel injection systems are to control the air-fuel ratio as efficiently as possible whilst limiting harmful emissions (49). The ECU is used to control the fuel injection system. At any given engine condition, the ECU will have a pre-programmed air-fuel ratio which it will try to achieve based on engine speed, accelerator pedal position and ambient conditions. This pre-programmed air-fuel ratio depends on many variables according to the purpose of the engine, but its general purpose is to generate sufficient power whilst maintaining efficiency, reducing harmful emissions, protecting the engine or to help auxiliary engine components to function efficiently. The ECU receives signals from various sensors in the air intake system to predict the air mass flow rate at any given point. This includes mass air flow, pressure, temperature and position of various intake components such as the compressor, throttle and intake valve variable valve timing. All these inputs allow the ECU to build an accurate prediction of the air mass flow rate and how it is likely to change in the following cycle. Consequently, this allows the ECU to calculate the required fuel mass flow rate to achieve the desired air-fuel ratio.

In GDI, the fuel is pumped from the fuel tank at low pressure, routed through a high-pressure pump and a regulator to keep a stable pressure in the fuel rail. For PFI systems the fuel rail is regulated to a lower pressure. In both systems the fuel injection is controlled by the amount of time the injector is open and the rail pressure. The ECU correlates injector open time and fuel pressure to generate fuel mass flow rate. This is achieved by sending a very short digital signal which activates an armature in the

injector, lifting the needle and allowing fuel to flow through. A high initial current is used to rapidly open a needle but any small delays in the opening and closing times are taken into account in the calibration of the control logic. In GDI systems the fuel then enters the cylinder at high pressure, which is necessary to atomise the fuel ready for combustion (50), whereas the fuel enters the intake port and is directed towards the back of intake valve in PFI systems (51).

The ECU is only predicting the fuel flow that will enter the cylinder using calibration data which can deviate from the real-world flow rate. A feedback loop has been installed to account for this, and functions by placing an oxygen sensor in the exhaust which sends a signal to the ECU (52). This allows the ECU to self-correct to obtain the desired air-fuel ratio. However, this loop can only compensate for a certain tolerance of error in the predicted fuel flow rate by adjusting fuel trim. Engine operation can be significantly hindered if the predicted error is too large (36).

2.1.3 Injector Design

2.1.3.1 GDI

Homogenous

The two primary types of combustion in a GDI engine are homogenous and stratified, which have distinct injector designs. Homogeneous operation aims to achieve an evenly spread homogenous mix of air and fuel throughout the cylinder in time for the combustion event. This is achieved by injection in the intake stroke to give the fuel sufficient time to mix with the air (49) (53). To further assist mixing a high fuel pressure of between 5-15 MPa is used with a multi-hole injector normally utilising a wide spray

angle to increase air entrainment and decrease droplet sizes, which in turn aids fuel atomisation and vaporisation, thereby promoting good combustion (49).

Stratified

Stratified injection aims to create a combustible cloud of fuel and air around the spark plug to initiate flame growth, while the rest of the cylinder is diluted and lean. This is achieved through precise late injection in the compression stroke (49). Location of the injector, nozzle design, fuel pressure, airflow and piston design work in tandem to achieve the desired fuel-air mixture around the spark plug. This is achieved in three main ways: spray guided, air guided and wall guided (Figure 2-2). Spray guided injection is when the injector is placed close to the spark plug. The fluid characteristics of the spray guide the fuel towards the spark plug, as it is sprayed on directly (46) (50). Air guided systems use the dynamics of airflow to carry the fuel to spark plug (46) (50) and often have the injector placed further away from the spark plug (49). Similarly, wall guided systems have the fuel injector placed further away (49) ,using the geometry of the piston to guide the fuel to its destination (46) (50). Normally a combination of one or two of these systems are used, along with a specifically designed injector nozzle to fit with the mixing approach (49). Injectors utilising nozzles with multiple small orifices at their tip, known as multi-hole injectors are often favoured because they create a fine atomised mist of fuel leading to more stable fuel spray patterns with respect to in-cylinder conditions and cyclic variations and due to their improved customisability (54).

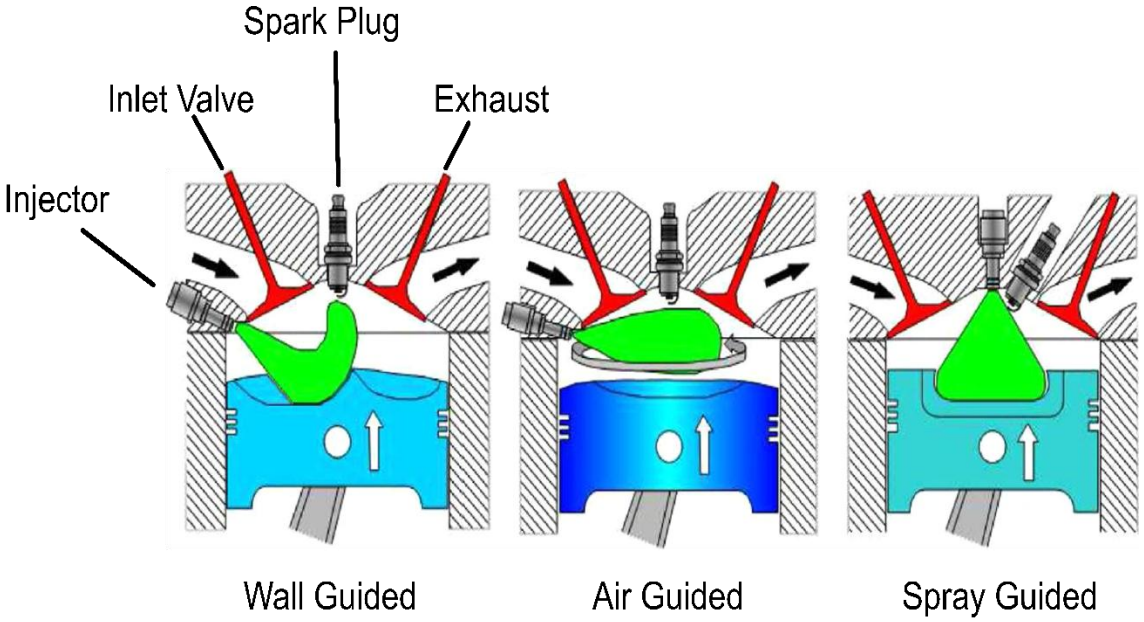


Figure 2-2: Types of stratified change (46).

2.1.3.2 PFI

PFI operation facilitates more homogeneous fuel distribution compared to GDI, as the fuel has more time to mix with air. PFI systems have improved upon single point injection by employing a dedicated injector for each cylinder. A critical design aspect is the location of each injector. The simplest design places the injector outside the cylinder head, aiming it at the intake port, while more advanced designs position the injector within the cylinder head (55). The objective is to direct fuel towards the hot surface of the intake valves. The intake valve, heated from combustion, facilitates rapid evaporation of the fuel droplets (25). This process is essential for ensuring effective vaporisation of the fuel, allowing for uniform mixture with the incoming air, thereby promoting efficient combustion.

Positioning the injector near the intake valve ensures that a portion of the injected fuel collides with the hot intake port and valve surfaces, forming a liquid film on these

surfaces (56). However, the liquid film can have negative implications such as pooling and puddling if the surface is too cold and does not allow for fast evaporation. This can significantly affect combustion behaviour (57) and is best avoided through optimised injection timing and fuel spray characteristics, allowing for the optimum air-fuel mixture formation process (51). Research indicates that directing the fuel spray towards the intake valves leads to improved, in-cylinder fuel distribution, which is crucial for optimising combustion efficiency and minimising emissions in spark ignition engines (58).

2.1.4 GDI vs PFI

2.1.4.1 Fuel Efficiency

Increased fuel efficiency is one of the key advantages of GDI compared to PFI (59) (60), with reported estimates of improvement of up to 15 % (7). Gains have been attributed to reduced pumping losses, improved mixture thermodynamic properties, increased compression ratio and reduced heat transfer. Conversely GDI was found to show reduced combustion efficiency and increased frictional losses compared to PFI.

Pumping Losses

Alkidas et al (7) tested at 7 setpoints split across near idle conditions, low load and medium load. The near idle and low load conditions both use stratified injection and medium load used homogenous injection. Fuel savings due to reduced pumping losses were largely due to stratification at lower loads reaching as much as a 26 % increase in efficiency compared to PFI. This is because the diluted charge allows for a low load to be achieved without the need for much throttling (53). The perceived benefit diminishes

to about 2-3 % as the load increases and a homogenous charge is used. The remaining increase is likely due to reduced throttling due to EGR being used in the GDI engine and not the PFI. The impact of EGR on pumping losses will be discussed later, in more detail, in the EGR section. Minimal EGR was used in the PFI engine possibly because it would have deteriorated the combustion.

Evaporative Cooling

The evaporative cooling generated by the injected fuel is greater in GDI compared to PFI, due to direct injection into the cylinder (61). This is because the majority of the evaporative cooling is done on the intake valve in PFI, as this is where most of the fuel is impinged. In contrast, the fuel is predominantly vapourised by the air charge in GDI (62). This allows for higher peak pressures to be achieved without damaging the engine and reduces the chance of engine knock (63), thereby allowing for an increased compression ratio (62). The reduction in knock also reduces the amount of fuel enrichment and spark retardation at high loads, which is done more aggressively in PFI to protect the engine (64) (65). Injecting excess fuel reduces fuel efficiency and also increases PM,HC and CO emissions (66) (67). The reduced knock propensity allows for more aggressive engine downsizing and boost pressure from turbochargers (59). This allows for the specific power to be increased, reducing low load engine operating time and can thus reduce pumping losses (3).

According to the equation for thermal efficiency of an Otto cycle engine (Equation 2-1) an increase in compression ratio directly increases thermal efficiency. Alkidas et al (7) demonstrated that GDI cooling benefits could increase the compression ratio from 9.4

to 11.2. This yielded an increase in efficiency of 3 % across all conditions. The increased compression ratio allows for increased maximum power output (63) and lower temperatures also increases volumetric efficiency, further increasing power (62).

Another benefit of reduced in cylinder temperatures is the increase in the charge mixtures ratio of specific heats (7). Equation 2-1 shows that an increase in the ratio of specific heats will increase efficiency. This is further enhanced by lean operation at low loads and by the presence of EGR in the GDI engine as both of these dilute the charge and help with cooling (65) (68).

The reduced in-cylinder temperature also resulted in lower heat losses from the cylinder, resulting in higher efficiencies, even when piston surface area was accounted for, as increased piston surface area would increase heat transfer in the GDI engine (7).

$$\eta_I = 1 - \frac{1}{r_c^{\gamma-1}}$$ *Equation 2-1: Otto cycle efficiency (69).*

Fuel Delivery and Control

Direct injection into the cylinder allows for better control of the fuel and air mixture in GDI engines. As there is no delay with the fuel travelling from the place of injection to the cylinder as in PFI (49), more precise control of the mixture can be achieved (70) (71), resulting in better driveability (49) primarily due to improved transient response (70) (4). GDI can also take advantage of different injection strategies not available to PFI, such as splitting injection over intake and compression strokes and strategies revolving around late injection timing, both of which can greatly improve efficiency and emissions

(7) (46). Split injection allows the total fuel load to be split over multiple injections. This allows for better mixing and improved homogeneity, comparable to a PFI engine, helping to decrease PM and HC emissions (72) (73). Stratification can only be used in GDI and allows for the potential of significant efficiency gains. However, there are some practical limitations that hinder stratification. Fuel stratification can only be used at low-medium loads, as the stratified spray gets too large with large loads which in turn increases soot emissions (50). Another disadvantage of fuel stratification is that it can lead to increased HC and PM emissions (5). As emissions regulations have got tighter regarding HC and PM emissions, the market has generally shifted away from stratified injection and back to its homogeneous counterpart (5). Therefore, homogenous mixture preparation will be the primary focus of the rest of this study.

Frictional Losses

A negative of GDI compared to PFI found by Alkidas (7) was increased frictional losses especially at low loads. This is due to the reduced pumping losses at low loads creating higher in-cylinder pressures. On top of this the increased compression ratio added more pressure across all loads. However, this was less of a problem at high loads, due to the frictional losses being a smaller proportion of the total power.

Combustion Quality

PFI has increased combustion efficiency compared to GDI, this is due to better mixing of air and fuel, as the air-fuel mix has more time to mix homogenously (64). Using stratified injection worsens the combustion quality in GDI further due to sub-optimal mixing (74).

2.1.4.2 Emissions

The poor mixing in GDI engines also leads to rich spots forming around the spark plug, thereby increasing PM, HC and CO emissions (75) (8). A greater proportion of fuel condenses on the surfaces of the combustion chamber, a phenomenon known as fuel impingement, which leads to increased PM, HC and CO emissions in GDI engines (76) (77). As the injector is directly exposed to these increased emissions in GDI engines, there is a greater probability of fuel deposit formation compared to PFI (46) (49). The spark plug is also impacted by poorer combustion quality as it causes quicker electrode degradation (50) (46). However, elements of PFI design can also lead to increased emissions especially if high amounts of liquid fuel films are found in the port and valve surfaces. This can lead to increased HC and PM emissions (78) and incomplete combustion (57). This liquid can be inducted into the cylinder further negatively impacting combustion quality and hence emissions, especially during cold starts (79).

2.1.4.3 Exhaust Aftertreatment

PM emissions are harmful to human health and the wider environment (80) (81), thus their reduction has become a target of regulatory reform (82). A GPF is necessary in GDI engines to be compliant with these regulations (83). This can make a GDI engine more expensive to develop than a PFI, while concurrently reducing fuel efficiency (84). The decrease in efficiency is primarily due to increased exhaust pressure and the GPF regeneration process (85), as more soot requires more filtration, resulting in increased back pressure. Regeneration is a process whereby excess accumulated soot in the filter is oxidised, which is necessary to prevent the GPF from degrading and prevents the

pressure drop from increasing further (86). Regeneration can be passive at conditions where exhaust temperature is high, as the conditions are sufficient to oxidise soot with excess oxygen, which is abundant in a decelerating engine (87). However, the converse applies at low load conditions where the exhaust temperature is not sufficient for oxidation and regeneration has to be done actively either via delayed ignition or air injection, both of which incur a fuel penalty (88). Therefore, reducing PM emissions is critical to reduce the accumulation of soot in GDI engines, to ensure exhaust back pressure and frequency of active regeneration are kept to a minimum.

The majority of gasoline engines operate at stoichiometric conditions and use a TWC to reduce tailpipe emissions. TWC are able to control emissions of NO_X, CO, and HC during stoichiometric combustion conditions (89). TWC technology is also effective in low-oxygen exhaust conditions typical of gasoline engines, ensuring efficient reduction of harmful pollutants (90). This is possible due to sufficient concentrations of reducing agents in a rich exhaust environment, which allows the TWC to efficiently catalyse the oxidation of CO and HC as well as the reduction of NO_X (91). Conversely, the TWC does not operate well in a lean environment with an abundance of oxygen and a scarcity of reducing agents (92). The poor operation of a TWC in lean conditions means that additional aftertreatment is required if a gasoline engine is to run lean, such as during stratified operation in a GDI engine. These treatments can be expensive and numerous, examples include Lean NO_X Traps (LNT) or Selective Catalyst Reduction (SCR) (93).

2.1.4.4 Warmup Time

Alkidas et al (7) hypothesised the impact of other factors relating to GDI efficiency compared to PFI which were not tested in their experimental setup. These included slower warmup times of the engine and aftertreatment systems due to the improved efficiency of the GDI engine, which results in less heat being ejected to the engine block and the exhaust. This results in reduced efficiency during the warmup phase, as the engine stays colder for longer, increasing frictional losses due to cold oil (59). Additionally, in order to increase the temperature of the aftertreatment into its operating window the engine operates in a manner to allow more heat to exit via the exhaust, reducing efficiency, and this operation will last longer with GDI (94).

2.2 Injector Fouling

2.2.1 Overview

The injector within the combustion chamber is exposed to a harsh environment in GDI engines, which leads to an increased proneness to fouling. Reduced combustion quality due to poorer air-fuel mixing (64) and increased PM, HC and CO (75) (8) also increase the likelihood of injector fouling (46) (49). This fouling has a negative impact on the performance of the injector, which consequently impacts engine performance and emissions.

2.2.2 Formation Mechanisms/ Processes

Fuel is deposited on the inside and outside of the injector. The scale of deposition and resulting impact on performance varies greatly depending on properties of the fuel, engine operating conditions and engine geometry. The deposits are generally formed in two different ways, low temperature auto-oxidation and high temperature pyrolysis, also called coking, or carbon deposition (12).

Carbon deposits are normally created at temperatures above 350 ^{o}C, as hydrocarbons decompose into elemental carbon and hydrogen or polymerise/ condense into larger polycyclic aromatic hydrocarbons, which can nucleate, forming even larger deposits. Metal catalysis of carbon deposition uses decomposition as the primary mechanism, whereas non-catalytic, thermal carbon deposition, utilises polymerisation. At lower temperatures when the fuel is in liquid form the reactions of alkyl radicals generating hydroperoxides and other products can cause deposit formation (95) (12).

2.2.3 Parameters Impacting Injector Deposits

2.2.3.1 Temperature

Temperature is a key parameter that influences deposit creation. According to Bacho et al (96) the maximum injector tip temperature should be more than the T90 of the fuel to accelerate deposit formation. In other words, volatilisation of 90 % of the fuel volume at the injector tip is needed to form deposits. Henkel et al (16) conducted a study where they measured the temperature of the injector tip and observed that as its temperature

increased, combustion products would accumulate on the nozzle, potentially resulting in increased PM emissions. This suggests that higher injector tip temperatures may contribute to the formation of deposits and increased emissions in GDI engines. Conversely Slavchov et al (15) found that external deposits decreased at high temperatures.

Medina (97) identified that the tip temperature plays a crucial role in the drying process of the injector tip, with higher temperatures leading to enhanced evaporation of the overlying fuel film. The study emphasises that liquid vapour pressure is strongly influenced by the tip temperature. Critical factors that impact tip drying include temperature and residence time of the overlying fuel film, which are subject to engine operating conditions. Engine temperature has also been found to impact deposit formation. Rounthwaite et al (98) found that higher engine temperatures can increase the severity of deposits. Moreover, Cheng et al (99) noted that temperature rise significantly impacts the performance of GDI injectors.

2.2.3.2 Injector Design and Injection Strategy

The structure of the injector, as discussed by Zhang et al (100), plays a significant role in determining the fuel film deposited on the injector tip, which in turn impacts, fuel atomisation, PM emissions and the likelihood of deposit formation (12). The injector position can also have an impact, such as in wall-guided GDI systems, where the fuel injector tip temperature is low due to the distance from the flame front and the air

movement around the injector tip. This low tip temperature contributes to reducing the amount of residual fuel, which can impact the formation of injector deposits (12).

The surface where the deposits form also has an impact. A non-catalytic surface may reduce the heat transfer of the surface and act as an inert substrate to collect carbon deposits which are normally thermally initiated in the liquid phase. Conversely, a catalytic surface can interact with the reactive species in the fuel to increase the number of deposits. Aradi et al (101) found that larger amounts of deposits were found on stainless steel walls compared to when using a glass insert.

The injection strategy employed can also impact fuel deposition. Split injection can decrease PM and HC emissions and thus injector deposits (72) (73). Sarmast et al (102) found that by adjusting the start of the first and second injections and varying fuel mass ratios, split injection can influence mixture formation and combustion processes, potentially enhancing combustion efficiency and reducing emissions, which may indirectly affect deposit formation on injectors. While split injection shows promise in terms of combustion control and emission reduction, it can also lead to negative impacts. Wang & Zhao (103) observed that narrowly spaced split injections with short dwell times could lead to increased cycle-to-cycle variation and emissions. This demonstrates the challenge of optimising injection strategies to balance combustion efficiency, emissions, and deposit formation in GDI engines.

The fuel injection quantity is crucial in GDI engines, requiring precise modulation to achieve optimal combustion and minimise fuel deposition (104). Timing of injection also

influences deposit formation as it can significantly influence PM emissions. According to Szybist et al (105) advanced injection timing can lead to fuel spray impingement on the piston, resulting in higher PM emissions, while delayed timing may not allow sufficient time for proper air-fuel mixing, potentially contributing to deposit formation on injectors. He et al (106) agreed, also finding that fuel injection timing has a significant impact on PM emissions and could be reduced by retarding injection. Qin et al (107) demonstrated an initial decrease of PM emissions while advancing injection timing followed by a subsequent increase after 340 CAD bTDC. These findings highlight the complexity of optimising injection timing to minimise deposits while ensuring efficient combustion and emissions control. The research also shows how small changes in the injection delivery strategy can impact emissions and efficiency and thus any deposits in the injector that could disrupt the injection timing and delivery are likely to have an impact on the ability of an engines ECU to suitably control engine emissions. Therefore, ongoing research efforts are essential to refine understanding and develop guidelines for selecting the most suitable injection timing strategies in GDI engines (106) (13), and to more deeply understand how this can impact/ be impacted by fuel deposits

Xu et al (12) demonstrated that increased injection pressure can suppress the formation of injector deposits by improving the rate of deposit removal, indicating that higher pressure levels can contribute to maintaining cleaner injectors and reducing deposit buildup. Furthermore, higher injection pressure has been associated with a decrease in PM emissions in GDI engines (13). However, there are conflicting findings regarding the impact of injection pressure on injector deposits. While higher injection pressure can

enhance air-fuel mixing and promote better evaporation, potentially reducing deposit formation (13), it can also present challenges. Li et al (108) observed that increasing injection pressure from 5 to 40 MPa significantly affected PM and HC emissions, highlighting a complex relationship between injection pressure and emissions which can influence deposits.

2.2.3.3 Fuel Characteristics

Distillation Properties

Some key fuel properties impacting deposition are its distillation temperatures such as T90, defined as the temperature at which 90 % of a fuel evaporates, or E150, defined as the volume of evaporated fuel at 150 ^{o}C. Aradi et al (101) found that increasing T90 reduced fuel injector plugging. Kinoshita et al (109) found similar results, where a T90 which was below the injector tip temperature would result in the evaporation of the liquid, leaving behind deposits. Conversely, high T90 led to a greater proportion of the fuel remaining as liquid and washing away with the next injection. The role of injector tip temperature is controversial as the claim made by Kinoshita et al (109) that T90 being higher than the injector tip has a significant effect on deposits was not supported by the test on 11 different fuels by Aradi et al (101). Other studies have not been able to demonstrate statistically significant correlations between T90 and injector deposits (110). Aradi also admitted that the data found in their results was too limited to establish definitive fuel composition cause and effect (101). A review paper by Xu et al (12) seconded that correlation between fouling and T90 needs to be further investigated due to the abundance of confounding factors involving fuel and engine parameters.

Olefins, Aromatics and Sulphur

Olefins are another factor that can influence the likelihood of a fuel to generate injector deposits. Studies have shown that higher olefin content in fuels can lead to an increased tendency to form deposits in injectors and intake valves (111) as well as PM emissions (12). Aromatics also impact injector deposits, as studies have demonstrated the aromatic content of gasoline can significantly increase the formation of PM emissions (112) (113) which has an established effect on fouling. Heavy aromatic components, such as those with a carbon number of C9 and above, have been found to contribute significantly more to PM emissions compared to lower aromatic compounds (114). Another key fuel constituent that can impact injector deposits is sulphur content (12). Similarly to aromatic and olefin content, higher sulphur content leads to increased PM emissions (13).

Oxygenated Fuels

Many modern gasoline compositions are mixed with oxygenated fuels such as ethanol. The inclusion of these components can also impact PM emissions from GDI engines. A study by Fatouraie (112) highlighted the importance of considering oxygenated content, along with carbon chain length and thermo-physical properties, in understanding the factors contributing to PM emissions. The presence of oxygen in fuel can influence the formation of injector deposits. A study by Slavchov (15) proposed an adsorption-precipitation model for the formation of injector external deposits in internal combustion engines. The model suggested that the combination of high temperature

and the presence of oxygen dissolved in the fuel can initiate reactions leading to deposit formation. A study by Stępień (115) found that gasoline blends containing 10-20 % (v/v) ethanol or butanol showed a logarithmic increase in injection duration due to deposits, whereas standard gasoline fuels showed a linear increase. Alcoholic fuels would initially generate more deposits but then stabilise quickly, whereas standard gasoline fuels exhibited continually increasing deposits. This was due to alcoholic fuels exhibiting intensive early deposit precursor formation but showing less sediment build-up and higher rates of removal than standard gasoline after the initial phase.

2.2.4 The Impact of Fuel Deposits on Injection, Engine Performance and Emissions

Deposits formed in the injector have a negative impact on injection and engine performance. Fuel injectors are designed to accurately meter fuel to the engine and deliver it in a precise pattern of fine droplets. Since the fuel passages are small, injectors are highly sensitive to small amounts of deposits in the critical regions where the fuel is metered and atomised. These deposits can reduce fuel flow and alter the spray pattern, degrading driveability, decreasing power, fuel economy and increasing emissions (95).

Reduction in flow rate is due to partial or complete obstruction of the injector nozzle caused by deposits (12). Jiang et al (14) found that fuel injectors had lost 23.5 % of nominal flow rate after a 55 hr deposit accumulation test. A reduced flow rate results in an increased injection duration being required to maintain the flow rate at pre-fouling levels. Increased injection duration can alter the spray pattern, droplet size distribution,

and fuel atomisation. This can subsequently negatively impact fuel-air mixing, combustion efficiency, and emissions control in the engine (13). These findings correspond with the 20 % and 93 % increase in HC and CO respectively observed by Jiang et al (14). Wang et al (116) found that a fouled injector consistently generated higher PM emissions of up to 58 % compared to a clean one across all engine conditions. Sandquist et al (117) found an increase of 80 % in HC emissions and significant misfires after a 60 hr “dirty up test”. Similar results were also found by Zhang et al (33) who attributed increased PM emissions to the injector tip-wetting effect, as fuel trapped in the deposits on the tip-dome of the injector could lead to diffusion flames and cause higher particulate emissions.

Pre-existing deposits on injectors have also demonstrated an impact on formation of further deposits. According to Slavchov (15), average temperature of the injector surface rises as deposits accumulate and act as insulating layers which impede heat dissipation. Consequently, as the injector tip temperature increases, it can initiate a cycle where higher temperatures facilitate further deposit formation, establishing a self-reinforcing mechanism.

Henkel et al (16) observed that fouled injectors reduced the quality of fuel atomisation, resulting in larger droplet sizes and reduced evaporation. This can cause deeper spray penetration, due to increased mass of the droplets resulting in less deceleration from air resistance. Reduced atomisation and increased penetration depth both increase wall wetting, which in turn increases PM emissions. This highlights the impact that injector deposition has on spray formation, which detrimentally impacts combustion efficiency

and emissions. The disrupted spray pattern and in-cylinder charge motion (118) can lead to incomplete combustion due to poor mixture preparation causing rich spots, which ultimately leads to increased PM emissions (119). This is especially prevalent during cold engine starts (120). Yue and Reitz (121) found similar results, demonstrating the quality of the fuel-air mixture around the spark plug (influenced by the spray pattern) is crucial for ignition and combustion efficiency. Any disruption in this mixture can result in higher emissions and reduced engine performance.

The precise pattern of fuel injection is critical for achieving some injection strategies. The ECU can compensate for small amounts of deposition via fuel trim, but high levels of deposition and any levels of spray distortion may not be accommodated within its computation. This results in reduced combustion quality, causing a loss in power and exhaust emission deterioration (15). In spray guided systems, injector deposits can distort the spray pattern, leading to uneven fuel distribution and incomplete combustion, impacting fuel distribution and combustion efficiency. In air guided systems, deposits can hinder the proper interaction between fuel droplets and air, impacting vaporisation and mixing processes. For wall guided systems, deposits on injector tips can alter fuel flow and spray characteristics, potentially leading to incomplete combustion and increased emissions (122).

2.3 EGR Cooler Fouling

2.3.1 Overview

Another area of interest with regards to engine deposits is in the EGR system. These systems function by recirculating a portion of the engine's exhaust gas back into the engine cylinders, which aids in decreasing the combustion temperature (123). EGR is present in PFI and GDI engines but is predominantly used in the latter due to their higher operational compression ratios and temperatures which lead to increased knock and NO_X emissions (124). EGR can mitigate the negative impacts of this by reducing peak temperature (68) (125), whilst retaining the benefits of GDI. EGR also improves thermal efficiency, (24) (68) primarily through reductions in heat (126) (127) and pumping losses (68) (21) (128). These benefits have led to EGR equipped engines achieving brake thermal efficiencies of over 40 % (129) (130), whilst maintaining low emissions levels. This is especially important given the recent trend in engine downsizing, which is accomplished by reducing engine displacement and using a turbocharger to increase specific power. However, increased specific power increases knock propensity, which both GDI and EGR can reduce (124).

2.3.2 Fouling Mechanism

EGR is often used with a heat exchanger (Cooler) to cool the exhaust gases, increasing intake density, reducing knock and reducing in-cylinder heat transfer (68) (131) (127). The high temperature exhaust gases and high levels of soot and HC emissions in GDI engines create a harsh environment for the Cooler. The high temperature gradient

between the exhaust gas and the Cooler walls drives the soot particles towards the wall through thermophoresis, which increases with higher Cooler inlet temperatures and soot concentration but decreases with flow velocity due to deposit removal (17) (18) (132) (19) (20) (133). This contrasts with the formation of internal injector deposits, which adhere to the nozzle via auto-oxidation and high-temperature pyrolysis, as here the mechanisms are pre-dominantly thermodynamics and shear stresses which gradually push and pull soot from the walls, resulting in a more porous and fragile deposit structure. Soot deposition reduces cooler effectiveness and increases pressure drop. Eventually the system reaches an equilibrium where the soot deposit thickness reduces thermal conductivity and hence thermophoresis to a level where soot is being deposited at the same rate it is being removed. The equilibrium is highly affected by transient engine behaviour, soot concentration, EGR inlet temperature and can vary greatly depending on the type of engine and test cycle. Condensation from HC also has a significant impact on both the packing structure and removal mechanism of the soot (19) (20).

2.3.3 Impact on Engine Performance

2.3.3.1 High Load (Knock)

Fouling can reduce EGR Cooler effectiveness to an extent that the knock mitigation benefits of EGR are outweighed by the increased knock propensity due to higher intake temperatures. The mechanisms behind knock mitigation are primarily due to the dilution of the gases with a cool inert gas (21). Fischer (22) showed that an increased EGR outlet temperature significantly reduced the impact of EGR on BSFC and exhaust

temperature. Fischer et al (22) demonstrated an increase in EGR rate decreases BSFC at lower EGR Cooler outlet temperatures due to the MFB50 being advanced, which also allows for lower exhaust temperatures. Siokos (21) demonstrated the relationship between EGR and intake temperature with respect to knock. Increasing EGR rate reduces knock propensity until the intake temperature is high enough to induce knock. This was demonstrated by Fischer et al (22) who showed that with higher EGR Cooler outlet temperatures, an increase in EGR rate did not reduce BSFC with increasing EGR rate. Similar results being found by Bozic (23) who found that end-gas temperature was the primary cause of knock as similar peak end-gas temperatures had similar levels of knock, regardless of EGR rate. Szybist (24) (127) found that EGR ability to mitigate knock was diminished at high boosted loads. This is disadvantageous as knock is most likely to occur at high loads. Furthermore, EGR Cooler fouling is most prominent at high boosted loads because the high exhaust temperatures will lead to more thermophoresis. A combination of EGR knock mitigation effectiveness being reduced and high EGR Cooler fouling rates at high boosted loads, results in high EGR rates being likely to increase knock more than it can reduce it. However, EGR is still beneficial at high boosted loads even with little knock mitigation due to its ability to limit exhaust temperatures, protecting exhaust components and limiting the need for over-fuelling. Over fuelling is a method where excess fuel is injected into the engine, causing the temperature to drop as the fuel is evaporated, however this drastically reduces fuel efficiency (21). As smaller downsized engines with high boosted loads and hybrid vehicles become more important in reducing the impacts of global warming so too will the need to limit EGR Cooler fouling.

2.3.3.2 Low Load (Efficiency)

The benefits of EGR vary with speed and load. Knock is unlikely at low loads and increasing intake temperature at these conditions can be advantageous. This is often done through internal EGR with higher temperatures than external cooled EGR. This was studied by Siokos (21) who found that internal EGR increased efficiency at lower loads more than cooled external EGR, mainly due to reduced pumping losses. Similarly, Alger (128) conducted tests with HP uncooled EGR which performed more efficiently than cooled EGR at low loads. Higher intake temperatures can also increase the typically long combustion duration of high EGR rate engine operation, assist combustion stability and vaporisation of fuel (131).

2.3.3.3 Pressure Drop

EGR Cooler fouling also results in an increased pressure drop across the Cooler, which can have varying affects depending on the setup of the powertrain components, including engine (turbocharger and aftertreatment) and can especially impact lower load conditions. There are three common setups for EGR: LP, HP pre-intercooler and HP post-intercooler. LP takes exhaust gases post-turbine and recirculates it pre-compressor. Both HP setups take the exhaust pre-turbine and deliver it post-compressor with one delivering it before the intercooler and the other after.

The most common design in an HP loop is post intercooler to make use of the vacuum found downstream of the throttle, as pre-throttle designs often have an insufficient vacuum to induce EGR flow (particularly at low speed and high load) (131) (134). An alternative design involves re-introducing the EGR pre-intercooler and moving the

throttle upstream, but this reduces the control of the throttle over air flow and is not preferred (128) (131) (134). Throttling to induce EGR at high loads when it is not normally required will increase pumping losses and more throttling will be required with an increased pressure drop from fouling. At high loads, exhaust temperatures are high and a highly effective EGR Cooler is necessary to cool the EGR in post intercooler setups, whereas in pre intercooler setups the EGR outlet gas can be further cooled by the intercooler, making them less susceptible to EGR Cooler fouling. Therefore, pre-intercooler setups such as LP are favourable at higher loads where low intake manifold temperatures are critical in order to reduce knock. LP also requires no additional throttling at high loads. At low loads the pressure difference across the EGR loop is often higher with HP compared to LP due to the low pressures post throttle (128) (131) (134) making HP less sensitive to rises in pressure drop due to fouling. It is therefore beneficial to reduce fouling at all speeds and loads to allow for either setup to be used depending on the criteria of the engine design.

2.3.4 Summary

The above literature review has demonstrated the importance/ impacts of controlling intake manifold temperature and exhaust back pressure at both high and low load and with LP and HP external EGR configurations. The formation of deposits on the EGR Cooler (EGR cooler fouling) has a direct impact on both phenomena as it would increase intake manifold temperature and exhaust backpressure with demonstrated detrimental consequences on fuel economy, tailpipe emissions and engine malfunction. Therefore, this work aims to comprehensively investigate the reduction of EGR Cooler deposit

formation by using fuel additives and thus their impacts on fuel economy, emissions and EGR Cooler performance. The study has developed a new accelerated cycle with varying engine operation conditions (temperature, flow rates, exhaust composition) to understand the impact of fuel additives on injector deposits and its consequences on fuel flow rate (injection duration), particle and gaseous exhaust emissions as well as the effectiveness and *dP* of an EGR Cooler. The potential impacts of EGR Cooler fouling on engine performance are predicted considering the cooler effectiveness experimental results and by comparing this to literature. The impacts of EGR Cooler effectiveness on intake temperature for HP post intercooler, HP pre intercooler and LP loops were assessed. EGR cooler *dP* was compared to the pressure difference across the EGR loop for each setup.

2.4 Intake Valve Deposits

2.4.1 Overview

A further engine component that is susceptible to fuel deposits is the intake valve. This is primarily a problem with PFI systems, as the intake system is fully exposed to fuel spray. This is in contrast to GDI, where exposure is only partial (113). IVD can negatively impact engine performance and can cause engine valves to get stuck and cause engine malfunction in extremes (26). PFI engines have established advantages over GDI engines with regards to lower CO, HC and PM emissions, reduced frictional losses and reduced cost (referenced in 2.1.4.2). It is therefore of importance to investigate the deposits associated with PFI systems.

2.4.2 Formation Mechanisms/ Processes

The two most researched mechanisms for the formation of IVD are those created by fuel and oil. There are many factors that impact both mechanisms and this has led to different studies having variable results. Some studies claim that fuel parameters are the main reason for deposit creation (30) (31) (34), while others claim that oil has a much more significant impact than fuel (29) (135) with some evidence that engine oil cleans or prevents deposit buildup (136) (137). Research also acknowledges that fuel has a significant impact alongside engine oil (27) (28) (10). The possible reason for these contrasting views is that it is difficult to isolate all the variables found in an engine. Factors such as valve temperature, intake temperature, fuel boiling points, fuel composition plus additives, oil composition and additives, valve and intake geometry and engine speed and load can affect whether deposit formation is oil or fuel based. This review will now elaborate on this in more detail.

2.4.2.1 Fuel Based Deposits

Formation of fuel deposits in a PFI setup is primarily due to the injection of fuel directly onto the back of the valve or into the intake system upstream of the valve. This maintains the valve in near-constant contact with the fuel (27). Cheng (27) suggests that fuel derived deposits originate from heavy fuel fractions in liquid form which are condensed in the intake system. This liquid fuel forms on the valve tulip and the heat of the intake valve turns it into solid deposits. Another formation mechanism is suggested by Stępień (138) where the precursors to deposits are partially oxidised fuel in the gaseous phase. The formation process involves radical-initiated reactions producing

oxidation products that condense on hot surfaces. This is followed by pyrolysis or polymerisation.

Daneshgari (30) found similar results, whereby formation of deposits on the intake valve is caused by the high-boiling components of the gasoline, such as paraffin and polycyclic aromatic hydrocarbons, which could act as pre-cursors to deposit formation. The deposits were then formed via graphite crystal buildup through crystallisation, within a certain temperature range. Ramadhas (28) came to a similar conclusion, demonstrating deposition on intake valves is linked to higher temperatures, driving fuel vaporisation and oxidation of components.

Both Cheng and Daneshgari (27) (30) also found that fuel injection had the potential to wash away deposits. Daneshgari found that deposit formation started on the injector side of the valve and eventually formed on the opposite side, with the injector side having more deposits generally (30). Similarly, Esaki (29) also found that the injection could have a cleaning effect as they found that one third of the deposits were washed away on the intake side of the valve due to fuel dissolving the existing deposits which also prevented further deposits. This claim is also supported by Gail et al (10) who found a washing effect of the fuel, especially if they were comprised of heavy olefins. In addition to washing, the injection cooled one side of the valve by 80 ^{o}C compared to the shadow side, and as will be discussed later the valve temperature plays a significant role in deposit formation.

2.4.2.2 Oil Based Deposits

Oil can find its way onto the intake valve in several ways, for example via the valve stem guide (28) and crankcase blowby fumes (137). Oil was found to both generate and clean deposits in a similar fashion to its fuel-based counterpart. Following their preliminary results with fuel-derived deposits, Cheng (27) doped the fuel in their engine with 0.25-2 % engine oil to assess its impact. They found some oils generated significant thick deposits and others either cleaned the fuel deposits or had negligible impact. Cheng and Bitting (27) (31) suggest that oil and fuel derived deposits look visibly different. Bitting reports fuel deposits look like a “cauliflower” and are dry and “flakey”, with a larger impact on engine drivability. Conversely, Cheng suggests that fuel derived deposits are thin and porous whereas oil deposits are thick, wet and “oily”. However, after conducting further research Cheng suggests that fuel derived deposits can also often appear “oily” as well and concludes that the two deposits cannot be differentiated purely by looks and that the morphology is more dependent on valve temperature.

Esaki et al (29) proposed a mechanism for the formation of oil derived IVD. The process consists of three stages: initial, growing and final. The initial stage occurs when there are no deposits at low temperatures. The larger components of oil and fuel drain off the surface of the valve, leaving smaller components which become viscous due to thermal or oxidised reactions causing adherence. Subsequently, the growing stage starts after the agglutination, where the deposits continuously accumulate on the valve. At this stage, the rates of oxidative reactions, such as dehydrogenation, partial oxidation, and hydroxylation, competitively increase with increasing valve temperature in the outer portion of deposits. The oxygen concentration then drops around the partially oxidised

products, causing carbonisation to occur in the inner regions of the deposits. This inner region sees an increase in pre-carbonised products coming from parent materials. In the final stage, the deposits become amorphous and carbonaceous aggregates. The amount of deposits changes with repeating cycles of growth and breakaway. Injected fuel was found to either dissolve or suppress the oil deposits throughout these stages, with Esaki reporting only a few heavy fractions of fuel among the deposits. They did not find much evidence supporting a direct contribution of the fuel to the formation of deposits. However, they demonstrated dissolution of fuel into engine oil increased deposits.

2.4.3 Parameters Impacting Intake Valve Deposition

2.4.3.1 Temperature

Cheng (27) suggested the main parameter that impacts either oil or fuel having the dominant effect on deposition is the boiling range of these substances. This theory is supported by Daneshagari (30) who suggests the relationship between the boiling point of a fuel and operating temperature of the valve is the determining factor in the formation of fuel deposits. Daneshagari (30) suggested that two temperatures relating to the fuels boiling point are of significance. These are the Nukiyama temperature and the Leidenfrost temperature. The Nukiyama temperature is above the boiling temperature, where many bubbles form within the fuel, significantly increasing the evaporation rate of the fluid up to a point when the fluid has a minimum contact time on the surface. The fuel droplets start to become spherical at a higher temperature (Leidenfrost), thereby reducing heat transfer to the droplet and increasing the amount of time the fuel remains on the valve. Daneshagari (30) reported that the

aforementioned temperature points were below the operating window of most intake valves, provided high boiling fractions of a fuel were removed. This suggests that there is a critical temperature where the formation of IVD will be influenced predominantly by fuel composition, a finding that was corroborated by Cheng (27) and Repsol (35).

Valve temperature seems to be one of the most important parameters impacting intake valve deposition. Cheng, Daneshgari, Repsol and Nomura (27) (30) (35) (139) found that IVD peaked at temperatures between 200-250 ^{o}C and Repsol (35) also found that the deposited mass was negligible at temperatures below 70 ^{o}C and above 300 ^{o}C. This is due to the Nukiyama and Leidenfrost temperatures described above and because at low temperatures no boiling occurs. As temperature is increased rapid evaporation around the Nukiyama temperature results in many deposits, then as the temperature is further increased to the Leidenfrost temperature the evaporation rate decreases and consequently so does the deposition rate. Then after this temperature the deposits become hard and brittle, negatively impacting the consolidation of the deposits (30) (27). Stępień (138) also suggests that above a certain temperature deposits levels reduce because of the lack of condensation of precursors.

2.4.3.2 Fuel Characteristics

The composition of fuels and their additives play a key role in intake valve deposition. As mentioned in section 2.4.3.1 the boiling point of the fuel is a critical parameter with regards to what temperature deposition occurs at and is probably responsible for why researchers testing at similar valve temperatures find very different results regarding the morphology and chemical composition of the deposits. The addition of certain

hydrocarbon chains can have an impact on deposition, likely due to changing boiling points and consequent change to the Nukiyama and Leidenfrost temperatures (30). Gail et al (10) found that adding olefins from C6-C12 had no significant effect but adding C-16 olefins with a high boiling point contributed to washing the fuel. This is similar to what Daneshgari (30) found when using a fuel with significant amounts of high boiling point substances added to it. Ansomboon (140) found that higher olefin content led to an increased tendency to form deposits, as when olefin content in gasoline increased from 5 to 10 %, deposits increased by 30.6 %.

Gail (10) also found that aromatics impacted deposits. Increasing the number of aromatic rings increased the mass of the deposits but by a small amount. However, heavy aromatics such as triphenylmethane increased the deposit mass more significantly. This was attributed to aromatics with three or more rings and heavy aromatics with a boiling point over 340 ^{o}C remaining on the valve surface.

Alcoholic content has also been found to impact IVD. Chapman (32) found that E85 (85 % Ethanol, 15 % Gasoline) market fuels generated over double the IVD of a baseline gasoline fuel, whereas E10 generated less than half. Bennett (141) also reported that baseline ethanol fuels generated more IVD than baseline gasoline by a significant amount. Bitting (31) found that 10 % ethanol generated four times as many deposits as a base fuel with no additives. Other alcohols have also been reported to increase IVD with Bitting (31) reporting that IVD increased by 6 % with a 3 % methanol blend and that a 10 % oxinol fuel generated 2.5 times more deposits than the base fuel with no additives.

2.4.3.3 Engine Operation Conditions

Engine conditions also play a critical role in the generation of IVD. Cheng (27) found that intake temperature showed a significant negative correlation with IVD. Fuel was observed to have completely vaporised in the intake manifold at temperatures above 110 ^{o}C, corresponding to a reduction in deposit mass to negligible amounts. This was attributed to high intake temperature vaporising all the fuel and leaving behind no liquid fuel to form deposits. Cheng also demonstrated a similar relationship between coolant temperature and deposit formation to that found with valve temperature, but this is largely attributed to the direct impact that coolant temperature has on valve temperature. This was also the case with spark timing where Cheng (27) found that changing the spark timing in isolation also showed the exact same trend as changing valve temperature and this was also attributed to spark timings direct correlation with valve temperature. Cheng also found that engine load had a similar effect on valve temperature and hence deposits. They found that medium load conditions generated the most deposits as at low load the valve temperature was too low and at high loads even though there was more fuel available to generate deposits the valve temperature was above the critical temperature and this had a dominating effect, thus deposits were low. Gail (10) also found that low-medium loads generated the most deposits, especially with respect to deposits made per unit of fuel consumed. They demonstrated cyclic loads with periods of acceleration and idling increased deposit formation. Air-fuel ratio was also found to impact valve deposition as Cheng (27) found that rich air-fuel ratios generated the most deposits, despite the cooling effect of fuel. This can be explained by the abundance of fuel available for deposit generation, but this effect would depend on

the valve temperature. Another factor that influences valve temperature is pre-existing deposits. Grant and Mason (34) found that valves with existing deposits had temperatures that were 2-5 ^{o}C higher than that of the clean valves, which would affect the production of further deposits.

2.4.3.4 Other Parameters

Other investigated parameters included valve timing, coatings, valve rotation and EGR. Valve and injection timing can have an impact on how the fuel is atomised and the amount of fuel that impinges on the inlet valve. Depending on the timing of the injection with respect to valve timing the fuel may evaporate, puddle or rebound (142) and the atomisation and impingement on the valve can significantly impact valve deposition. Bitting (31) found that valve coating delayed initial build-up of deposits although overall deposition was unchanged. Cheng (27) concluded that valve material had minimal effect as formation processes were more physical as opposed to chemical. Similarly, valve rotation was found to have little effect on the overall deposited mass but did allow for a more even distribution of the deposits. Therefore, flow over the valve was less disrupted and the additives had a larger surface area of deposit to impinge upon thus helping with cleaning (27). The effect of EGR on IVD formation was also investigated by Cheng (27) but was found to have minimal effect.

2.4.4 Impact of Intake Valve Deposits on Engine Performance and Emissions

2.4.4.1 Drivability

IVD can have an adverse effect on engine performance. They have been proven to reduce fuel economy, power and driveability while increasing CO emissions (9). The impact of IVD on efficiency and CO emissions was initially reported by European markets but later became a problem for their American and Japanese counterparts (27). This was a well-known problem at the time especially when carburettors were used but the problem still persisted with PFI as they are more closely controlled in terms of fuel management and are therefore sensitive to changes in air-fuel ratio (27). The problems created by IVD are especially prevalent during cold start conditions (34). Bitting (31) found that IVD mass was directly related to warm-up drivability concerns. This was primarily attributed to porous “sponge” like deposits that absorb fuel which results in a leaner mixture than expected in the combustion chamber. This is especially problematic in fast/lean burn engines or engines with a narrow control window for combustion (9). Daneshgari, Costa and Cheng (143) (144) (27) corroborated these findings. The problem was exacerbated in transient conditions (145) and is a current phenomenon demonstrated by Costa (144) who proved that the IVD are capable of absorbing as much n-heptane and isooctane as is delivered into the combustion chamber per cycle, which demonstrated the sponge-like properties of the deposits having a significant impact on fuel absorption. Arters (146) tested the drivability index of engines with and without IVD and found the presence of IVD increased the frequency of misfire/partial burn cycles

and lower IMEP during acceleration periods. This would be felt by the driver as stumble, hesitation and lack of power. These characteristics were also reported by Gething (147).

2.4.4.2 Engine Power

The fuel absorption problem with IVD does not manifest when the engine is warm, however other issues persist (31) (27). Tupa and Koehler (9) reported that there are generally two types of deposits that impact drivability. One type are low deposit volumes that are uniformly spread over the intake valve tulip area and tend to create drivability problems after 12,000-38,000 km of driving. This type causes the sponging effect discussed in section 2.4.4.1 and is only a problem during cold start. In contrast, heavy and thick deposit types create large enough structures to physically disrupt air flow over the valve. Consequently, power is restricted at high loads and fuel economy, combustion behaviours and emissions are impacted at low loads. Tupa reported that a simulation in Japan using two machined valves representing valves with 30,000 km and 50,000 km worth of deposits resulted in a power decrease of 5-25 %. This experiment was repeated more recently and showed a full load power loss of 4 % and 1.9 % at part load (145). Taniguchi (148) also reported power loss of 5-10 % depending on the type of valve (with clean valves having lower losses compared to dirty ones), with power losses of 25-35 % for extremely dirty valves. This demonstrates a very considerable impact of IVD on performance.

2.4.4.3 Efficiency and Emissions

In addition to power losses, efficiency and emissions can also be impacted by IVD. Evidence shows deposits increase NO_X emissions (149). Taniguchi (148) demonstrated dirty valves produced around double the NO_X emissions of clean valves across a range of spark timings, with a maximum reported increase of around 1000 ppm. Tupa (9) reported that during engine idle, CO emissions increased by 5-20 % after 10,000 km of driving and then were further increased by 10-35 % after 50,000 km of driving (these distances represented 0 % and 50 % intake port restriction due to deposits respectively). Tupa also reported that fuel economy dropped from 1-2 % to 5-7 % at the same distances. Glawar (145) found that the deposits increased combustion duration by 3 CAD, thereby decreasing fuel economy. Price (150) also found a statistically significant increase of fuel consumption by 1 % ($p < 0.05$) A study by Merola (142) observed soot emissions reduced when less fuel deposits were on the intake valve as the lower amount of deposited fuel induced the formation of less intense diffusive flames that are sources of soot particles. Engines that are designed to rely on precise delivery of air (e.g. high swirl and lean burn) were also found to be significantly disrupted by IVD. This is because air swirl into the cylinders can be greatly disrupted by deposits, degrading vehicle drivability (147). This is corroborated by Taniguchi (148) who found that heavy IVD could drop peak power by 34 % in high swirl engines. The swirl ratio was found to decrease by 44 %, which could lead to greater cycle-cycle variations and further drivability problems, as well as causing the rate of combustion to retard.

2.5 Deposit Control Additives

2.5.1 Mechanisms

Maintaining low deposit levels in engines is crucial for optimal performance and using DCA is an effective method to accomplish the above (151). DDA are a common type of DCA used for cleaning injectors, intake valves and other engine components. They are dissolved in fuel using a nonpolar hydrophobic group and bind to deposit particles with a polar hydrophilic group (152) (12). Certain DDA have the polar group joined to the hydrocarbon chain directly, whereas other DDA have the polar group joined through a molecule such as polyisobutylene-succinimide. The polar group adheres to deposits and uses detergent action to remove deposits from metal surfaces (152). DDA can provide a protective coating to stop deposition on metal surfaces (153) (12). To guarantee DDA fuel solubility and aid in clearing deposit particles, a carrier oil is usually employed in conjunction with them (152). They work in two modes: keep-clean (prevent deposits) and clean-up (remove existing deposits). DDA can be utilised at different doses depending on the needed function and are frequently found in multifunctional additive packages (12).

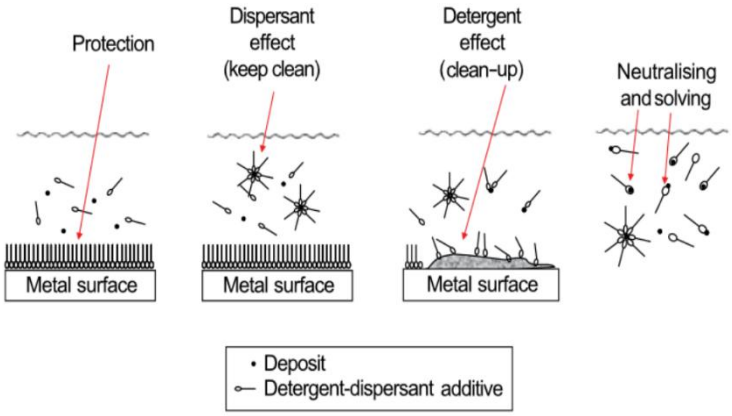


Figure 2-3: Mechanism of DDA (152).

2.5.2 Types of Additives

Cheng (27) observed that a polyether-amine addition reduced deposits by 10 %. According to Ansomboon et al (140), the most successful DDA resulted in a considerable reduction in deposits, from 176.9 mg with baseline fuel to 13.9 mg. Daneshagari (143) demonstrated additives and paraffins could impede or prevent the formation of deposits. Dispersants for gasoline detergents are frequently made of polyolefin amines, particularly polyisobutylene amines (PIBA) (152). 200 ppm of PIB (polyisobutylene) in gasoline maintained intake valve cleanliness in an Opel Kadett engine during a standard CEC (Coordinating European Council) F-05-A-93 test, while 30-150 ppm of poly-1-butene oxide as a carrier fluid and 0.1 % PIB were found to be beneficial in the CEC F-16-T-96 process (154). Combining polyolefin amines with polyetheramines (PEA) has been shown to prevent CCD, making them an effective DDA (155). DDA based on PIB-succinamide, PIB-amine, polyisobutene-amino alcohol, and PEA can prevent and eradicate IVD in both keep-clean and clean-up modes due to their exceptional heat stability in high-temperature zones (152). In gasoline engines, a mixture of a succinimide

detergent, a fluidiser (PEA, polyether, or a combination), and a Mannich detergent is a highly successful way to reduce IVD (156).

2.5.3 DCA in GDI Engines

DCA can prevent injector deposit buildup in GDI engines, but they have to withstand the temperature regime which varies from 60-150 ^{o}C at the fuel injector (157). Zhang et al (33) conducted a 55 hr test comparing additivated fuel with regular fuels. They found that additivated fuels performed better at maintaining fuel flow rate through injectors. PEA are a standard DDA for both PFI and GDI (151). Their high efficacy has kept them in use despite being older (Generation IV). PEA contain primary amino groups attached to the end of a polyether backbone (152). Additives for GDI engines use poly butene amines and PEA with a narrow molecular mass distribution and synthetic oils as carrier fluids, effective up to 400 ^{o}C (157). Combining aromatic esters of polyalkyl-phenoxyalkanols with PEA provides a fuel additive that controls engine deposits and is correlated with the octane requirement increase (ORI) (158). The latest generations of Mannich bases (Generation V and VI) are capable of preventing deposit formation and removing existing deposits in combustion chambers (151). These additives have demonstrated effectiveness in preventing fouling at injector tips (159) (151). Tests comparing Mannich bases and commercial PIBA and PEA based additives in a GDI engine revealed that Mannich bases performed six to seven times better than commercial additives (151). In another test, the best PEA additive reduced flow by 8 %, while the best Mannich base reduced it by 3 %, with the worst Mannich base achieving 5.7 % reduction (151). Conversely, China et al. (39) reported superiority of PIBA in a study comparing them to

Mannich bases and PEA. Detergents have been found to increase deposits in some situations, making it important to use the correct dosage, typically between 400 and 1000 ppm (12).

2.5.4 Impact on Exhaust

DDA account for approximately 40–50 % of the additive market, emphasising the importance of studying their effects on emissions (153). While detergent additives do not directly impact exhaust gas emissions, they reduce deposits that negatively impact engine performance. As mentioned previously deposits can increase many engine out emissions, therefore reducing these deposits with DCA is critical. Zhang (33) concluded that DDA are beneficial for reducing NO_X emissions and can significantly impact PM reduction. PM emissions from deposits are a particular concern in GDI engines and DCA have been proven to reduce them (16). Henkel (16) also found that DCA could successfully clean dirty injectors, reducing PM emissions to pre-fouling conditions. This is especially important in the modern day with legislative bodies imposing ever stricter environmental standards regarding PM to protect the health of their citizens (13).

As discussed in section 2.2.4, fouled injectors lead to increased soot emissions, creating a negative feedback loop where the higher soot levels create further injector deposits, which subsequently increases EGR Cooler fouling (160). This demonstrates how the two types of fouling are linked and this study aims to investigate the two phenomena together. Fuel additives have been shown to prevent this negative feedback loop and thus reduce EGR Cooler deposits (12). EGR Cooler deposits reduce the thermal conductivity of the Cooler walls and constrict the pipe diameters leading to reduction of

Cooler effectiveness and increased exhaust back pressure, leading to friction loss and increased *dP* (161). This may ultimately lead to engine failure (162). The direct relationship between DCA and EGR Cooler Fouling have not been studied in the same test in literature before and this study aims to fill this research gap.

2.5.5 DCA in PFI Engines

Studies on IVD and PFI deposits and their effect on emissions have been inconclusive. Research indicates that reducing IVD with fuel detergents can lower HC and CO emissions compared to untreated fuel. However, there have been observations of a negative effect on CO and NO_X emissions, likely due to increased CCD (152). A U.S. study reported increased engine knock with more DDA (163). A Venezuelan study (164) found that DDA significantly reduced CO (6-10 %) and HC (13-24 %) emissions in test trucks, although NO_X emissions increased by 2-3 % and fuel economy improved by 0.5-1 % (28). An evaluation by the European Commission, ACEA, and EUROPIA estimated that using detergents could reduce CO emissions by 10-12 %, HC by 3-15 %, NO_X by 5 to -5 %, and improve fuel economy by 2-4 % (165).

Repsol (35) successfully employed DCA to decrease IVD to minimal levels; nevertheless, some deposits were caused by mild instability at higher temperatures, indicating that dose and valve temperature are important factors in efficacy. Deposit levels rose with valve temperature in additivated fuels but dropped in non-additivated fuels, according to Grant and Mason (34). Additionally, they observed that certain additives were more or less successful at decreasing deposits depending on their composition. According to

Bitting et al (31), while certain commercial additives increased IVD, the proper dosage of additions decreased deposits in fuels containing alcohol and additives.

2.5.6 Impact of Alcoholic Fuels on DCA Composition

Modern fuels often contain a percentage of ethanol which significantly alters its polarity and solubility, complicating the dissolution of gasoline's conventional detergent-emulsifying additives and leading to deposit formation. There is evidence demonstrating increased deposit formation attributed to ethanol-containing fuels with standard additives compared to their non-ethanol counterparts (166). Similar issues were noted by Brennan and Yeakey (167). As a result, Engines fuelled with ethanol blends require specially formulated detergent additives with different chemical structures that are soluble in ethanol-gasoline mixtures of any ratio (152).

2.5.7 Summary

DDA usage provides several significant advantages (152). These additives help maintain a clean fuel supply system, ensuring that fuel flows smoothly and without obstruction. This cleanliness promotes uniform fuel injection, which is crucial for optimal engine performance. Additionally, DDA enhance combustion efficiency, leading to a more complete burn of the fuel, which improves engine performance and reduces noise and vibrations. As a result, the overall driving experience is smoother, with better engine responsiveness and power. Furthermore, the use of DDA can lead to lower fuel consumption and reduced maintenance costs, as the engine remains cleaner and more efficient. Finally, these additives contribute to a decrease in harmful exhaust emissions,

making the vehicle more environmentally friendly. By understanding and effectively utilising these additives, the performance and longevity of engines can be significantly enhanced, along with reduced environmental impact through lower emissions.

2.6 Accelerated Fouling Test Methods

2.6.1 Overview

Fouling on all the components mentioned so far builds up slowly over the lifetime of an ICE. Thus, it is necessary to create an accelerated test procedure that can replicate years of deposit build up in a short time in order to test the effectiveness of fuels and the impact of varying engine conditions on deposit formation. This helps fuel and engine manufacturers to rapidly develop products that can reduce the formation of deposits. It also allows researchers to understand the deposition process as well as additive function in less time and at lower cost.

Several methods have been reported in literature for various types of engine deposits. These methods vary depending on the variable investigated. A few methods use full scale engine tests and others use benchtop experimental rigs to simulate engine conditions.

2.6.2 Injector Fouling

Accelerated injector fouling tests generally vary fuel and additive properties as well as physical parameters to observe their effect on deposit formation. Some standardised tests have been developed, such as the CEC F-98-08 DW10 cycle for diesel injectors (168)

(169) (170) (171). There is no standardised test to quantify GDI deposits from the American ASTM or European CEC. All gasoline related fouling tests only analyse PFI engines (172). The CEC has been working on developing a method since 2016 and Volkswagen have developed an inhouse procedure (172) (36). This is similar to the DW10 test, which consists of “keep clean” test, followed by a “dirty up” test and concluded with a “clean up” test. The “keep clean” tests assess how a fuel can prevent deposit build up, while the “clean up” test uses a fuel on injectors that have previously been fouled via a “dirty up” test to investigate how effective they are at cleaning.

The types of tests described in literature vary in specific aspects. Some tests use engines controlled by dynamometers (39) (33), while others let the engine run free to save on operating costs (96). A few tests also use whole vehicles (173). Time taken to run the tests also varies, with some short tests lasting less than a day (39) and some taking multiple days (33). The “keep clean” test by the CEC lasts 48 hr (36) with the aim of assessing if fuels can keep the injector pulse width from increasing above 5 % of its original value (11). The CEC expects a fuel to maintain an injection pulse width increase below 25 % during a 48 hr “dirty up” test and a 90 % injector pulse width recovery is expected after a 24 hr “clean up” (36) (11).

The results from accelerated fouling methods vary greatly, impacting the ability of the difference between a reference fuel and an additivated fuel to be assessed easily. Some short tests produce significant deposits, while others lasting days observe minimal change. For example China et al (39) observed that a reference fuel resulted in a 20 % loss in injector flowrate and the additive reduced this to a 2 % increase over the test.

Conversely, Zhang (33) only saw an average fuel flow rate loss of 2.3 % and 1.8 % for a reference fuel and additive respectively. Evidence proves that adequate methodology is superior to duration of a test where quantity of deposits is concerned.

It is important to find the correct engine speed, load and an effective cycle to operate the test. Some studies run at constant load for the entire test (e.g. standard CEC GDI tests, Zhang (33), Henkel (16) and Joedicke (174)) and some run cyclic tests (such as China and Rivere (39)). The standard Diesel DW10 cycle starts at 20 % load for 2 min, then ramps up to 60 % load in steady state for 7 min. This is followed by a sharp drop to 20 % load. This cycle repeats itself, increasing to 80 % load and the next cycle is at 100 % load. The 100 % load condition is repeated 4 times as the whole sequence repeats itself. The CEC GDI test runs at steady state of 2000 rpm / 56 Nm for a “keep clean” test and the “Dirty up” and “Clean up” cycles work similarly to the DW10 cycle. Afton chemical used the CEC cycle and saw varying results with reference fuels from 5-50 % increase in injection time over 48 hr (36). China and Rivere (39) repeated a 6 min cycle 160 times to generate significant results. The cycle started with 30 s at idle followed by a 15 s ramp up to 5000 rpm / 2.5 bar BMEP where the engine stayed for 300 s, then the cycle ramped back down to idle to repeat the cycle. China and Rivere (39) chose a high-speed low load condition as they had found from previous tests that this achieved a high injector tip temperature. Badawy (175) also used a transient cycle sweeping from idle to 8 bar IMEP at 2000 rpm over 54 hr. They observed an average flow rate difference between clean and coked injectors of 5.6 %, significantly less than other transient cycles such as that done by China and Rivere (39). Henkel (16) ran their test at multiple steady state conditions, starting at 2000 rpm / 2 bar BMEP for 30 min then moving to 2500 rpm

/ 6bar BMEP for 4 hr, before reverting to 2000 rpm / 2 bar for 30 min. This was followed by a clean-up test. Henkel (16) reported significant changes in emissions and combustion which was attributed to deposits. Joedicke (174) managed to achieve a 23.5 % reduction in injector flow rate after a 55 hr steady state test at 2000 rpm 5 bar, significantly more deposits than Zhang (33) who also used a steady state test for a similar time. A similar 30 hr steady state test at 2000 rpm/ 5 bar with the addition of a cold start was performed by Jiang (14) however they only saw a 2 % change in injector pulse width, a considerable contrast to the 23.5 % reduction in flowrate by Joedicke (174). Another factor that can assist deposit formation is a hot soak at the end of the test to allow the deposits to stabilise (171).

The varying results throughout the above mentioned studies can be attributed to varying engine injector strategy or design and air motion and differing fuel compositions among other differences. It is therefore important to understand the engine that is being used in order to make an adequate accelerated fouling cycle. Brinklow et al (171) aimed to do this by mapping their engine prior to running the fouling tests. The parameters of interest were the fuel return temperature, EGR rate, injection timing, duration and pressure. As discussed in section 2.2.3, these parameters all have an impact on the formation of injector deposits. High fuel return temperatures were targeted as they correlate to high fuel temperatures and high EGR rate was expected to make high in-cylinder PM emissions. Two operating points were identified. One was a high-power point to increase injector temperature, which was followed by a low power point with low injection pressure and fuel flow rate to let the deposits stabilise. The effect of the total test duration was studied. It was reported that an 8 hr cycle alternating between

high and low load every 15 min, followed by a 4 hr soak, could generate deposits that restricted injector flow by 11 %, a greater value than when they ran the 44 hr DW10 cycle on their engine. The cycle was repeated up to 4 times, but the injector flow rate loss plateaued after the first 2 cycles.

The speed and load of the proposed high power operating point was investigated. It was found that increased speed had more of an impact on deposit formation than load. This was theorised to be due to higher loads having increased fuel pressure for only a small increase in injector tip temperature, and higher speeds leading to more injections per second. The high pressure of these injections can induce a shear force on the injector wall, sharply increasing temperature. This was also observed in a study by Kinoshita (109) who found that when maintaining load, an increase in speed would generally increase injector nozzle temperature.

The time spent at each operating point was also proved to have an impact. It was concluded that more deposits were generated by spending less time at the high power point. This is possibly due to less time being spent at operating points where the high fuel pressure and fuel flow rate can wash away the deposits. A longer time at lower injection pressure could allow more time for deposits formed during the high injector temperature phase to solidify.

The frequency at which the engine cycled between the two phases was also important. It was found that higher frequencies resulted in more deposits. This is because the injector is still hot from the high power setpoint, but the pressure and flowrate are low enough to not wash away deposits at the transition point from high to low power. This

may help to explain how China and Rivere (39) achieved high deposits in a short test, as they cycled between loads every 6 min. The addition of a high-speed idle test proved useful as it increased injector flow loss by 109 %, due to the poor quality of combustion promoting the production of soot.

An injector flow loss of 11 % was observed with a baseline fuel following a 20 hr test utilising the above conditions. Two additives were used showing flow losses of 8.72 % and 7.27 %. This is a significant difference and demonstrates the value of research into optimised shorter test cycles, improving the cost-effectiveness of additive testing for manufacturers.

The study by Brinklow (171) is one of few studies that explains in detail how an accelerated injector deposit formation cycle was created and this study aims to build on this knowledge. In addition to this a novel concept in this study is not to purely assess the different parameters that can impact the rate at which injector deposit growth can be accelerated but also to outline an approach that will assist with finding these parameters as quickly as possible. This study will detail the steps taken with different trials to aid future researchers to use the same techniques or improve upon them.

The level of control of the engines parameters also impacts how effectively an accelerated fouling method can be created. For example China and Rivere (39) had control of the lambda control loop, blow by, EGR, intake temperature, coolant temperature, fuel temperature and fuel pressure. Some of these variables were found to have a significant impact on deposit formation (such as fuel temperature), while

others had negligible effect (such as EGR, blowby and intake temperature). Strict control of these parameters improves reliability and replicability of the experimental design.

The injector cleaning process is also important and varied from study to study. Some studies used the same injectors that were cleaned between different tests (39),while others used new injectors in every test (33). Most studies used ultrasonic cleaning methods with a cleaning fluid for the injectors (39) (36) (33).

The type of fuel being used also makes a difference This is likely due to the relationship between T90 and the injector temperature previously mentioned. Some tests such as the DW10 use additives like zinc to purposefully increase deposit formation (171). Different engines also have distinct maps and hence different injection strategies which will cause great variation between engines at the same speed and load.

2.6.3 EGR Fouling

Accelerated fouling methods are also used to generate deposits in EGR systems. As the EGR Cooler is not within the combustion chamber there are less parameters impacting it. As mentioned in section: 2.3.2 the main parameters that impact EGR Cooler fouling are exhaust temperature, flow velocity and particle concentration. These factors generally have less trade-offs with each other compared to those that impact injector deposits. For example, a hot injector tip might be needed to create deposits, so high speeds and loads might be suitable in this sense, however this will also impact the fuel pressure, injection timing, lambda and so on, making it difficult to obtain the optimum condition for fouling. In contrast, generating exhaust conditions with high

concentrations of soot, low flow velocity and high temperature are factors that can be more easily controlled with EGR fouling and do not necessarily conflict with each other.

As the EGR is outside the engine it is easier to make custom setups, such as that done by Abarham (176) who artificially heated the walls of the Cooler to observe the impact of temperature gradient on deposition. The Cooler was specially designed out of Pyrex to allow for observation of the process. Storey et al (37) used a custom surrogate tube instead of a full size EGR Cooler as they could achieve better control of the conditions. A similar approach was taken by Lance et al (177).

Most studies use the engine as a deposit generator when researching EGR Cooler fouling (176) (37). The Cooler is not often used in a functioning EGR system as this can add variability to the process. This is because EGR Cooler fouling can affect engine properties, thereby impacting exhaust composition, temperature, and flowrate, all of which perpetuate Cooler fouling. Therefore, it is recommended to extract exhaust gases circulating in the cooler away from the engine.

2.6.4 Intake Valve Fouling

The accelerated methods for testing IVD also vary greatly between different studies. There are standardised tests ran by the American ASTM and the European CEC. The CEC methods include CEC-F-05-93 performed in an OHC 4-cylinder engine, where the engine runs through a 60 hr low load test profile on an engine test stand. The intake valve weight is measured along with a rating of the IVD and photos. The CEC-F-16-96 test is conducted on a 1.9 l water cooled boxer otto engine type 2 series. A drive cycle is used

with a cool down and soak phase along with a compression test. The sticking tendency of the intake valve is studied at low temperature during the compression test. The CEC-F-20-98 is performed on a 2 l 4-cylinder engine with 4 valves per cylinder. A 60 hr low load test profile is used on an engine stand. The studied outcomes are intake valve mass, CCD mass and piston top deposit mass (36). The deposits are expected to be kept below a certain mass when using an additivated fuel. Typical IVD mass for base and additivated fuels are shown in Table 2-1.

Table 2-1: Summary of standard valve deposition tests (138).

Test	Engine	Test description	Typical Deposits	
			Base fuel	Additivated fuel
CEC F-05-93	MB M102E 2.3 dm³	60 hr dyno	200-500 [mg/valve]	≤ 30 [mg/valve]
CEC F-20-98	MB M111 2.0 dm³	60 hr dyno	300-800 [mg/cyl]	≤ 50 [mg/valve]
ASTM D 5500	BMW 318i 1.8 dm³	16 000 km vehicle	290 [mg/valve]	≤ 100 ≤ 50 [mg/valve]
ASTM D 6201	FORD 2.3 dm³	100 hr dyno	300-1000 [mg/cyl]	≤ 50 [mg/cyl]
ASTM D 5598	Chrysler PFI 2.2 dm³ Turbo	16 000 km vehicle	20-40 [% flow loss]	≤ 5 [% flow loss]
ASTM D 6421	Chrysler PFI 2.2 dm³ Turbo	44 hr dyno	25-50 [% flow loss]	≤ 10 [% flow loss]

Different approaches have been taken in other studies to generate IVD, with variable control of parameters. For example Cheng (27) had good control of many engine parameters such as coolant temperature, spark timing and intake temperature. Cheng (27) used a single cylinder engine with two injectors in the intake system. They used a fuel trap to filter liquid fuel in the intake manifold, which led to no deposit formation.

Conversely, significant amounts of deposit were formed when the fuel trap was removed. Having this level of control in the setup helped to characterise the impact of liquid fuel. They also had control over oil leakage, by collecting any potential oil leaks from the valve stem seal in an oil cup placed on the stem. This additional level of control allowed confirmation that all deposits were fuel derived. Cheng successfully generated 103 mg of fuel derived IVD in 180 hr, with sufficient deposits after 2 hr to repeatably observe the impacts of different fuels on deposits formation.

The methods used to measure deposits varied between testing strategies. Repsol (35) measured the weight of a small metal bushing placed close to the valve in the intake port before and after the test. The instrument had thermocouples in it allowing for the temperature to be recorded. This saved time as the engine did not need to be disassembled to remove the valves after every test for weight measurement. Cheng (27) used a custom built intake valve that had four pieces of metal laying on a machined part of the valve tulip. They covered a quarter of the valve each and could be removed independently to assess how deposit formation varied around the valve. Each quarter piece also had its own thermocouple to record exposure to fuel injection and airflow and how this impacted temperature.

Other examples of experiments conducted on engine test rigs can be found here (29) (28) (31) (10). Bitting (31) found that different cycles were needed for different engines to represent results seen in the field when conducting engine dynamometer tests. They reported that a 60 hr transient acceleration/ deceleration cycle was more representative of real-world results than a test that moved between various steady state conditions

every 5 min. They also found that a different test consisting of a cycle with a 2 min idle followed by various accelerations and decelerations helped to attain more realistic results in larger engine sizes. Gail (10) used low and high load cyclic cycles alongside a low load steady state cycle and the standard CEC cycle. They found that that the constant speed low load cycle generated the most deposits in 100 hr, but the cyclic low load cycle generated the most deposits per unit of fuel consumed. It is important to consider the amount of fuel consumed as IVD tests can be between 50 and 100 hr long and multiple tests may be needed to quantify the impact of fuel additives. Maintaining low fuel consumption while maximising deposit formation is essential to ensure the testing process (and fuel development by extension) is cost-effective.

Physical simulations performed on experimental rigs can be utilised to further enhance cost-effectiveness. Lacey et al (38) created a bench top laboratory test that could generate IVD in a short period of time. This was done by constructing a physical simulation of the intake manifold with a fuel injector, intake runner and valve. The valve stem was hollowed out so a small electrical heating element could be inserted, allowing for precise control of valve temperature. This is a key advantage in comparison to using regular engines, as the temperature can be isolated and controlled without impacting related parameters. Air is passed through the constructed intake manifold and valve via a pre-heated compressed air tank. The results from the apparatus were found to correlate well with standard BMW and Ford IVD tests. The test also only lasted 20 hr, thus time was saved in the test duration compared to the standard 60 hr cycles, and money was saved by negating the need for a full engine and dynamometer setup.

Daneshgari (30) used an even simpler simulator, where they passed fuel over a heated aluminium bar. The bar was heated so that one end was 400 ^{o}C and the other was 120 ^{o}C, representing the temperature range of intake valves. The bar was tilted so that fuel drops could slide from the hot to the cold end. This allowed them to investigate the impact of temperature and boiling points on intake valve deposition. The simulator was subsequently used to identify which temperatures were most likely to create IVD, which helped develop a test cycle to create IVD in an actual engine.

The current study aims to build upon the methodology of physical simulations found in literature. The results from the above studies show that simple experimental rigs can replicate the results seen in real engines, mainly with respect to valve temperature. However, valve temperature is impacted by several factors such as valve speed, air and fuel mass flow rates and coolant temperature among others. The novelty of this work is the design of a rig that allows for the physical simulation of all these variables to understand their impact on fuel derived intake valve deposits in a real engine cylinder head. The experimental rig built in the current study aims to allow the user to investigate these variables and determine which variables are truly necessary to allow a simulation to accurately replicate a real engine.

3. METHODOLOGY

This chapter outlines the methodologies employed in the experimental research, including the set-up of the engine test cell, engine type and characteristics, instrumentation, control and emissions analysis for both the GDI Injector Deposits and EGR Cooler Fouling Chapters. The proof of concept test plan for the Intake Valve Deposit Experimental Rig is also described here.

3.1 Engine Setup and Facilities.

3.1.1 Engine

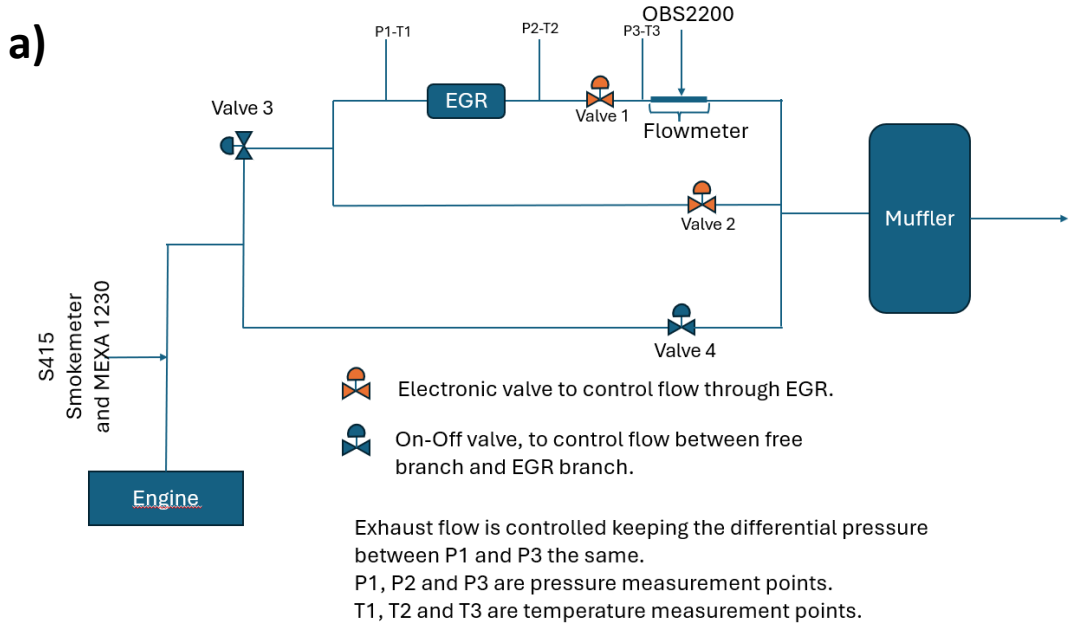
The experiments were conducted using the engines detailed in Table 3-1. These are both modern production GDI engines utilising a multi-hole injector, which are water-cooled, four-stroke and turbocharged.

Table 3-1: Engine specifications.

Engine Specification	Injector Study Test Engine	EGR Cooler Study Test Engine
Compression ratio	10.5	10.5
Displacement	1.199 l	1.395 l
Stroke	90.5 mm	80 mm
Bore	75 mm	74.5 mm
Emissions Standard	Euro 6	Euro 6b

A schematic of the exhaust layout used in both the GDI and EGR Cooler tests, along with photos of the physical setup for both experiments are presented in Figure 3-1, which illustrates the placement of the emissions measurement probes and other instrumentation. The exhaust gases went away from the engine via the EGR Cooler, with a Low Pressure Loss (LPL) valve (Valve 1) being used to control volumetric flow rate through the EGR Cooler system. This was controlled so that the pressure difference between P1 and P3 measured at the start of a test cycle would remain constant, for each engine operating condition respectively. This was used in conjunction with Valve 2 which assisted to keep the engine back pressure constant throughout the test and to maintain constant EGR flowrate. During the engine warm up phase Valve 3 was shut with Valve 4 remaining open, to divert exhaust away from the EGR Cooler until the engine stabilised. The valve positions were then reverted to begin testing.

The engine was controlled using a dynamometer, which facilitated power absorption from the engine. The dynamometer was used to measure brake torque and the rotational speed of the engine. The engine speed and load were controlled separately, with torque control allowing for accurate adjustments. The ECU could not be controlled in the Injector Study and EGR Cooler Study test engines. In both experiments involving the engine, an engine map was created so ECU variables could be related to engine operating conditions.



b)

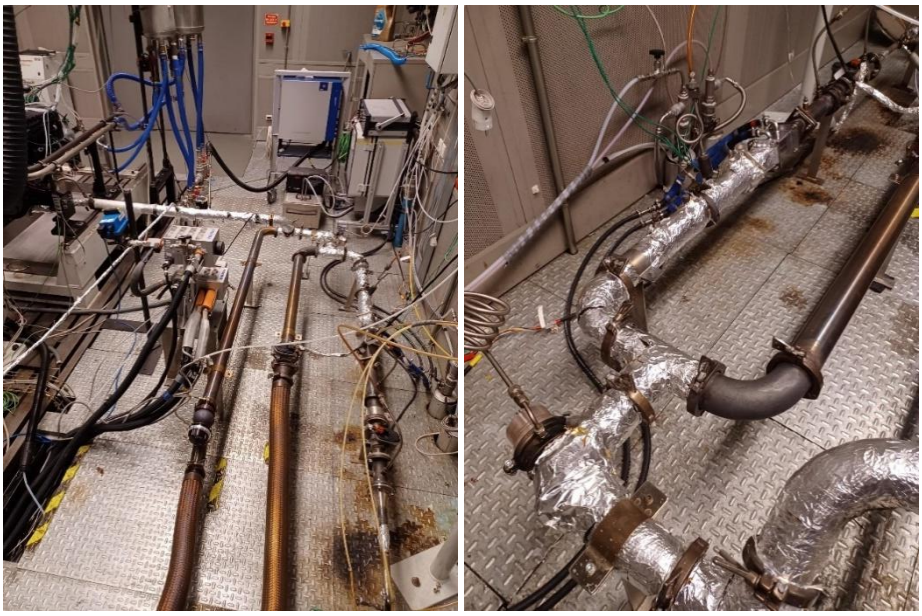


Figure 3-1: a) Exhaust layout, b) Photographs of the exhaust layout.

3.1.2 Fuel Properties

The Base fuel properties for all experiments are shown in Table 3-2. For the Injector study one additive was used with both the Base Gasoline and Renewable fuel and for the EGR Cooler Fouling experiments three separate additives were used initially, and the

best performing additive was then used for further comparative experiments with a Reference Fuel. The details of the additives cannot be disclosed in this study. The reference and Base Gasoline fuels were chosen to represent commonly used fuels in commercial vehicles that were available at the time of experimentation, with the renewable fuel chosen as a representative of commonly used ethanol blended fuels.

Table 3-2: Fuel properties (approximate value for confidentiality, ** range of values used for confidentiality).*

Parameter	Base Gasoline (Injector Study)	Base Renewable Fuel (Injector Study)	Reference Fuel (EGR Cooler Study)
Density at 15 ^{o}C [kg/m^{3}]	735	*765	728.6
Octane Index [-]	97.5	95.8	95
Oxygen Content [%m/m]	1.7	** > 3, <6	0.7
Ethanol [%v/v]	0.34	**>5,<20	7.8
Methanol [%v/v]	0	<1*	0.5
Ethyl tert-butyl ether [%v/v]	10.56	<1*	0.9
Aromatics [%v/v]	22.4	*30	42.5
Olefins [%v/v]	16	*5	29.0
Vapour Pressure [kPa]	74.3	58.9	71.7
Initial Boiling Point [^{o}C]	31	37.1	29.0
E70 [%]	33.4	39.8	42.5
E100 [%]	60.9	48.7	65.0
E150 [%]	91.6	75.5	95.8
Calorific Value [MJ/L]	30.2	29.8	Not provided

3.1.3 Emissions and Instrumentation

The concentration of emissions in the engine exhaust was measured using the Horiba OBS 2200 system for gaseous emissions (NO_X, THC, CO, CO_2). The OBS 2200 utilises several different methods for accurate detection under varying environmental conditions. The system employs Non-Dispersive Infrared (NDIR) detection for CO and CO_2, Flame Ionisation Detector (FID) for THC and Chemiluminescence Detection (CLD) for NO_X. The accuracies of each emissions measurement are displayed in Table 3-3, in all cases the emissions were measured using "Range Low" if the concentration was suitable, in order to improve the accuracy of measurements.

During operation, the OBS 2200 continuously measures emission concentrations and records data such as exhaust flow rate and environmental conditions including atmospheric temperature, humidity, and pressure. The OBS 2200 was able to sample emission concentrations at a frequency of 1 Hz. It measured concentrations of CO and CO_2 as percentages, while other species such as NO, NO_2, and THC were measured in ppm.

Soot was measured using the AVL 415SE (Smoke Meter), which utilises the filter paper method to determine the FSN and soot concentration in mg/m^3. The AVL Smoke Meter employs a variable sampling volume and thermal conditioning of the exhaust gas to ensure consistent results. A user-defined volume of exhaust gas is extracted from the exhaust pipe using a probe which is subsequently drawn through clean filter paper. The volume of exhaust gas drawn through the filter paper is then measured using an orifice flow meter. The blackening of the filter paper caused by soot is detected by an optical

reflectometer head. From the degree of blackening and a calculated effective length, the soot content in the exhaust gas is calculated. As a result of the sample volume being near constant, the measured values remain accurate over the period of sampling. A microprocessor controls and monitors the whole measuring procedure, which is carried out entirely autonomously including the calculation of the paper blackening and effective length. Soot was also measured via a Horiba Mexa 1230 PM by a Diffusion Charging (DC) method. Hot dilution was considered to prevent nuclei mode, with the dilution ratio of the soot diluter set to approximately 40.

The emissions were collected from the exhaust using a probe, as illustrated in Figure 3-2. The probe was positioned in the transverse axis of the exhaust pipe, with multiple smaller orifices machined into it, facilitating an even distribution of the exhaust. All the emissions analysers were also routinely purged throughout all experimental test procedures via an electronically controlled three-way valve which switched between diverting ambient air or the exhaust through the analysers at a fixed frequency.

Table 3-3: Emissions measurement equipment accuracy.

Emission	Analyser	Repeatability	Range Low	Range High
CO	Horiba OBS 2200	± 2.5 % of full scale	0 - 0.5 vol %	0 – 10 vol %
CO_2	Horiba OBS 2200	± 2.5 % of full scale	0 – 5 vol %	0 – 20 vol %
THC	Horiba OBS 2200	± 2.5 % of full scale	0 -1000 ppmC	0 - 10,000 ppmC
NO_X	Horiba OBS 2200	± 2.5 % of full scale	0 – 100 ppm	0 – 3000 ppm
Soot	AVL 415SE	± (0.005 FSN + 3 %)	0-10 FSN	N/A
Soot	Horiba Mexa 1230 PM	± 1 % of full scale	0 to 1000 µg/m³	N/A



Figure 3-2: Emissions probe.

3.1.4 Engine Instrumentation and Data Acquisition

Pressure transducers were used to monitor the pressure at certain places along the gas route. Endress + Hauser DELTABAR 5 PMD75 and ABB 266DSHHSSB2A1 pressure transducers were used for the pressure difference across the EGR Cooler and LPL valve as these were critical measurement points and these transducers are specifically designed for measuring pressure differentials as well as being highly accurate and robust. They also have additional communications capabilities allowing them to be easily integrated into the control system required to maintain near constant exhaust back pressure throughout the experiments. Calibrated K-type thermocouples were used to measure the temperature.

For the experiments in the injection duration chapter the injection duration and spark timings were measured using a current probe which was linked to an encoder, whereas in the EGR Cooler Fouling study they were measured from the engines ECU.

The equipment used for data acquisition along with their repeatability is listed below:

- Fuel Measurement Equipment: AVL PLU Fuel balance (± 0.3 %) for fuel consumption measurement.
- Injection and Spark Timing Measurement System:
    - Kistler Kibox.
    - Chauvin Arnoux Current Probe e3n.
    - Kistler 2614C11 encoder (± 0.5 CAD resolution).
- Intake Flow Measurement: ABB flowmeter (± 0.8 %).
- Temperature Measurement: Type K thermocouples (± 1.5 ^{o}C or ±0.4 %).
- General Pressure Measurement: Keller PR-33X transducers (± 0.05 % of full scale).
- Pressure Difference across EGR System: Endress + Hauser DELTABAR 5 PMD75 pressure transducers (± 0.05 %).
- Pressure Difference Across LPL Valve: ABB 266DSHHSSB2A1 (± 0.06 %).
- Lambda: measured using MEXA 7000 Oxygen sensor (± 0.5 % of full scale).

3.1.5 Fuel Injector Cleaning

For both the GDI and EGR Cooler tests the following cleaning method was employed at the end of every test:

- Dismount injector and take photographs.
- Clean the injector using a detergent mix (e.g. Spezialreiniger Alkalisch 5 %) in an ultrasonic bath for 90 min.
- Take photographs of clean injectors.
- Place the injectors back in the engine.

3.2 Intake Valve Deposit Experimental Rig

The details of the design, manufacturing and assembly processes of the rig are explained in chapter 6, where the completed components and the final rig are presented with calculations and discussions explaining how the final designs were created. The completed rig was then tested using the below methodology.

3.2.1 Proof of Concept Testing

To determine whether the finished product complied with a PDS (described in chapter 6), a proof of concept test was executed. The mass of the IVD was examined at various valve temperatures to see if the experimental rig could successfully generate deposits similar to that of an ICE. It was determined from literature that the most important factor impacting the formation of IVD was valve temperature. Prior research suggested that most deposits formed within a critical temperature range. This critical temperature

was to be determined by preliminary testing. Testing the temperature control system's capacity to precisely regulate the valve and Cylinder Head temperatures was another aspect of the proof of concept. The behaviour of various control parameters was recorded and used to assess the control system's performance.

Two sets of preliminary tests were carried out (Table 3-4). The first set of tests were to test the ability of the experimental rig to operate with dynamic tests. This began with an initial 2 hr exploratory dynamic test which was conducted to identify any potential issues with the equipment, which was then followed by a 9 hr dynamic durability test. Static tests were then run to give a comparison between the results.

The following static tests were then used to study the impact of changing the valve temperature while keeping all other variables the same. These tests used static valves as it reduced complexity and hence setup time allowing for more testing to be done per day. To enable one test to be executed per day the duration was reduced to 5 hr, the decision was then made to increase the fuel flow rate but to maintain the air-fuel ratio for these shorter tests, with the theory being that this would increase the chance of observing significant IVD in the short duration. These tests aimed to identify the critical temperature for IVD formation outlined in section: 2.4.3.1.

Table 3-4: IVD proof of concept test conditions.

	Test	Duration (hr)	Valve Temperature (°C)	Cylinder Head Temperature (°C)	Intake Temperature (°C)	Intake Pressure (bar)	Air Mass Flow rate (kg/hr)	Fuel Mass Flow rate (kg/hr)	Air-Fuel Ratio	Camshaft Speed (rpm)
Dynamic	1	2	240	67	27	2	9	0.77	11.76	620
	2	9	290	67	20	2	9	0.77	11.76	620
Static	3	9	290	67	20	2	9	0.77	11.76	0
	4	5	330	67	22	2.7	13	1.11	11.76	0
	5	5	370	67	22	2.7	13	1.11	11.76	0
	6	5	250	67	22	2.7	13	1.11	11.76	0
	7	5	210	67	21	2.7	13	1.11	11.76	0
	8	5	170	67	18	2.7	13	1.11	11.76	0

To measure the mass of the deposits, the valves were weighed before and after the test using an Ohaus Pioneer scale with 0.1 mg precision, with typical IVD mass ranging from 2.5-20 mg per valve. After each experiment each valve was measured three times with the mean being used as the final result, the valves were then partially cleaned and finally fully cleaned (with 3 measurements and a mean being taken after each step). Post-test the valves were left for at least 12 hr to allow deposits to solidify and any residual fuel to evaporate. This was followed by the partial clean consisting of a 5 min soak in ethanol so the solidity of the deposits could be analysed. The mass was measured again, and then the full clean occurred, where the valves were thoroughly cleaned using a solvent and manual abrasion with a cloth to remove the deposits as completely as possible. This clean mass was used as the pre-test mass for subsequent tests. The IVD mass was calculated as the difference between the first post-test measurement and the pre-test mass. This process was repeated for all following tests to ensure accuracy and consistency in the results. Each valve was marked so the two valves could be differentiated and so that the orientation could be determined. The orientation was kept consistent between tests.



Figure 3-3: Ohaus Pioneer scale being used to weigh a valve.

4. GDI INJECTOR FUEL DEPOSITS

4.1 Introduction

As previously noted in the literature review and research focus sections, there is a growing interest in GDI engines due to their enhanced fuel efficiency compared to PFI engines. However, one of the challenges associated with GDI technology is the potential accumulation of fuel deposits on injectors, which impact engine performance, PM and gaseous emissions as well as fuel efficiency. It is therefore beneficial to address this issue to maintain the advantages of GDI technology while minimising its environmental and operational drawbacks. This is particularly pertinent considering the regulatory requirements concerning PM emissions.

The composition of the fuel and the presence of any fuel additives can influence the formation of deposits. This chapter examines the influence of a conventional Gasoline and a Renewable fuel, in conjunction with an Additive, on the formation of injector deposits over the course of an accelerated injector fouling test cycle. Furthermore, the impact of the Additive on both fuels is investigated to assess the importance of developing additives that are specifically tailored to fuels with different properties. A comprehensive examination is conducted to ascertain the influence of varying fuels and additives on the formation of injector deposits and how different engine operating conditions can influence the formation of injector deposits. In addition to this the impact of the deposits on engine PM and gaseous emissions as well as fuel consumption is studied.

The methodology employed to create the accelerated fouling cycle is also explained, with the aim of addressing the lack of existing literature about which engine and cycle parameters can be exploited to create injector deposits in a relatively short period of time. This is a crucial aspect, as fuel and additive developers require a method to simulate the formation of injector deposits in a shorter timeframe, which would otherwise take years in the real world. This chapter also considers the techniques used to develop the accelerated fouling cycle from the outset, given the limited existing literature on this topic as well. This represents an area of inefficiency in the testing of new fuels and additives, as a significant amount of work is often required to first develop the fouling cycle with a new engine before fuel testing can commence. This chapter aims to provide a framework for such a process.

4.2 Methodology

4.2.1 Development Procedure for Discovery of an Accelerated Injector Deposit Formation Cycle

The methodology for finding an accelerated deposit formation test cycle involved multiple steps including initial mapping, lean and agile experimentation, sequential experimentation and the final test cycle. The overarching philosophy with the technique employed to find the final test cycle was to vary multiple test parameters simultaneously, as opposed to a more thorough but time consuming One-at-a-time (OAT) approach. This allowed for rapid identification and optimisation of engine and cycle parameters that lead to significant injector deposit formation, which is essential

for testing the impacts of different fuels and additives efficiently. The primary method for assessing the level of the injector deposits was through monitoring injector duration time and from visual inspection of the injectors before and after the test cycles.

The engine, cleaning and exhaust layout described in the main methodology section was used to conduct experiments on injector deposits. This chapter starts with defining a process used to generate a test Cycle which accelerates the formation of fuel-derived deposits on the fuel injectors which is then utilised to study the impact of Renewable fuels and Additives on deposits formation. The process used for the development of the Cycle is shown in Figure 4-1. Special attention was paid to certain parameters which were understood to relate to injector fouling including but not limited to the parameters in Table 4-1. It must be noted that engine control parameters could not be recorded or modified (locked ECU), but they could be measured indirectly via methods outlined in the main methodology section.

For the following chapter the definitions of various parts of the developed test *Cycle* are displayed in Figure 4-2. Where a *Cycle* refers to the entire test *Cycle*, a *Sequence* refers to one repetition within the *Cycle,* and the *Sequence* is then made up of varying engine *Setpoints* (engine operating conditions) with a ramp between them if multiple *Setpoints* are used.

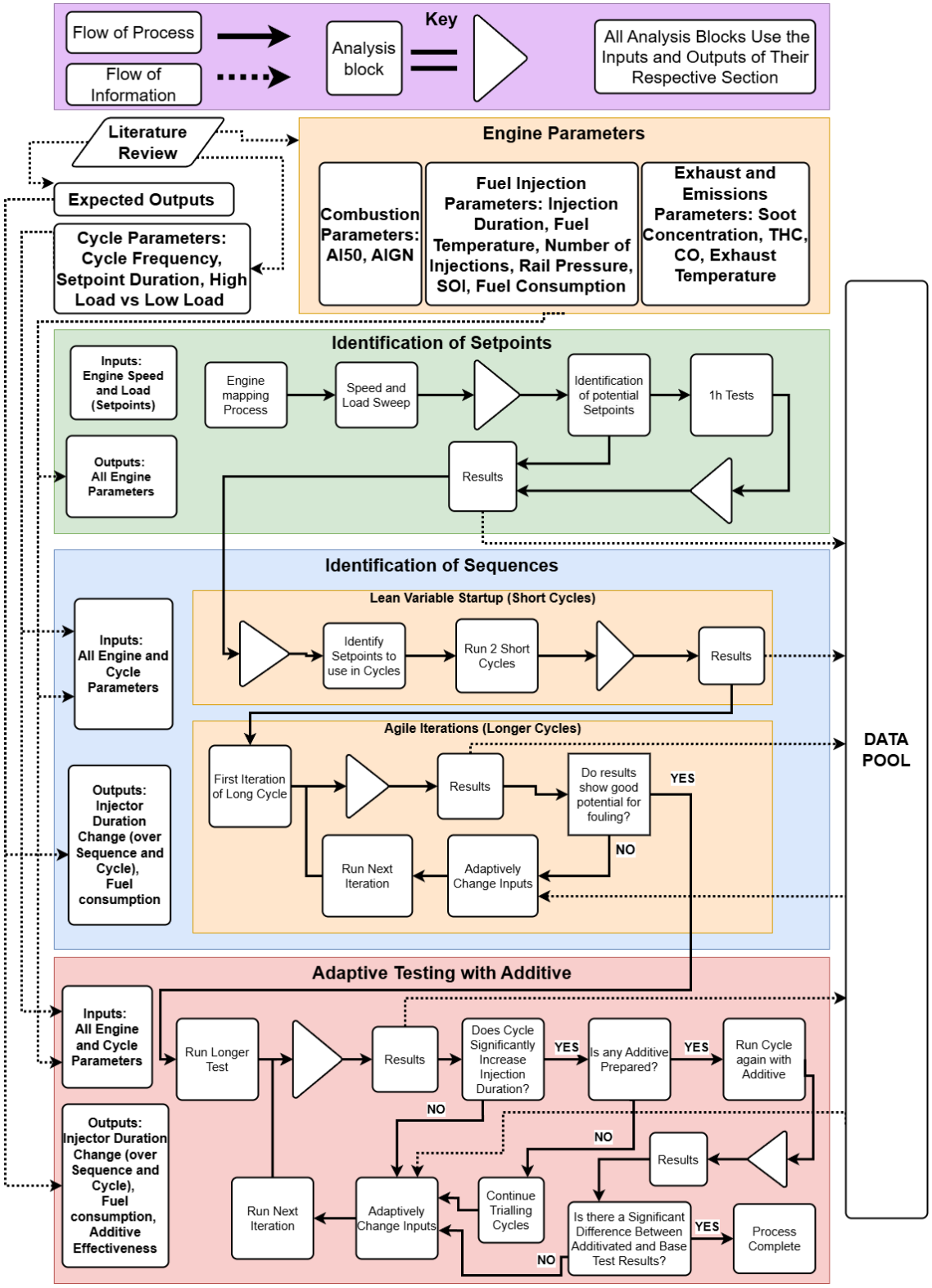


Figure 4-1: Flowchart of process used to develop accelerated fouling Cycle.

Table 4-1: Variables that were adjusted throughout accelerated fouling Cycle development process.

Engine *Setpoints*	Speed (1250 to 4500 rpm) and load (6 bar IMEP to full load)
Fuel Injection Parameters	Number of injections, fuel temperature, injection pressure, SOI, and injection duration
Combustion Parameters	MFB50, AIGN
Exhaust and Emissions Parameters	Soot concentration, THC, CO, exhaust temperature
Cycle Characteristics	*Sequence* duration, *Setpoint* duration

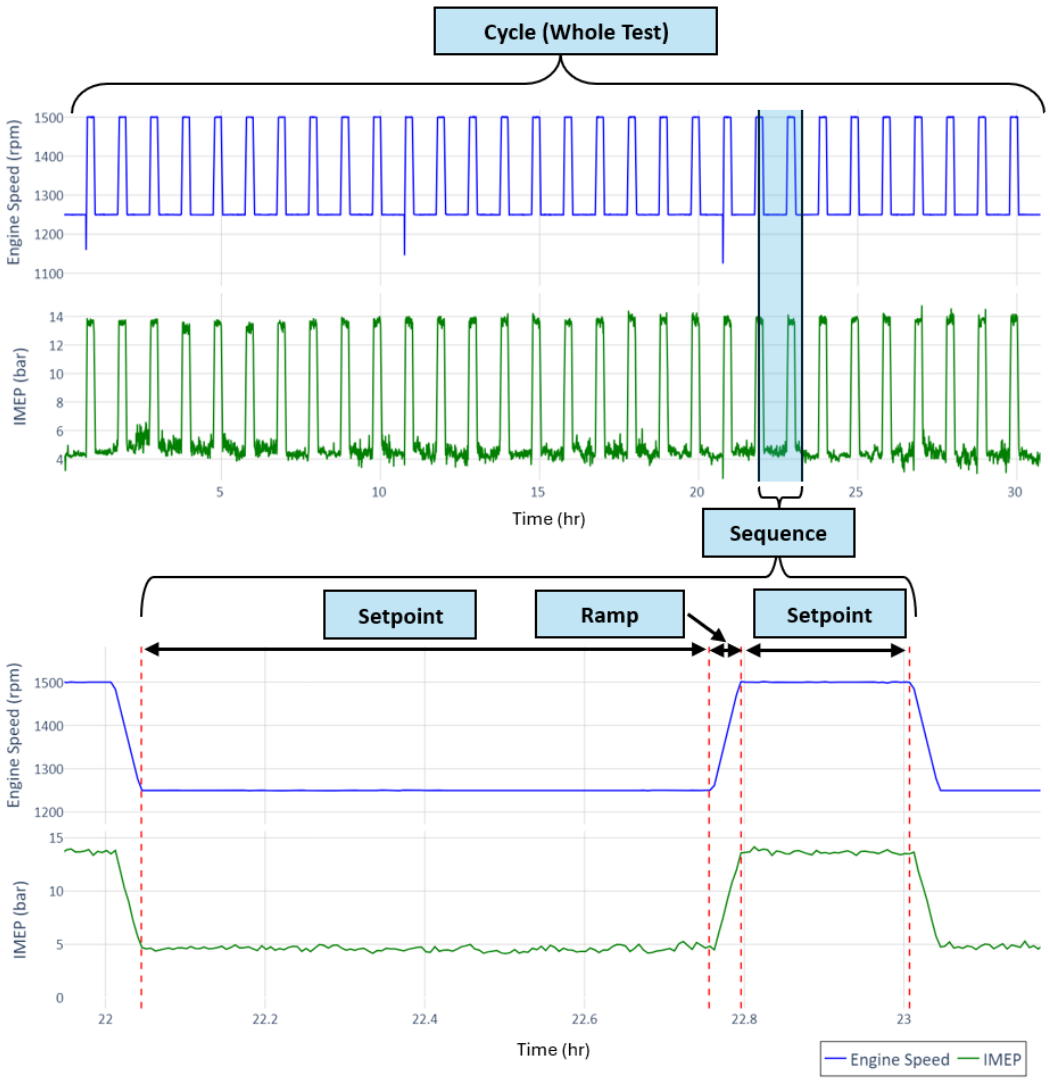


Figure 4-2: Definition of Cycle Parameters.

The first stage of the *Cycle* development process was to identify key *Setpoints* using the above parameters. This was achieved by reviewing literature to identify engine output parameters that showed a correlation with injector deposit generation. Once this was established a set of preliminary experiments (engine mapping) were carried out, which consisted of running the engine for a short duration (approximately 2 min) across a wide range of engine speeds (1250 to 4500 rpm) and loads (6bar IMEP to full load). This information was then analysed so that engine *Setpoints* could be correlated to potential engine output parameters that could impact injector deposit formation. The method employed in the analysis of this section of the procedure was an Exploratory Data Analysis (EDA), where visual plots consisting largely of contour maps and bar graphs were made to identify key *Regions* of the engine map. As the ECU could not be modified it was also vital to identify how ECU parameters reacted at different *Setpoints*, and the engine mapping process provided this.

The chosen *Setpoints* were further explored and measured over a longer duration (1 hr) to confirm the experimental results found from the engine map and to explore if any amount of injection duration increase could be seen. An increase in injection duration would indicate a restriction in the injector nozzle and hence the potential presence of injector deposits, providing a method for assessing injector deposits in-situ. Visual analysis of the injectors was also used to identify the presence of deposits. The analysis of both the map and the 1 hr tests were used to build an understanding of how the engine behaved at different *Setpoints* and this data was used to determine which *Setpoints* would be used for further exploratory testing. The data was also added to

what is shown as the *Data Pool* in Figure 4-1. The *Data Pool* was used throughout all stages of the procedure and was continuously updated and used to inform decisions.

The second stage of the procedure consisted of a variety of *Cycles* composed of *Setpoints* selected from the results of the EDA from the previous stage. In addition to engine parameters that were known to impact injector deposit formation, literature was also reviewed to study which *Cycle* parameters (such as those shown in Figure 4-1) impacted injector deposit formation. The first *Cycles* were relatively short in total duration (7.5 hr) cycling between high speed – low load *Setpoints* and low speed - high load *Setpoints*. These short tests provided a lean startup, where minimal time and resources were used to build foundational knowledge on how a multitude of engine and *Cycle* parameters impacted the outputs (Figure 4-1). The *Setpoints* and *Sequences* that showed the most change in injection duration or displayed characteristics such as high soot or other parameters indicating high potential levels of injector fouling were chosen to propose longer (22.5 hr) *Cycles*. These *Cycles* varied further *Cycle* parameters such as *Sequence* and *Setpoint* duration. The results from these tests underwent another EDA after each iteration so that the input parameters of each iteration could be compared to the outputs and then adapted in an agile manner.

The governing principle of this phase was to adaptively modify parameters in a simultaneous manner, thereby facilitating the acquisition of a comprehensive *Data Pool* with a lean number of tests. The ensuing results were then subjected to real-time analysis through a comparison with established literature and results from the *Data Pool*. This approach enabled the rapid implementation of agile iterations, where

multiple variables were changed simultaneously. An agile iteration is when the plan for each iteration is loose with the results of one test changing the plans for the following ones as the acquired knowledge in the *Data Pool* changes, making the tests agile. This allowed for the identification of the most influential parameters with greater speed. Once the results of the EDA showed a wide range of data on which parameters had a correlation with injection duration increase, the parameters were tested further in the next stage.

The following test *Cycles* were then run for at least 37.5 hr with a Base Gasoline fuel (Table 3-2) and different doses of an Additive (The details of the Additive are unable to be disclosed in this work). The Cycles were changed adaptively with the aim of assessing which *Cycle* and engine parameters could not only generate deposits in a short period of time but also changed the behaviour of the Additive so that a clear difference could be seen between the Additivated and Base test results. The *Cycle* duration was also increased to between 50-75 hr for the later, more finely tuned *Cycles* so that any small differences between the Additive and Base Gasoline test results would be clearer. After each iteration the process shown in Figure 4-1 was followed where firstly the injection duration increase was analysed. If the increase was significant then the *Cycle* was repeated with the Additive if there was any prepared. This is an important factor as the Additive was both time consuming and expensive to create, meaning if the Additive was still being produced, time should not be wasted waiting and instead further *Cycles* should be ran to add to the *Data Pool*. After each *Cycle* an EDA was done to add more results to the *Data Pool*. When a *Cycle* demonstrated that it could both successfully

show a significant increase in injection duration and a noticeable difference between the Base and Additive fuels the process was complete. This process provides a method for future researchers to follow, to effectively create their own test *Cycle* for additive testing, saving on cost, fuel and time used in the process of developing accelerated fouling procedures. The different *Cycles* also allowed for an understanding of how the Additive functioned at various engine and *Cycle* parameters, which can aid in the development process of the Additive.

The final test *Cycle* was then run with a Renewable fuel (Table 3-2) with the same Additive as was used with the Gasoline. Both the Base Gasoline and Renewable test *Cycles* were repeated to ensure repeatability. The results for these tests were analysed in more detail to observe how each fuel and Additive combination impacted injector deposit formation. The impacts of the deposit formation on engine performance were also analysed via changes in carbonaceous emissions and fuel consumption. A final round of tests was then run using a GPF in order to assess the likely impacts of any increase in soot levels in a modern vehicle with a GPF.

4.2.2 Analysis Techniques

To analyse how different sections of a *Sequence* impacted injection duration, the *Sequence* was split into multiple *Phases*, displayed in Figure 4-3 which shows the injection duration evolution over both *Setpoints* over the course of one *Sequence*. To analyse the data, the raw data was first smoothed using a LOESS function. Three *Phases* of the *Sequence* were then identified, *Initial, Post Start, and Total,* which are labelled in

Figure 4-3 where the beginning and the end of each *Phase* is measured by using the average injection duration in a window of ± 1 min. Note this timing was sometimes changed for example in *Cycles* where a *Setpoint* duration might be less than 5 min, the transition point from *Initial* to *Post Start* was brought forward to approximately 2.5 min.

To analyse the evolution of output parameters over a whole *Cycle* firstly the *Initial Phase* data shown in Figure 4-3 was filtered out so that the evolution over the whole *Cycle* was comparing data that was recorded at a consistent section in each *Sequence*. Then a trendline using the LOESS function as seen in Figure 4-3 was used on the filtered Injection duration results. The LOESS line at this stage used a small window for the locally estimated values, to allow the LOESS regression curve to follow the raw data more accurately, thus any raw results that deviated from this line by more than 15 % were removed as anomalies. 15 % was chosen as the limits of the data as this is where the vast majority of the data lied. The LOESS regression was then repeated with a larger window size on the filtered data to capture the trend over the whole *Cycle* as opposed to small changes within a *Sequence*. As the data was measured at 1 Hz over multiple hours, the data was then finally condensed by averaging the results of each hour in order to save on computational time.

To calculate confidence intervals for results showing the evolution of parameters over whole *Cycles,* the Standard Error at each hour was calculated from each repeat of a *Cycle* with the same fuel. As the Standard Error was calculated at each timestep using only two samples from different days these confidence intervals represent the probability of how much a trendline will vary from day to day. As repeats were only executed for the

Base fuel runs, the Additive runs used the same confidence intervals as their Base counterparts, normalised to their own values. Confidence intervals for *Sequence* analysis, e.g. comparing how much the *Initial, Post Start* and *Total Changes* varied between fuels, used data from every *Sequence* in a *Cycle* that used the same fuel (including any repeated runs).

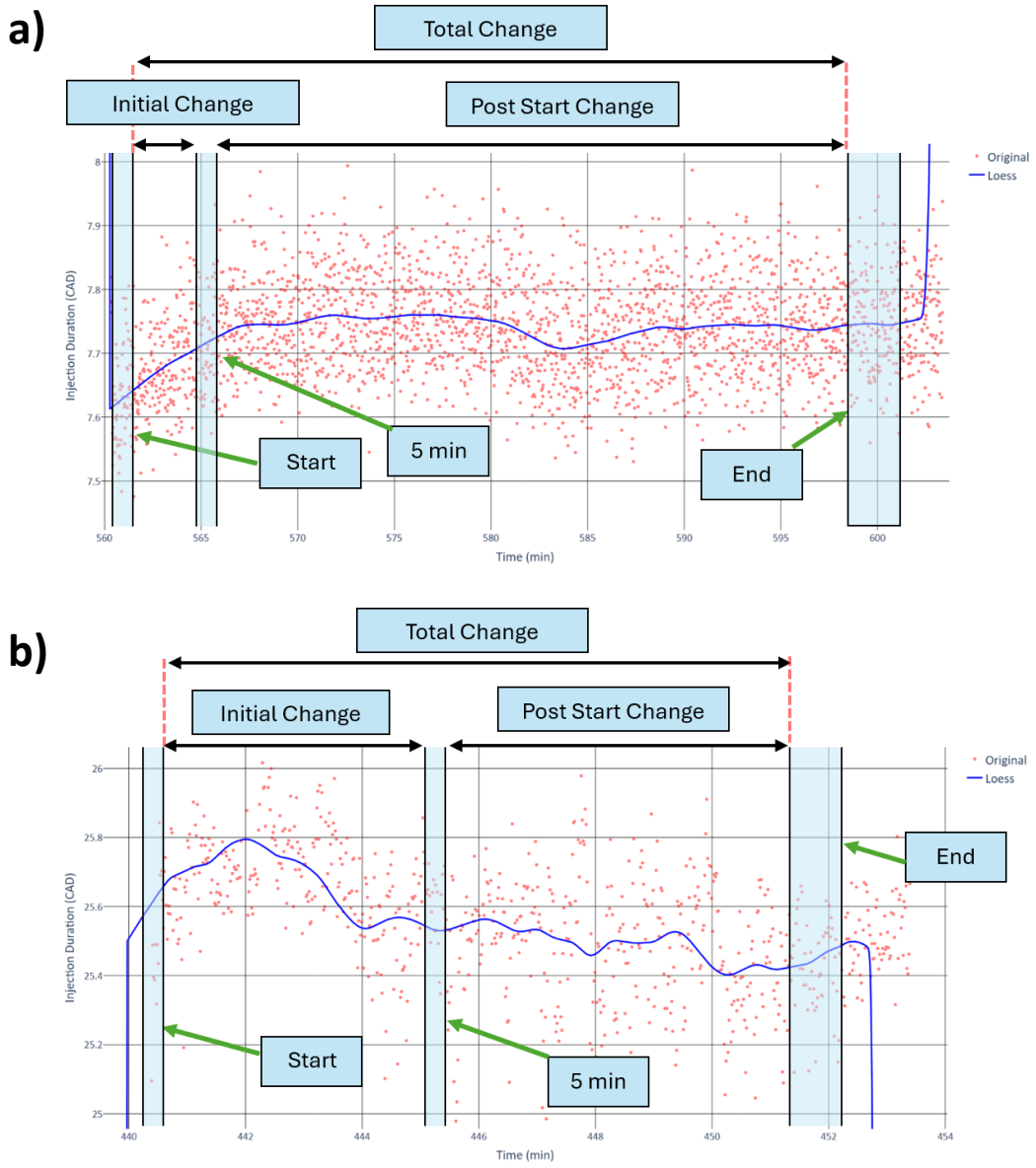


Figure 4-3: Definition of Phases of injection duration change throughout a Sequence at a) 1250 rpm 6 bar IMEP b) 1500 rpm 16 bar IMEP.

4.3 Results and Discussion

4.3.1 Development Procedure for Discovery of an Accelerated Injector Deposit Formation *Cycle*

4.3.1.1 Identification of Setpoints

Engine Mapping

The process began with sweeping the engines operation range to create a contour map of various engine parameters (Table 4-1) against engine speed and load. High soot emissions *Regions* (defined by engine speed and load) are identified in Figure 4-4: *Region* 1: mid/high engine speed (3000-4500 rpm) and low load (4-10 bar IMEP); *Region* 2: low speed (1000-2250 rpm) and mid load *Region* (12-19 bar IMEP); *Region* 3: low/mid-engine speed (2000-3000 rpm) and high load *Region* (19-23 bar IMEP). *Setpoint*s that lied within these 3 *Regions* were selected for longer 1 hr duration tests, represented by white dots on Figure 4-4. *Region* 1 was chosen as it had high levels of soot (Figure 4-4) and presented a high level of THC and CO emissions. *Region* 2 was also highlighted due to its high levels of soot and the high load aimed to create high in-cylinder temperatures. Furthermore, *Region* 3 was also selected primarily due to the high THC and CO concentrations, respectively.

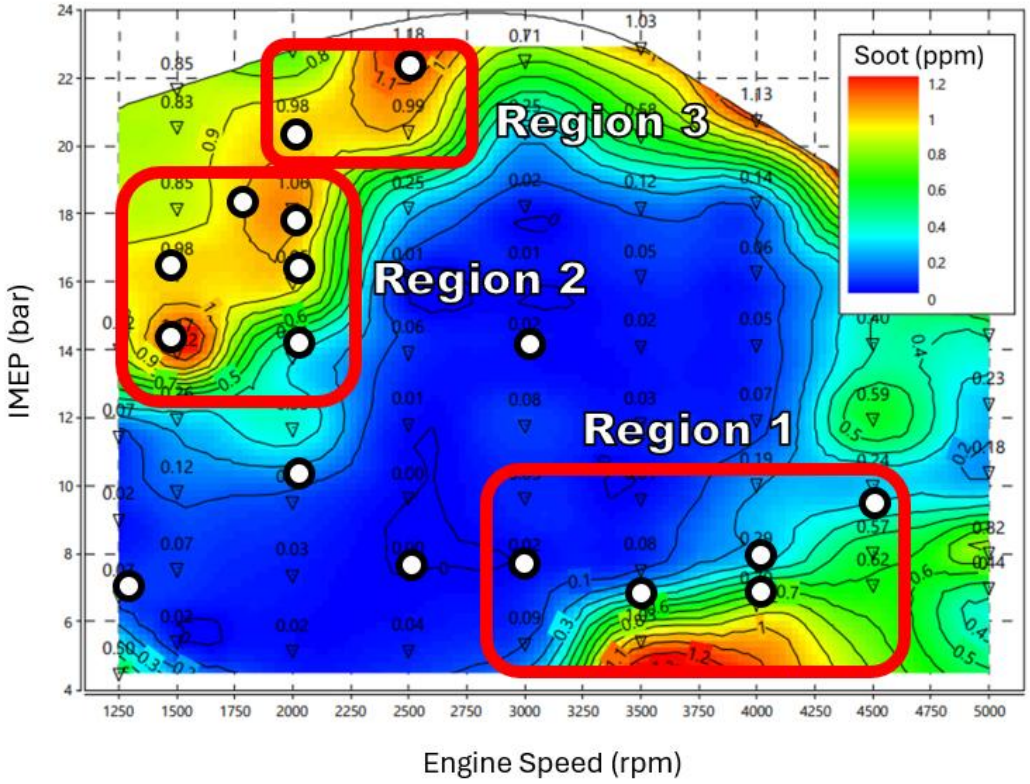


Figure 4-4: Soot emissions contour map.

Further engine parameters were considered in the selection of the *Setpoints,* such as injection strategy. *Setpoints* located in *Region* 2 used a split injection strategy. This was to investigate what was discussed in section 2.2.3, that injection strategies can impact PM emissions which can then in turn impact injector deposit formation, thus, some of the selected *Setpoints* with 2 and 3 injection events were chosen. Injection timing has also been shown to impact PM emissions and combustion chamber deposits, so *Setpoints* across a range of SOI values were employed. Injector tip temperature could not be measured directly but it was hypothesised that there are other parameters which could represent thermal effects on injector deposits. AIGN and MFB50 could be used to be qualitatively relate with injector temperature, and to observe if the deposits had any impact on combustion duration and flame growth, so *Setpoints* with varying values for

these parameters were also chosen. As mentioned in section 2.6.2 higher fuel temperatures can increase injector deposits. To investigate this some *Setpoints* were chosen in high fuel temperature *Regions*.

The engine map effectively gave an overview of how key engine parameters behaved across a range of *Setpoints* providing a fundamental foundation of knowledge to inform future decisions. This was necessary as the engine did not have a locked ECU so parameters such as fuel pressure, SOI, AIGN and more could not be regulated and thus the map was necessary to choose *Setpoints* for the next stage. The process could be made faster by having control of the ECU and therefore control of some of the aforementioned important parameters. Another improvement could be to have more measurement points such as a way of measuring injector tip temperature directly, such as that done by Kinoshita et al (109).

Stability of *Setpoint*s

The soot, THC and CO emissions were further measured during a longer measurement time (1 hr) than in the case of the engine mapping. The obtained trends were the same with regards to which *Setpoints* generated high soot/ THC/ CO in the engine mapping. The 1 hr tests allowed for the repeatability of the original map to be confirmed, especially with regards to soot as this seemed to vary significantly throughout the test, which was attributed to settling time. During the 1 hr tests the engine would finish the 1 hr run at one *Setpoint* and immediately ramp to the next *Setpoint*. In some cases, the soot level took approximately 20 min to settle after the ramp. This demonstrates the need to check the results of an engine map where not much settling time was allowed

between *Setpoints*. The mapping procedure was adequate in identifying which *Regions* were likely to have high soot and then the 1 hr tests confirmed this.

Table 4-2 shows the increase in injection duration divided by the increase in fuel consumption during the 1 hr duration experiments for the *Setpoints*. The normalisation/ compensation of dividing the increase in injection duration by the increase in fuel consumption is to account for the variability in fuel mass flow rate due to uncontrolled parameters such as ambient conditions and various ECU/ dynamometer control variables, which could impact injection timing. The increase in fuel consumption could be due to injector deposits as mentioned in the literature review section 2.2.4, but this was deemed unlikely in these short tests, especially as with close analysis of the fuel consumption rate, the fuel consumption would often jump sporadically and not gradually increase like what would be expected with deposits. It is important to identify this as if not it could lead to some *Setpoints* appearing to be much more effective than they actually are after 1 hr. This was only necessary for these 1 hr tests due to their relatively short duration meaning a small fuel consumption change could cause a significant percentage change of injection duration. In addition to this in longer tests the likelihood of an increase in fuel consumption being due to deposits is increased.

Once compensated for by fuel consumption, the increase in injection duration was deemed too small to be of much significance after such a short test. Only three *Setpoints* showed greater than 1 % increase and these were generally at low fuel flow rates with low injection duration times to begin with, where a small random change would be a greater percentage of the total duration time, thus amplifying the percentage increase.

In addition to this there was often some random variation in most engine parameters during the first 10-15 min as the oil temperature settled after a speed or load change, so percentage changes were taken with reference to an average around the 20th min and the 60th min, essentially making the tests shorter. It was therefore deemed important to allow the engine and dynamometer control systems such as the coolant temperature, air temperature and exhaust flowrate control mechanisms time to settle in future tests.

Table 4-2: Summary of stability (1 hr) test results. The shade of red indicates how high a value is comapred to the average. Setpoints in yellow were chosen for the next section.

Setpoint		Injection duration/Fuel consumption (% Increase)	Soot (FSN)	CO (%)	THC (ppm)
Speed (rpm)	IMEP (bar)				
1500	14	0.20	0.003	0.65	527.81
1500	16	-0.55	0.070	0.87	654.27
2000	14	0.61	0.002	0.51	479.02
2500	8	0.69	0.000	0.35	536.25
3000	8	0.79	0.005	0.36	479.68
4000	8	1.23	0.050	0.50	424.42
4000	6	0.55	0.035	0.41	487.23
4000	7	0.80	0.030	0.40	466.53
4500	10	-0.08	0.010	0.53	368.89
2000	21	-0.22	0.025	0.90	580.99
2500	23	0.14	0.048	0.80	436.64
1750	18	-0.63	0.021	0.86	610.81
2000	18	-0.06	0.015	0.77	554.62
3500	7	1.51	0.006	0.46	468.57
2000	11	1.19	0.000	0.41	447.08
3000	14	0.13	0.001	0.46	420.64
1250	6	-0.11	0.000	0.60	717.70

Summary

Time was saved in the 1 hr tests by targeting *Setpoints* that had interesting parameters, identified by the EDA from the Engine Mapping process. However, this could be improved by making the 1 hr tests either longer or shorter, because it took approximately 20 min for some readings to stabilise at each *Setpoint* the test could be made faster by only testing for 20 min rather than 1 hr. This would be a viable technique as the 1 hr duration was not long enough to see significant change to injection duration. Therefore, if tests longer than 20 min are to be ran, they should be made longer than 1 hr so that more information can become clear, helping to advise decisions in later *Cycles*, otherwise 20 min would suffice if the aim were only to test repeatability of the engine map.

4.3.1.2 Identification of Sequences

The results of the 1 hr steady state tests were analysed to identify which *Setpoints* had the best potential to generate injector deposits, and these were combined in a *Cycle* to allow for simultaneous analysis of the impacts of different *Sequences* that transitioned between high and low load and the impact of engine parameters on injection duration over a longer time period than 1 hr.

Lean Variable Startup

Two *Cycles* (*Cycle* 1 and *Cycle* 2) composed of two steady state *Setpoints* were determined from an EDA of the *Data Pool*. Both *Cycles* were composed of a 90 min *Sequence* repeated 5 times leading to a total duration of 7.5 hr each (Table 4-3). *Cycle* 1 consisted of a high speed-low load (*Region* 1) *Setpoint* and a low speed-high load (*Region*

3) *Setpoint*. 4000 rpm 8 bar IMEP was chosen as it showed the highest soot emissions of all the high-speed low load *Setpoints* (Table 4-2). 1500 rpm 16 bar IMEP was chosen due its high output of soot, CO and THC, its multiple injection strategy and high fuel temperature. 2000 rpm-21 bar IMEP was chosen in *Cycle* 2 to represent a slightly higher speed and load than 1500 rpm 16 bar IMEP with poor combustion quality evidenced by its high levels of CO and THC and moderately high soot concentration (Table 4-2). It also had a later SOI than 1500 rpm-16 bar IMEP which was thought to be an interesting point of investigation. 4000 rpm 7 bar IMEP was selected as it had similar results to 4000 rpm 8 bar IMEP, but with a lower load, in an attempt to find the lowest load at 4000 rpm that could produce stable and consistent results.

Both *Cycles* showed a reasonable increase in injection duration over the *Cycle*. *Cycle* 1 led to an increase in injection duration at the high load *Setpoint*, but not at the low load *Setpoint*. *Cycle* 2 also led to an increase in injection duration at the high load and the low load *Setpoint* contributed more towards injection duration than in *Cycle* 1.

Table 4-3: Summary of short Cycle test results (first 9h continuously at 1500 rpm 16 bar IMEP, followed by cycling between 1500 rpm 16 bar IMEP (60 min) and 4000 rpm 7bar IMEP (30 min).*

	Setpoint		*Setpoint* Duration	*Cycle* duration	Injection duration		
Cycle	Speed (rpm)	IMEP (bar)	(min)	(h)	Start (CAD)	End (CAD)	(% Change)
1	1500	16	60	7.5	25.9	26.59	2.7
1	4000	8	30		28.497	28.24	-0.9
2	2000	21	60	7.5	45.62	46.86	2.7
2	4000	7	30		27.22	28.02	3.0
3	1500	16	*	22.5	25.82	26.78	3.7
3	4000	7	*		28.16	28.23	0.2
4	1500	16	60	22.5	26.22	26.91	2.6
4	4000	7	30		27.16	27.64	1.8
5	1500	16	60	22.5	30.97	31.37	1.3
6	2000	21	60	22.5	45.32	46.14	1.8
6	4000	7	30		26.90	27.50	2.2

Agile Iterations

The next iteration was *Cycle* 3 with a longer duration of 22.5 hr, which was proposed based on the *Setpoints* from *Cycles* 1 and 2 that increased the injection duration the most. *Cycle* 3 simultaneously tested the impact of these *Setpoints* and also tested steady state testing against cyclic by combining 9 hr at steady state at 1500 rpm 16 bar IMEP followed by 9 hr cycling between 1500 rpm 16 bar IMEP and 4000 rpm 7bar IMEP. The injection duration quickly increased up until the first 9 hr (steady state operation). However, when the cycling started the rate at which the injection duration increased reduced.

Based on the current *Data Pool*, three new *Cycles* also with a duration of 22.5 hr were investigated (*Cycle* 4, *Cycle* 5 and *Cycle* 6). *Cycle* 4 retained the *Sequence* of *Cycle* 1, but

7 bar IMEP was used instead of 8 bar IMEP for the low load to address an injection control issue. The low load *Setpoint* of 7 bar IMEP was more effective than the 8 bar IMEP used in *Cycle* 1 as the low load injection duration also increased during *Cycle 4*. *Cycle* 6 kept the *Sequence* of *Cycle* 2 but with a longer duration. Increasing the *Cycle* duration while maintaining the *Sequence* did not lead to a larger injection duration increase. *Cycle* 5 was planned to further observe the impacts of running at steady state at the same *Setpoint* that successfully increased injection duration in *Cycle* 3, however the results showed the lowest injection duration increase so far. Suggesting that steady state testing may not be as effective as cyclic testing.

4.3.1.3 Analysis of Sequences and Setpoints

Cycling Between Loads

The impact of cycling between low speed-high load and high speed-low load was identified in section 2.6.2 as an effective way of making deposits. The short test *Cycles* successfully demonstrated this, as all *Cycles* that used this method increased the injection duration significantly. This combination works well because the high combustion temperatures at high load increase the fuel injector tip temperature above the fuels T90 allowing deposits to form, however at high loads the high fuel pressure also washes away the deposits. Therefore, the transition point from high to low load can be beneficial as there is still residual temperature from the high load *Setpoint* but the fuel pressure will be less. The high frequency injections at high speed can also help to keep the injector at a relatively high temperature (171). This can be observed by noting that, despite *Cycle* 3 increasing injection duration during its steady state phase, the pure

22.5 hr steady state test (*Cycle* 5) exhibited the lowest combined injection duration increase of all. In contrast, the *Cycles* that varied their *Setpoint*s demonstrated greater injection duration increase. An EDA was carried out using figures such as Figure 4-6 to provide a more detailed examination of this phenomenon. It suggests that in both *Cycles* 4 and 6, the transition point from high to low load is where the majority of deposits are generated, this will be discussed in more detail in section 4.3.1.4: Cycling Between Loads.

Impact of *Setpoint*s

The results from the previous *Cycles* were analysed to identify an effective *Cycle* moving forward. The high load *Setpoint* was chosen to be 1500 rpm 16 bar IMEP from *Cycle* 4 as it showed the largest overall Injection Duration Increase in Table 4-3. Closer analysis of the *Phases* of the *Sequences* shown in Figure 4-6 suggested that the combination of S*etpoints* used in *Cycle* 6 showed more of an increase in the average *Sequence* injection duration increase. However, the overall results from Table 4-3 were deemed to be more reliable, as explained in section 4.3.1.4: Cycling Between Loads. A combination of both results from Table 4-3 and Figure 4-6 provided useful information in regards to choosing a *Cycle* that was likely to create deposits and this was added to the *Data Pool* over time as more *Cycles* were completed. This iterative based adaptive understanding was integral to the process of creating the accelerated fouling *Cycle*.

1500 rpm 16 bar IMEP was also chosen as it generated more soot, as demonstrated in Table 4-2. It is possible that the fuel temperature also impacted injection duration as at 1500 rpm 16bar IMEP the fuel temperature was on average 2 ^{o}C higher than at 2000

rpm 21 bar IMEP. This was found in literature (178) (179) to make a significant impact on injector deposits and this helps to support that theory. Both *Setpoints* also used multiple injections with the first injection being at a similar time, however the second and third injections were later at *Setpoint* 2000 rpm 21 bar IMEP (Table 4-4). In theory a later SOI should generate more deposits as the injector tip temperature will be higher at the time of injection. From these results though it seemed this either had no impact on deposits or it had a smaller impact than other parameters such as soot concentration and fuel temperature. Perhaps the reason for this is because even though SOI2 and 3 are later at 2000 rpm 21 bar IMEP they are not late enough to see a significant rise in injector tip temperature above the T90 of the fuel. This is because at the latest SOI of 111 CAD bTDC the piston is only approximately a third of the way through the compression stroke and the intake valve has likely only just closed, thus the temperature will not be much higher here than at the CAD of SOI3 when operating at 1500 rpm 16 bar IMEP. To investigate this further an open ECU would be needed to study the impact of SOI independently, however this was not possible with the setup and was beyond the scope of the study.

Table 4-4: SOI at high load Setpoints.

Setpoint		SOI 1 (CAD bTDC)	SOI 2 (CAD bTDC)	SOI 3 (CAD bTDC)
Speed (rpm)	IMEP (bar)			
1500	16	256.5	212	129
2000	21	262	150	111

Summary

The short test *Cycles* saved time by using a Lean Variable Startup, utilising two short 7.5 hr long *Cycles*, which proved sufficient in duration to observe injection duration increase but short enough that 2 *Cycles* could be ran in a day. This quickly confirmed that cycling between *Setpoints* chosen from the *Data Pool* had potential to generate deposits. The longer 22 hr tests built on this and helped to identify any anomalies and closer analysis of the *Sequences* (section 4.3.1.4: Cycling Between Loads) gave more insight into what was an effective test *Cycle*. These tests achieved this whilst simultaneously testing the effectiveness of steady state and cyclic *Cycles*. In total 105 hr were used to add knowledge to the *Data Pool* regarding the impacts of varying *Cycle* parameters and using different *Setpoints* in different combinations. As will be discussed later this information was useful for future adaptive iterations thus proving the effectiveness of this style of testing.

4.3.1.4 Adaptive Testing with Additive

For the next stage of testing the high speed-low load *Setpoint* of 4000 rpm 7 bar IMEP was chosen as it generated high amounts of soot in the 1 hr long tests and as discussed transitioning to high speed-low load from low speed-high load was likely to be effective at making deposits, so this *Setpoint* was tested further. *Cycle* 4 was increased in duration to 37.5 hr and named *Cycle* 7, this can be seen in Table 4-5. The *Cycle* successfully created deposits as shown by the 4.81 % increase in injection duration and by the photographs in Figure 4-5. This was achieved in 10.5 hr less than the *Cycle* duration of the standard CEC test (48 hr) (36), satisfying one objective to develop an accelerated

injector fouling method in a short amount of time. However, further testing was required to investigate Additive behaviour.

The *Cycles* that were tested are shown in Table 4-5, they were iteratively changed in the manner outlined in Figure 4-1. The decisions made and a discussion of the *Cycle* results with respect to both *Cycle* and engine parameters can be found below. Further discussion involving the Additive can be found in section 4.3.1.4: Summary of all Developmental Procedure Results.

Table 4-5: Adaptive testing with additive cycle results.

	High load *Setpoint*			Low load *Setpoint*					Injection duration (% increase) / (% per 10 hr)		
Cycle	Speed (rpm)	IMEP (bar)	duration (min)	Speed (rpm)	IMEP (bar)	duration (min)	fuel pressure (bar)	Duration, total (hr)	Base	Additive	Fuel used per injection duration% increase (kg)
7	1500	16	60	4000	7	30	200	37.5	4.81 / 1.28	4.85 / 1.29	43.6
8	1500	16	30	1500	11	30	242	50	2.81/ 0.56	NA	63.3
9	1500	16	30	1250	6	30	185	50	6.5 / 1.3	NA	22.6
10	1500	16	15	1250	6	30	185	48.5	4.42 / 0.91	3.15/ 0.65	25.8
11	1500	16	5	1250	6	15	185	62	4.31 / 0.7	4.88 / 0.77	29.2
12	1500	16	15	1250	6	45	185	75	6.76 / 0.9	2.09 / 0.28	23.7

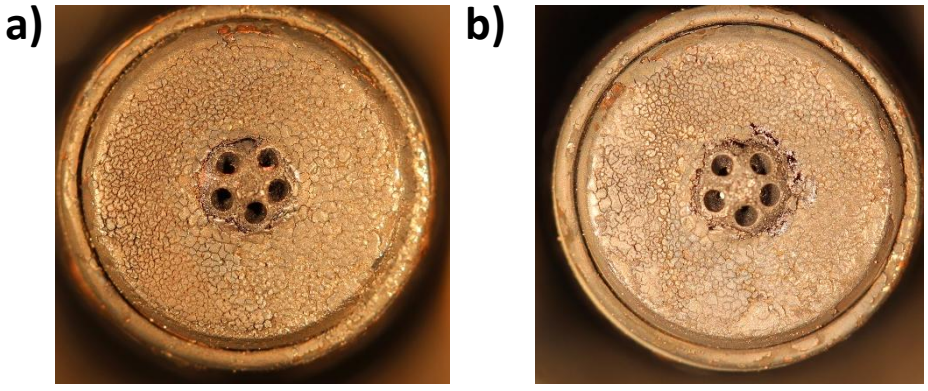


Figure 4-5: Photos taken after Cycle 7 a) no Additive, b) with Additive.

Setpoint Duration and Choice of Low Load *Setpoint*

Firstly, tests were run to search for a new low load *Setpoint* and also to investigate the impact of *Setpoint Duration*. *Cycle* 8 reduced the high load *Setpoint* duration but maintained the same low load *Setpoint* duration. The high speed-low load *Setpoint* from *Cycle* 7 was swapped for a low speed-mid load condition in *Cycle* 8. *Cycle* 9 further reduced the speed and load which proved effective as a larger injection duration than *Cycle* 8 was observed in *Cycle* 9. The speed was reduced based off the theory that the Additive needed more residence time (time between injections) on the injector to clean the deposits, and a lower speed would allow this. Furthermore, the fuel pressure is 15 bar higher at 4000 rpm compared to 1250 rpm so this could also contribute to the Additive not having enough time on the deposits, as it gets washed away. When comparing *Cycle* 7 and *Cycle* 8 to the other *Cycles* in Table 4-5 the additives ability to prevent injection duration at the low load *Setpoint* of 1250 rpm 6 bar IMEP was clear, so this was used for further iterations.

The benefit of using a low load *Setpoint* was confirmed because both *Cycle* 7 and 9 had a larger impact on injection duration increase than *Cycle 8*. This is because *Cycle* 8 which used a higher load of 11bar IMEP at its low load *Setpoint* had a fuel pressure of 242 bar compared to 185 bar at 1250 rpm 6 bar IMEP and 200 bar at 4000 rpm 7bar IMEP. Another difference between the low load *Setpoints* was that approximately double the THC was generated at 1250 rpm 6 bar IMEP compared to 4000 rpm 7 bar IMEP (Table 4-2). This has been demonstrated to help generate injector deposits in literature (171), but as the normalised injection duration percentage increase per 10 hr was similar between Cycles 7 and 9, it appears to have made minimal difference here.

Sequence Duration

As well as changing the low load *Setpoint, Cycles* 7, 8 and 9 also changed *Sequence* duration, which as mentioned in the literature review has been demonstrated to impact injector deposition. This information was used to generate *Cycle* 10 and as both *Cycles* 9 and 10 successfully increased injection duration, whilst using a relatively low 25 kg of fuel per percentage increase of injection duration, *Sequence* duration was further experimented with. Using this information, the *Cycle* was again changed adaptively so that *Cycle* 11 continued to decrease *Sequence* duration. Table 4-5 shows that by decreasing *Sequence* duration in *Cycles* 10 and 11 the level of injector deposits seemed to decrease compared to *Cycle* 9. In the literature review it was outlined that decreasing the *Sequence* duration generally increased deposit formation (171) as it generated more transition points from high to low load. This discrepancy may be due to the *Setpoint* duration at both high and low load also changing as well as the ratio between them. An EDA after these *Cycles* showed that there was a balance to be struck between *Sequence* duration and various S*etpoint* durations, which is explained later in 4.3.1.4: Cycling Between Loads.

After the Additive had been prepared it was used in *Cycle* 10. The Additive was more effective than that seen in *Cycle* 7 but by a small amount, so it was deemed necessary to investigate the impact of further *Cycle* parameters. Further investigation was done into the impact of *Sequence* duration on additive effectiveness with *Cycle* 11. The Additive was ineffective during *Cycle* 11, as it marginally increased the injection duration, therefore it was deemed that a *Sequence* duration of less than 20 min had a negative impact on additive effectiveness.

Cycling Between Loads

The data discussed from all *Cycles* ran so far shows that there is a balance that needs to be struck between *Sequence* duration and *Setpoint* duration at both high and low load *Setpoints*. The data also suggests that these impact both injection duration increase and the effectiveness of the Additive. To gain a better understanding of this, closer analysis of how the injection duration changes over a *Sequence* was carried out. This was done by splitting the *Setpoint* duration into three *Phases* as discussed in the methodology (Figure 4-3), where an example can be seen in Figure 4-6, which shows that in the shorter *Cycles* (*Cycles* 4 and 6), in the *Initial Phase* the largest increase is observed at the *Setpoint* 4000 rpm 7 bar IMEP. This largely continues into the *Post Start Phase* especially with the data from *Cycle* 6. 4000 rpm 7 bar IMEP appears to also have the largest contribution to the *Total Change.* This helps to support the theory of most of the deposits being formed in the *Initial Phase* of the high speed-low load *Setpoint*, it also shows that the high load *Setpoint* is important too in aiding the low load *Setpoint* in producing deposits as the increase is higher in *Cycle* 6. This is potentially due to the higher load *Setpoint* of 2000 rpm 21 bar IMEP providing more suitable temperatures for deposit formation during the transition point. Another point of interest with the low load *Setpoint* of 4000 rpm 7 bar IMEP is that it created the joint largest increase in injection per 10 hr in Table 4-5. This is likely because as mentioned in the literature review section 2.6.2, increasing engine speed results in higher nozzle temperatures. This supports the hypothesis that injector deposits increased with injector nozzle temperature.

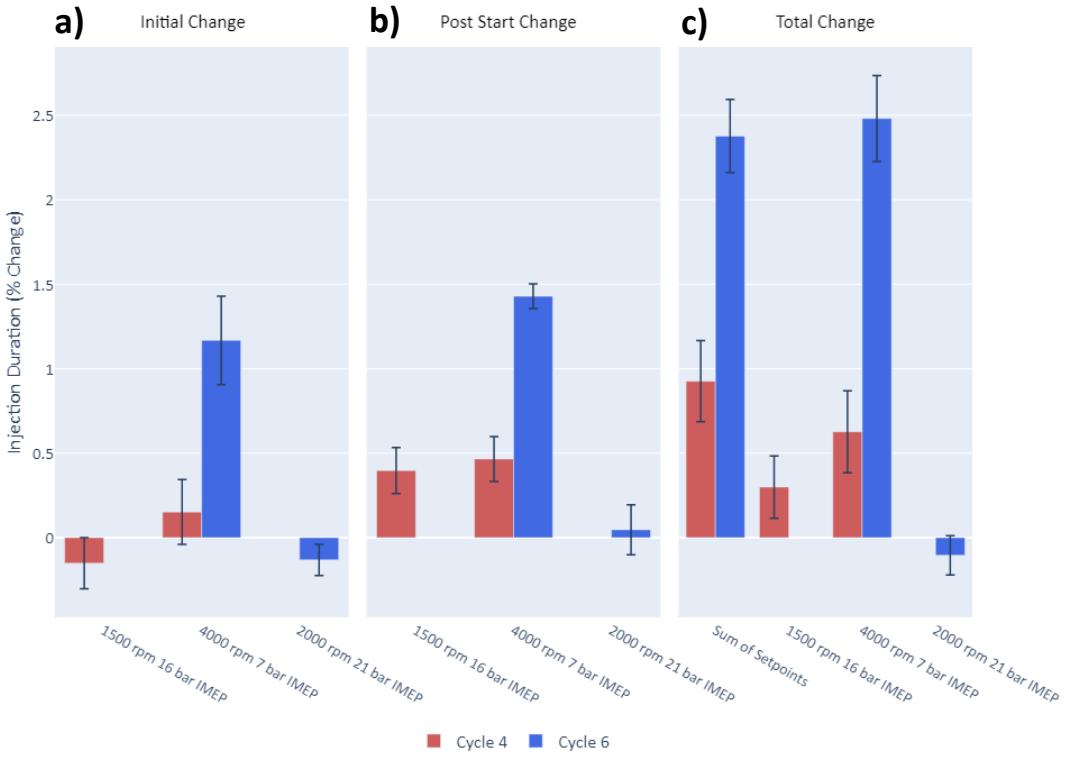


Figure 4-6: Average increase in injection duration of all Sequences used in Cycles 4 and 6, averaged over a whole Cycle a) Initial Change, b) Post Start Change, c) Total Change. Error bars represent 90 % confidence intervals.

The *Sum of Setpoints*: *Total Change* represents the average increase of one *Sequence* after both the high and low load *Setpoints* have passed. In theory the *Cycle* with the largest *Sum of Setpoints*: *Total Change* should correlate with the *Cycle* with the largest total injection duration increase. However, by reading Figure 4-6 alone, the *Sum of Setpoints*: *Total Change* would suggest that *Cycle* 6 exhibited far more deposition than *Cycle* 4, but *Cycle* 6 shows slightly less of an overall increase in injection duration across the whole *Cycle* than *Cycle* 4 (Table 4-3). Similar results can be seen in the analysis for the *Cycles* that used Additives in Figure 4-8. In these *Cycles* the *Sum of Setpoints*: *Total Change* also varies significantly compared to results taken over the whole *Cycle*, showing a discrepancy with the results in Table 4-5. This discrepancy could be for many reasons

including the settling time of the injection control system, in the *Initial Phase* this is still happening and is possibly responsible for the large changes in injection duration in the *Initial Phase* which occurs over a relatively short time period compared to the *Post Start Phase*. This could also explain why *Cycle* 6 increased injection duration across all phases more than that in *Cycle* 4, because the high load was different in each *Cycle*, possibly resulting in different transition patterns between the loads. However, even though the absolute value of *Sum of Setpoints: Total Change* has little correlation with the injection duration change per 10 hr shown in Table 4-5, the results from *Cycles* 7, 10, 11 and 12 (Figure 4-8) as well as *Cycles* 4 and 6 (Figure 4-6) show that, the *Post Start Change* in all *Cycles* is generally positive at the low load *Setpoint* and negative (or lower than the low load *Setpoint*) at the high load *Setpoint*. *Post Start Change* occurs after the majority of the variance due to settling time has passed and therefore demonstrates that the low load *Setpoint* creates more deposits and the high load *Setpoint* removes them due to higher fuel pressure.

Comparing the Injection duration change between the Base fuel and Additive in Figure 4-8 further helps to discount errors caused by settling time. Because if the *Initial Change* results were purely because of settling time then it would be expected to see similar results with both fuels, however there is a significant difference between the Additivated and Base Gasoline results in the *Cycles* which also saw the Additive reduce injection duration increase over the whole *Cycle* (*Cycles* 10 and 12). In *Cycles* 10 and 12 the difference between the Base and Additivated fuels is generally largest in the *Initial Phase* of the low load *Setpoint* suggesting that deposits are indeed mainly generated

after transitioning from high to low load. The discussion on the impact on the additives is continued in section 4.3.2.2: Impact of Additive.

The current *Data Pool* after the above *Phase* analysis and results from Table 4-5 seemed to indicate that in general that the balance between high and low load *Setpoint* duration leans towards having increased low load *Setpoint* duration. This information was used to make the final iteration in *Cycle* 12, In which the low load time was increased further, the *Sequence* Duration was brought back to that of the *Cycle* with the highest injection duration increase (*Cycle* 9) and more time was spent at low load compared to high load in a similar way to *Cycle* 10 which so far was the only *Cycle* that had seen an impact from the Additive. These adaptive changes saw an impact from the Additive with *Cycle* 12 being the most effective *Cycle* in terms of additive injector deposit prevention, whilst also significantly increasing injection duration.

Fuel Consumption per *Cycle*

It is also important to address the amount of fuel used in order to see a change in injection duration. Table 4-5 shows this parameter and it can be seen that the *Cycles* that spent 30 min or more at high load (*Cycles* 7-9) generally consumed more or the same fuel per increase in injection duration than *Cycle* 12, but without any effectiveness from the Additive. Thus, it was deemed unnecessary to increase the duration at high load further because although increasing the time from 15 min to 30 min seemed to have a small impact on injection duration, it consumed slightly more fuel as naturally spending more time at high load would. The largest fuel consumption value came from *Cycle* 7, due to the low load *Setpoint* having a high engine speed, resulting in high fuel

consumption, it did however see the joint highest injection duration increase, but at a much higher fuel cost than other high deposition *Cycles* such as *Cycles* 9 and 12.

Summary of all Developmental Procedure Results

The above results suggest that there was a fine balance between which *Cycle* and engine parameters could both create deposits and have an impact on the Additive effectiveness. In terms of creating sufficient deposits *Cycle* 7 was successful with a short duration and also with a short amount of development time to create the *Cycle*. Further demonstrating that the combination of a high speed-low load *Setpoint* and low speed-high load *Setpoint* is an effective way of creating injector deposits quickly, however this did come at a significant fuel cost. *Cycle* 9 also created a similar number of deposits when normalised for time, along with *Cycle* 12 which produced a slightly lower injection duration increase rate, but still a significant amount. *Cycles* 9 and 12 achieved this with a fuel consumption rate nearly two times lower than that seen with *Cycle* 7, suggesting that a low speed-low load *Setpoint* is more cost effective than a high speed-low load *Setpoint*.

The inclusion of a low load *Setpoint* of some kind was necessary to produce deposits as demonstrated by the lowest injection duration increase being found with *Cycle* 8. Other parameters that appeared to assist with increasing injection duration were a *Sequence* duration of at least 20 min as demonstrated by *Cycle* 11 having the second lowest injection duration increase. A high load *Setpoint* duration of at least 30 min also increased injection duration as observed by the injection duration increase being reduced as the high load *Setpoint* duration was decreased from *Cycles* 9-11. However,

Cycles 12 and 10 being the only *Cycles* where the Additive had a positive impact suggests that firstly a high load *Setpoint* duration of at least 15 min and spending more time at low load compared to high load allowed the Additive to be effective. However, it is essential to not reduce the high load *Setpoint* duration of the *Sequence* too much or the Additive will be ineffective, as seen in *Cycle* 11. It is thus important to have both a sufficiently long high load and low load *Setpoint* duration, whilst maintaining a low enough *Sequence* duration to gain the benefit of cycling between loads.

Carrying out analysis of the Injection Duration Change over a whole *Cycle* and of *Phases* throughout a *Sequence* in real time helped to provide evidence to the *Data Pool* that gave valuable insight into how cycling between high and low load helped to generate deposits quickly, and which phases of *Setpoints* added and removed deposits. The *Phase* analysis also demonstrated which phases impacted Additive performance. This allowed the impacts of *Sequence* duration, *Setpoint* duration and different *Setpoints* to be estimated while the iterations were adaptively changed. This process simultaneously provides a framework for an efficient way of developing accelerated fouling procedures for testing fuel additives in the future, as well as providing analysis into the impact of several *Cycle* and engine parameters on injector fouling and the behaviour of fuel additives.

4.3.2 Effect of Fuel on Injector Deposits, Fuel Consumption and Emissions

4.3.2.1 Overview

Cycle 12 was used to study the impact of different fuels and additives on injector deposits and their effect on combustion and emissions. A Base Renewable fuel and the

incorporation of an Additive (same Additive as the one used throughout the preliminary testing) to the Renewable fuel were selected to be studied. These experiments ran for 75 hr with both Base fuel *Cycles* and were analysed in more detail than the preliminary tests with the focus being on how the Additive and different fuels could impact injector deposits and how this in turn impacted carbonaceous emissions and combustion properties.

4.3.2.2 Fuel Injection System

Injection Duration Change

Impact of Additive

The percentage increase in injection duration was measured at both *Setpoints* with the results being averaged to create the Combined result. Figure 4-7a shows the evolution of the Combined percentage change over the whole *Cycle,* and Figure 4-7b shows the final Combined Injection Duration percentage increase, with the uncertainty of the measurement. The percentage change seen in Figure 4-7 was taken with reference to an average of the first 3-5 hr of the entire *Cycle*. This was due to the data being variable in the first 2 hr.

The 75 hr duration experiment successfully demonstrated the accumulation of injector deposits. This is evident from the 6.5 % injection duration increase with the Base Gasoline fuel (Figure 4-7). The Additive was successful at reducing the impact of deposits on injection duration, evidenced by a drop of approximately 4 % compared to the Gasoline fuel. The Additive however was less effective at reducing the increase in injection duration with the Renewable fuel.

Figure 4-8 shows the analysis of how injection duration changes throughout the *Phases* of a *Sequence* for all *Cycles* that used Additives from Table 4-5, and additionally Figure 4-8d includes the results from the Renewable fuel tests.

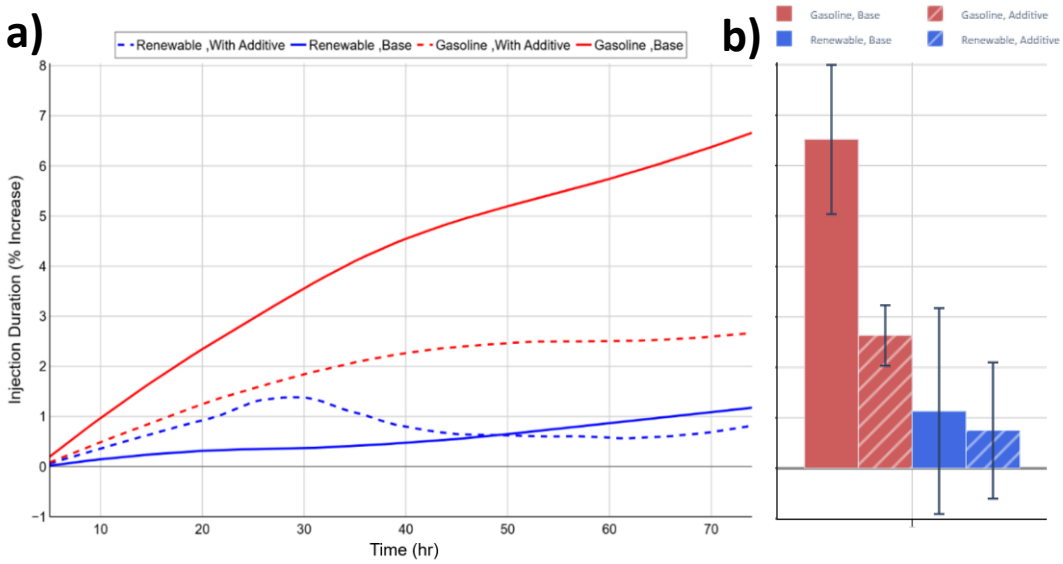
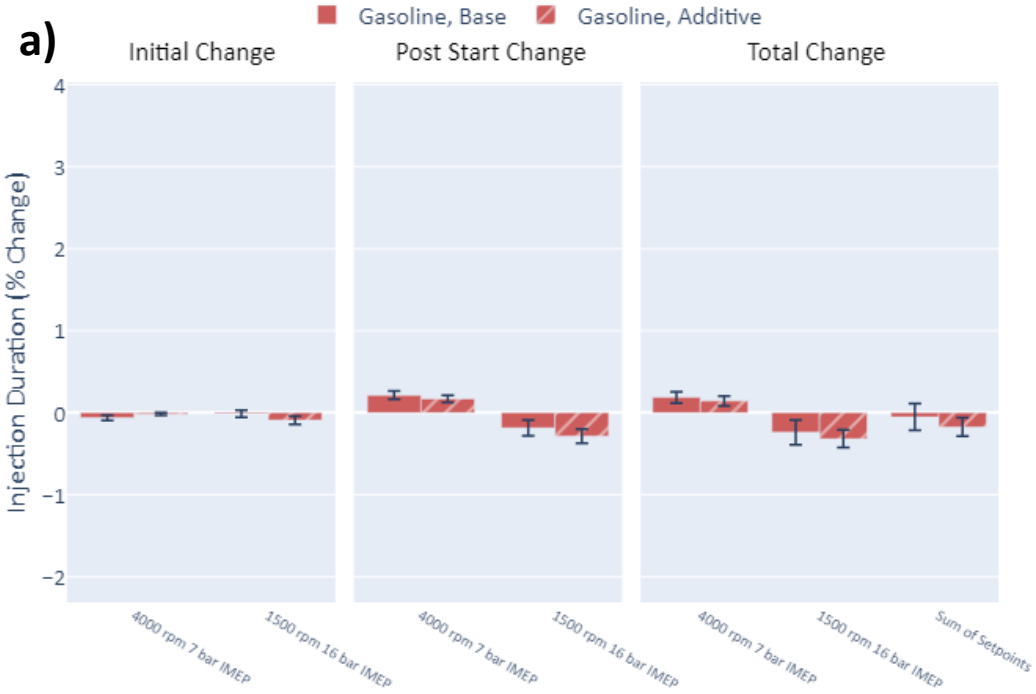
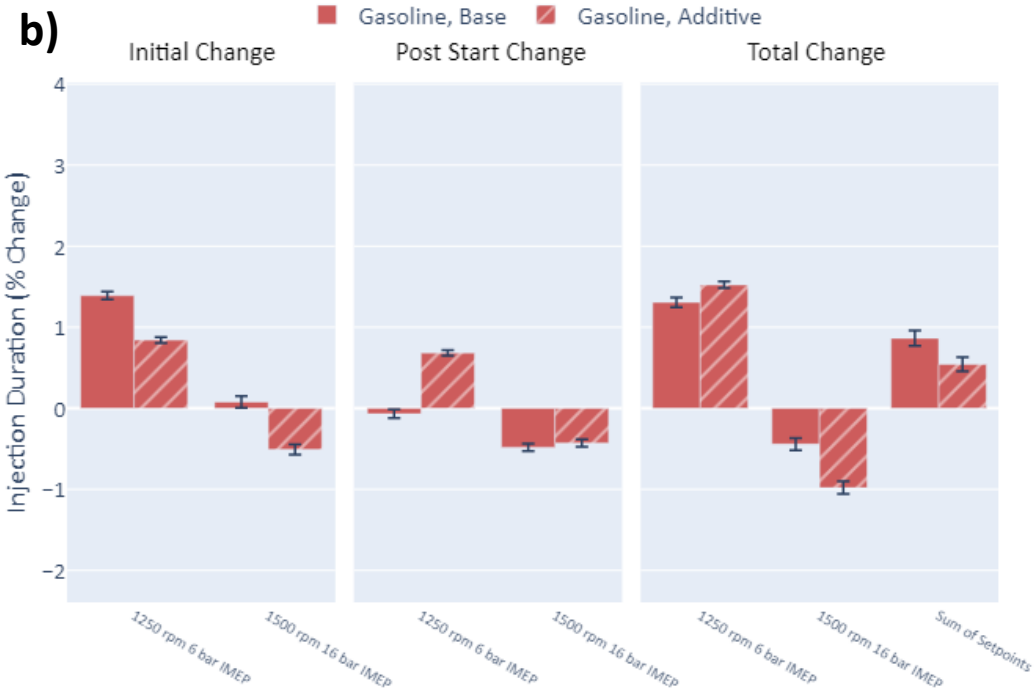


Figure 4-7: Injection Duration Percentage Increase of Cycle 12 a) Evolution of Injection Duration of both Setpoints combined, b) Percentage increase of Injection Duration, from the start to the end, combined average of both Setpoints.


a)
Gasoline, Base
Gasoline, Additive
Initial Change
Post Start Change
Total Change
Injection Duration (% Change)
4
3
2
1
0
−1
−2
4000 rpm 7 bar IMEP
1500 rpm 16 bar IMEP
4000 rpm 7 bar IMEP
1500 rpm 16 bar IMEP
4000 rpm 7 bar IMEP
1500 rpm 16 bar IMEP
Sum of Setpoints


b)
Gasoline, Base
Gasoline, Additive
Initial Change
Post Start Change
Total Change
Injection Duration (% Change)
4
3
2
1
0
−1
−2
1250 rpm 6 bar IMEP
1500 rpm 16 bar IMEP
1250 rpm 6 bar IMEP
1500 rpm 16 bar IMEP
1250 rpm 6 bar IMEP
1500 rpm 16 bar IMEP
Sum of Setpoints

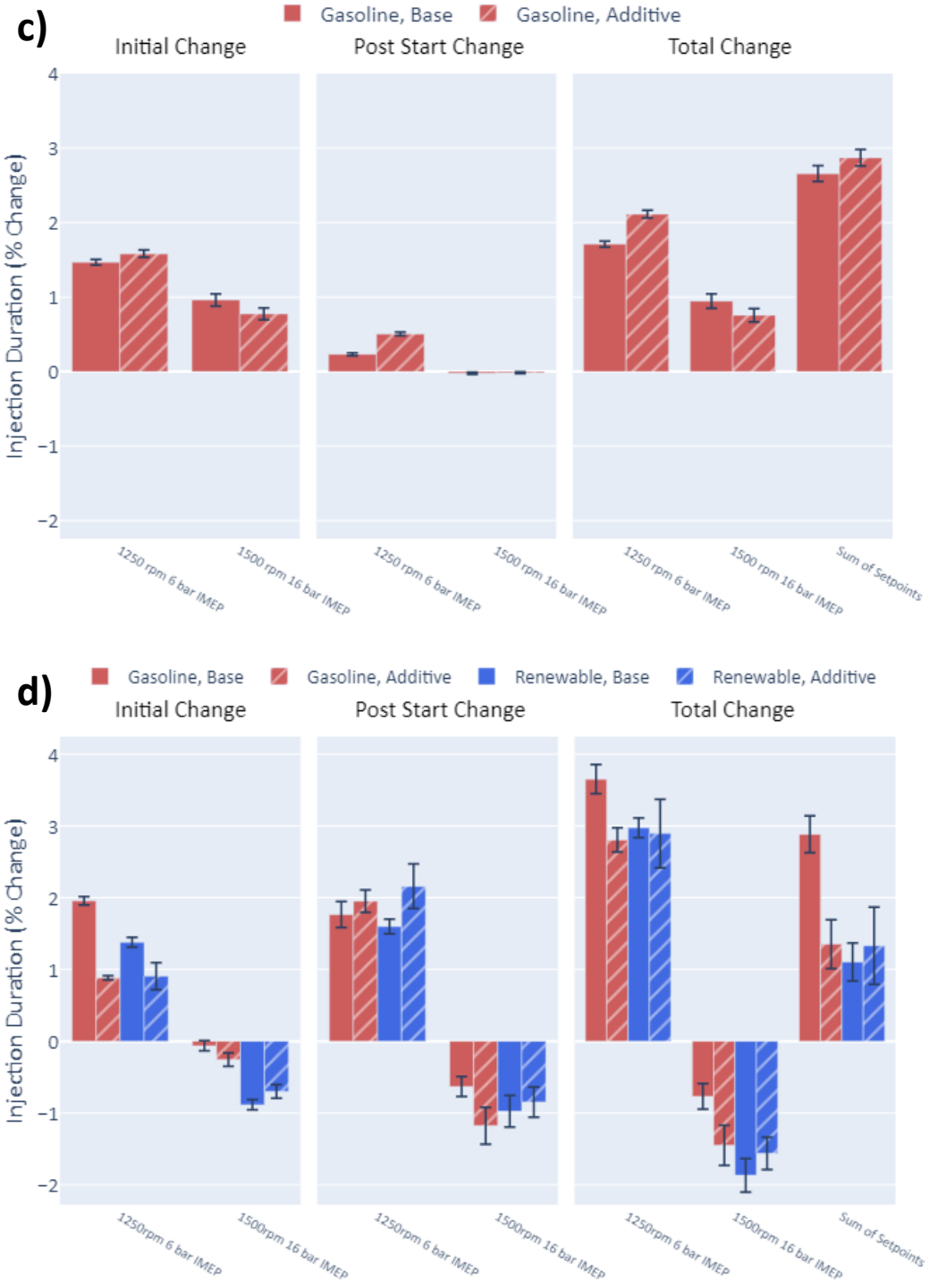


Figure 4-8: Average increase in injection duration of both Setpoints of a Sequence and their sum, averaged over a whole Cycle (including repeats) a) Cycle 7, b) Cycle 10, c) Cycle 11, d) Cycle 12. Error bars represent 90 % confidence intervals.

Low Load (Gasoline)

At low load in the *Initial Phase* there is a substantial difference between the Base and Additive fuels in *Cycles* 10 and 12. This corresponds well with results from Table 4-5 and Figure 4-7 where *Cycles* 10 and 12 were the *Cycles* that showed a difference between the Additive and the Base fuel with regards to overall injection duration percentage change, and Cycles 7 and 11 did not. The similarities between the Base and Additive results across all phases in *Cycle 7* provides further evidence to the Additive having minimal impact at the *Setpoint* 4000 rpm 7 bar IMEP. As discussed, this is primarily due to the Additive not having enough residence time on the injector.

At the low load *Setpoint*, in general the Additive makes the biggest difference in the *Initial Phase*, this is especially true for *Cycle* 12 and is also evident in *Cycle* 10. These results provide further evidence that the majority of the deposits are formed in the *Initial Phase* of the low load *Setpoint* and that the Additive has a significant impact in this phase. In the *Post Start Phase* the additives effectiveness appears to decrease, and in the case of *Cycle* 10 it even increases injection duration more than the Base Gasoline, suggesting that the Additive is less effective later in the *Setpoint*. The reason for this is unclear as by comparing *Cycles* 10 and 12 (Table 4-5), the additives ability to reduce injection duration increase has a positive correlation with low load *Setpoin*t duration. The last 15 min of the *Post Start Phase* in *Cycle* 12 was checked to investigate if it was responsible for the discrepancy in increased injection duration in the *Post Start Phase* of *Cycle* 10 compared to *Cycle* 12, but it showed the same trend as the rest of the *Post Start Phase* in *Cycle* 12, suggesting that the reason for the discrepancy may also be influenced by the high load *Setpoint.*

High Load (Gasoline)

The results from *Cycles* 10 and 12 showed that the Additive decreased injection duration at the high load *Setpoint* more effectively than the Base Gasoline, but this was not true of *Cycles* 11 and 7. This can be seen in the *Initial Phase* of *Cycles* 10 and 12. This is interesting as this too aligns well with the *Cycles* that showed the best overall difference in Injection Duration Increase with the Additive (Table 4-5). This suggests that the Additive is more effective at cleaning the deposits with high fuel pressure than the Base Gasoline.

In the high load, *Post Start Phase* the Additive appears to be more effective at cleaning in *Cycle* 12 compared to *Cycle* 10. This possibly helps to explain the positive correlation between the additives ability to reduce injection duration increase and low load *Setpoint* duration. It is theorised that a longer duration at the low load *Setpoint* with low fuel pressure (such as in *Cycle* 12) increases the Additive contact time with the existing injector deposits, allowing them to be washed away more easily in the subsequent high load *Setpoint*. Additionally Cycle 11 which had a short high load *Setpoint* duration in addition to a short low load *Setpoint* duration*,* saw no Additive reduction in injection duration compared to *Cycle* 12 with a longer duration at both *Setpoints.* This suggests that the high load *Setpoint* duration also assists Additive effectiveness as there is more time for it to clean the deposits following a long low load *Setpoint* where it has had time to soak into the deposit.

Low Load (Renewable fuel)

With regards to the Renewable Fuel the Additive did marginally reduce the injection duration increase in the *Initial Phase* of the low load *Setpoint*, but then marginally increased injection duration in the *Post Start Phase.* As discussed in section 2.5.6, there is the possibility that DCA should be specifically formulated for use with ethanol blends to be effective, possibly explaining the ineffectiveness of the Additive with the Renewable fuel. Alternatively, the quantity of deposits formed with the Base Renewable fuel was not sufficient for a significant difference with the Additive to be observed.

High Load (Renewable fuel)

At high load the Additive was also ineffective with the Renewable fuel as it seems that the Base Renewable fuel was already effective at cleaning the deposits and the Additive did not enhance this, resulting in both having similar changes in injection duration in all phases of the high load *Setpoint* duration.

Total Change

A combination of the Base Gasoline showing more fouling at low load and less cleaning at high load is reflected in Figure 4-8 in the *Sum of Setpoints: Total Change.* As mentioned in section 4.3.1.4: Cycling Between Loads, the absolute value of *Sum of Setpoints: Total Change* does not correlate with the overall change of Injection Duration seen in Table 4-5 and Figure 4-7 but the difference between the fuels does. From Table 4-5 and Figure 4-7 it can be said with more certainty that the Base Gasoline resulted in an increased injection duration time as these results compare the injection duration evolution across the whole *Cycle*. This difference comes from deposits, which must have

been generated at some point in the *Sequence.* Figure 4-8 shows a clear difference between the Additivated and Base Gasoline in the *Initial Phase* of both *Setpoints,* in *Cycles*, 10 and 12, and also in the high load *Post Start Phase* of *Cycle 12*. In both of these *Cycles* the average injection duration change over a *Sequence* (*Sum of Setpoints: Total Change*) is lower with the Additive than with the Base Gasoline, which aligns with the results seen in Figure 4-7 and Table 4-5. In addition to this *Cycles* 7 and 11 show minimal change in *Sum of Setpoints: Total Change* results when using base and additivated fuels, again aligning with the overall injection duration change results in Table 4-5 and Figure 4-7. So even though the absolute value for *Sum of Setpoints: Total Change* may be skewed by settling time, the differences between the fuels aligns well with results taken over the evolution of the whole test *Cycle*. This provides further evidence that the observations made from Figure 4-8 are due to fuel deposition and not engine control.

To further test the reliability of these *Cycles,* the results seen in Figure 4-8 were segmented into thirds for each *Cycle* (Appendix A). This was done to observe if the reason for the Base Gasoline fuel having an increased *Initial Change* at low load was due to the injection control system having to make larger adjustments due to fouling at the end of the test. However, as the results maintained the same trend in the first third of the *Cycle* with relatively clean injectors to what was seen in the final third when the injector nozzles were restricted, this does not seem to be the case.

Renewable Fuel and Gasoline Comparison

Figure 4-7 and Figure 4-8 show that the Renewable fuel reduced injection duration increase compared to the Base Gasoline fuel. The shape of the trendlines in Figure 4-7a

generally show a plateau later in the *Cycle*. This is especially evident with both the Additivated fuels and the gradient of the Base Gasoline trendline can also be seen to decrease in the second half of the *Cycle*. In contrast the Base Renewable trendline appears to be linear. As mentioned in the literature review section 2.2.3.3 it was found that fuels containing alcohol like the Renewable fuel have been found to create logarithmic trends where initially the injection duration increases rapidly due to intensive early deposit precursor formation but then a higher removal rate causes a plateau later on. This can be seen in the trendline of the Renewable fuel with the Additive but not so much with the Base Renewable fuel. However, it must be noted that the Renewable fuel did not change the injection duration much to start with, so maybe this trend would be seen if using a different test *Cycle*, which would allow more deposition with the Renewable fuel. Stępień (115) found in their study that the Gasoline trendline was linear until 50 hr of testing, which is similar to what is seen in Figure 4-7a, however after approximately 50 hr the Gasoline trendline also starts to plateau slightly, suggesting that it too has an equilibrium point. The Additivated Gasoline starts to plateau earlier in the *Cycle* and by the end the gradient is nearly zero. This appears to be one of the main benefits of the Additive, in that it brings the equilibrium point between formation and removal of deposits down so that it is reached earlier in the *Cycle*.

Low Load

Figure 4-8 shows that on average the *Initial Change* after transitioning from high to low load was lower with the Renewable fuel compared to the Base Gasoline fuel. This demonstrates that less fuel was being deposited in this *Phase* compared to the Base

Gasoline. The Renewable fuel shows similar levels of *Post Start Change* to both the Base and Additivated Gasoline fuels. The reason for the Renewable fuel generating less deposits in the *Initial Phase* of the low load *Setpoint* is due to the Renewable fuel having a lower E100 and E150 than the Gasoline fuel. E100 and E150 represent the proportion of fuel that has evaporated at 100 and 150 ^{o}C respectively. This results in the Renewable fuel evaporating at a higher temperature. As discussed in section 2.2.3.1, if most of the fuel evaporates on the injector tip then deposits are left behind, otherwise the remaining liquid fuel is washed away with the following injection. This helps to support the claims of Aradi and Kinoshita (101) (109) who claimed that as a fuels T90 increases there is less injector deposition. As the injector tip temperature was not directly measured in these tests the exact relationship between fuel evaporation temperatures and the injector tip temperature is uncertain, this is something that could be investigated in future studies. The Gasoline fuel also had a higher olefin content than the Renewable fuel which was found in literature to increase injector deposition. This is supported by the increased levels of fouling seen with the Gasoline fuel. The increased level of aromatics in the Renewable fuel seemed to either have no impact on injector deposition or it was cancelled out by the other factors mentioned above being more dominant.

High Load

When inspecting Figure 4-8, it can be seen that the majority of the difference between the Renewable and Gasoline Base fuels appears to have come from the high load *Setpoint*. Where the Renewable fuel reduced the Injection Duration Change significantly in the *Initial Phase* of the high load *Setpoint*, which continued but with less of a

difference in the *Post Start Phase*. This is likely due to fuels containing ethanol having a strong cleaning effect (115).

Visual/Optical Inspection of Injectors

The deposits on the injectors are also visually evident, this can be seen by comparing the pre-test (Figure 4-9) images to the post-test images (Figure 4-10). This is especially interesting with the Renewable fuel as even though the evolution in injection duration (Figure 4-7) did not provide much evidence for injector deposits, deposits are clearly visible in Figure 4-10c and d. The injectors appear to have darker deposits when running with the Renewable Base fuel compared to the Gasoline Base fuel, which supports findings by Slavchov (15), who as mentioned in the literature review, predicted that the presence of oxygen in alcoholic fuels would lead to higher levels of external injector deposits. Figure 4-10c shows zoomed in photos of the injector nozzle after running with the Renewable Base fuel. The majority of the deposits have built up around the outside of the injector tip as well as around the front face of the injector facing the camera. However, the inside of the nozzles appears relatively clean. The photos from Figure 4-10d show that the Additive was successful in reducing the buildup of deposits on the outside of the nozzle with the Renewable fuel, the deposits also appear to be lighter in colour compared to the Base test results. The appearance of the injectors looks similar after both the Base Gasoline test and the Gasoline Additive test, especially around the nozzle. However, the outside of the injector does look darker with the Base fuel compared to the Additivated fuel.



Figure 4-9: Photos of the three injectors, clean, pre-test.

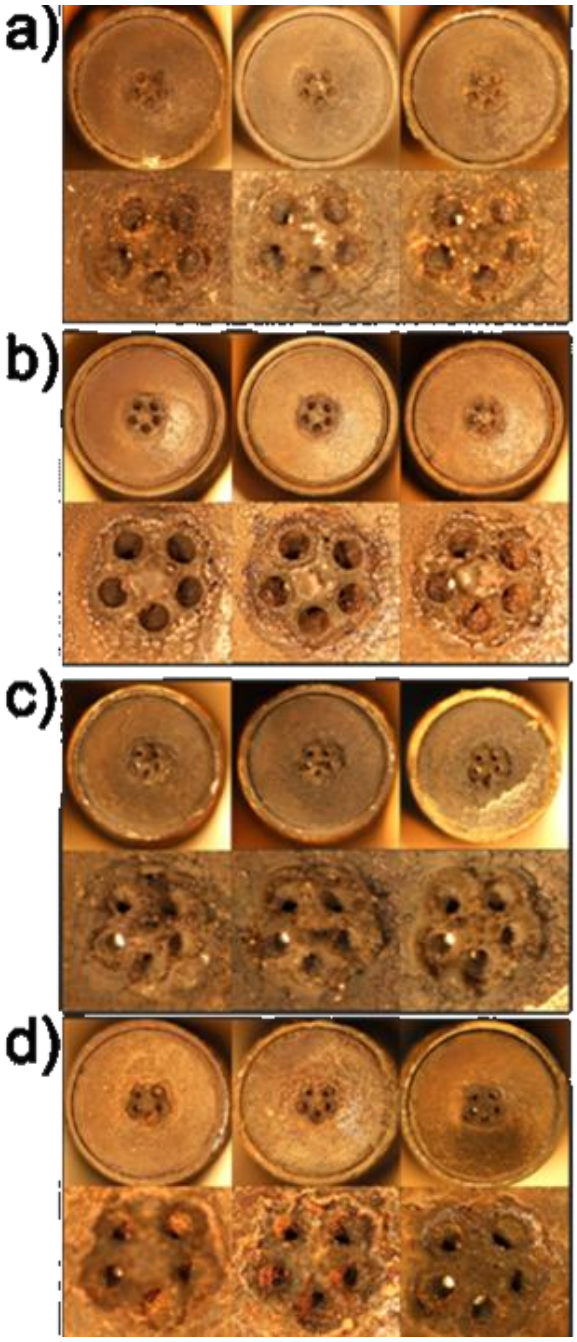


Figure 4-10: Photos of external deposits and nozzle deposits from a) Gasoline Base Fuel, b) Gasoline with Additive, c) Renewable Base, d) Renewable with Additive.

4.3.2.3 Impact on Engine Performance, Fuel consumption and Emissions

Fuel Consumption

The fuel consumption (Figure 4-11) did not change by more than ± 1 % throughout all the tests. This therefore had little impact on the injection duration. It can also be deduced that with little change in fuel consumption there was an insignificant change in the efficiency of the engine. This is especially interesting with regards to the Renewable fuel which showed extensive deposit build up around the nozzle, which as discussed in the literature section: 2.2.4, has been known to disrupt injection patterns and reduce efficiency but did not appear to have an impact in this study.

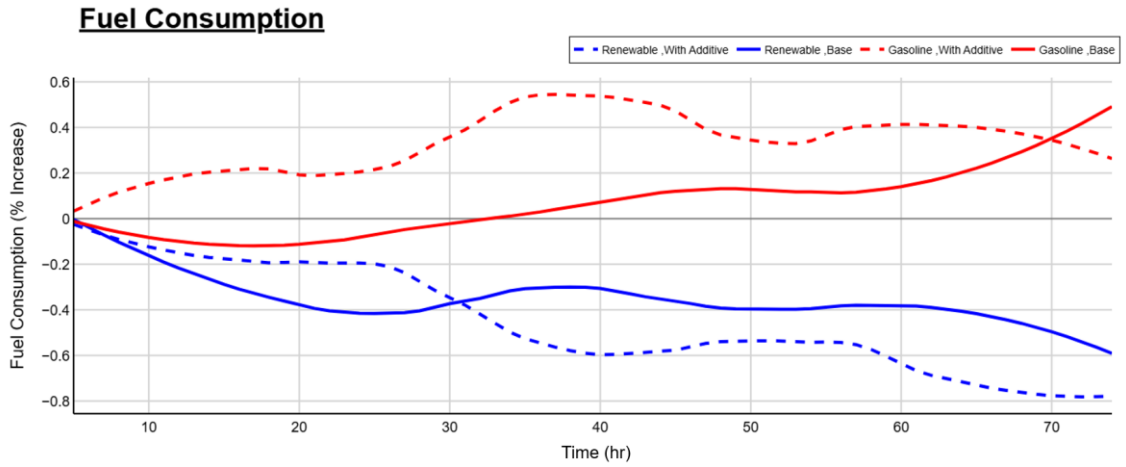


Figure 4-11: Fuel consumption change throughout Cycle 12 (averaged across Setpoints).

THC and CO

The emissions for THC and CO are shown in Figure 4-12 and Figure 4-13. These both remain relatively unchanged and even decrease in some cases. It must be noted that the 10 % CO decrease in Figure 4-13 only represents a decrease of 0.08 % in volumetric concentration. Any changes that were observed were insignificant as the THC and CO emissions results day-day variation was more than the overall evolution observed

throughout the experiment. This, along with the fuel consumption data remaining unchanged further suggests that there was no or an insignificant change in combustion efficiency due to the internal and external deposits buildup. In addition to these results, combustion timings and durations were found to be insignificantly impacted throughout the test, further suggesting there was little impact on combustion quality.

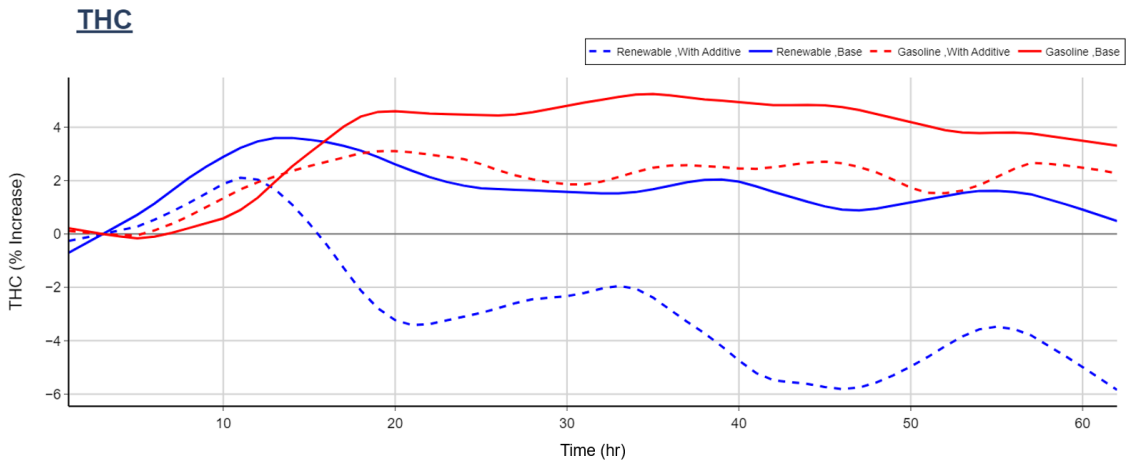


Figure 4-12: THC change throughout Cycle 12 (averaged across Setpoints).

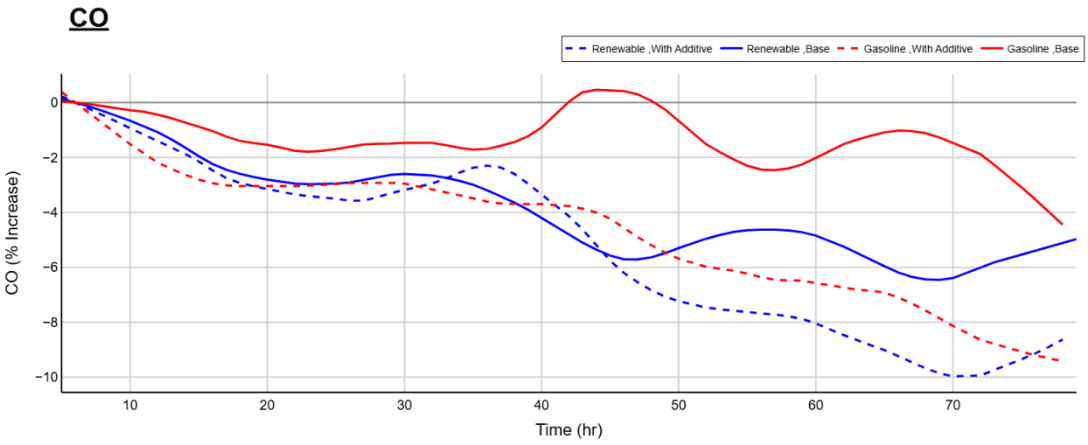


Figure 4-13: CO change throughout Cycle 12 (averaged across Setpoints).

Soot

The increase in FSN from the start to the end of *Cycle* 12 is shown in Figure 4-14. Soot increased throughout the experiment for all fuels and additives at the high load condition. The low load condition however saw a relatively small increase and started with minimal soot in the first place as shown in Table 4-2, so further discussion is concentrated on the high load *Setpoint*. At the high load *Setpoint* both fuels experienced an increase of approximately 0.035 FSN throughout the test with both the Base fuel and Additive (Figure 4-14). Figure 4-15 shows that the Renewable fuel started and ended the test with more soot than the Gasoline, this is due to the increased aromatic content in the renewable fuel increasing soot and PM emissions, as discussed in section 2.2.3.3. However, the Renewable soot results do appear to plateau after 40 hr, whereas the Gasoline tests seem to a carry on rising, suggesting that with a longer *Cycle*, the Gasoline would carry on increasing its soot emissions, whereas the Renewable would not.

The increase in soot throughout the experiment is likely due to the deposit buildup on the inside and outside of the injector nozzle, disrupting fuel spray patterns. This hypothesis is supported by the fact that the soot increases with all the fuels and additives which all showed external deposit buildup in Figure 4-10. The high FSN value of the Renewable fuel throughout the *Cycle* is responsible for the high levels of external injector deposits in Figure 4-10c and d, which initially increases the FSN values further, however the low levels of internal injector deposits in the Renewable tests do not result in the FSN levels rising continuously. On the contrary, the constant increase of the Gasoline FSN compared to the logarithmic trend of the Renewable fuel suggests that

over time the larger buildup of internal injector deposits (indicated by the injection duration increase) in the Gasoline tests will continue to increase FSN.

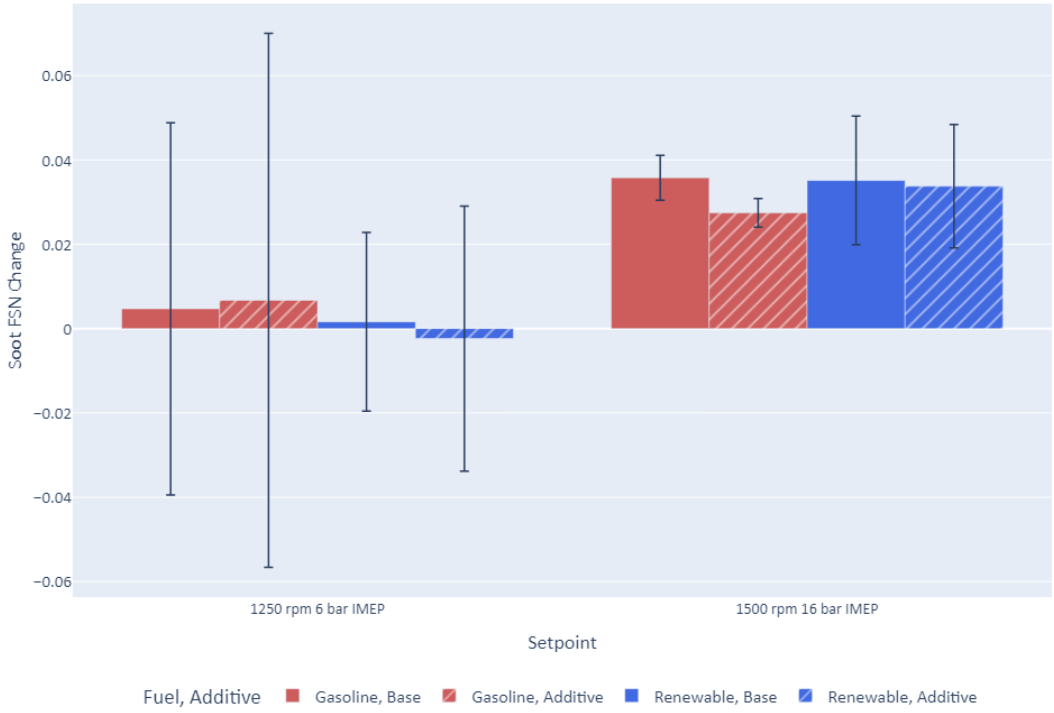


Figure 4-14: Change in FSN at the end of the Cycle compared to the beginning.

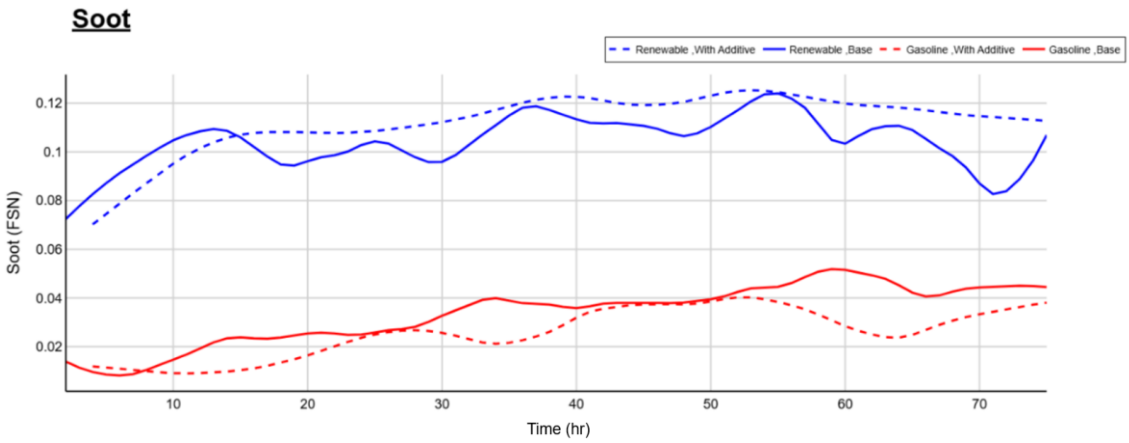


Figure 4-15: Evolution of soot at 1500 rpm 16 bar IMEP.

There is a small reduction in the soot FSN change seen in Figure 4-14 with the Additive, possibly due to its reduced level of internal injector deposits. However, the difference

in soot is less pronounced than the difference in injection duration, suggesting the external deposits seen in both the Additivated and Base Gasoline results also influence the soot levels. It would appear that the Additive is more effective at cleaning inside the nozzle and less effective at mitigating the impacts of external injector deposits.

A further test was conducted using a GPF. The results from this test (Figure 4-16) show that at both high and low loads the GPF was capable of significantly reducing the soot output of the engine with the Renewable Fuel to a comparable level with the Base Gasoline fuel. Thus, the increased soot observed with the Renewable fuel is not a cause for concern as long as a GPF is used to mitigate it.

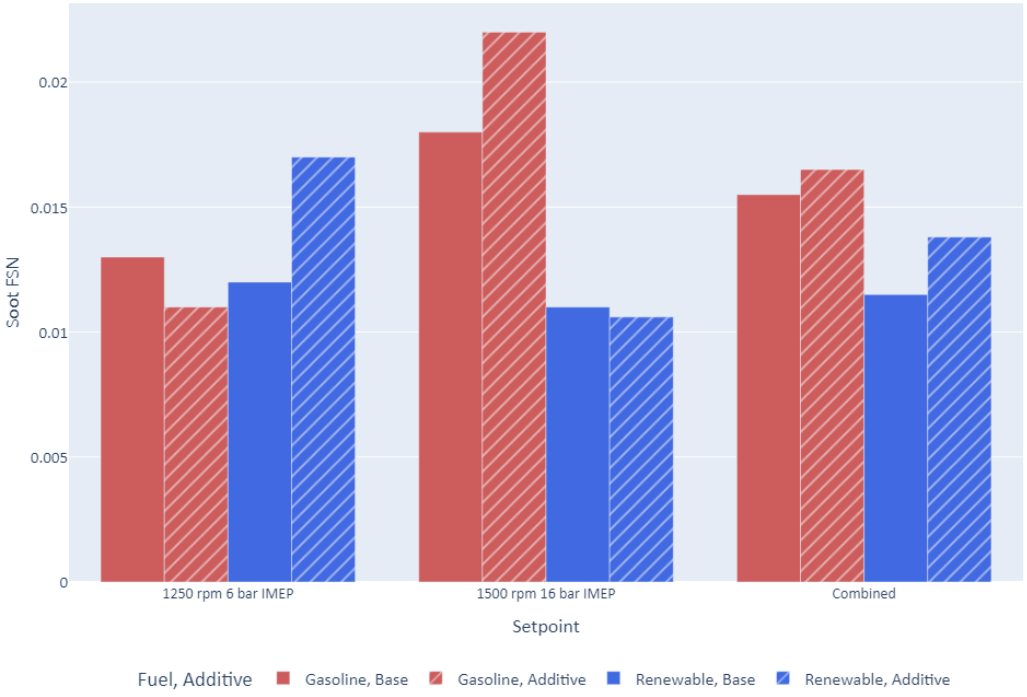


Figure 4-16: Soot Results (FSN) from the end of each Cycle with GPF.

4.4 Conclusion

The research confirmed that cycling between high and low loads is critical in order to generate injector deposits quickly. This was due to the *Initial Phase* of the low load

Setpoint (after transitioning from high load) retaining residual temperature from the high load *Setpoint*, combined with the low fuel pressure of the low load *Setpoint*, allowing for the rapid generation of injector deposits.

The process of adaptive and iterative testing was successful, because a total 105 hr of *Cycle* testing in addition to approximately 20 hr of *Setpoint* testing resulted in *Cycle* 7 which could successfully generate significant injector deposits in 37.5 hr. The most important parameters in terms of generating this *Cycle* were found to be low fuel pressure at low load, and the temperature generated at high load. Other engine parameters such as SOI, THC and PM emissions did not seem to correlate significantly with injection duration increase. In terms of *Cycle* parameters, a balance needed to be struck to generate deposits, where the *Setpoint* duration at both loads was at least 15 min but the *Sequence* duration had to be short enough to allow for multiple transition events from high to low load.

The adaptive process took a further five *Cycles* to create a sufficient *Data Pool* to show a range of results for additive effectiveness. This took longer due to the delicate balance of engine and *Cycle* parameters required to both generate deposits and change the effectiveness of the Additive (allowing for analysis of which parameters impact the Additive to be analysed). It was concluded that the Additive had its most significant effect during the *Initial Phase* of the low load *Setpoint* when being used with Gasoline. In addition to this it also increased the removal rate of the injector deposits when operating at the high load *Setpoint.* Furthermore, it was found that in order to see a significant difference between Base and Additivated Gasoline *Cycle* results, a longer

duration at low load was required in conjunction with a high load *Setpoint* duration of at least 15 min. This was theorised to be due to the Additive needing sufficient time at low fuel pressure where it could soak into the existing deposits. Sufficient additive residence time was also found to aid cleaning as the Additive was less effective in preventing deposit accumulation at a high speed-low load *Setpoint*, whereas it demonstrated enhanced efficacy at a low speed-low load *Setpoint*.

The Renewable fuel also impacted the injector deposit results, both internally and externally. Internally the Renewable fuel generated less deposits at low load due to its higher evaporation temperature and lower olefin content. It also removed more deposits at high load due to the effective cleaning properties of ethanol. The Additive however was less effective at the high load as it could not add to the already effective cleaning of the Base Renewable fuel and could not reduce low load deposition in the *Initial Phase.*

The results from all sets of fuels had minimal impact on fuel consumption, CO and THC but did impact soot emissions. The Renewable fuel generated more soot initially due to the significant external deposits on the injector and high aromatic content, which also then led to higher initial soot levels, but this did not impact injection duration. However, the soot levels with the Renewable fuel stopped increasing whereas the Gasoline soot emissions continued increasing throughout the *Cycle*. The Additive marginally decreased the soot levels with the Gasoline fuel but not the Renewable fuel. When a GPF was used, the soot emissions from all fuels were then brought to approximately the same level.

5. GDI ENGINE EGR COOLER FOULING

5.1 Introduction

With the growing trend of engine downsizing and turbocharging the combination of GDI and EGR is becoming more popular. It is common practice to utilise a heat exchanger (EGR Cooler) in conjunction with an external EGR system, with the objective of increasing intake density while simultaneously reducing knock and in-cylinder heat transfer. However, EGR Coolers are susceptible to fouling from high-temperature exhaust gases, soot and HC emissions. As discovered in the previous chapter different fuels and injector deposits can lead to increased levels of soot in a GDI engine exhaust and thus it is important to study the impacts of poor exhaust quality on exhaust components such as the EGR Cooler.

The fouling can result in reduced effectiveness of the EGR Cooler, leading to increased outlet temperatures as well as reduced flow rate due to the build-up of deposits increasing the pressure drop across the Cooler. This fouling can be reduced through the use of additives which by reducing CCD and injector deposits, can change the composition of the exhaust to one which is less likely to cause EGR Cooler Fouling. This is investigated in this chapter by comparing the impact of three different additives on EGR Cooler performance, as well as a brief analysis of their impact on injector behaviour. The results are then contextualised by estimating the potential impact of the change in EGR Cooler performance on BSFC and MFB50 in various EGR configurations.

5.2 Methodology

Three additivated fuels (Fuel Add 1, Fuel Add 2, Fuel Add 3) were experimentally investigated along with a reference gasoline fuel (Ref Fuel). The fuels were tested over a variety of *Setpoint*s, selected to cover a wide range of emissions, temperatures and flow rate levels, to accelerate the formation of deposits in the injector and EGR Cooler. The *Setpoints* and *Cycle* are shown in Table 5-1.

Table 5-1: Engine operating Setpoints.

Setpoint	Speed (rpm)	BMEP (bar)	THC (ppm)	Soot (FSN)	EGR Cooler Inlet Temperature (°C)	Exhaust Volumetric Flow rate (m^3/min)
1	1250	7	2303	0.011	250	0.4
2	1250	9	1961	0.013	270	0.47
3	4000	8	1550	0.067	555	1.1

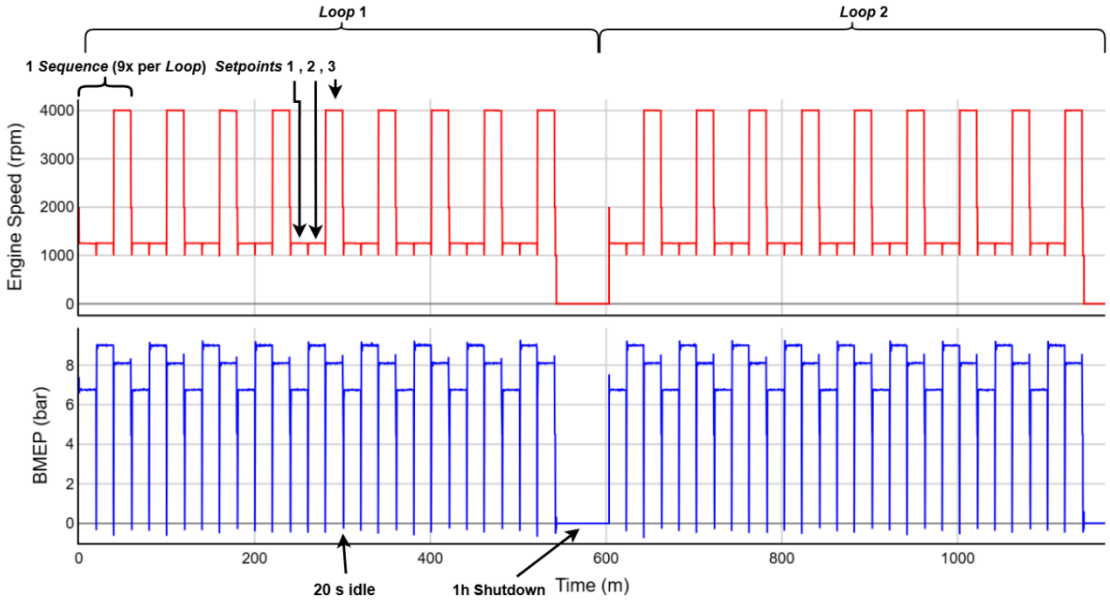


Figure 5-1: Graph showing how speed and BMEP change for the first 2 Loops of the Cycle.

Between each experiment the fuel injectors were cleaned and prepared for the new fuel. Figure 5-1 shows the *Cycle* used in the experiment consisting of *Loops* of 9 *Sequences* of 3 *Setpoints* going from *Setpoint* 1-3 sequentially, with a 20 second idle period between each *Setpoint*. The engine stayed at each *Setpoint* for 20 min. After 9 *Sequences* the engine shutdown for 1 hr, completing a *Loop*. 7 *Loops* were carried out with the Reference Fuel and Fuel Additive 1. Further tests were conducted with the other two additives but as it was observed they were having minimal impact on EGR Cooler deposit formation, these tests were ended after 4 *Loops.* Valves 1 and 2 (Figure 3-1) would be adjusted to keep the flowrate constant for each *Sequence* at the same *Setpoint*. This kept the combined *dP* across the Cooler, valve 1 and valve 2 constant, keeping total engine backpressure constant when operating at a particular engine *Setpoint* regardless of fouling levels.

5.2.1 Analysis of EGR Cooler Effectiveness and Impact on Engine Performance

The variation of injection duration at each *Setpoint* throughout the test was compared to the variations of soot, THC and fuel consumption to establish a relationship with fuel-derived injector deposit formation. EGR Cooler performance was quantified by effectiveness and *dP*. The impact of reduced EGR Cooler effectiveness on intake temperature and engine performance for the scenarios was estimated using equations 2-11 assuming an EGR rate of 15 %. These scenarios are shown in Figure 5-2. Scenario 1 was designed to represent an LP EGR loop with no GPF (with temperatures representative of the experimental facility), (Figure 3-1) where the cooler out

temperature would be adiabatically mixed with the intake pre compressor. Scenario 2 represents a theoretical HP EGR loop that would have the same EGR Cooler outlet temperature as the EGR outlet temperature from the actual experiment. This temperature then mixes with the intake manifold. Scenario 3 predicts how a higher EGR inlet temperature would impact the intake manifold temperature in an HP setup. The position of the EGR is further (3.65 m) from the engine than in a real vehicle leading to an unrealistic EGR Cooler inlet and outlet temperatures for an HP setup. Therefore, a more realistic inlet temperature value (940 ^{o}C) is chosen based on Fischer (22), who investigated a comparable engine (in terms of engine displacement, number of cylinders, turbocharger and power) equipped with an HP EGR loop experimentally evaluated at 15 % EGR. Fischer's experiments were conducted at a higher load than the *Setpoint*s in this study which aligns well with the purpose of Scenario 3: to observe the impact of a fouled EGR Cooler when operating under full load engine *Setpoint*s. Scenario 4 represents an HP pre intercooler setup and was only used with reference to *dP* and not temperature.

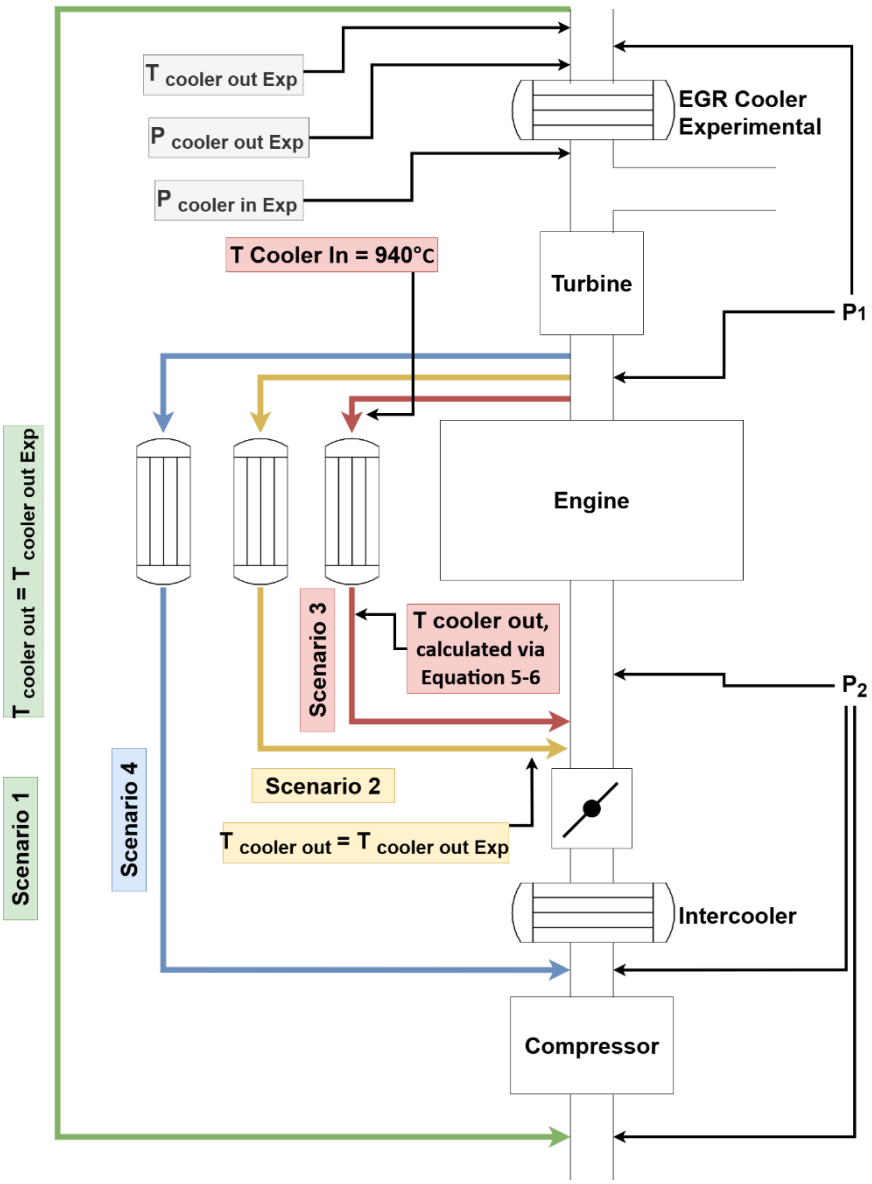


Figure 5-2: Schematic showing the different scenarios used in analysis.

The theoretical EGR Cooler exit temperature was calculated by estimating the heat transfer coefficient of the real EGR Cooler by using the experimental results. An assumption was made to use the EGR Cooler effectiveness that was found experimentally. In reality the effectiveness would likely be lower in Scenario 3 compared to the experimental results, due to increased inlet temperature and thus fouling. However, this scenario still shows a useful insight into the potential impacts of Cooler

fouling. Equation 5-2 (derived from Equation 5-1) represents the heat transfer across the EGR Cooler, by estimating the temperature difference between the gas and the Cooler wall with the Logarithmic Mean Temperature Difference (ΔT_{LMTD}) and using Equation 5-4, the EGR exit temperature (T_{h2}) can be obtained. ΔT_{LMTD} was calculated as a parallel flow heat exchanger (Equation 5-3) (counter flow was also tried but did not make a significant difference to the final results). When using the EGR inlet temperature of 940 °C, ΔT_{LMTD} would be different to the experimental data, but $\frac{L}{u}$ would be the same. It was assumed that UA (Equation 5-5) would not change with 940 °C EGR Cooler inlet temperature, because the average bulk gas temperature does not vary significantly. Therefore, gas properties such as thermal conductivity which determine U will remain largely unchanged. The other terms of Equation 5-5 such as $R_f + R_w + R_{conv,c}$ would also remain unchanged due to the coolant having a much higher heat capacity than the gas and consequently the neighbouring wall temperature would be largely unchanged.

$$\int_{t1}^{t2} \dot{Q}\, dt = \int_{t1}^{t2} UA(\Delta T_{LMTD})\, dt \qquad \textit{Equation 5-1}$$

$$\dot{Q} = (t_2 - t_1)\, UA\, \Delta T_{LMTD} = \frac{L}{u} UA(\Delta T_{LMTD}) \qquad \textit{Equation 5-2}$$

$$\Delta T_{LMTD} = \frac{(T_{h2} - T_{c2}) - (T_{h1} - T_{c1})}{\ln\left(\frac{T_{h2} - T_{c2}}{T_{h1} - T_{c1}}\right)} \qquad \textit{Equation 5-3}$$

$$\dot{Q} = \dot{m}\, c_{p,avg}\, (T_{h2} - T_{h1}) \qquad \textit{Equation 5-4}$$

$$\frac{1}{UA} = R_{conv,g} + R_f + R_w + R_{conv,c} \qquad \textit{Equation 5-5}$$

As a next step to estimate the Cooler outlet temperature for Scenario 3, the heat transfer (*Q*) is calculated by using the experimental data (estimating ΔT_{LMTD} by Equation

5-2) and using Equation 5-4. Equation 5-2 can be rearranged to find $\frac{L}{u}UA$ (Equation 5-6) and by using experimental data and assuming the coolant temperature to remain the same, the outlet temperature for Scenario 3 with an inlet temperature of 940 ^{o}C is estimated (Equation 5-6).

$$\frac{Q}{\Delta T_{LMTD}} \approx \frac{L}{u}UA \approx \frac{\dot{m}\, c_{p,avg}\,(T_{h2}-T_{h1})}{\frac{(T_{h1}-T_{c1})-(T_{h2}-T_{c2})}{\ln\left(\frac{T_{h2}-T_{c2}}{T_{h1}-T_{c1}}\right)}} \qquad \textit{Equation 5-6}$$

The intake manifold temperature was calculated using Equation 5-7 (all scenarios), where air and EGR properties changed depending on the scenario. The intake manifold temperature is calculated assuming adiabatic mixing between the EGR Cooler exit and the pre compressor flow (Scenario 1) and experimental intake manifold measurement points, upstream of the hypothetical EGR mixing point (Scenario 2 and 3).

The post compressor temperature (Scenario 1) was estimated using Equation 5-8. The adiabatic compressor efficiency was calculated from the experimental results and was assumed unchanged with the added flow rate from the EGR system.

$$T_{new} = \frac{c_{p,air}\; T_{air}\;(1-EGR_{\%}) + c_{p,EGRt}\; T_{EGR,cooler\ exit}\;\; EGR_{\%}}{c_{p,air}\;\;(1-EGR_{\%}) +\; c_{p,EGR}\;\;\; EGR_{\%}} \qquad \textit{Equation 5-7}$$

$$T_{out} = T_{in} + \frac{T_{in}}{\eta_{comp}}\left(\frac{P_{in}}{P_{out}}^{\frac{\gamma-1}{\gamma}} - 1\right) \qquad \textit{Equation 5-8}$$

As Scenario 1 represents LP EGR the air and EGR flow mix passes through the intercooler after the compressor, to predict the intake manifold temperature post intercooler the following method was used. $\frac{L}{u}UA$ (from Equation 5-6) is calculated from the experimental results, adjusted for the increased flow rate through the intercooler. Of the terms in Equation 5-5 only gas convection will change with mass flow rate, with the

other terms remaining near constant due to the temperature increase in the intercooler being small. Equation 5-9 is found by rearranging Equation 5-5 and representing $R_{conv,g}$ with the gas forced heat transfer coefficient and representing the other terms as a constant. Equation 5-10 approximates the gas heat transfer coefficient via the Nusselt's number, approximated via the Dittus-Boelter equation, as the flow was predicted to be turbulent within smooth pipes (180). All terms except for mass flow rate are constant so are grouped into the constants *K* and *C.* Then substituting Equation 5-10 into Equation 5-2, representing *u* in terms of $\dot{m}, \rho \text{ and } A$, bringing *L,* $\rho \text{ and } A$ into the constant *K* and rearranging yields Equation 5-11. This equation relates $\frac{Q}{\Delta T_{LMTD}}$ to $\dot{m}$, both of which can be calculated from the experimental data. $\frac{Q}{\Delta T_{LMTD}}$ is calculated the same way as with the EGR Cooler (Equations 5-2 – 5-6) and $\dot{m}$ was recorded. By plotting $\frac{Q}{\Delta T_{LMTD}}$ against $\dot{m}$ at all *Setpoint*s with a range of flow rates a line of best fit of the form seen in Equation 5-11 could be plotted and allowed $\frac{Q}{\Delta T_{LMTD}}$ with increased $\dot{m}$ to be approximated and then T_{h2} was found from Equation 5-6.

$$U\,A = \; h_g\,A + C \;\;,\;\; C = Constant \qquad \textit{Equation 5-9}$$

$$U\,A = \frac{Nu\;\; k_g\;\; A}{d} + C \;=\; \frac{0.023\;\; Re^{0.8}\;\; Pr^{0.3}\;\; k_g\;\; A}{d} + C \;=\; \frac{0.023\;\; (\frac{\dot{m}\,L}{A\;\mu})^{0.8}\;\; Pr^{0.3}\;\; k_g\;\; A}{d} + C \qquad \textit{Equation 5-10}$$

$$U\,A = K\,\dot{m}^{\,0.8} + C \;\;,\qquad K = constant$$

$$Q = \frac{L}{u}(K\,\dot{m}^{\,0.8} + C)\;\Delta T_{LMTD} \;\leftrightarrow\; \frac{Q}{\Delta T_{LMTD}} = \; K\,\dot{m}^{\,-0.2} + C \qquad \textit{Equation 5-11}$$

The *dP* caused by fouling of the experimental EGR Cooler, named *EGR Cooler dP*, was calculated by subtracting $P_{Cooler\ out\ Exp}$ from $P_{Cooler\ in\ Exp}$ (Figure 5-2). This was compared to a theoretical *Total EGR dP*, calculated by subtracting P_2 from P_1 to give

context to the impact of *EGR Cooler dP* increase due to fouling. $P_2$and P_1 are pressure readings taken from the experimental data in the locations where the theoretical EGR system from each scenario would enter and exit the intake and exhaust respectively. This is different for each scenario and is shown in Figure 5-2.

5.3 Results and Discussions

5.3.1 Impact of Fuel on Engine Operation Parameters and Carbonaceous Emissions

The change in injection duration throughout the experiment is shown in Figure 5-3. An increase in injection duration suggests either fuel flowrate has been restricted requiring a longer injection for the same injected mass, or an increase in injected fuel mass due to reduced efficiency or both. The change in injection duration was divided by the change in fuel consumption so that the small changes seen would be due to a restriction of the injector nozzles. Fuel flow rate (Figure 5-4) is calculated by dividing air mass flow rate by lambda.

Injection duration increases less with Fuel additive 1 than with the other fuels at all engine *Setpoint*s. Fuel additive 2 and 3 reduced injection duration increase at *Setpoint* 2 and Fuel additive 2 also reduced injection duration at *Setpoint* 1. Although the change in injection duration with the Reference Fuel is only approximately 1 % it does appear to steadily increase over a long time, indicating the increase to be due to fouling over time. The injection duration increase from Fuel Additive 1 is consistently lower

throughout the test at all *Setpoint*s and fluctuates around 0 %, this is because the Additive successfully prevented the formation of nozzle deposits.

It can be observed that there is no significant trend on the variation on fuel consumption throughout the test. It is therefore likely that the changes in injection duration are due to fuel flowrate restrictions due to the formation and accumulation of fuel-derived deposits in the injector. It can also be hypothesised that none of the fouling caused by these fuels had a significant impact on engine efficiency.

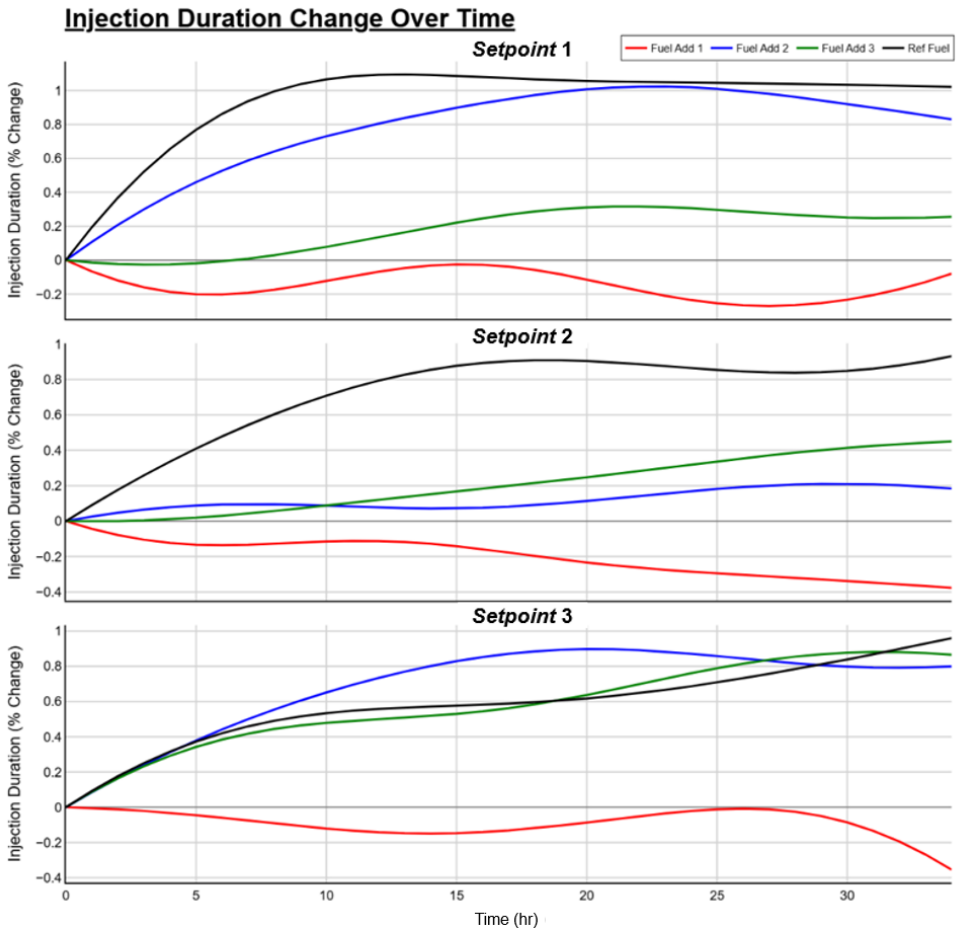


Figure 5-3: Evolution of injection duration throughout test.

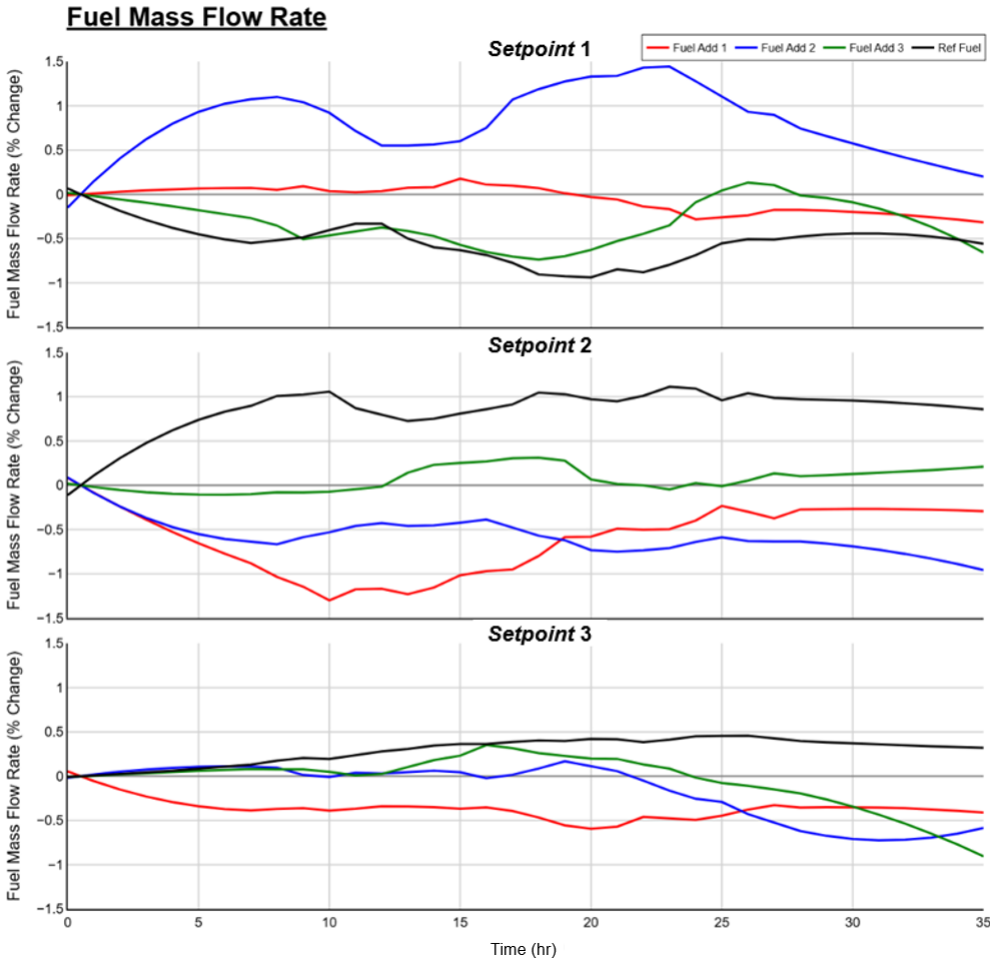


Figure 5-4: Fuel mass flow rate.

THC emissions increased throughout the accelerated method for all fuels (in particular for the Reference Fuel), except for Fuel Additive 1 (Figure 5-5).These results support the hypothesis of injector deposits restricting fuel flow, and disrupting fuel spray patterns and the diffusion flame, leading to an increase in HC emissions. This is also supported by other studies elsewhere (174) (117).

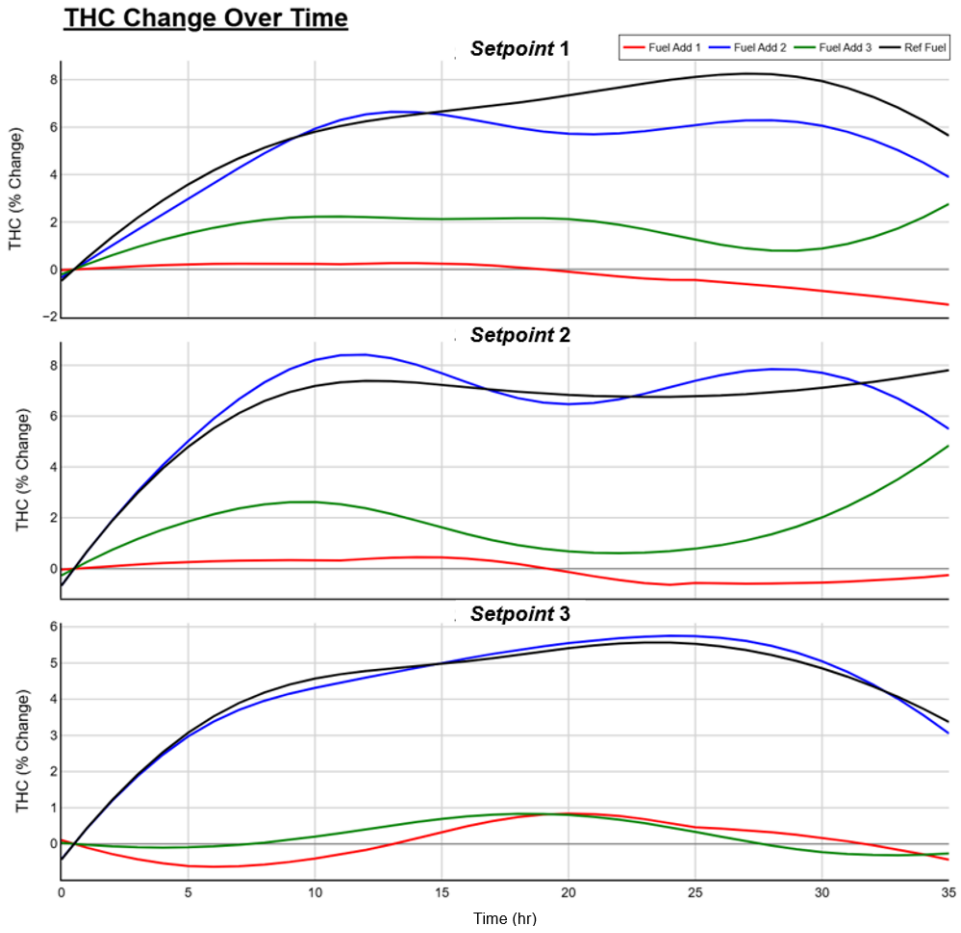


Figure 5-5: THC measured at EGR Cooler out.

Figure 5-6 shows soot emissions. A notable observation includes the soot emissions increasing significantly in the first few hours of the *Cycle* for most fuels and *Setpoint*s. This increase in soot emissions is a consequence of deposits being formed on the injector during the first stage of the *Cycle*, which has been proven to increase soot emissions (181).(39) (182) (116). It has been reported in literature that high particulate emissions lead to deposits forming on the injector (12) (71) (12), which will then in turn generate more particle emissions. Fouled injectors have been proven to increase soot emissions drastically, mainly due to how the deposits distort the spray formation and how deposits on the injector tip impact combustion (182). After the first exponential increase in soot

emissions, the soot levels remain constant or slightly increase. The capabilities of Fuel additive 1 to control injector deposit formation/accumulation should be highlighted, evidenced by obtaining the lowest increase (or even not increasing) with respect to injection duration, HC and soot results. The contents of the additive cannot be disclosed here but the results show that an effective additive can reduce injector fouling and hence avoid any detrimental impact on combustion efficiency and emissions, as well as have the potential to reduce fouling of components downstream (e.g. EGR Cooler) as is shown below.

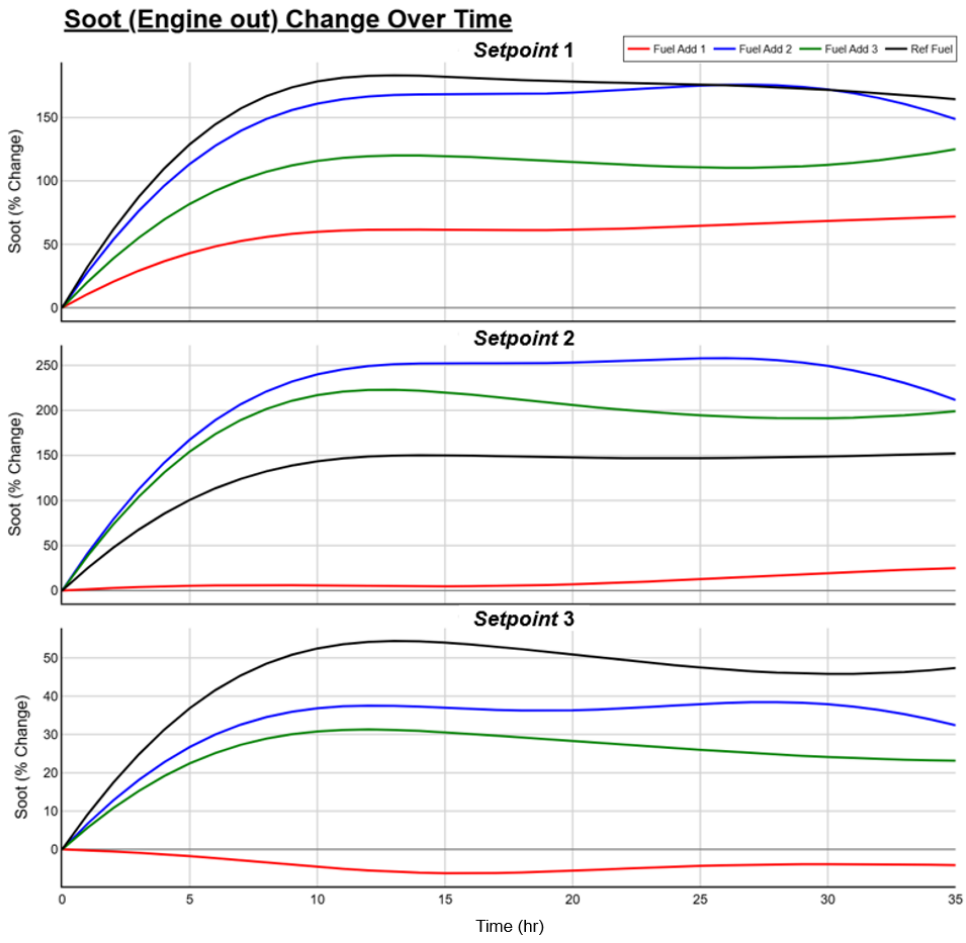


Figure 5-6: Soot measured at engine out.

5.3.2 Impact of Fuel on EGR Cooler Performance

To observe the impacts of the fuel on the EGR Cooler performance, *dP* (Figure 5-7) was measured and the average Cooler effectiveness (Equation 5-12 and Figure 5-8) was calculated throughout the accelerated injector deposits *Cycle*. In this section, only Fuel additive 1 and the Reference Fuel are shown as they showed the largest differences in EGR Cooler performance.

$$\epsilon_{EGR} = \frac{c_{p,avg}(T_{h2} - T_{h1})}{c_{p,avg}(T_{c1} - T_{h1})} \qquad \textit{Equation 5-12}$$

Equation 5-13 represents the fouling factor, essentially how much soot is deposited (20). In summary the fouling factor increases with an increase in the soot concentration, EGR inlet temperature, and the hydraulic length of the cooler, and decreases with an increase of gas velocity (20).

$$R_{\dot{f}} = \frac{K_1 C_s}{K_2 k_d u} \cdot \{1 - \left[\frac{T_w}{T_0} + \left(1 - \frac{T_w}{T_0}\right) . \exp\left(-4 \, . St \, . \frac{L}{D}\right)\right]^{Pr.K_{th}}\} \qquad \textit{Equation 5-13}$$

$$St = 0.023 Re^{-0.2} Pr^{-0.6}$$

At *Setpoint* 3 the EGR inlet temperature is approximately 300 ºC higher than the other *Setpoint*s, resulting in more fouling, represented by the largest change in *dP* (Figure 5-7) and effectiveness (Figure 5-8). The exhaust temperatures entering the EGR Cooler for *Setpoint*s 1 and 2 are 250 and 270 ºC respectively, hence why they have similar effectiveness changes throughout the experiment. The flow gas velocity at *Setpoint* 3 is approximately double that of *Setpoint*s 1 and 2, but the effectiveness drops (Figure 5-8) as temperature has a larger impact than flow velocity.

At *Setpoint*s 1 and 2 the Cooler fouling has a larger impact on *dP* in terms of percentage change than Cooler effectiveness, so the *dP* is more likely to have a larger impact on engine operation at these types of *Setpoint*s. Engine restarts result in moments of effectiveness recovery as can be seen in Figure 5-8 every 10 hr, when the engine has been shutdown. This was seen by Teng et al (20) who found similar results.

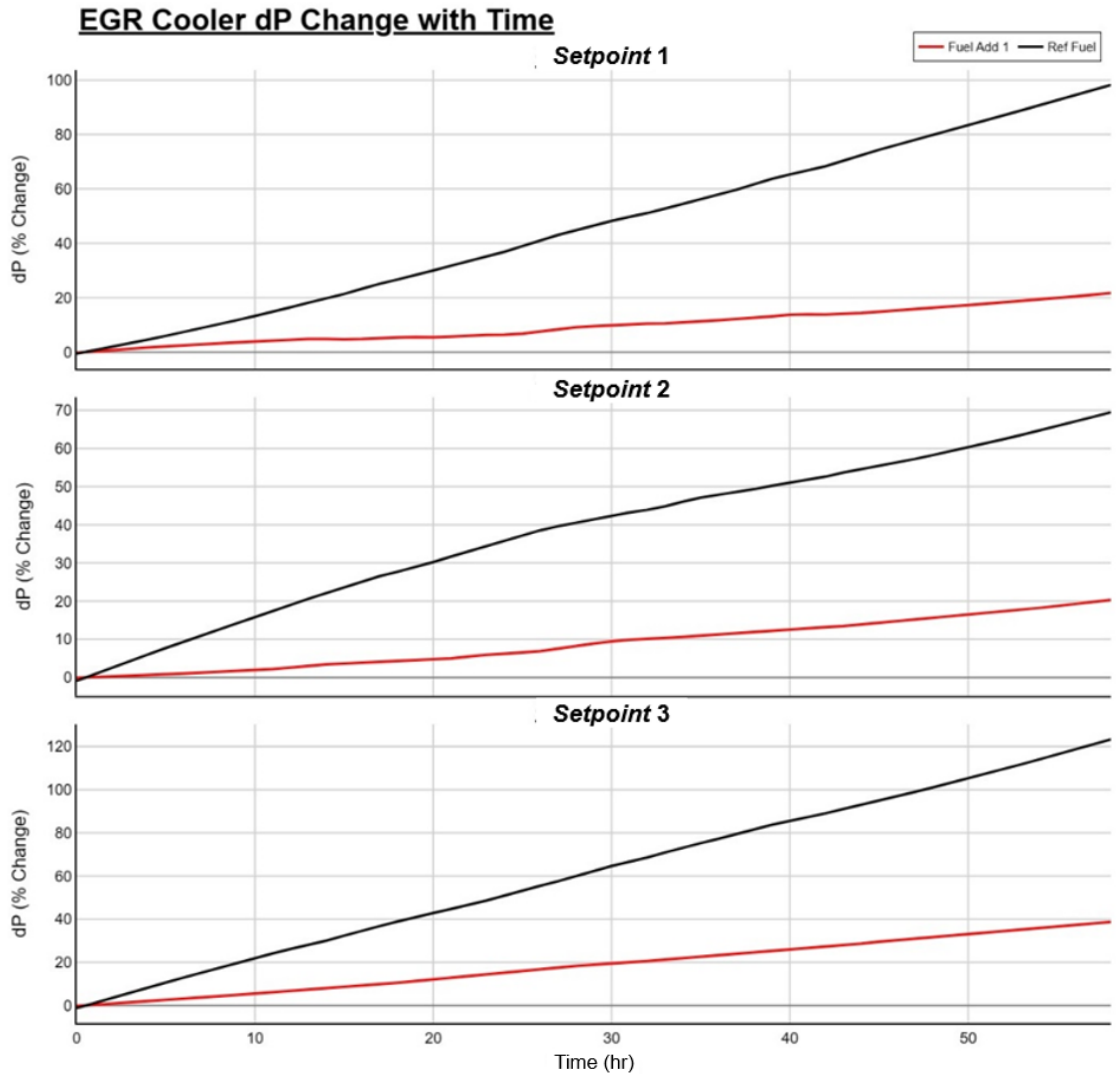


Figure 5-7: EGR Cooler dP change with time.

Fuel additive 1 shows the smallest rise in *dP* and the least change in EGR Cooler effectiveness. The small impact on effectiveness and *dP* over 60 hr when using Fuel

Additive 1 shows that this additive significantly reduced fouling compared to the Reference Fuel, especially at *Setpoint* 3. This is possibly due to Fuel additive 1 showing a lower increase in both THC and soot. As per Equation 5-13 an increased level of soot concentration will lead to more EGR Cooler fouling. It has also been discussed in literature that HC condensate does increase soot deposition as the wetted section is more efficient at catching soot particles and hence the deposition layer is thicker (19).

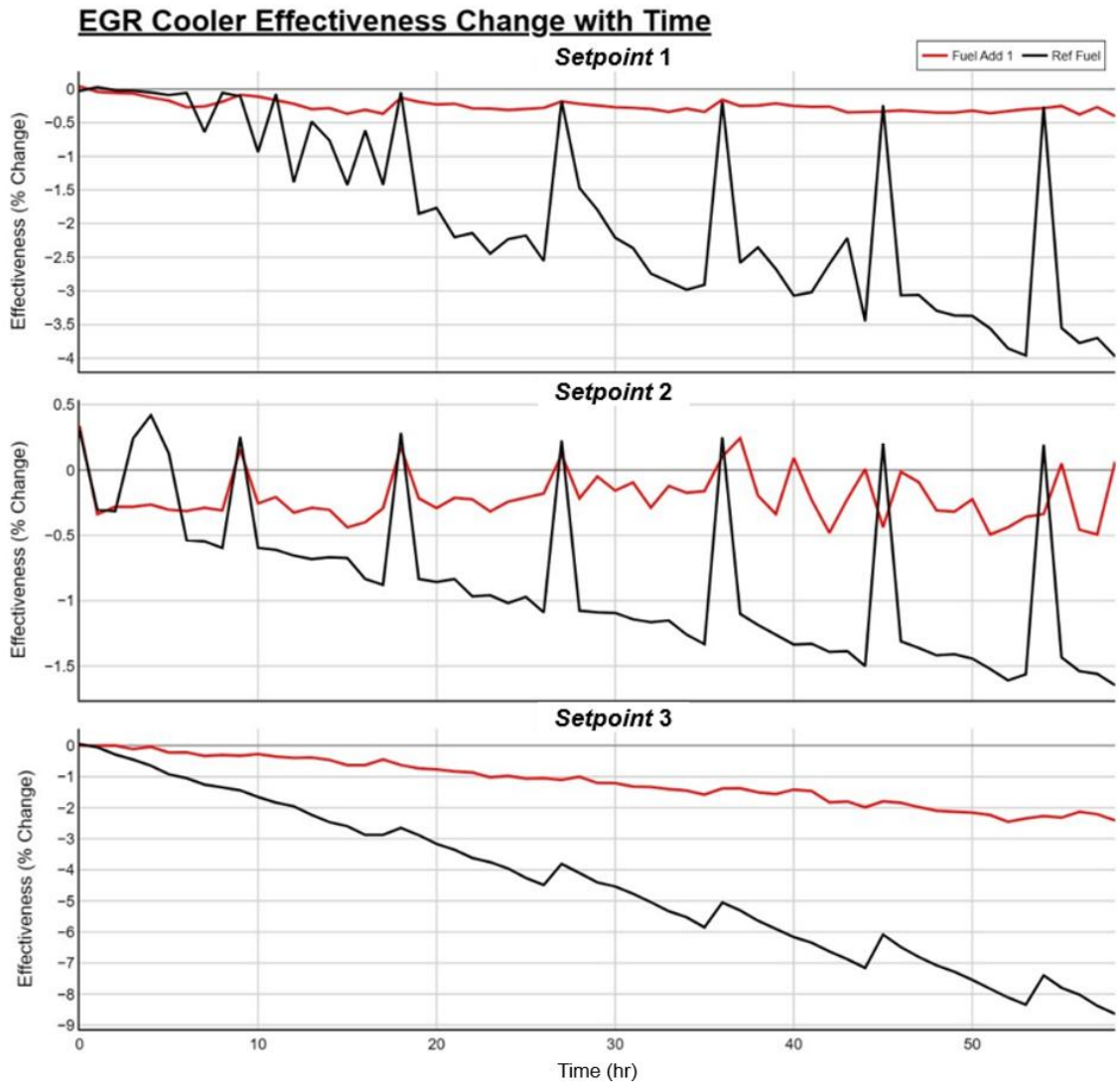


Figure 5-8: EGR Cooler Effectiveness change with time, all fuels.

5.3.3 Impact of Fuel-Derived EGR Deposits on EGR Cooler and Engine Performance for Various EGR Scenarios

5.3.3.1 Intake Manifold Temperature and Engine Performance

In regular EGR operation the EGR flow would enter the intake system increasing intake manifold temperature. An increase in intake manifold temperature can have varying effects depending on the engine condition. The intake temperatures (both at the start and end of the experiments) as well as the estimations of *BSFC* and *MFB50* for scenarios outlined in section 5.2.1 are shown in Table 5-2. The *BSFC* and *MFB50* estimations are obtained according to Fischer (22), who used 15 % EGR with a near identical engine to the one used in this study.

Scenario 1: The EGR inlet temperatures recorded in the experiment are representative of an LP loop where the EGR exit gases would be introduced into the intake before the compressor, defining Scenario 1. The temperature increase with the LP setup was considerably lower than for the HP setups (Table 5-2) due to the intercooler providing additional cooling. At *Setpoint* 3 the final temperatures are 24.5 ^{o}C and 22.5 ^{o}C for the Reference Fuel and Additive 1 respectively, resulting in a negligible change in *BSFC* and *MFB50*, according to Fischer (22). LP setups are still vulnerable to fouling though as cool inlet temperatures are required to protect the compressor and maintain high mass flow rates through the compressor (128). Sufficient cooling is also required to not create excessive post compressor temperatures and to limit over speeding (131).

Scenario 2: The intake manifold temperature increases by 2.7 °C (8.5 %) and 5.6 °C (17.4 %) at engine operation *Setpoint* 3 for Fuel Additive 1 and the Reference fuel, respectively. The engine *Setpoint*s 1 and 2 show a smaller increase in intake manifold temperature as the Cooler effectiveness does not change much due to the lower exhaust temperatures in comparison to *Setpoint* 3. The increased intake manifold temperature when using the Reference Fuel of 37.9 °C does not significantly affect the *MFB50* and *BSFC* compared to the 34.6 °C found with Fuel Additive 1 (22). This is because in the low intake temperature region the engine is not near the knock limit. Therefore, an increase in intake temperature will generate little knock allowing for high efficiencies.

Table 5-2: The impact of fuel, scenario and Setpoint on predicted intake manifold temperature and the predicted impact on BSFC and MFB50.

	Scenario	Fuel	Intake Manifold Temperature (°C)		Temperature increase		Predicted Increase when using Ref fuel Compared to Fuel Add 1	
			Start	End	(°C)	(%)	BSFC (%)	MFB50 (%)
Setpoint 1	1	Ref Fuel	16.7	16.9	0.2	1.1	NA	NA
		Fuel Add 1	16.4	16.4	0.0	-0.2		
	2	Ref Fuel	21.4	22.0	0.6	2.9	0.0	6.7
		Fuel Add 1	21.4	22.0	0.6	2.9		
	3	Ref Fuel	23.8	28.6	4.8	20.2	0.0	6.3
		Fuel Add 1	24.0	24.9	0.9	3.7		
Setpoint 2	1	Ref Fuel	15.8	15.8	0.0	0.3	NA	NA
		Fuel Add 1	15.5	15.5	0.0	0.1		
	2	Ref Fuel	20.9	20.7	-0.2	-1.0	0.0	0.0
		Fuel Add 1	20.7	21.3	0.6	2.7		
	3	Ref Fuel	23.4	25.1	1.7	7.4	0.0	6.3
		Fuel Add 1	23.6	23.9	0.3	1.4		
Setpoint 3	1	Ref Fuel	23.3	24.5	1.2	5.0	0.4	12.5
		Fuel Add 1	22.1	22.5	0.4	2.0		
	2	Ref Fuel	32.3	37.9	5.6	17.4	0.0	0.0
		Fuel Add 1	31.9	34.6	2.7	8.5		
	3	Ref Fuel	40.1	50.0	9.9	24.8	1.2	6.3
		Fuel Add 1	39.4	43.0	3.6	9.1		

Scenario 3: Fischer (22) operated the engine at 4750 rpm 17 bar IMEP leading to exhaust temperatures of 940 °C with no EGR, whereas *Setpoint* 3 operated with turbine inlet

temperatures of 810 ^{o}C and EGR inlet temperatures of 550 ^{o}C; so the changes in *BSFC* and *MFB50* due to increased intake manifold temperature would be different compared to when the engine is operating at *Setpoint* 3. So, for a better representation of the effects of increased EGR outlet temperature at high loads this scenario was defined assuming that the 940 ^{o}C exhaust gas would enter the EGR Cooler straightaway. The higher exhaust temperatures increase the intake temperatures resulting in an intake manifold temperature at *Setpoint* 3 of 50 ^{o}C and 43 ^{o}C for the Reference fuel and Fuel Additive 1, respectively. Those intake temperatures lead to *BSFC* values of 245 g/kWh and 242 g/kWh (22) respectively, a 1.2 % change caused by a 1 CAD retard in combustion. This represents a modest but not insignificant change in *BSFC*. If the intake manifold temperature was to increase over 50 ^{o}C, the *BSFC* would increase considerably with just a small increase in temperature (22). By using this information with the trends seen in Figure 5-8 it can be predicted that the EGR Cooler effectiveness will continue to decrease with time causing intake manifold temperatures to increase to more than 50 ^{o}C with the Reference Fuel. This would result in large *BSFC* increases considerably impacting engine high load performance. Furthermore, the decrease in EGR Cooler effectiveness with an EGR inlet temperature of 940 ^{o}C would likely be larger as the Scenario 3 calculations used the same Cooler effectiveness as *Setpoint* 3, and thus did not account for the increased levels of fouling that would occur with an increased EGR Cooler inlet temperature of 940 ^{o}C as according to Equation 5-13.

The *BSFC* increase above is primarily due to spark retard, however with higher inlet temperatures further fuel consumption penalties could be encountered through fuel enrichment. This is likely to occur if, as predicted, higher exhaust temperatures lead to

higher levels of fouling than seen in the experiments. This would require the spark to be further retarded, resulting in higher exhaust temperatures (65)(183), creating a negative cycle. It is possible that the increased knock would result in reduced downsizing and compression ratios, impacting efficiency across the whole engine range. Su et al (184) increased compression ratio from 9.3 to 10.9 with cooled EGR, this would be unachievable with heavy fouling.

In all scenarios the increase in temperature is less obvious at *Setpoint*s 1 and 2. This is primarily due to lower exhaust temperatures resulting in less soot deposition and less heat being added to the intake. As mentioned earlier, research has shown that at lower temperature engine conditions increasing intake temperature has a negligible impact on engine efficiency and can even be beneficial. Thus, the increase in intake temperature at *Setpoint*s 1 and 2 is unlikely to have a negative impact on engine performance.

5.3.3.2 Pressure drop (*dP*)

The formation of EGR Cooler deposits will affect *dP* across the Cooler (*EGR Cooler dP*) and thus over the whole EGR loop. The experimental *dP* values obtained across the EGR Cooler at the start and end of the experiments are shown in Table 5-3. The *Total EGR dP* was estimated for Scenarios 1, 2 and 4 as described in the methodology and Figure 5-2.

Scenario 1 (LP setup): A large *Total EGR dP* was found at *Setpoint* 3, and much lower values found at *Setpoint*s 1 and 2. At *Setpoint* 3 the 33.8 mbar *EGR Cooler dP* found with the Reference Fuel at the end of the experiment represented 20.5 % of the *Total EGR dP*, while 19.7 mbar is found with Fuel additive 1 representing 12 %. At *Setpoint* 1 the increased *EGR Cooler dP* with the Reference fuel also represented a significant portion

of the *Total EGR dP*. The *Setpoint* where *EGR Cooler dP* was predicted to have the largest impact on the overall EGR flowrate in Scenario 1 was *Setpoint* 2. This is because both fuels resulted in an *EGR Cooler dP* that was larger than the *Total EGR dP* itself. If the *EGR Cooler dP* is larger than the *Total EGR dP* then the pressure gradient between the exhaust and the intake will not be enough to overcome the *dP* across the Cooler resulting in no EGR flow. EGR Cooler fouling in an LP loop can be mitigated through the use of a GPF which would filter most of the soot from the exhaust and reduce fouling, however this would decrease pressure downstream of itself reducing *Total EGR dP*. In this situation the exhaust back pressure can be increased through the use of an exhaust valve to assist EGR flow, however the increased exhaust back pressure increases engine pumping losses and therefore comes at a fuel penalty (185). It is therefore beneficial to reduce EGR Cooler fouling to levels where these additional components are not necessary.

Scenario 2 (HP post intercooler setup): The *Total EGR dP* for Scenario 2 is much higher than those obtained for Scenarios 1 and 4 at all *Setpoint*s, because the EGR flow enters the intake after the throttle. Therefore, the *EGR Cooler dP* only represents a small percentage of the *Total EGR dP* thus a low *EGR Cooler dP* is not so critical for the functioning of the EGR system in this scenario.

Scenario 4 (HP pre intercooler setup): The impact of increased *EGR Cooler dP* is more significant at *Setpoint*s 1 and 2 compared to *Setpoint* 3. At *Setpoint* 3 *EGR Cooler dP* makes up 10.9 % and 18.8 % of the *Total EGR dP* with the Fuel Additive and Reference fuel respectively. *Setpoint*s 1 and 2 have a much lower *Total EGR dP*, making *EGR Cooler*

dP critical for the functioning of the EGR system. This would be particularly key at *Setpoint* 1 where the *Total EGR dP* is negative, meaning that there would be no EGR flow. At this situation the intake would need to be throttled to make a positive pressure gradient, this throttling would also need to overcome the rise in *EGR Cooler dP* and would likely have an impact on engine efficiency.

In all scenarios and *Setpoint*s the impact of *EGR Cooler dP* is significantly less with the use of Fuel Additive 1 compared to the Ref Fuel. This is due the reasons discussed in section 5.3.2. In some cases, the additive almost halves the proportion of *EGR Cooler dP* compared to *Total EGR dP* suggesting that the use of an additive can significantly improve maximum EGR flow rates. This is most evident in the two pre intercooler scenarios 1 and 4 and at the low load *Setpoint*s (*Setpoint* 1 and 2).

Table 5-3: The impact of increased EGR Cooler dP due to fouling in the context of the total dP found across 3 typical EGR setups.

	EGR Cooler dP , Start of test (mbar)		*EGR Cooler dP* , End of test (mbar)				*EGR Cooler dP* (End of test) as a Percentage of *Total EGR dP*	
Setpoint	Fuel Add 1	Ref Fuel	Fuel Add 1	Ref Fuel	Scenario	*Total EGR dP* (mbar)	Fuel Add 1	Ref Fuel
1	3.2	3.2	4.1	6.6	1	15.7	26.1	42
					2	45	9.1	14.7
					4	-5	-82	-132
2	2.8	2.8	3.4	4.8	1	3	113.3	158.3
					2	150	2.3	3.2
					4	0.1	3400	4750
3	14.1	14.8	19.7	33.8	1	164.5	12	20.5
					2	362	5.4	9.3
					4	180	10.9	18.8

5.4 Conclusions

This study assessed the impacts of different engine operating *Setpoint*s and fuel additives on EGR Cooler fouling. The impact of fuel additives on the mechanisms behind the fouling were also investigated. Another purpose of this study was to put the potential impacts of EGR Cooler fouling into context by predicting its impact on engine performance and thus demonstrating the contextual benefits of using fuel additives.

The impact of using fuel additives to control fuel-derived deposit formation in the fuel injector and EGR Cooler has been investigated within the same test *Cycle*, allowing the direct impacts of the Additive on fouling to be observed. A new method to accelerate injector and EGR Cooler deposit formation has been developed and successfully applied to denote the impact of fuel on the formation and growth of those deposits. The method is composed by various experimental engine operation *Setpoint*s leading to a sequence of emissions (e.g. HC and soot), temperatures and flowrates prone to forming deposits. The experiments have clearly showed that fuel additives could reduce EGR Cooler fouling, with Fuel additive 1 proving the most effective. This was attributed to Fuel additive 1 producing the least soot and THC emissions.

The reduced EGR Cooler fouling was represented by a lower *EGR Cooler dP* when using the fuel additive. The reduced *dP* with the additives was found to be a significant portion of the *Total EGR dP* when using LP and HP pre intercooler setups, leaving HP post intercooler as the optimum setup in terms of *dP*.

The use of Fuel Additive 1 significantly increased Cooler effectiveness with respect to the Reference Fuel, which was predicted to lead to a reduced intake manifold

temperature with EGR and hence improved *BSFC*. The impact on *BSFC* was predicted to be highest at high load with an HP EGR setup. Calculations predicted further impacts with a longer test and higher engine speeds and loads. At lower loads the fouling was much less severe because lower exhaust temperatures were predicted to have a negligible impact on engine performance in terms of intake temperature. Pre intercooler EGR systems were also predicted to be minimally impacted by EGR Cooler fouling with regards to intake temperature increase.

EGR Cooler fouling has a significant impact on HP and LP setups at different engine *Setpoint*s. Pre intercooler setups may be impacted little in terms of intake temperature at high load *Setpoint*s but are susceptible to *dP* increases at low engine speeds. This leaves HP post intercooler, but this is susceptible to increased intake temperature due to EGR Cooler fouling which causes knock at high loads. However, HP is less susceptible to knock at lower loads and the increased *Total EGR dP* makes HP less vulnerable to an increase in *EGR Cooler dP*.

In conclusion EGR Cooler fouling significantly limits the benefits of both HP and LP EGR loops, such as downsizing and increased compression ratios by limiting their performance across a range of engine operating *Setpoint*s and this study has demonstrated that an effective way of mitigating this is by using fuel additives which reduce soot and THC emissions.

6. DEVELOPMENT OF AN EXPERIMENTAL METHOD TO INVESTIGATE FUEL DERIVED DEPOSITS ON ENGINE INTAKE VALVES.

6.1 Introduction

The experimental facility and method developed in this chapter aimed to emulate engine conditions that cause fuel derived IVD formation while reducing running costs and fuel consumption compared to experiments on a full vehicle/engine operated with fuel combustion. The experimental method and setup aimed to be controllable for independent adjustment of key parameters selected from critical analysis of relevant literature to analyse their impact on deposit formation.

The structure of this chapter is as follows. Firstly, the Product Design Specification is described along with its justification. The description of the final experimental rig is split up into sub systems which were built to satisfy each point of the PDS. Each sub system had its own more detailed specification and the design and manufacturing process of the components that make up each subsystem are outlined in detail. Finally, the measurement process of some preliminary tests which aimed to demonstrate a proof of concept of the experimental rig is described along with the results and discussion of how the experimental rig performed.

6.2 Design and Manufacture

6.2.1 Product Design Specification

The final developed experimental rig can be seen in Figure 6-1, the rig utilised a cylinder head from a commercial 4-cylinder engine. This engine was chosen to closely emulate the conditions of most modern vehicles which use multi-cylinder engines. The engine used PFI, targeting the bridge between the two intake ports for each cylinder (Figure 6-2). The subsystems and components of the experimental rig are labelled in Figure 6-1, these are explained in their respective sub-sections. Most of the components were designed especially for the rig and some components were modified from existing apparatus such as the fuel injection system.

To meet the design objectives, the following specifications were established:

- Cylinder Head temperature controllable and measurable from ambient to 90 ^{o}C. Adjusting the Cylinder Head temperature is key to observe its impact on valve deposition as Cheng (27) found that most deposition occurs from liquid fuel pooling in the intake port and impinging on the valve. Controlling the Cylinder Head temperature affects the intake port temperature and hence condensation, it also helps achieve realistic heat distribution across the valve, by transferring heat from the Cylinder Head to the valve via conduction.
- Valve temperature controllable and measurable from ambient to ~370 ^{o}C. To simulate conditions causing intake valve deposition, valve temperature is the

most critical factor, as detailed in section 2.4.3.1. Precise regulation is essential since the critical deposition temperature window can be as narrow as 20 ^{o}C (35).

- Valves actuated similarly to a regular engine in a measurable way. For realistic valve behaviour, valves should actuate via camshaft rotation and valve springs, as opposed to stationary valves used in other experimental rigs (section 2.6.4). This setup can help determine if valve movement impacts deposition and cleaning compared to stationary valves. The location of fuel impingement on the valve and the air flow affects deposition and cleaning. Realistic valve actuation, achieved by camshaft usage, better emulates the fuel impingement on the valves in real engine conditions.
- Fuel mass flow rate, injection pulse width and injection frequency adjustable and measurable. Fuel delivery must be adjustable, necessitating control over injection frequency and pulse width to replicate various common injection strategies. The fuel pressure should match those in a PFI system.
- Intake air mass flow rate, pressure and temperature adjustable and measurable. Regulating intake air temperature is crucial for analysing fuel evaporation and condensation behaviour in the intake port. Adjustable intake pressure and flowrate also allow for the behaviour of the air and fuel charge motion to be monitored so its impact on deposit formation can be analysed.
- Fuel vapour must be safely extracted to reduce the chance of spontaneous combustion in the system and to keep operators from being exposed to harmful vapours.

- The mass of the valve must be measurable to allow the mass of the deposits to be measured.

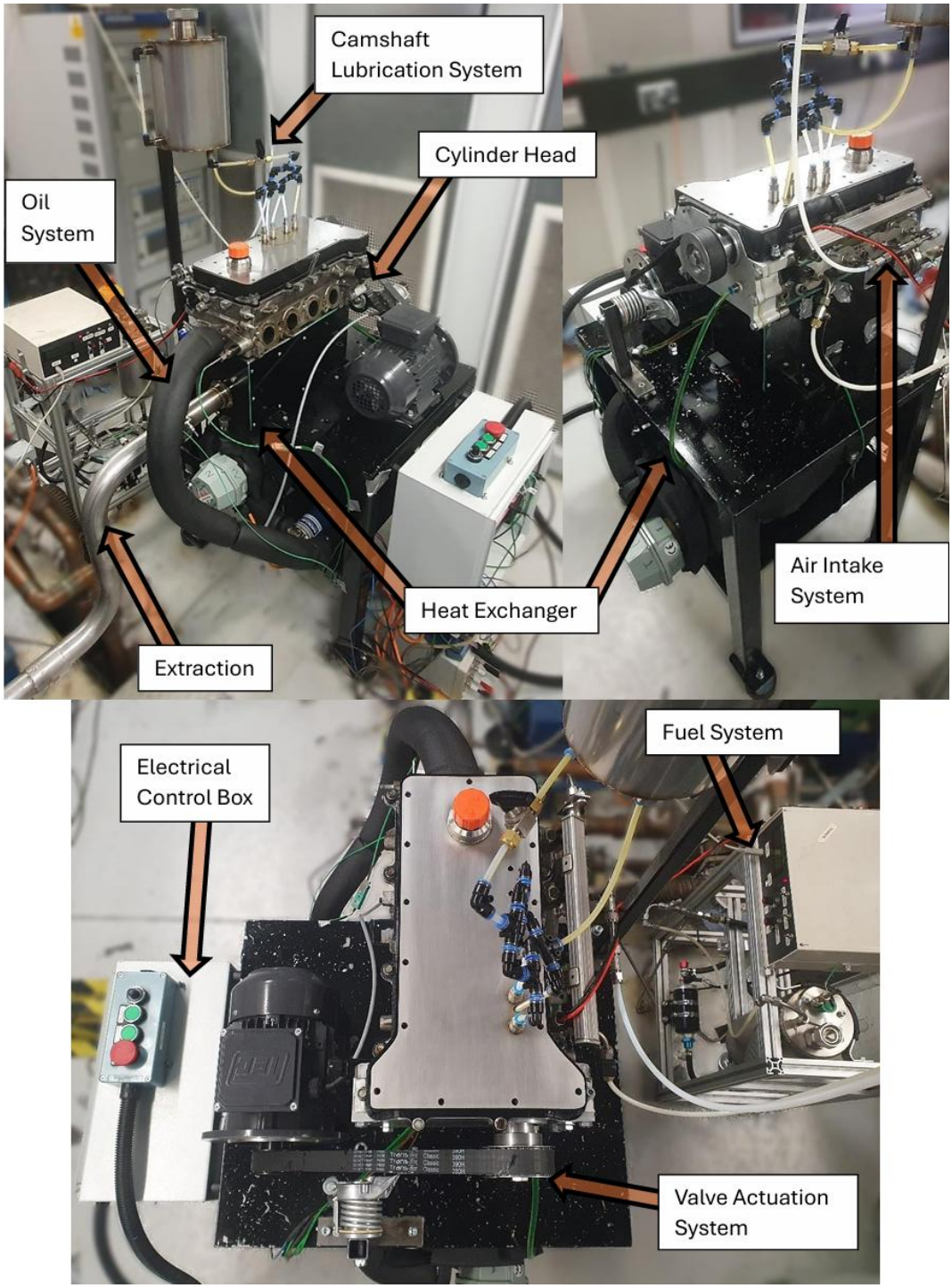


Figure 6-1: Intake Valve Fuel Deposits Rig.

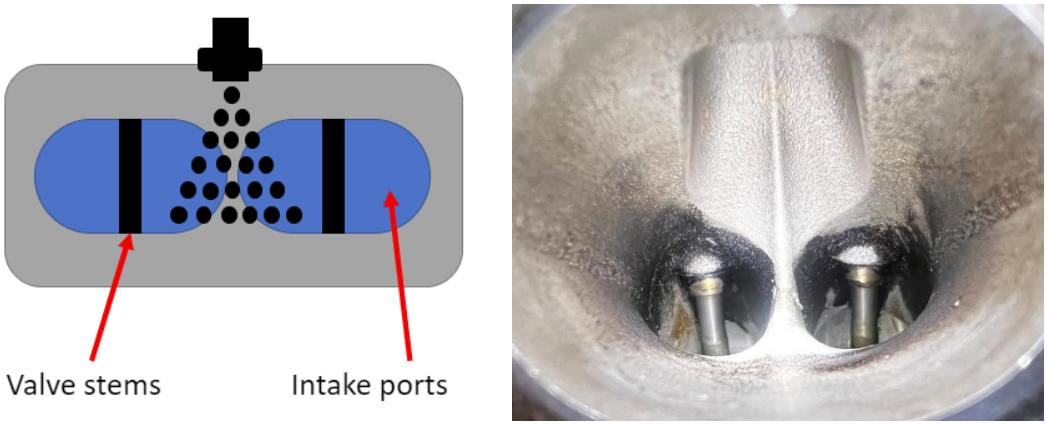


Figure 6-2: Fuel injector location.

6.2.2 Design and Manufacture of the System to Modify Cylinder Head Temperature

6.2.2.1 Design Specification of the Subsystem (Heat Exchanger and Oil Delivery)

Oil was selected as the heat transfer medium to the Cylinder Head due to its high boiling point, allowing for the maximum expected temperature in the Heat Exchanger of 110 ^{o}C to be comfortably maintained, oil could also simultaneously lubricate the camshaft system. The oil was designed to circulate around the coolant jacket of the Cylinder Head as this wrapped around the valve stems and the area just above the valves, effectively transferring heat to the valves. The oil was designed to be heated via a Heat Exchanger which was designed to control the Cylinder Head temperature by providing heated oil to the Cylinder Head. The components of this subsystem were built to meet the following specifications.

Table 6-1: System to modify Cylinder Head temperature: Specification.

Component	Specification
Cylinder Head	Must withstand temperatures of 90 ^{o}C
	Modifications to the Cylinder Head should allow the oil to pass through the Cylinder Head without leakage
	Allow a portion of the oil to be bypassed to the camshaft bearing system for lubrication
Heat Exchanger	Must withstand temperatures 20 ^{o}C higher than those found in the Cylinder Head (110 ^{o}C)
	Capable of relieving pressure from heated oil
	Deliver sufficient heat to the rest of the oil system
	Sufficiently insulated to maintain heating efficiency
	Be able to measure the temperature within the Heat Exchanger
Oil Delivery System	Capable of pumping liquid from Heat Exchanger to Cylinder Head
	Drain liquid from Cylinder Head
	Maintain Cylinder Head temperature at the set value
	Withstand temperatures of 20 ^{o}C higher than those found in the Cylinder Head (110 ^{o}C)
Power/ Control Electronics	Maintain steady state Cylinder Head temperature with fluctuations of less than ±5 ^{o}C
	Control both the Cylinder Head and Heat Exchanger temperatures so that they remain below their maximum operating temperatures
	Have safety shutdown procedures in the event of overheating

6.2.2.2 Cylinder Head

To circulate the oil through the coolant jacket, the base of the Cylinder Head needed to be sealed to prevent leaks. Figure 6-3a shows passages highlighted in red in the base of the Cylinder Head where coolant normally flows to the engine block. A base plate (Figure 6-3b) was designed to block these holes, and in certain places (indicated by the labels on Figure 6-3a) allow oil flow from the coolant jacket to the camshaft bearings, enabling simultaneous heating and lubrication of the Cylinder Head and camshaft. The gasket plate was designed so that the oil would flow in from the left, through the coolant jacket

as well as the camshaft bearings, and then drain from the coolant jacket from the right, as indicated by the red arrows (Figure 6-3a).

Figure 6-3b shows the final plate design and Figure 6-3c shows its respective CADD model and 3D scan overlaid with the labels from Figure 6-3a. In Figure 6-3b channels where the oil is diverted from the coolant jacket to the bearings can be observed. To create these channels steel plates were welded to the underside of the gasket plate. Figure 6-3c shows how the design was aligned to the Cylinder Head to ensure all the correct openings were aligned and that space was left for valve actuation.

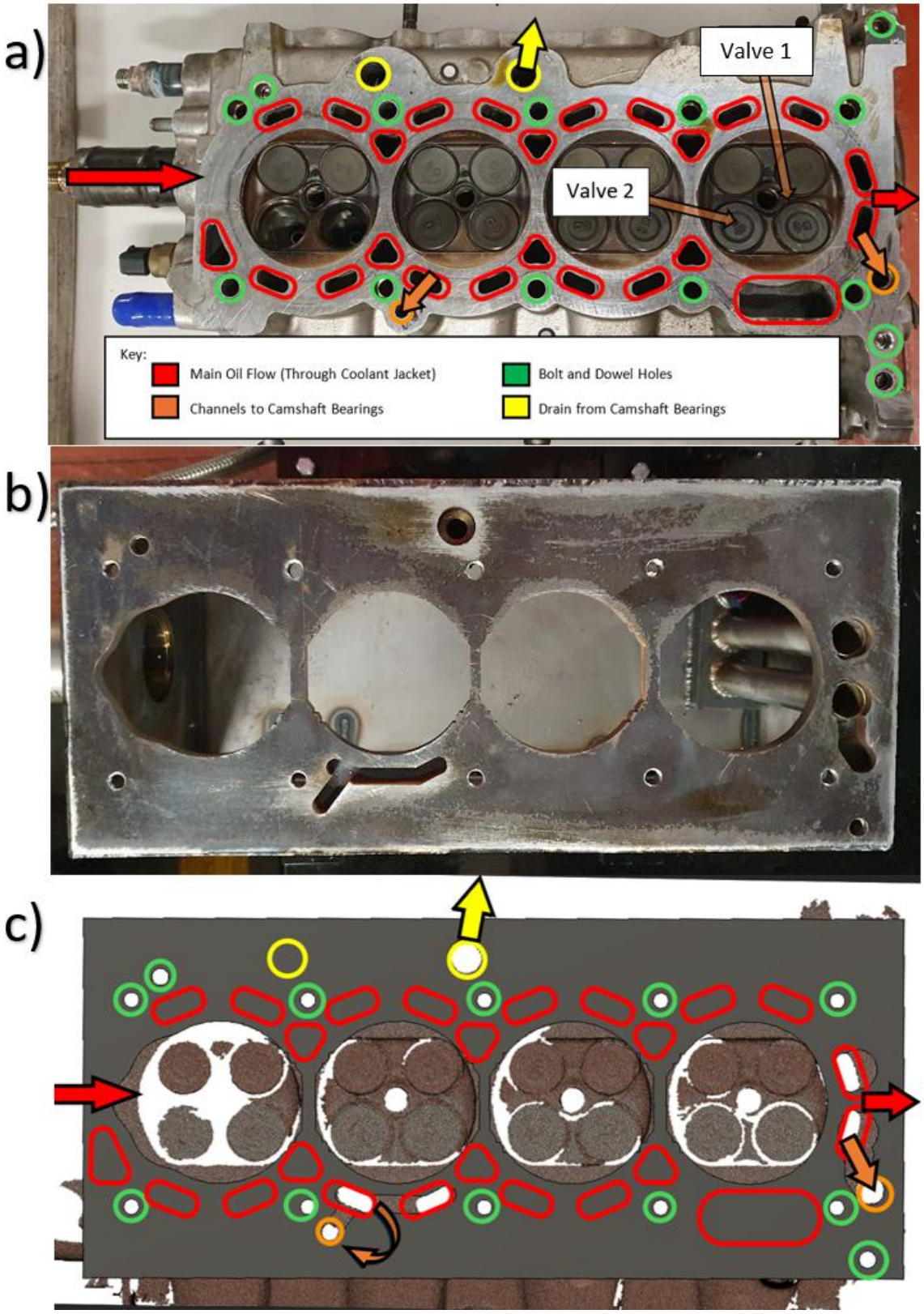


Figure 6-3: Cylinder Head gasket plate design a) oil channels, b) gasket plate, c) 3D scan and CADD model.

The underside of the base plate was attached to a box to collect air and fuel vapour from the intake valves (Figure 6-4). The air-fuel mixture passed through one set of intake valves, while the others allowed only air, creating a lean mixture in the extraction box, preventing combustion on the hot valve and aiding fuel vapour extraction. The extraction box featured sealable windows on the side. These windows were necessary for valve spring compressor tool to access the underside of the valves, to remove the valves to measure their mass. A large outlet was designed at one end which could be attached to the exhaust extraction. A smaller opening allowed thermocouple and heater wires to pass through. Pipework was included in the design to channel the oil, (Figure 6-4). This system is explained in more detail in the Oil Piping System section.

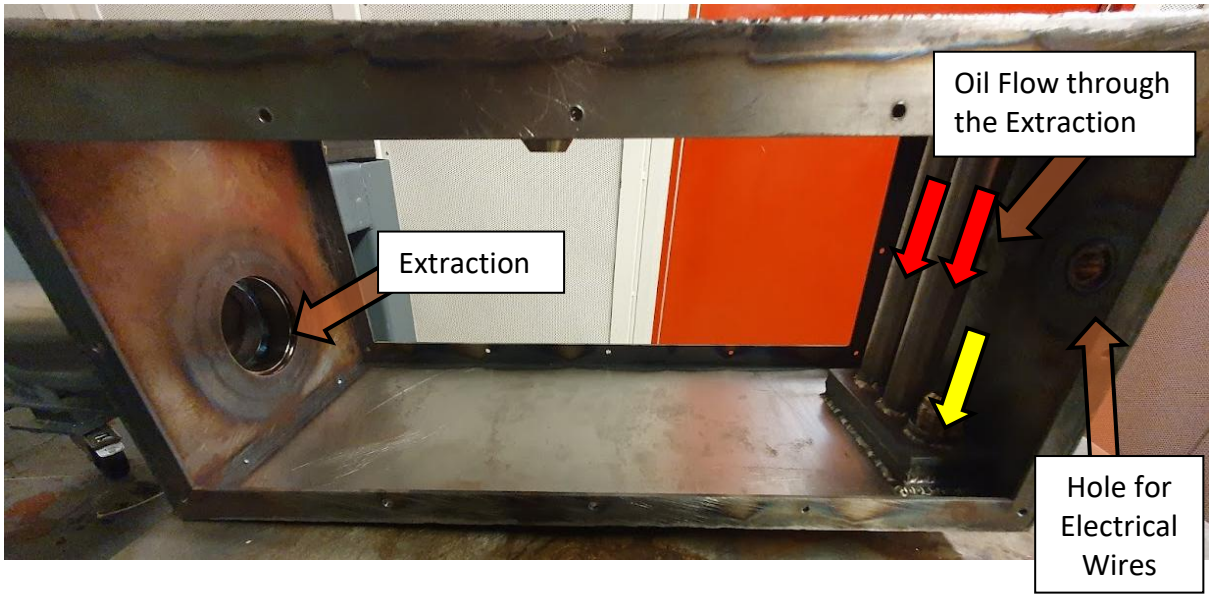


Figure 6-4: Extraction box.

The base plate was 10 mm thick ensuring rigidity to withstand high torque from Cylinder Head bolts and to support welding of the extraction box side plates. Mild steel was chosen for its weldability and cost-effectiveness. The extraction box and base plate were

designed in 2D CADD for water jet cutting followed by welding, a process chosen for its cost and time efficiency, and to minimise base plate warping for an adequate gasket seal. This was preferred to laser cutting as the high heat caused warping of the base plate. A multi-layered-steel gasket was used to seal the gasket base plate to the Cylinder Head.

6.2.2.3 Heat Exchanger

The original engine design lacked the necessary data to estimate the heat transfer to the coolant jacket. Consequently, the power required from the Heat Exchanger could not be determined. Therefore, the Heat Exchanger was designed to provide a substantial amount of power, anticipating the potential need for additional capacity. Two 1.75 kW immersion heaters were selected to fulfil the power requirements. Immersion heaters were chosen due to their high efficiency and low cost. These heaters could also withstand the high temperatures found in the Heat Exchanger. These were placed in opposing corners (Figure 6-5) providing good heat distribution, which was measured via thermocouples placed in the centre of the heaters. The hole for the oil outlet was left slightly above the base so that any debris that might be in the oil system would sink below it and not enter the rest of the system. JIC (Joint Industries Council) hose fittings were then welded to the inlet and outlet orifices. An inlet opening was drilled in the fill cap that allowed for an extra return pipe coming from the Cylinder Head to enter the tank (Figure 6-5c).

The Heat Exchanger was designed in 2D (Figure 6-5a) but was laser cut instead of water jet cut. This was because many items such as plugs and threads for heater and pipe fittings would have to be welded to the box. These items were generally made of thick

stainless steel by manufacturers and thus, to help with weldability the plates making up the box also had to be reasonably thick so that they would not burn during the welding process. 6 mm stainless steel was chosen for this and the cost of water jet cutting rises significantly with thicker materials, especially stainless steel because of its hardness and resistance to abrasion. Laser cutting was therefore chosen as warping was not a huge concern for this box as small amounts of warping could be compensated for in the welding process.

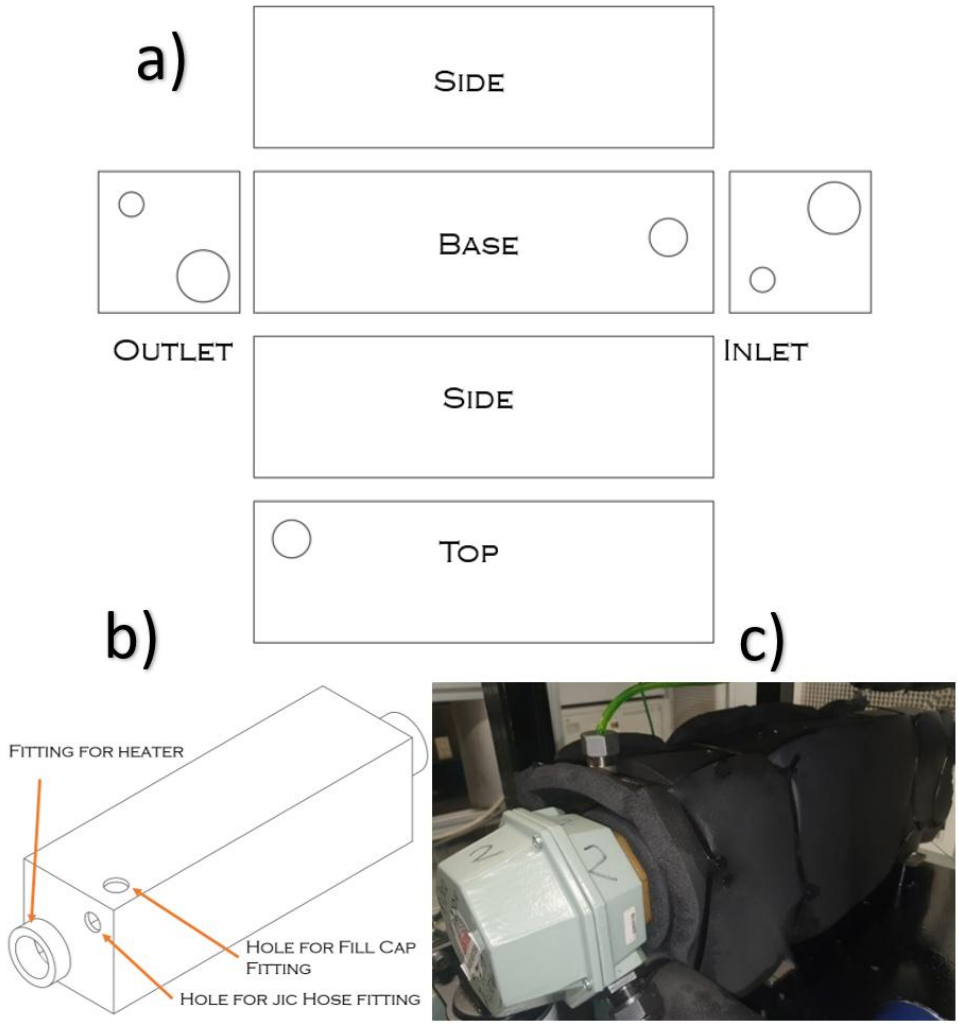


Figure 6-5: Heat Exchanger CADD a) 2D plates, b) Isometric view, c) Photograph with Insulation.

6.2.2.4 Oil Piping System

Hot oil first travels from the Heat Exchanger through a filter to a 12 V electric oil pump (Figure 6-6). A 90 W Mocal Electric Oil Pump EOP2 was chosen as it could withstand temperatures up to 175 ^{o}C and was designed for automotive processes so would have sufficient pressure and flowrate to drive the oil. The manufacture recommends that the pump runs only when the oil is above 70 ^{o}C to prevent damage, so it was placed close to the Heat Exchanger to keep it as hot as possible.

The oil was then pumped to the Cylinder Head via Goodridge stainless steel braided hoses with JIC fittings chosen for their high heat resistance, flexibility and quality to ensure no leaks. These braided hoses were connected to the Cylinder Head and Heat Exchanger via JIC "weld-on" adaptors, unless stated otherwise. To fix these pipes to the Cylinder Head an adaptor was machined out of a billet of steel which was welded to a hose tail connector on the Cylinder Head, originally used to connect to the coolant hoses. Another coolant pipe hose tail connector from the Cylinder Head was also used in the same way to secure a thermocouple and the final one was blanked off with a silicon cap (Figure 6-6).

The oil then circulated through the coolant jacket and up to the camshaft bearings as previously discussed. To allow the oil to drain back down from the bearings a hose was secured to the underside of the gasket plate in the location of the bearing drain (Figure 6-3), which then attached to the drain junction via a hose (Figure 6-6). The drain junction then rejoined the bearing oil with the main circuit which was draining from the coolant jacket. To drain the oil from the coolant jacket, two outlets were designed in the gasket

plate and two steel pipes were welded to the underside of this (Figure 6-4 and Figure 6-6). These two pipes were then welded to the drain junction. Another braided hose was then used to connect the drain junction back to the Heat Exchanger, completing the circuit through an orifice cut into the base of the drain junction.

Another drain was also installed in the Cylinder Head and Camshaft Extension (described in section 6.2.4.3) that drained into the fill cap of the Heat Exchanger box (Figure 6-5c). This aided with the draining of the oil from the upper section of the Cylinder Head after the oil had passed through the camshaft bearings. The design of this custom-made face plate can be seen in Figure 6-15 and is described in more detail later. All hoses were then insulated to reduce heat loss saving on heating energy and also helping to stabilise the heater control.

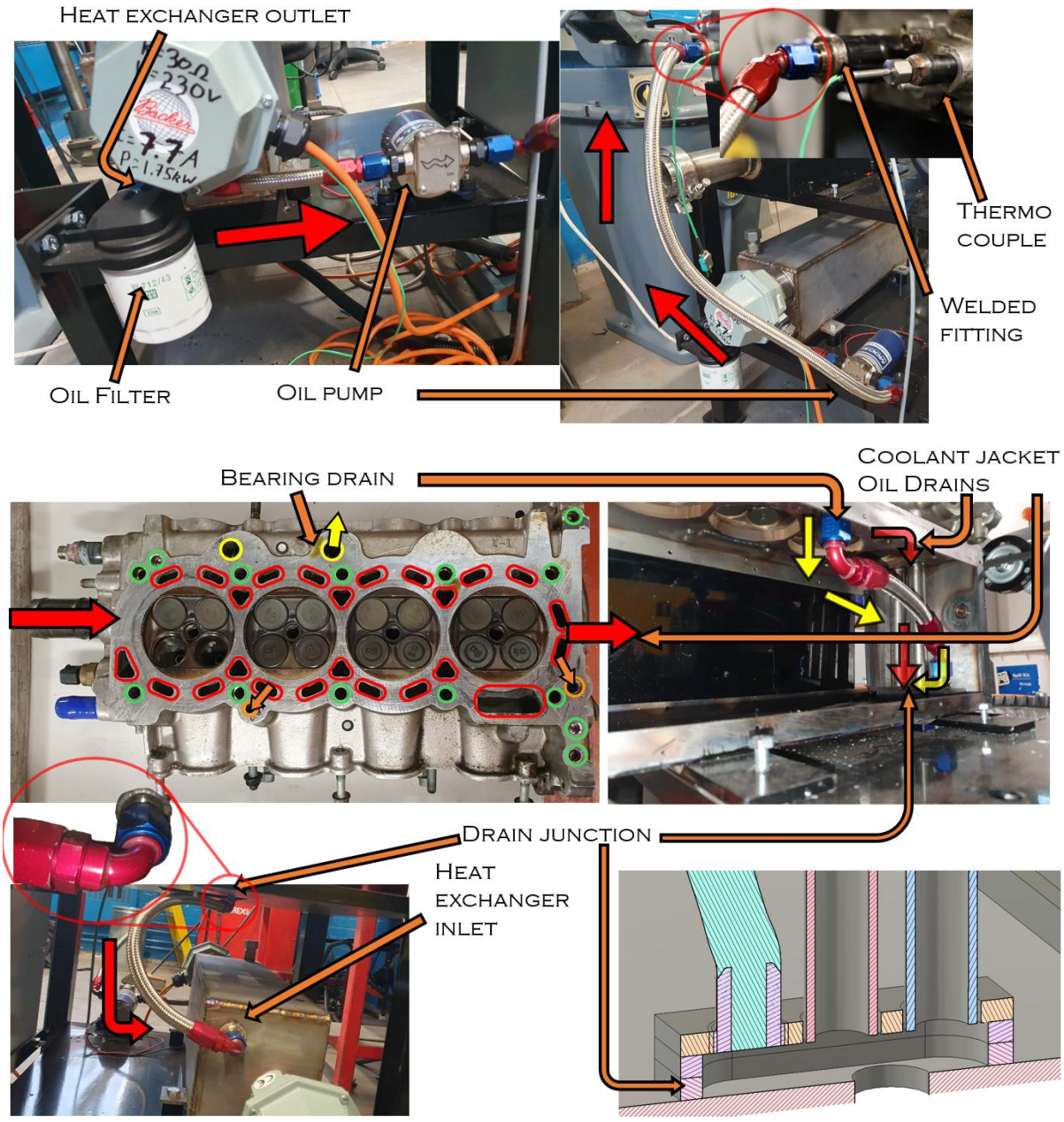


Figure 6-6: Oil system design.

6.2.2.5 Power/Control Electronics

Components and Electrical Diagram

To control the oil system temperature a custom PID controller was made using an Arduino UNO R3. The control system had additional components to a standard PID controller including safety checks and automation. Temperatures were measured using

K-type thermocouples connected to a Maxim Integrated MAX31855PMB1 module board. The MAX31855 amplified the thermocouple signal and transferred it to the Arduino via SPI (accuracy of ± 2 ^{o}C) , to be read by the Adafruit_MAX31855 library. Two thermocouples were used: one for the Cylinder Head and one for the Heat Exchanger. The temperature measurement acted as the feedback in the PID control loop, with the output being a Pulse Width Modulation (PWM) signal to a Solid State Relay (SSR). This SSR controlled the immersion heater's power output. Due to the high current drawn by the heaters, each was wired to a separate power outlet and SSR. A smaller SSR controlled the pump. Push to break buttons and a potentiometer adjusted the PID settings, while an OLED display showed inputs and outputs. An LED indicated SSR operation.

The PID control components are shown in Figure 6-7. An insulated metal plate separates the low voltage logic control from the high voltage side to shield from electrical noise and short circuits. The user interface, including the OLED display, LED, buttons, and potentiometer, were mounted on the face plate for easy interaction. Thermocouple amplifiers were attached to a 3D printed bracket for easy attachment and detachment.

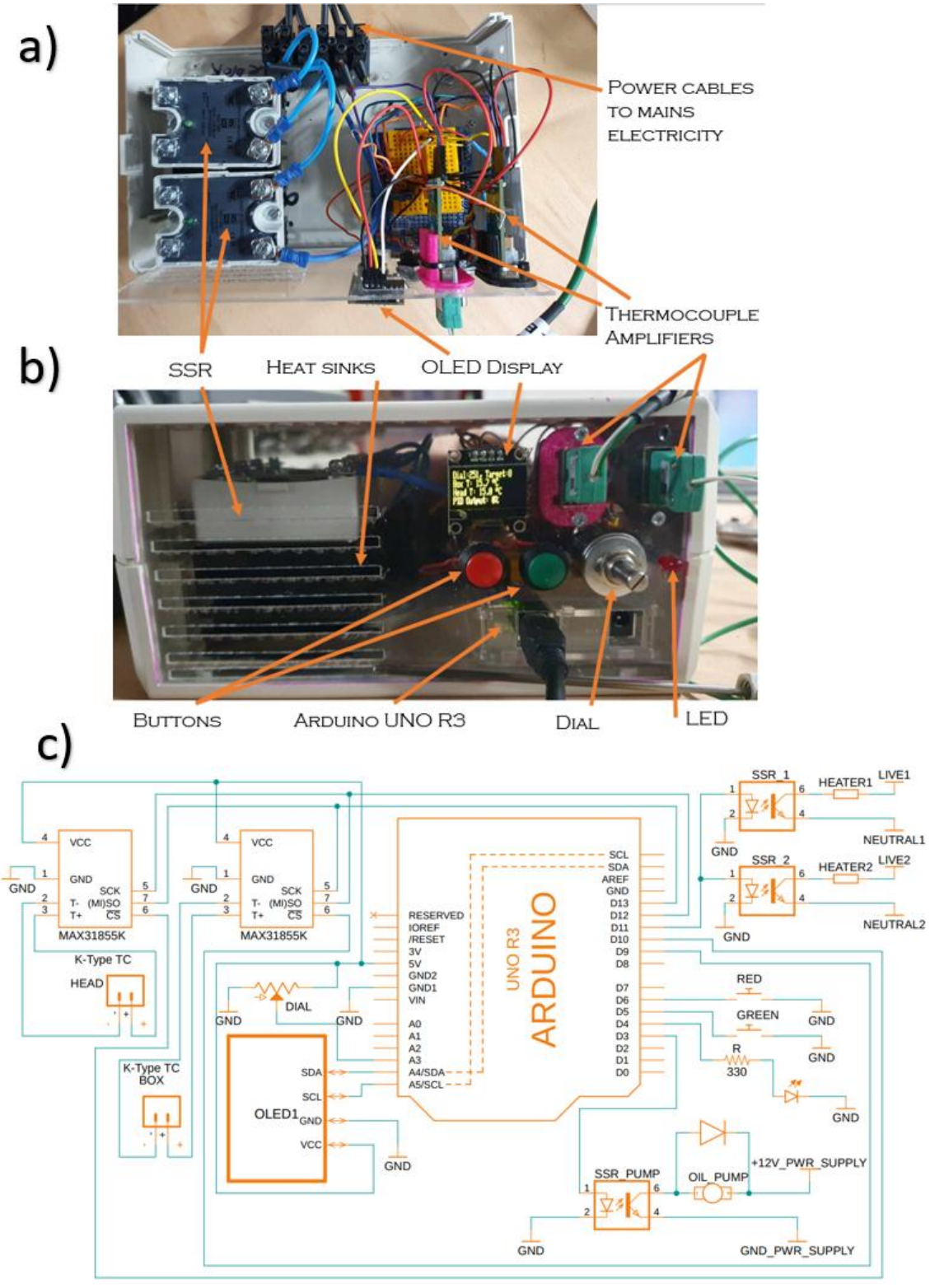


Figure 6-7: PID electronics: Controller Box a) Internal wiring, b) User interface c) Electrical schematic.

Cylinder Head Temperature Control Programming

The full code is available in Appendix B with comments throughout. The sections below, along with the comments in the code provide an in-depth explanation.

The setup section initialises temperature readings, the OLED display, buttons and sets the digital pin controlling the SSR to 30Hz. The code is split into four loops: *Main loop*, *PID control*, *Cool down*, and *Buttons*. All functions used throughout the code are stored at the bottom of the code. The *Main* and *Button* loops run continuously, while the *PID control* and *Cool down* loops activate based on input signals. The signals to determine which loop is used is decided in the *State Check* section of the *Main* loop. The *Main loop* also checks control, safety and filters signals, in addition to sending variables to the serial monitor for troubleshooting. The *Buttons* loop detects button presses to control state changes and set target temperatures.

The *Main loop* starts with the *Serial Print* section followed by the *State check*. The analogue input from the potentiometer is mapped to a value between 0 and 110, representing the available setpoints that the user can choose with the potentiometer. Then the signal filter in the "*Nan Check Loop*" counts *Not a Number* (nan) errors from thermocouple signals over 30 seconds. If more than three errors are recorded, the *Cool Down* loop is activated to shut off the controller as a genuine error has probably occurred in this case.

Control and Safety Checks

Control checks monitor temperature readings to determine which thermocouple is used for feedback and whether to activate the pump. Initially, the Heat Exchanger (box)

thermocouple is used. The control check function switches control to the Cylinder Head (head) thermocouple once the box temperature is above the pump's operating temperature and the head temperature is above a certain percentage of the target. Other checks manage pump activation and ensure it does not switch on and off too quickly, preventing damage.

Safety checks monitor temperatures for temporary or emergency shutdowns. If temperatures exceed preset safety thresholds, a temporary shutdown reduces the SSR output to zero, until the temperature is reduced and the PID loop then continues. If higher thresholds are breached, the PID control and heaters shut down, and the pump carries on running for a short duration to assist cooling. A restart is required to reset the system, ensuring the user acknowledges the issue.

PID Control

The *PID control* loop starts on the initial startup and is deactivated by pressing the red button, which when pressed again reactivates the loop. The loop's refresh rate is controlled by elapsed time. If a temporary shutdown is detected, the SSR and LED are turned off until temperatures drop below the threshold. In this loop both temperatures are recorded and passed through the signal filter. Then both temperatures are averaged via a moving average in two ways. These are two moving averages with different smoothing factor (alpha) values. One uses a small smoothing factor to quickly react, which generates a "safety average" and the other uses a slower but more stable moving average. The latter moving average is what is used by the main *PID control* loop and

temperature readings. Either the box or head moving average is sent to the PID algorithm and this choice is determined by the checks in the *Main loop*.

The time is then recorded and then both average temperatures, PID output percentage, the potentiometer output and target temperature are all displayed on the OLED display.

Target temperature and PID constants are then sent to the PID algorithm. If the checks have not activated the pump, then the target temperature is ~80 ^{o}C and the PID constants are lower than when the pump is on. The 80 ^{o}C target temperature is set 10 ^{o}C above the operating temperature of the oil pump to assist with the cold start. When the pump is activated the PID constants are increased, to provide more heating power, and the target temperature is set to the users input from the potentiometer.

The PID values are calculated using Equation 6-1 and summed to create the total PID output. The integral I_{n+1} is further influenced by a saturation limit, which defines the maximum integral value to prevent excessive buildup during the oil's long warm-up time. If the integral value exceeds the saturation limit, an integral check determines if the next iteration will increase or decrease the integral value. If it increases, the integral value remains capped; if it decreases, Equation 6-1 is reactivated. The integral is used only when the real temperature is within 40 ^{o}C of the target to avoid excessive power usage and localised boiling around the heaters during initial startup.

$$P = E \times k_p$$

$$I_{n+1} = I_n + (E \times k_i)$$

$$D = k_d \times \frac{\Delta E}{\Delta t}$$

Equation 6-1: PID Calculations

Table 6-2: PID Calculations Symbols.

Symbol	Description
P	Proportional Value
E	Error Value
k_p	Proportional Gain
I_n	nth Integral Value
k_i	Integral Gain
D	Differential Value
k_d	Differential Gain
$\frac{\Delta E}{\Delta t}$	Error Rate of Change

The Arduino maps the PID output value between 0 and 255, the PWM output range of an Arduino UNO R3. An absolute maximum value ensures controlled startup power. This value, determining the maximum PID output to the SSR, is smaller when the pump is off and increases when the pump is on. The PID output is zero if a negative value is calculated by Equation 6-1 or if the total time is less than 5 seconds, allowing the thermocouple amplifiers to stabilise and gather enough readings for a smooth moving average. Finally, the PID loop writes the filtered PID output to the SSR, activates the LED if the output is above 0, and resets variables for the next iteration.

The *Cool down* loop is activated by pressing the red button or a shutdown trigger. This resets the variables, ensuring a safe restart, if the user decides to trigger the PID loop again. Temperatures are monitored, and the pump is turned off after a short duration. If the emergency shutdown was triggered, then the user must reset the Arduino to acknowledge the warning message and restart when safe.

6.2.3 Design and Manufacturing of the System to Modify Valve Temperature.

6.2.3.1 Design Specification of the Subsystem

To control valve temperature efficiently, an electrical heater was attached directly to the valve. This design ensures precise temperature control and energy savings. The specification for the attachment method was:

Table 6-3: System to modify valve temperature specification.

Component	Specification
Cartridge Heater	Provide sufficient power to heat both valves to 370 ^{o}C
	Fit within the packaging constraints underneath the valves
Valve mounted heater bracket	Hold the cartridge heaters to the valves
	Withstand high speeds and forces
	Avoid colliding with the Cylinder Head and gasket plate
	Move with the valves
	Hold a thermocouple in position to measure valve temperature
Power/Control Electronics	Maintain steady state valve temperature with accuracy of ± 5 ^{o}C
	Have safety shutdown procedures in the event of overheating

The final design (Figure 6-8) features two cartridge heaters secured to the intake valves with an aluminium bracket.

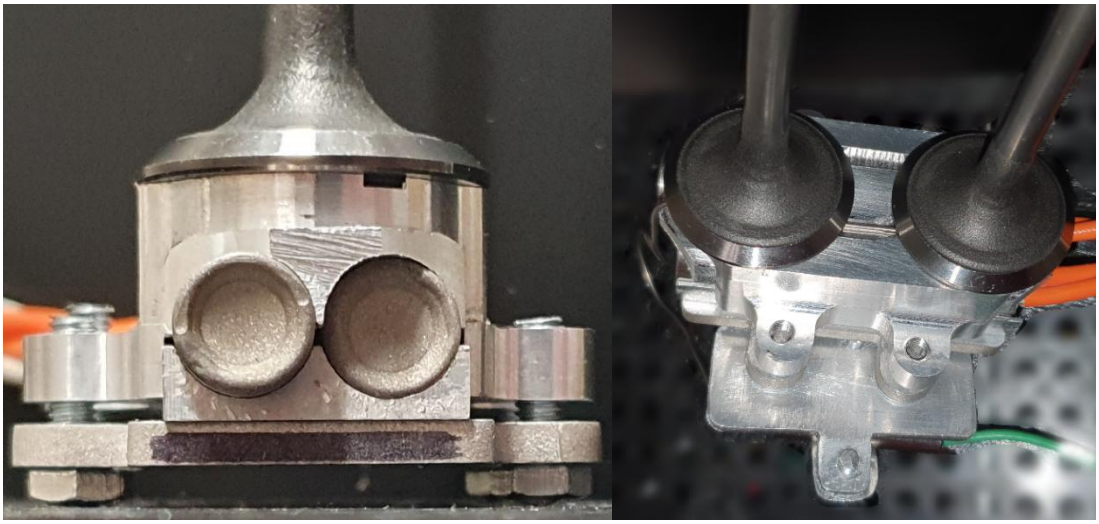


Figure 6-8: Valve heater and holder final design.

6.2.3.2 Cartridge Heater

The 3D scan used for the gasket plate in the Cylinder Head section also aided in designing the valve heaters and holders, by checking for collisions during valve movement and gauging size. Figure 6-9a shows the 3D scan and Figure 6-9b-e show the valve heater and holder in the CADD model.

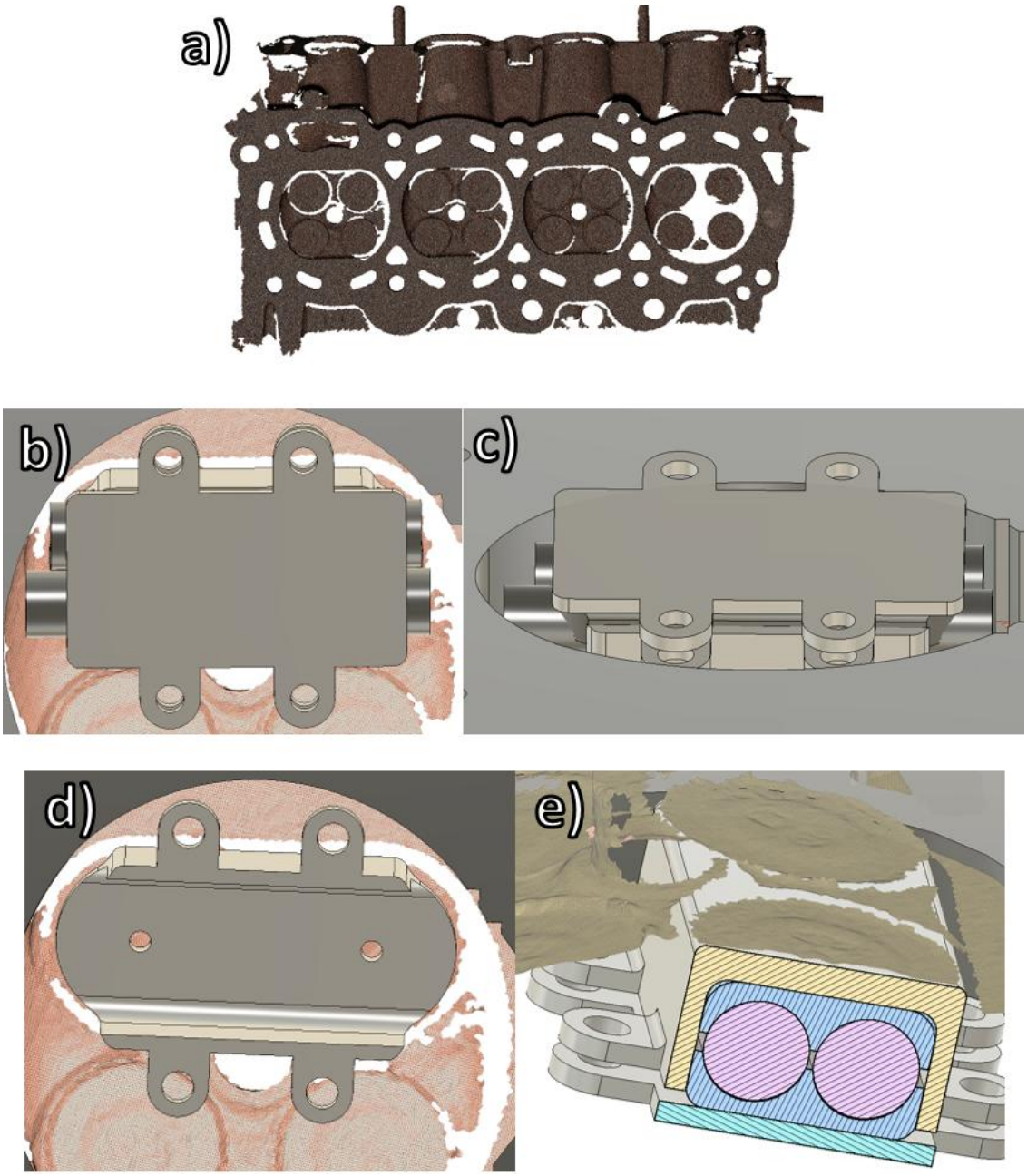


Figure 6-9: Valve heater CADD model a) 3D scan, b) imported model of heaters and holder, c) checking for collisions between holder and gasket plate, d) aligning upper bracket with valves, e) cross section view.

Heater sizing was determined by defining the physical boundaries via the CADD model and valve heat loss calculations using Equation 6-2. Heat transfer coefficients from Cerdoun (186) were used, covering the valve seat, stem, stem/port, and combustion

face. These coefficients were used in Equation 6-2 along with measured surface areas and predicted temperature differences to approximate the rate of heat loss from the valve via conduction to the Cylinder Head and convection to the air flow, allowing the required heating power to be estimated. The highest ΔT value, 350 ^{o}C (370 ^{o}C minus room temperature of 20 ^{o}C), was used to ensure that sufficient power could be achieved. The maximum temperature of 370 ^{o}C was based on previous experiments (35).

$$P = h \times \Delta T \times A \qquad \textit{Equation 6-2}$$

The Heat transfer coefficient *h* varied with engine speed, this was simulated across a range of 3000 to 7500 rpm by Cerdoun (186). At 3000 rpm, approximately 500 W was needed to heat both valves to 370 ^{o}C; at 7500 rpm, 800 W was required. By checking the CADD model for packaging restrictions (Figure 6-9b,c) it was determined that the largest possible heater that could fit in the space under the valves and within the Cylinder Head gasket plate was two 50 mm length, 10 mm diameter cartridge heaters, providing 800 W.

Since the heaters are placed under the valve, a proportion of the heat will transfer away from the valve, therefore a significant safety factor was deemed necessary. A Safety factor of 1.6 at 3000 rpm was sufficient but 1 at 7500 rpm was not. Additional methods to assist heating included using Cylinder Head heat, as the valve seat contacts the Cylinder Head for over half a rotation of a camshaft, this reduces ΔT, along with heating of the intake air. This adjustment lowered the required power to 430 W (safety factor 1.8) and 670 W (safety factor 1.2) for 3000 rpm and 7500 rpm respectively. The safety

factor at 7500 rpm was deemed too low, thus, a speed of 3000 rpm with a comfortable safety factor of 1.8 was chosen and was used to define the valve speed specifications in section 6.2.4.

6.2.3.3 Valve Mounted Heater Bracket

A bracket was designed to secure the cartridge heaters under the valves, in a compact fashion to minimise chances of a collision. The design also aimed to maximise contact surface area with the valve (Figure 6-9d,e). The design (Figure 6-10) features two cartridge heaters clamped side by side with a small gap left between them to allow for some thermal expansion. The jaws were secured by an upper bracket bolted to a base plate, with another small gap between them. This allowed the base plate to flex slightly as the bolts were tightened, ensuring that the heaters were firmly clamped.

Graphite paper was used to improve thermal conduction, filling air pockets with malleable, thermally conductive graphite. Graphite was chosen as it could withstand high temperatures that the alternative thermal pastes could not. Aluminium, chosen for its thermal conductivity and strength-to-weight ratio, minimised bracket weight to handle high valve acceleration (up to 7000 m/s^2). The acceleration was estimated from valve movement modelled as a sine wave. The period of the wave was measured from the cam lobe geometry (estimating valve opening duration) and the amplitude from the radius of the cam lobe.

To manage high inertial forces, the bracket was securely fastened by drilling holes in the top so it could be bolted to the base of the valves (Figure 6-10d and e). Hole locations were measured using the 3D scan of the Cylinder Head's underside, accurate to within

0.1 mm. The bolt diameter was carefully chosen since the valve stem was only 5.5 mm in diameter and there was little depth from the base of the valve before transitioning to the thin stem. Therefore, if the hole was drilled too deep or wide the material that remained would be extremely thin. An M4 bolt was selected as larger bolts would over-stress the thread. This is because a thread depth equal to the thread diameter is necessary to ensure that the thread cut into the valve is not over stressed and consequently stripped. Therefore, to manufacture the thread the hole would need to be drilled at least to a depth equal to its diameter, plus extra depth to give clearance to the tapping tool. As the valve diameter was only 8mm at a distance of 6.5 mm away from the valve base, anything larger than an M4 would have left a wall thickness of less than 1.5 mm, and any slight machining inaccuracy could cause this to be even thinner leading to failure. An M4 bolt was the largest bolt that allowed for a sufficient wall thickness of 3mm and ensured sufficient proof load in the bolt.

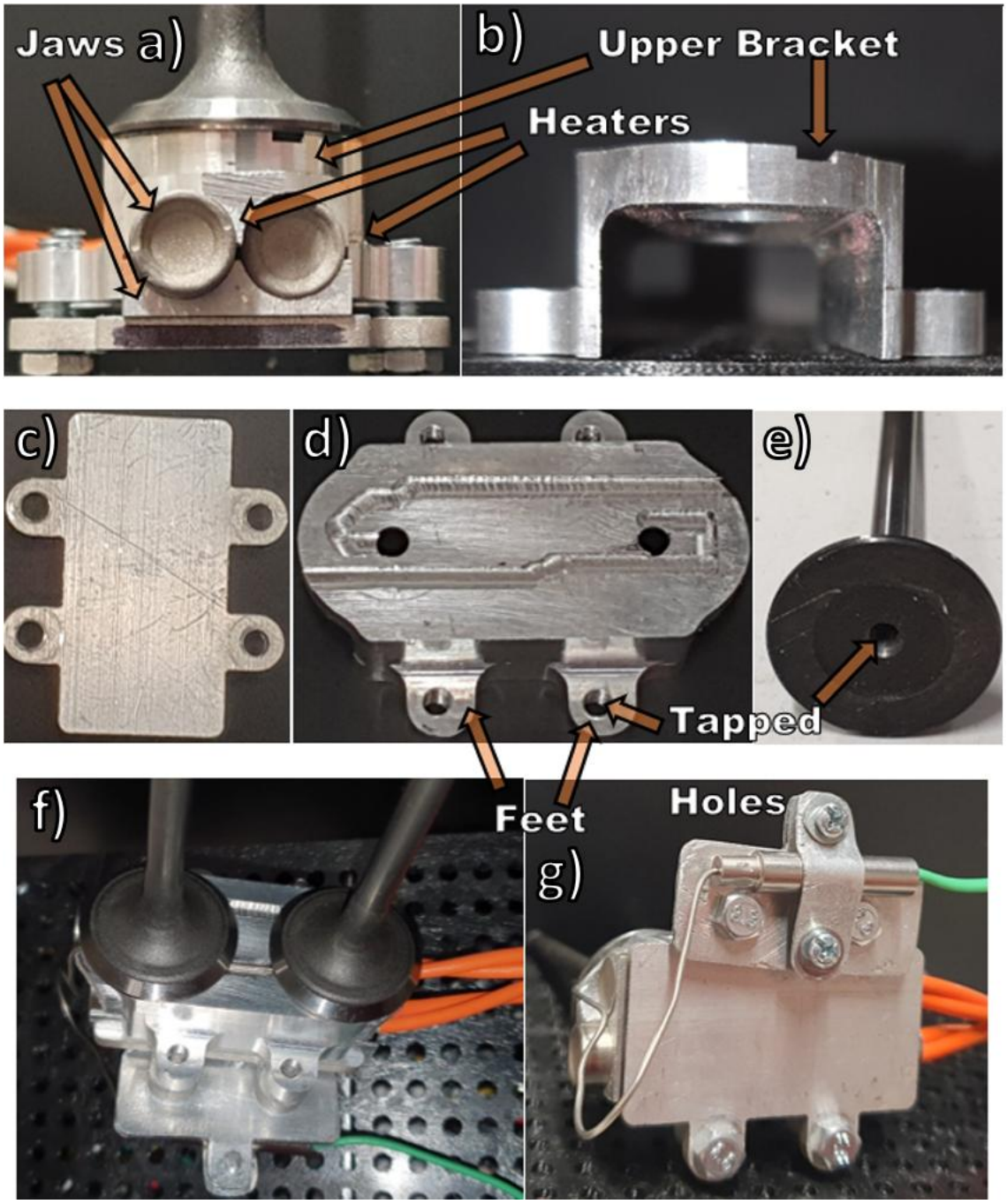


Figure 6-10: Cartridge heater bracket design a) jaws, b) upper bracket front view, c) base plate, d) bolt holes and thermocouple placement, e) valve, f) valve attachment and thermocouple, g) thermocouple bracket.

The groove in Figure 6-10d was designed to fit two 1 mm thermocouples around the tight corners near the bolt holes. When clamped by the valve (Figure 6-10f), vertical

movement is prevented and the bend around the corner stops horizontal movement. Two grooves were cut for both valves so the user can choose multiple places to measure from along the groove cut to a depth of 1.05 mm. The 0.05 mm clearance avoids over-compression of the thermocouple. The rest of the thermocouple is then secured by a bracket (Figure 6-10g).

The bracket was manufactured using CNC machining, water jet cutting, and milling. The upper bracket, the most complex part, required CNC machining for precise and complex dimensions. To confirm the accuracy of the CADD model (Figure 6-9) and prevent collisions with the Cylinder Head and gasket plate, the upper bracket was first 3D printed as a prototype (Figure 6-11). Once the prototype confirmed no collisions and proper alignment with the valve centre, CNC machining began. CNC machining's time-consuming nature limited its use to parts needing high precision. The base plate was manufactured using a water jet cutter, suitable for its 2D shape and because its distance from the valves ensured no collisions, so the ± 0.5 mm tolerance of a water jet was sufficient. The jaws were produced using a manual milling machine, allowing accurate machining without requiring the cost and time of CNC.

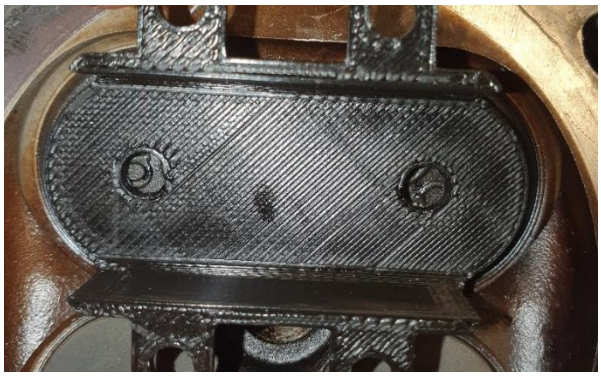


Figure 6-11: 3d print of upper bracket.

The CNC machining was performed on a pocket NC machine. An aluminium billet was first roughly machined with a manual mill to within 2 mm of the final dimensions, to save on time and to ensure the top surface of the upper bracket was square to the sides and parallel to the base. This alignment was crucial as the pocket NC's axis is referenced to the bed face holding the piece (Figure 6-12a).

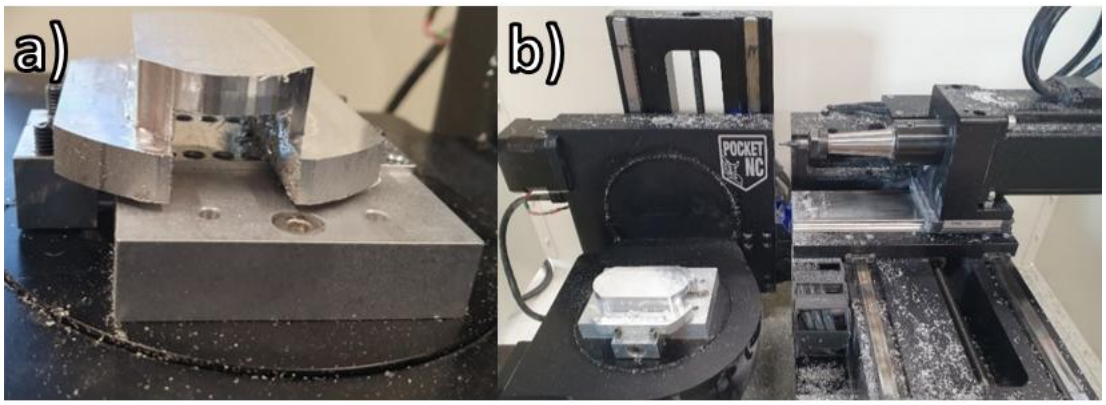


Figure 6-12: CNC machining process a) upper bracket on the clamping face of the pocket NC after the underside had been cut, b) Pocket NC machine.

For the valve's threaded holes (Figure 6-10e), the valve stems were placed in a lathe, and a 3.3 mm diameter, 6 mm deep hole was drilled into the centre. A tapping tool then cut a 4.5mm deep M4 thread.

The jaws were manually machined from an aluminium billet using a milling machine. Though not as capable of producing complex shapes as the CNC machine, the milling machine's larger tools and higher power allowed for quicker machining of the simple jaw shapes which were cut from a single piece.

6.2.3.4 Power/Control Electronics

The temperature of the cartridge heaters was controlled using a PID algorithm like the one used for the Cylinder Head oil temperature controller. However, this setup required fewer automation and safety checks. Unlike the oil system control, which necessitated two thermocouples for the Cylinder Head and the Heat Exchanger, the valve temperature control system only required one thermocouple. This thermocouple was positioned in the groove shown in Figure 6-10d, with the tip against the bolt in the centre of the valve. An additional thermocouple could be placed in the other groove for recording purposes, but it was not essential for control.

To prevent initial overheating during the time it took for the thermocouple to respond to the initial heat rise, the PID was tuned to limit the initial temperature increase of the cartridge heaters. This precaution was crucial, especially if the valve heaters were accidentally turned on without any air or fuel passing over them. In the absence of convective cooling, the heaters could significantly overshoot the target temperature. Therefore, the maximum PID output as well as some of the constants were limited until a specific threshold temperature was reached.

The controller utilised the same components as the oil controller but required only one SSR due to the lower power of the heaters. This time, the box was 3D printed to fit the components and to separate the high and low voltage sides, an aluminium plate was inserted between two 3D printed walls. This design reduced assembly time, improved cooling with strategically placed ventilation apertures, and conserved 3D printing material (Figure 6-13).

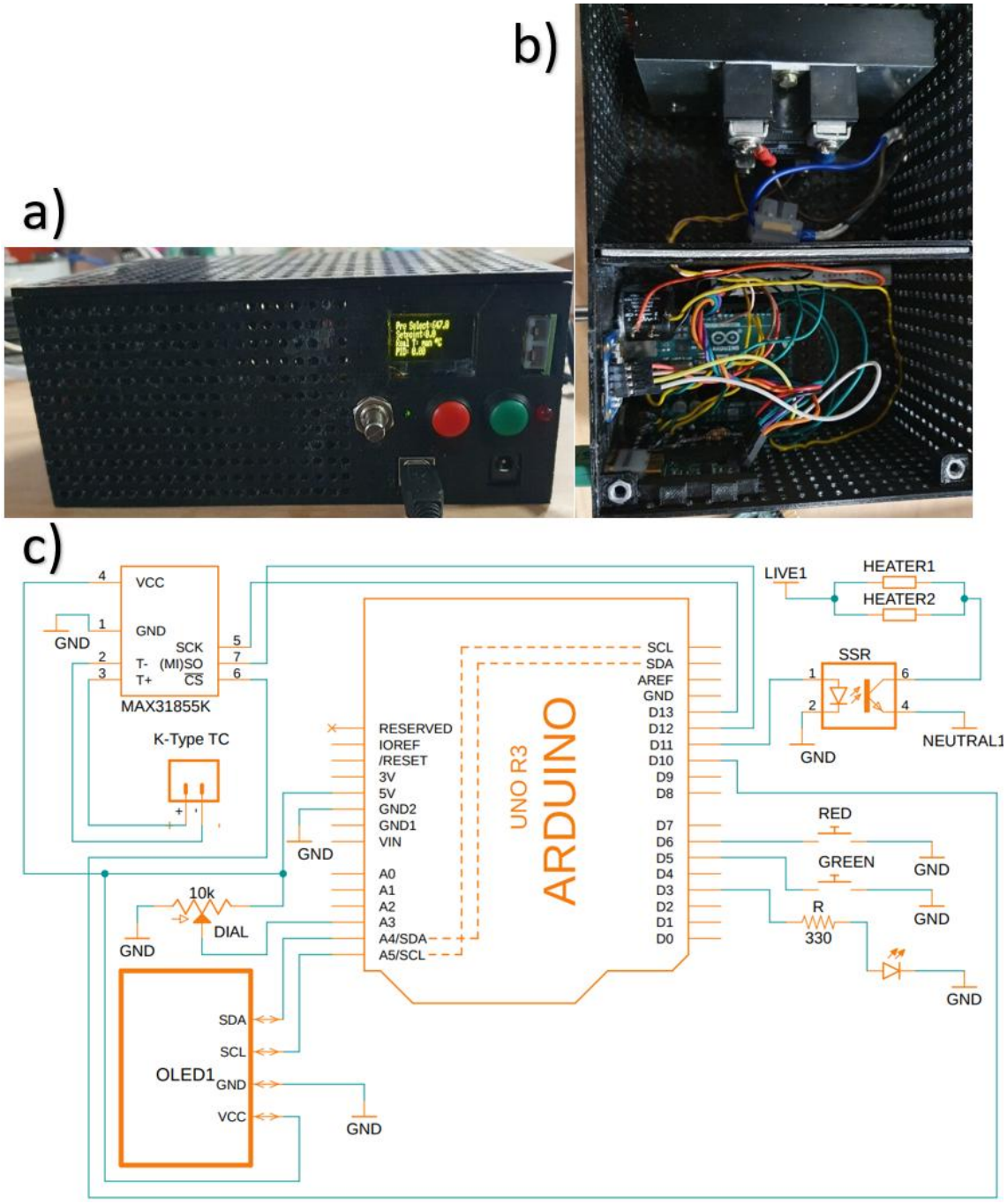


Figure 6-13: Valve temperature controller box a) user interface, b) internal wiring c) Electrical Schematic.

6.2.4 Design and Manufacturing of the System to Actuate Intake Valves

6.2.4.1 Design Specification of the Subsystem

Table 6-4: System to actuate valve specification.

Electric Motor	Provide the camshaft with sufficient torque, allowing it to provide similar valve speeds to those found in an engine with crankshaft speeds of up to 3000 rpm
	Emergency shutdown capability
	Be attached to the camshaft in a way that allows for easy removal of the camshaft from the Cylinder Head
Cylinder Head and Camshaft Extension	Allow access to the camshaft so it can be attached to the Electric Motor
	Seal oil inside the Cylinder Head
	Withstand maximum operating temperature of the Cylinder Head (90 ^{o}C)
Camshaft Lubrication System	Provide the camshaft with a consistent flow of oil, ensuring sufficient durability to enable the completion of the IVD generation tests
	Integrate with the Cylinder Head Extension
	Circulate oil back into the Heat Exchanger

The valve heaters were predicted to be capable of offsetting the convective cooling from the air intake at a mass flow rate equivalent to approximately 3000 rpm, which equates to a camshaft speed of 1500 rpm. Achieving 1500 rpm consistently required acceptable durability, lubrication and control. To achieve this the camshaft was attached to an electric motor with a speed controller and was lubricated via the oil system in section 6.2.2.4 and an additional lubrication system. The manufactured system is shown in Figure 6-14.

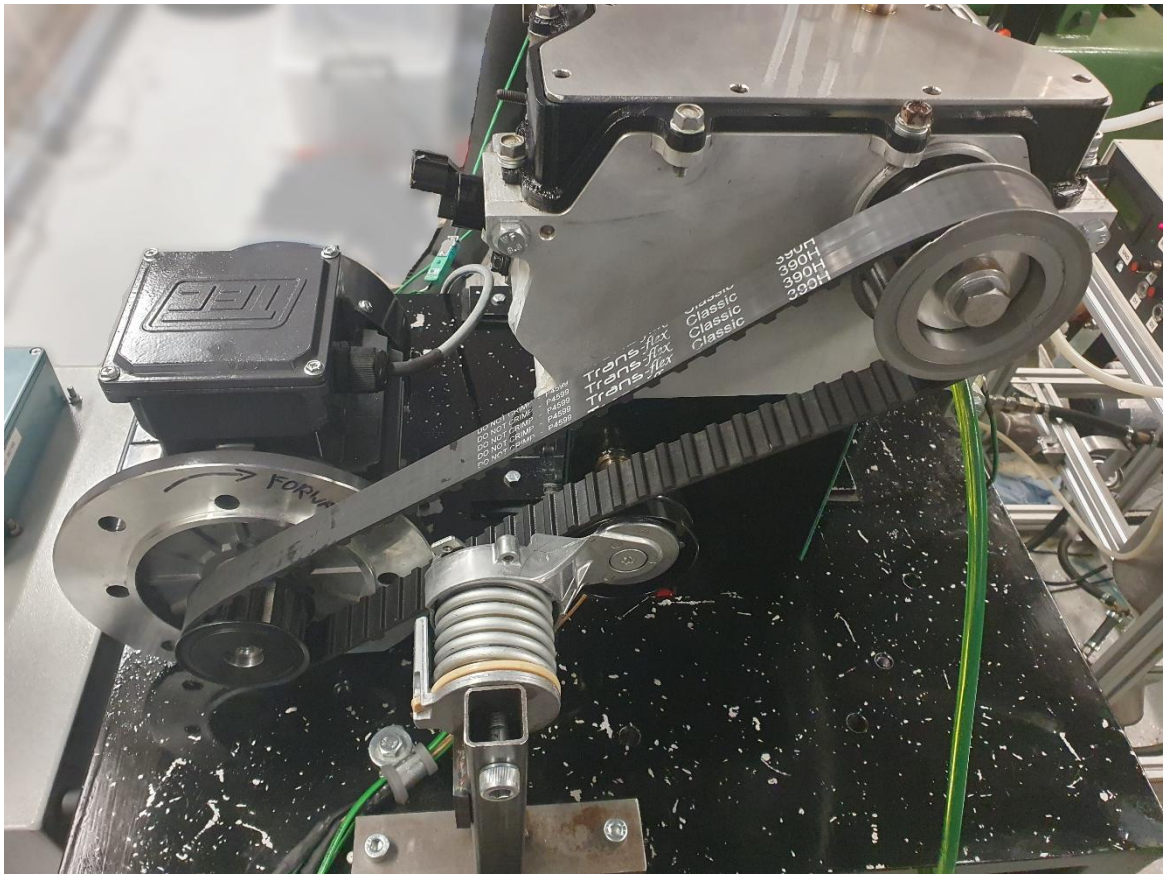


Figure 6-14: Camshaft control system.

6.2.4.2 Electric Motor

To achieve realistic valve speed emulation, the camshaft was selected due to its capability to mimic real engine behaviour. An electric motor of 0.55 kW, operating on 3-phase AC power with an inverter using 1-phase AC electricity, was chosen for its ability to maintain higher torque output and efficiency across a wide speed range and for its durability. By using the acceleration value found in section 6.2.3.3 and information from (187), it was decided that a 0.55 kW 3 phase AC motor would be used. This was used with a gear ratio where the torque at the camshaft was 1.2 times the torque at the motor, this helped to achieve sufficient starting torque and to keep the motor close to its optimal operating speed when testing below a camshaft speed of 1500 rpm. To lower

the torque required by the motor, the camshaft was halved to actuate only two valves, which was sufficient as one valve was needed for fuel injection and the other for diluting the fuel in the extraction box. This was a cost-effective method as it allowed low power motors to be used, which were significantly cheaper than their high power counterparts. The motor was also provided with an emergency stop button.

6.2.4.3 Cylinder Head and Camshaft Extension

To connect the camshaft to the motor, a drive system utilising a belt and pulley was constructed. An extension had to be designed (Figure 6-15) so that the Cylinder Head could accommodate the pulley since the end of the camshaft in the original engine design was located inside the Cylinder Head. As the Cylinder Head was removed from the rest of the original engine there was now no timing chain cover to stop oil leaking out the timing chain end of the Cylinder Head, thus, a new cover was designed to prevent this. Using CADD and a 3D scan of the Cylinder Head the complicated profile of the Cylinder Head could be modelled. The final design can be seen in Figure 6-16. The design is comprised of multiple aluminium plates, designed to be cut via water jet, due to the efficiency and cost-effectiveness of the process compared to traditional machining. Water jet was the favoured 2D manufacturing process as some parts of the design had a high thickness, and as discussed earlier water jetting is cheaper than laser cutting with thick sheets of material. All the plates were 10 mm thick except the two sides which were 35 mm thick, and the plug. The plates were designed to be adhered to the Cylinder Head using a high temperature and chemical resistant epoxy adhesive. Epoxy was chosen as the cast aluminium Cylinder Head could not be welded to.

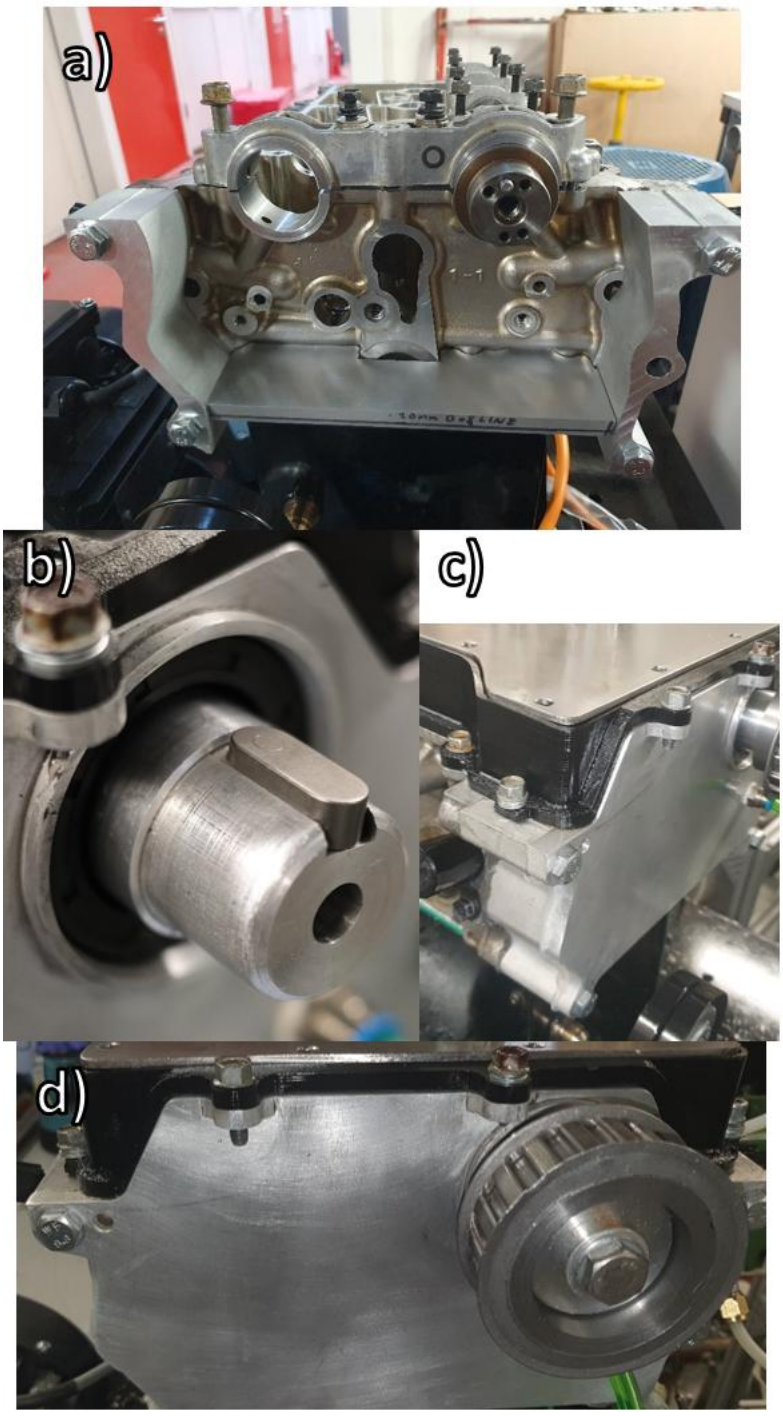


Figure 6-15: Cylinder Head extension a) base and side plates, b) camshaft extension, c) assembled extension (side), d) assembled extension.

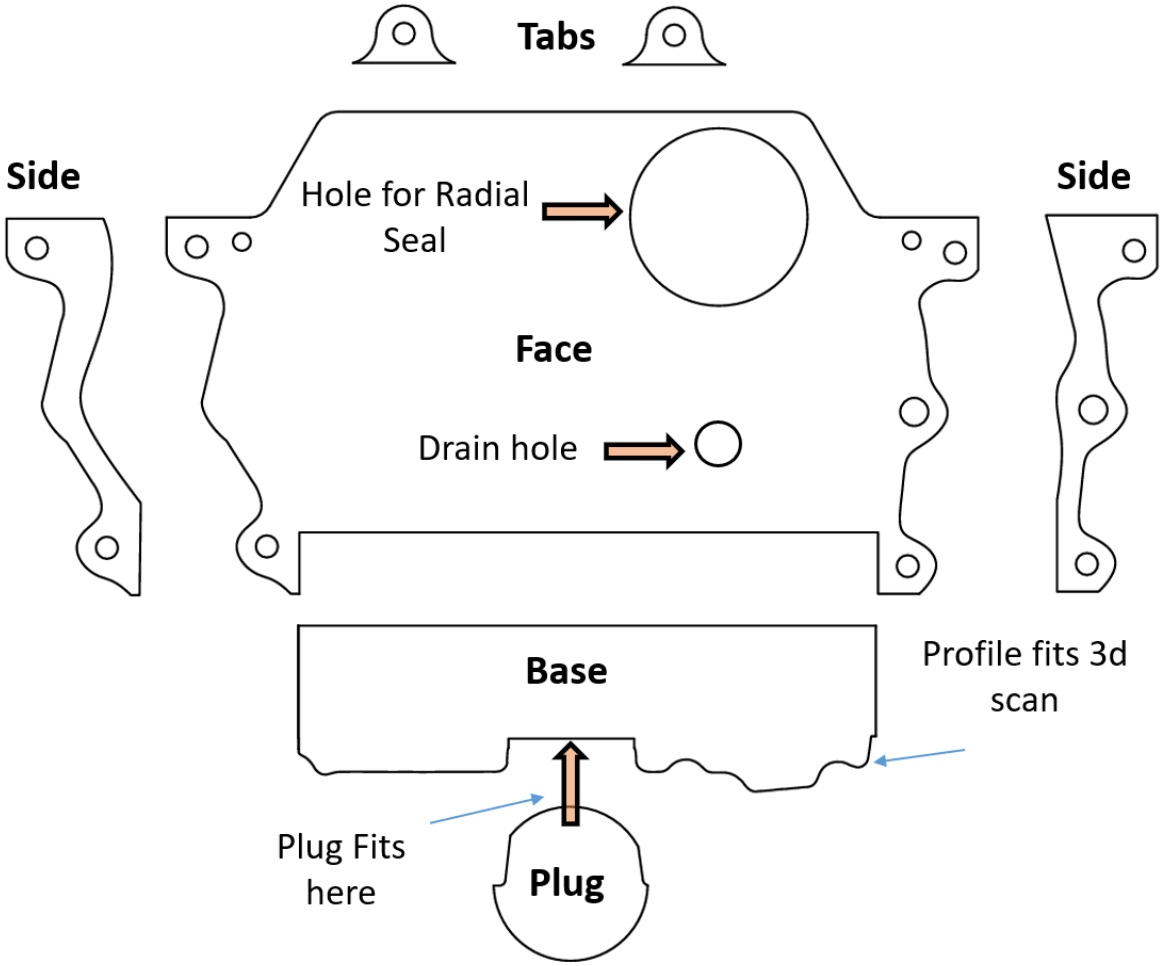


Figure 6-16: 2D design of Cylinder Head extension.

A camshaft extension was designed to protrude through the face plate so that a pulley could be secured to the end of it. To seal the oil from exiting through this opening a radial seal was used. Radial seals require a tight concentric tolerance of ± 0.25 mm with the rotating shaft they are sealing around. This tolerance is smaller than the manufacturing tolerance of the water jet cutter so the diameter of the opening was designed slightly over sized so a machined cylinder could fit into the face plate. The drawing for this part can be seen in Figure 6-17.

A final fitting was designed to fit into the drain hole (Figure 6-16), providing an extra oil drain from the valve section of the Cylinder Head back to the Heat Exchanger box (Figure 6-5c). The drawing for the camshaft extension can be seen in Figure 6-18, this protruded through the radial seal and was bolted to the pulley (Figure 6-15d). Torque was transferred to the camshaft via a dowel pin and keyway on the camshaft extension.

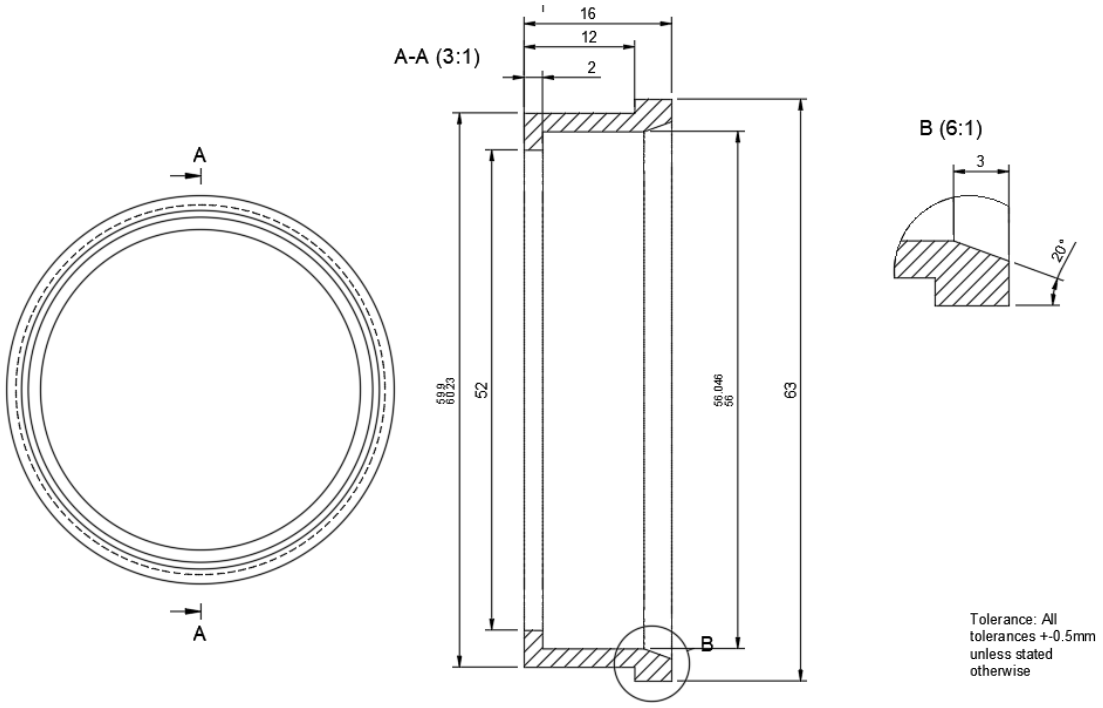


Figure 6-17: Drawing for seal to face plate adapter.

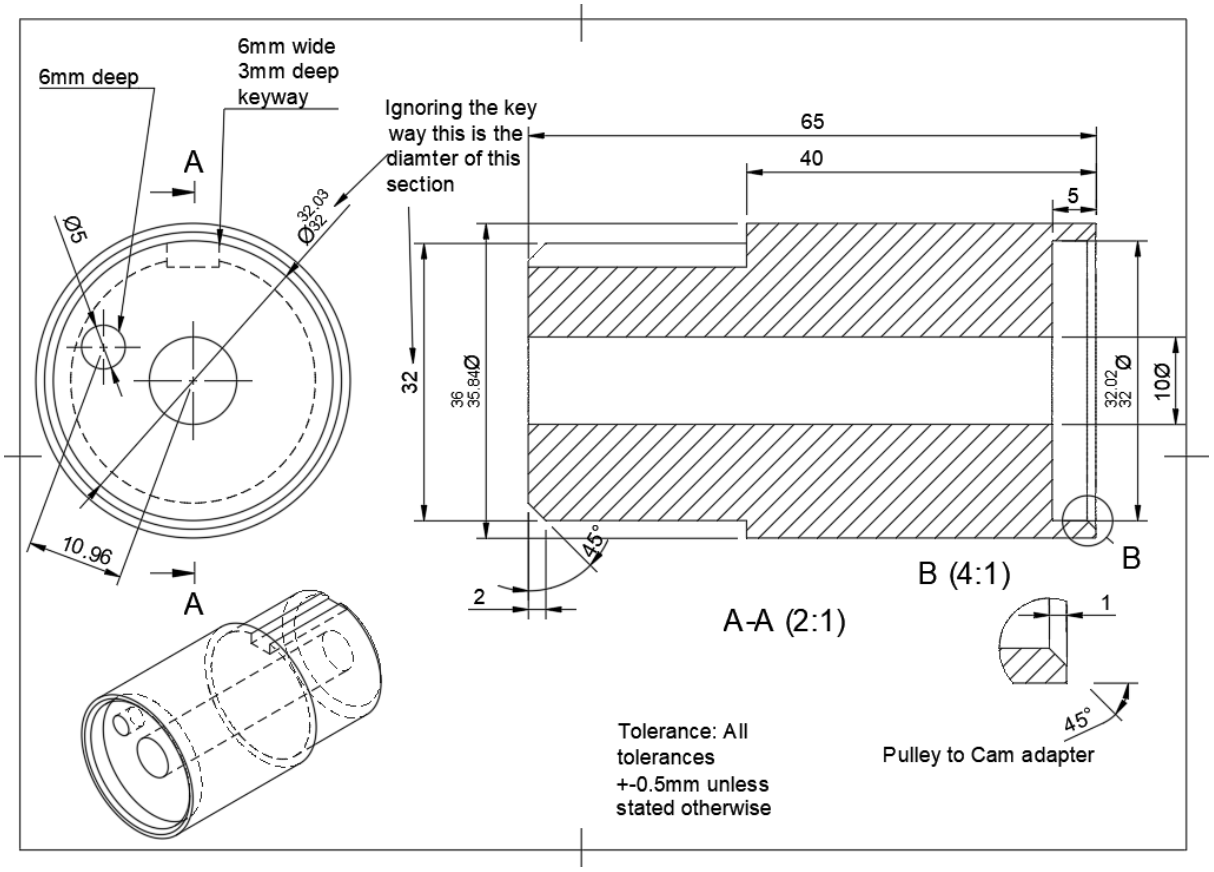


Figure 6-18: Camshaft extension.

The Cylinder Head extension side plates were fastened to the original bolt holes for the timing belt cover and then the base plate was put into position between them (Figure 6-15a). The outer face plate seen in Figure 6-15d was then clamped into position which held the base plate. In this position the base plate was welded to the 2 sides forming a rigid group. The parts were then removed and the rigid group of the base plate and sides, with the plug in the correct position (Figure 6-16), were then secured to the Cylinder Head using the epoxy. Once the original epoxy had set, a continuous bead of epoxy was run around the interior edge of the combined base plate and sides where it met the Cylinder Head, to provide a seal. After this was completed, the front face was then

sealed to the base plate and sides using silicon. This section was not adhered so that in the future it could be removed if any maintenance was necessary.

The camshaft extension and seal to face adapter were turned on a lathe from aluminium to the tolerances required by the radial seal. The seal to face adapter was then bonded to the extension face plate with epoxy. The radial seal was fitted before gluing, concentricity was ensured by placing the camshaft in its natural position and rotating it within the radial seal whilst the position of the seal adapter was adjusted.

The Cylinder Head extension meant that a new valve cover was required (Figure 6-19). The new cover was designed using CADD and a 3D scan of the Cylinder Head's top. A 3D-printed polycarbonate base was chosen for its high temperature resistance, strength, cost-effectiveness, and ability to follow the complex Cylinder Head bolt pattern while the stainless-steel lid was water jet cut for durability and ease of welding. The Valve Cover was designed to be secured to the Cylinder Head and aluminium Cylinder Head extension with bolts and adhered tabs (Figure 6-16), using an O-ring chord for sealing (Figure 6-20). The 3d print was designed to house nuts as shown in Figure 6-20 to secure the stainless-steel lid to the 3d print. This allowed the lid to be removable which would be necessary for the alignment of the camshaft lubrication system which is described in the next section.

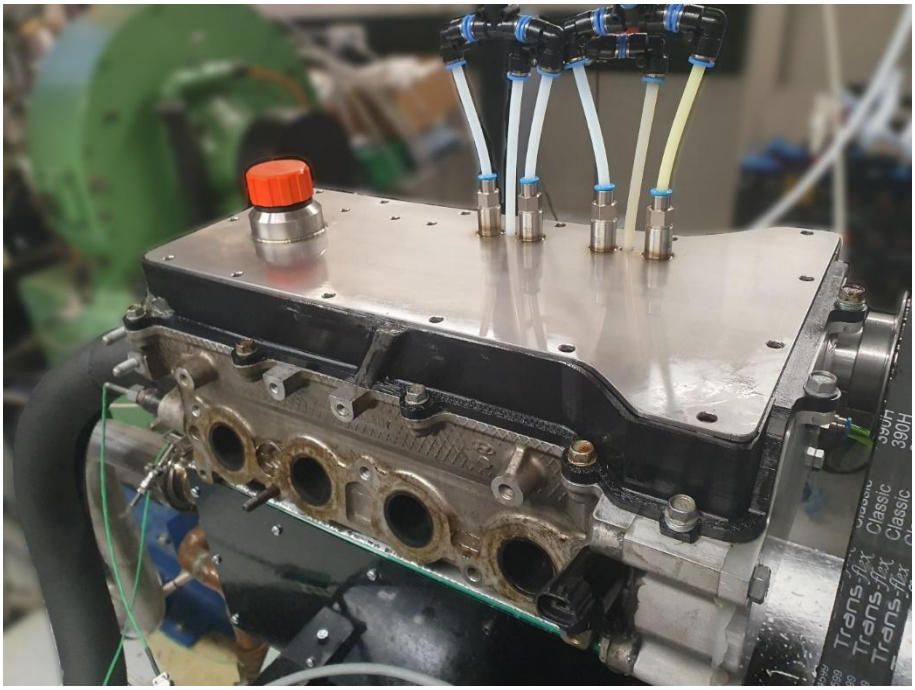


Figure 6-19: Valve cover.

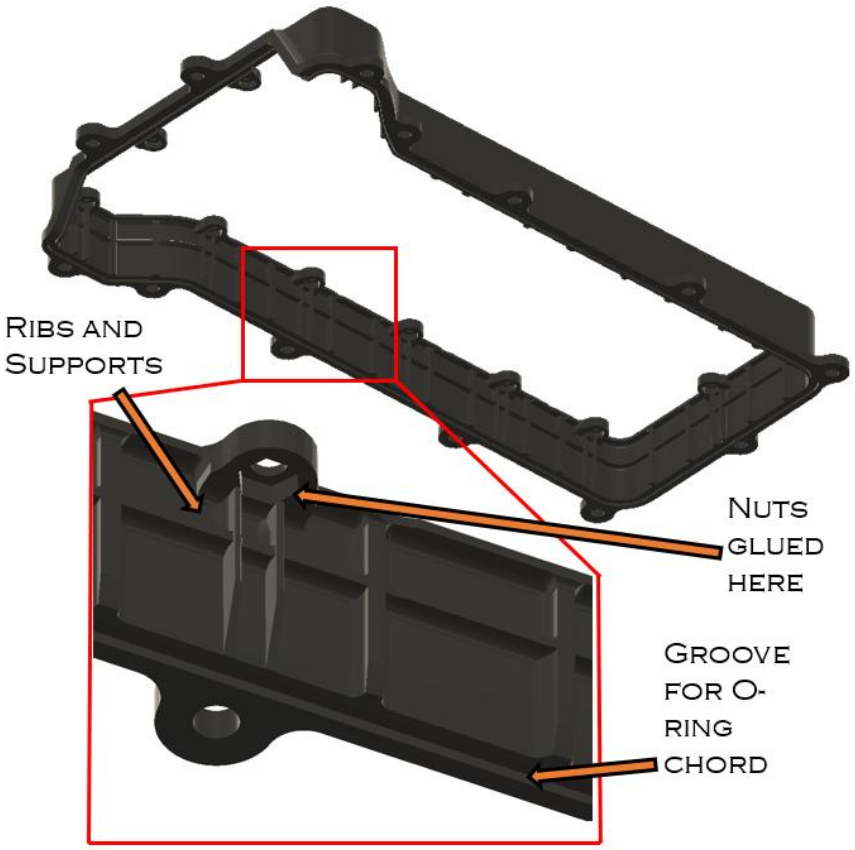


Figure 6-20: 3d print design.

The polycarbonate was printed using a Fused Deposition Modelling process on a large bed size within an environment maintained at a high temperature. As this was a challenging 3d print to make it was sourced externally. The Water Jet was also sourced externally, thus minimal manufacturing was required for this part. Only additional parts such as fixing the nuts into their housing and fitting the O-ring were done in house.

6.2.4.4 Camshaft Lubrication System

The camshaft lubrication was partly provided via the oil system described in section 6.2.2.4 but after preliminary tests it was found that this did not provide sufficient lubrication to the camshaft. This is possibly due to one pump being used to move the heated oil through the coolant jacket and up to the bearings whereas in a real engine these would be separate systems. Thus, a system was made to directly lubricate the bearings and the cam lobes. This was necessary as in a regular engine the cam lobes are lubricated by an oil mist that is created by components like the crankshaft and timing chain impacting the oil at high speed, however these components were not present in this system. The secondary lubrication system consisted of a 4 l tank elevated above the Cylinder Head (Figure 6-21), with plastic pipes directing oil to the camshaft bearings and lobes. The tank was pressurised initially to remove air locks and start the oil flow, which was then maintained by gravity. A shut-off valve allowed control of the flow to the cam lobes, and a sight glass enabled monitoring of the oil level. The tank's size ensured that it only needed refilling once an hour, with overflow managed by the Heat Exchanger. Fittings were welded and screwed into the stainless-steel lid to direct oil onto the cam lobes and bearings effectively (Figure 6-21). This system ensured that the valve

actuation system operated efficiently and remained lubricated to ensure good durability.

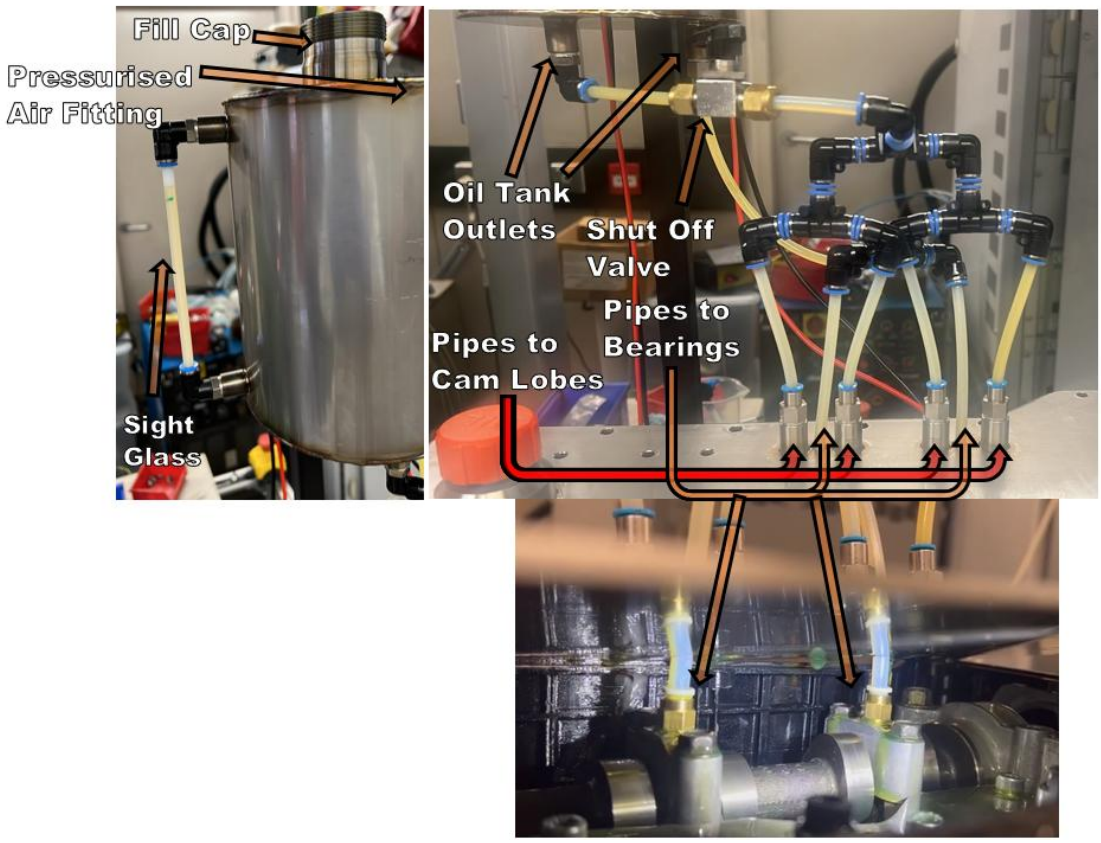


Figure 6-21: Camshaft lubrication system.

6.2.5 Design and Manufacturing of the Fuel Injection System

6.2.5.1 Design Specification of the Subsystem

Table 6-5: Fuel injection system specification.

Component	Specification
Fuel System	Deliver pressurised fuel to the fuel injectors
	Inject a consistent amount of fuel between tests
	Allow for control of injection timing, frequency and pulse width
	Store enough fuel for 1 hr of testing
	Must be compatible with fuel injection system from original engine

To deliver the fuel to the valve a fuel injection system was modified. This system is shown in Figure 6-22.

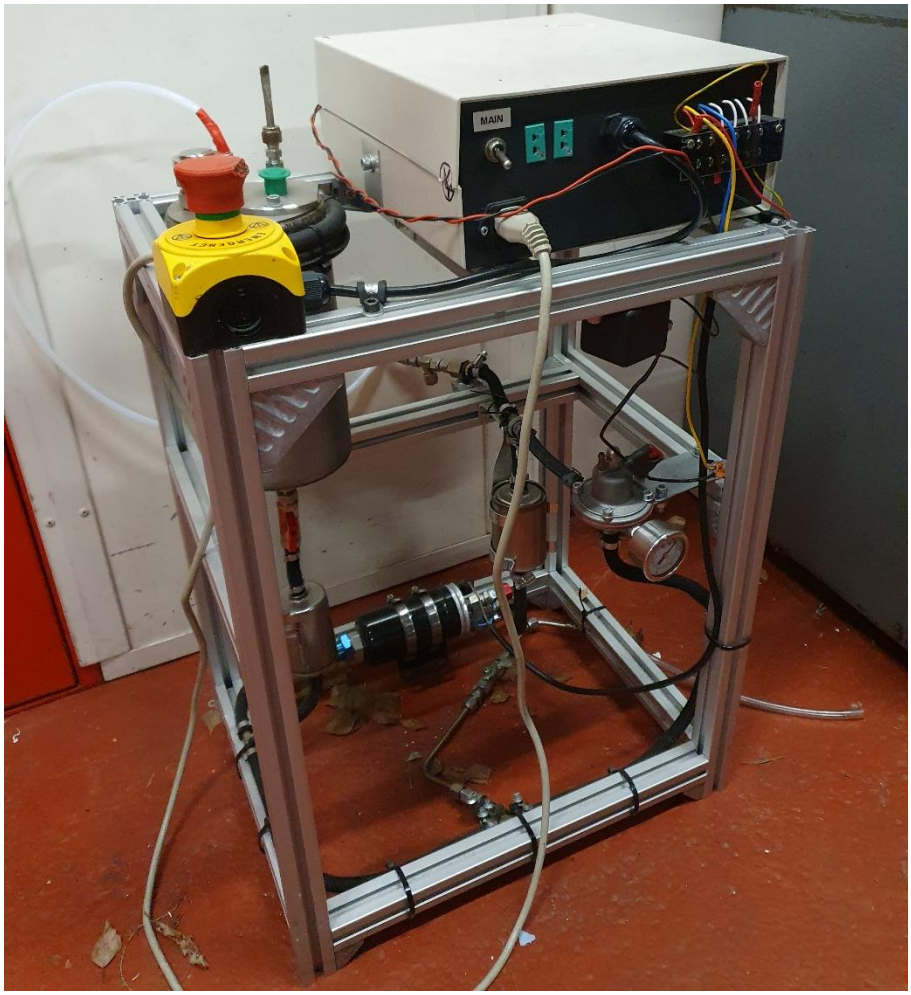


Figure 6-22: Fuel injection system.

6.2.5.2 Fuel Injection Delivery and Control

The fuel injection system in Figure 6-22 consisted of a fuel pump used to pressurise the fuel. The pressure was controlled by a regulator set to 3 bar. A filter was also installed along with a return pipe and a drain. The fuel injector solenoid was controlled by an Arduino MEGA which used PWM to control the injector pulse width, frequency and timing. The Arduino used a relay to engage the fuel pump and could also be shut off by an emergency shutdown button.

To adapt the fuel control system to the Cylinder Head the original fuel rail from the engine was chosen to be used. The fuel control system used a 1/8” fitting to attach to its original injector so a corresponding 1/8” fitting was adapted to fit onto the engines fuel rail. This can be seen in Figure 6-23. The adapter in Figure 6-23b was made by turning down a billet of stainless steel on a lathe and then welding a 1/8” fitting to it. A groove was cut into the adaptor for an O-ring to fit into. The adaptor was pressed into the inlet of the fuel rail (Figure 6-23c) via the plate seen Figure 6-23a. The plate was machined on a mill and was secured to the original bolts on the fuel rail. This secured the fuel system to the fuel rail.

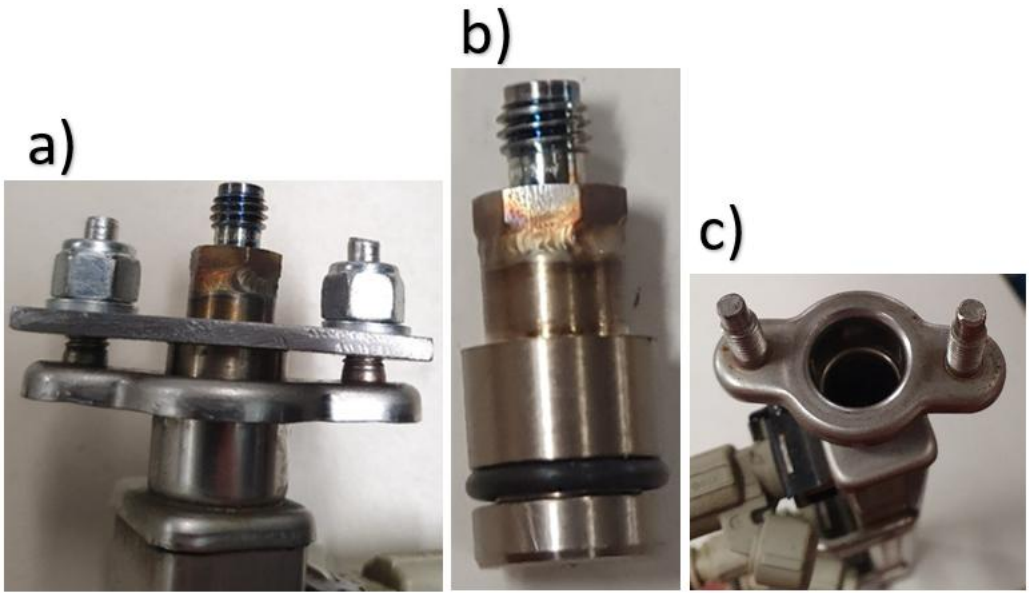


Figure 6-23: Fuel rail adapter a) full assembly, b) adapter, c) fuel rail inlet.

To control the fuel mass flow rate either the injection pulse width or frequency can be changed. To calculate the value of the fuel mass flow rate the pulse width or frequency is calibrated with respect to volumetric flow rate. This is achieved by measuring the volume of fuel injected into a container over a set amount of time at various pulse

widths or frequencies. The fuel volume can then be weighed to find the density of the fuel and thus the fuel flow rate can be calibrated to either pulse width or frequency.

6.2.6 Design and Manufacturing of the Air Intake and Extraction Systems

6.2.6.1 Design Specification of the Subsystem

Table 6-6: Air intake and extraction systems specifications.

Component	Specification
Pipework	Provide controllable and measurable mass flow rate across a range comparable to those seen entering a single cylinder in a modern engine
	Provide controllable and measurable pressure, up to the maximum values often seen in modern engine intake manifolds
	Provide controllable and measurable temperature, up to the maximum values often seen in modern engine intake manifolds
	Deliver air to the valve with fuel injection
	Deliver air to the other valves to dilute the extraction
Intake Gasket Plate	Integrate with the Cylinder Head
	Seal any air from leaking
Extraction	Safely extract fuel vapour
	Provide measurement of extraction temperature and emissions

6.2.6.2 Pipework

To adhere to the specification above it was decided to deliver intake air to the valve via pressurised air. Compressed air was delivered to the valves with and without fuel injection via separate pipe systems. The air going to the fuel injection valve was controlled in terms of mass flow rate, pressure, and temperature. The diluting air flow was only controlled by a shut off valve to turn it either on or off as control of this flowrate was not critical.

A diagram for the pipeline for the air intake and fuel injection is shown in Figure 6-24. The pressure is controlled and measured by a regulator connected to a compressed air line, this is then connected to a volumetric rotameter. A thermocouple is placed before the rotameter allowing for mass flow rate to be calculated from temperature, pressure and volumetric flow rate. The air then passes through a heated line and then to the intake port. A thermocouple is placed before the intake port and after the heated line. The output of the heated line is changed manually until the intake port temperature is at the required temperature.

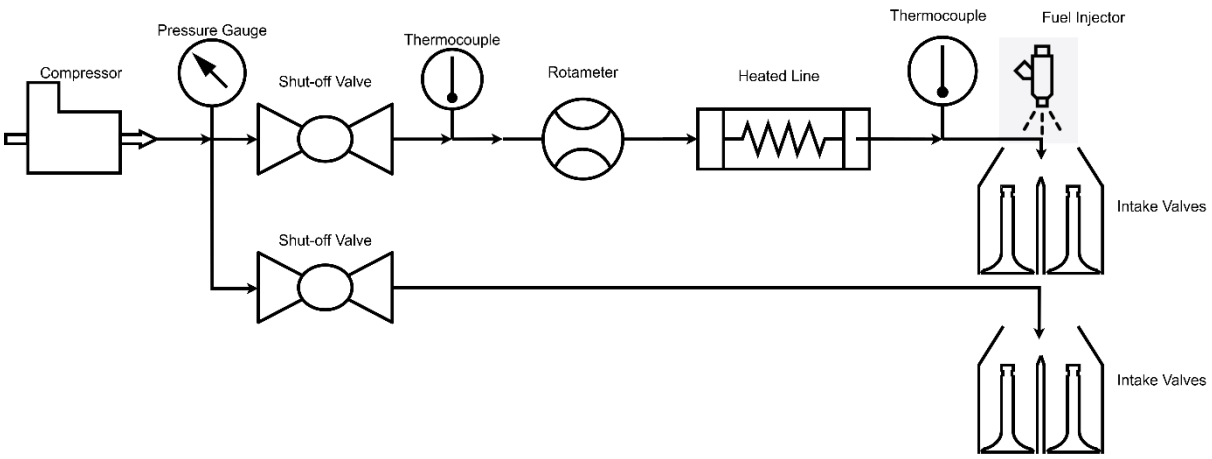


Figure 6-24: Intake air diagram.

6.2.6.3 Intake Gasket Plate

To attach the intake air to the Cylinder Head a custom plate was made which is secured to the Cylinder Head by the bolts from the original intake manifold and sealed with a gasket. The plate can be seen in Figure 6-25. The plate was manufactured by water jet cutting and was made from stainless steel. Stainless steel was chosen to increase the weldability of the stainless steel fittings used to connect to the intake pipeline. Water jet cutting was chosen to reduce the chance of warping, ensuring an air-tight seal. The

CADD was again modelled from the 3d scan of the Cylinder Head to align it with the bolt pattern from the original intake manifold and the intake ports. As shown in Figure 6-25 the port with the active fuel injection went to its own independent pipeline with a thermocouple and the other 3 joined together and went straight to the compressed air pipeline. All three intake ports were setup in case future tests involve using all four sets of valves.

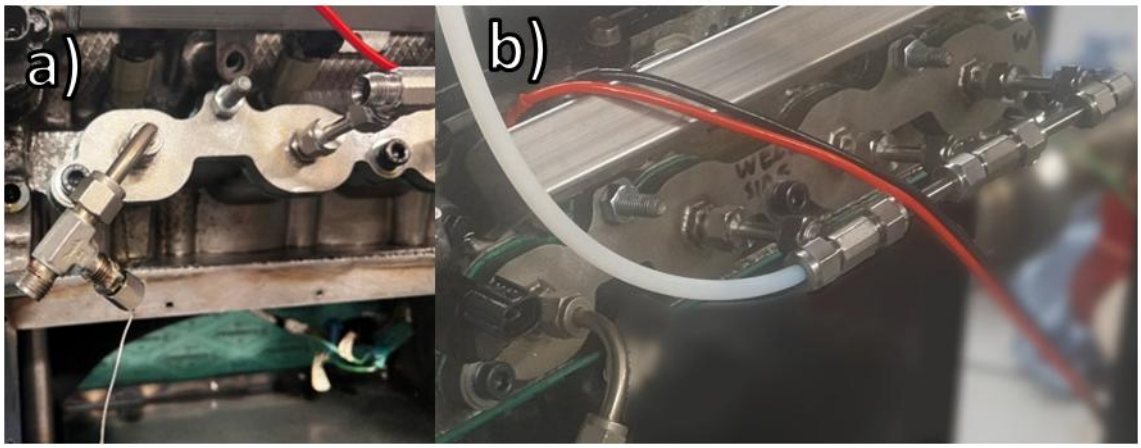


Figure 6-25: Intake plate a) pipe connections and thermocouple placement, b) fittings to other intake ports.

6.2.6.4 Extraction

The injected fuel mixes with the air in the intake port with the active injection and impinges on the valve. The remaining fuel vapour then dilutes with incoming air from the other intake valves, significantly reducing the risk of any combustion. The diluted air-fuel mix is then extracted from the extraction box. This was achieved by welding a 2” steel pipe to the outlet in the extraction box (Figure 6-4). A quick release V-band clamp was then welded to this pipe allowing for the whole setup to be attached to an exhaust system built in the engine lab. This also allowed the setup to be portable. Fittings were

welded into the exhaust so that a thermocouple and emissions analyser could be installed in the extraction. This is for safety reasons so any combustion would be seen by an increase in both temperature and combustion products CO_2 and H_2O.

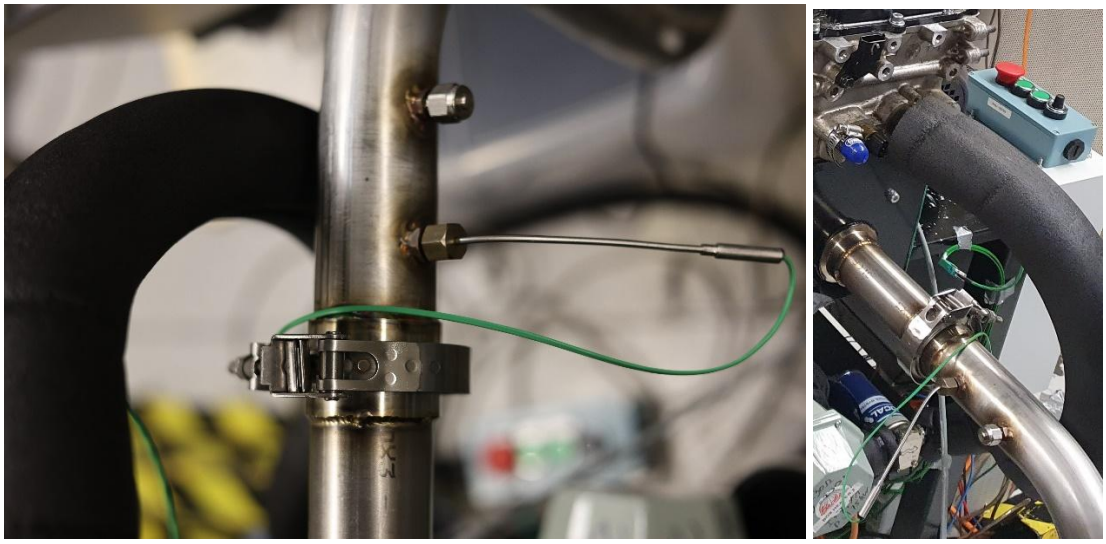


Figure 6-26: Extraction pipe and fittings.

6.3 Results and Discussion of Proof of Concept Testing

In order to ascertain the extent to which the product is capable of fulfilling the PDS, a series of preliminary tests, outlined in Table 3-4, were conducted for the purpose of proof of concept evaluation. The tests were primarily designed to identify potential issues and to refine the setup. Nevertheless, the tests yielded some intriguing insights that can inform future enhancements to the control of the setup and provide insight into its potential utility.

6.3.1 Impact of Temperature

The dynamic tests started with a short duration experiment of 2 hr of dynamic functioning (valve actuating via the camshaft) with a valve temperature of 250 ^{o}C. This was chosen as an estimate of where the critical temperature might lie, because as seen in section: 2.4.3.1 the critical temperature often laid within 200-250 ^{o}C. However in the studies by Cheng and Repsol (27) (35), the temperatures were measured on the valve tulip and in the intake port respectively. Whereas in this study the valve temperature was measured underneath the valve, adjacent to the heat source. Therefore, due to heat losses between the base and the valve tulip, it was hypothesised that in order to obtain a valve tulip temperature of 200-250 ^{o}C a temperature higher than this would be required on the base of the valve. The temperature was then further increased for experiment 2 (also dynamic conditions) along with the duration being increased after experiment 1 had confirmed the function of the dynamic valves. Significant deposits were observed after the two experiments.

Figure 6-27a shows the normalised mass of valve accumulated deposits on valve 1 and valve 2 independently for the duration of the test for all the experiments. There is some variability on the mass of deposits accumulated on each of the valves. This variability was partly attributed to the nature of the fuel injection. The fuel is injected in the intake runner and then splits between the two valves as seen in Figure 6-2, however the split may not be even. By observing Figure 6-27a, it can be seen that for the static tests that whichever valve has the most deposits per hr fluctuates. The difference between the valves was found to be statistically insignificant ($p < 0.1$). The difference between valve

mass with the dynamic tests is also statistically insignificant due to the small sample size, but it is worth noting that both dynamic tests showed valve 2 to have a higher mass (this was especially evident with the 9 hr test). This could be due to the dynamic valves resulting in a different air flow pattern pulling the fuel through the valves in a different manner compared to the static tests, however further dynamic tests would need to be executed to confirm this.

Figure 6-27b shows the sum of the IVD mass per hr from both valves against the mean temperature of the valves. A clear trend can be observed that bears resemblance to the findings reported by Cheng and Repsol (27) (35). A peak temperature of approximately 210 ^{o}C is indicated. Interestingly the peak temperature observed in this study is at a similar temperature to those reported by Cheng and Repsol (27) (35), despite the difference in valve temperature measurement location. The maximum sum of the deposits was 34.27 mg, recorded in a 5 hr test. This demonstrates the efficiency of this experimental rig as this was a sufficiently short test time to conduct a test, measure, and analyse results in 24 hr. 34.27 mg is predicted to be sufficient to observe the difference in deposit mass between fuels and additives, as it is significantly more than the 3.45 mg which Cheng (27) found to be sufficient to reliably compare fuels, additionally it is within a similar range of IVD per hr to the standard test results from Table 2-1. However, further tests are required to confirm the repeatability of the system.

The dynamic valve results in Figure 6-27b fit the same trend as the static valves, despite showing evidence for much more conductive heat loss. In addition to this the increased fuel flow rate from test 4 onwards appears to not impact the trend of the results,

perhaps suggesting that the air-fuel ratio is more important than the fuel flow rate. The overall trend is comparable to those observed in real engines, which is encouraging and provides evidence that the fundamental concept of the experimental rig is effective.

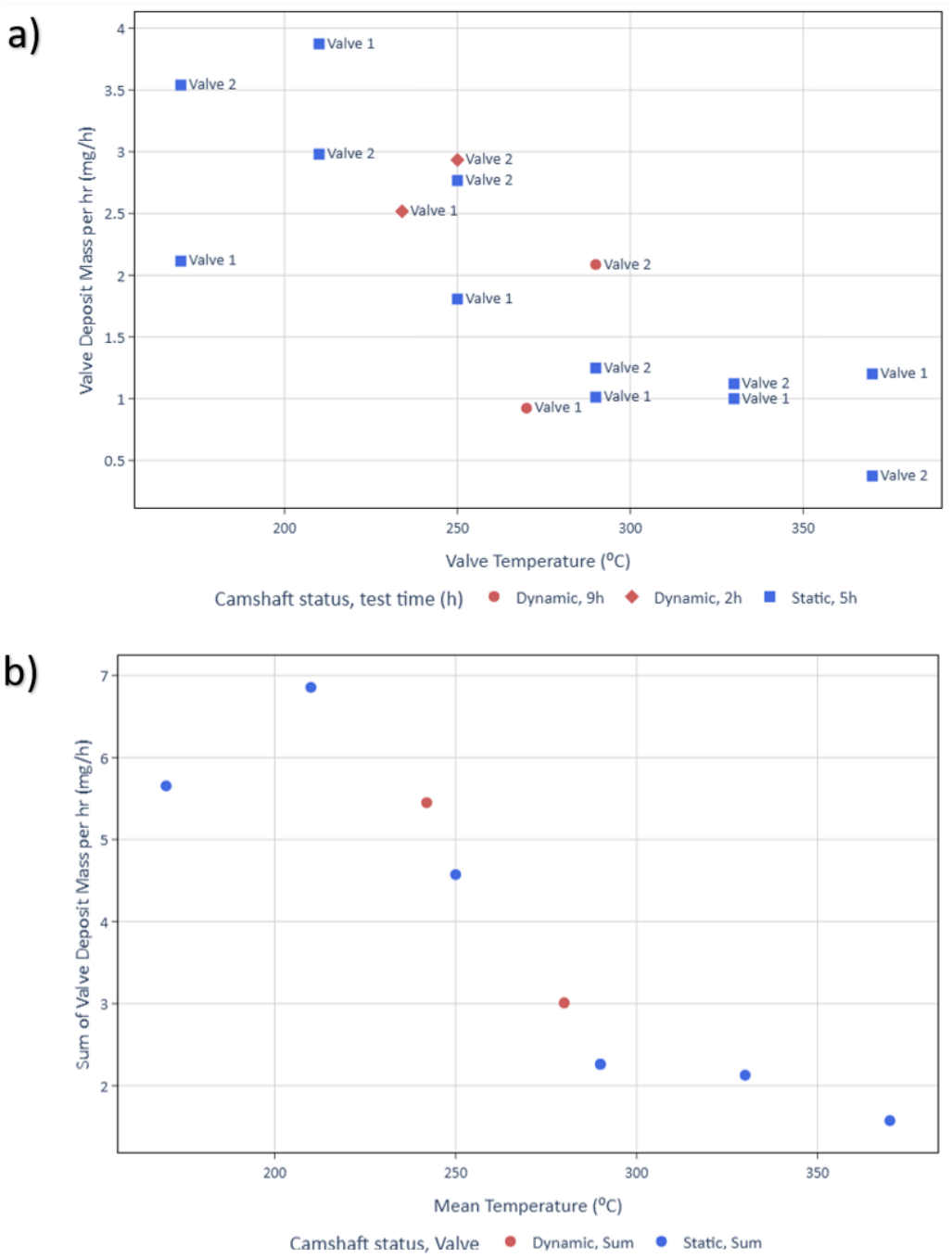


Figure 6-27: Impact of Valve Temperature on IVD mass: a) All results, b) Sum of valve mass against mean temperature (deposit mass is measured immediately after the tests and normalised against duration).

6.3.2 Distribution of Deposits

Following the conclusion of the experiments that significant amounts of deposits can be formed with the developed facility and method, photographic documentation was compiled, providing a visual representation of the distribution of deposits around the valves (Figure 6-28-Figure 6-36): the direction of the fuel injection is indicated by the arrow. In general, the distribution of the deposits appears to be related to the orientation of the valve in relation to the point of fuel injection. In static tests conducted at temperatures including and exceeding 250 ^{o}C, a faint silver deposit was observed on the upper surface of the valve tulip, which is oriented towards the fuel injectors. The reverse side of the valve is devoid of silver deposits, though it exhibits the presence of darker deposits. It is hypothesised that the side of the valve that is closest in proximity to the injector will accumulate the greatest quantity of fuel-based deposits in a concentrated area. This aligns with a finding by Gail (10) who found that the valve is 80 ^{o}C cooler at the location of fuel impingement, resulting in a temperature closer to the critical temperature of 210 ^{o}C when the rest of the valve is above the critical temperature. Resulting in deposits being concentrated in this area.

The majority of the reverse side of the valve is exposed to a small number of darker deposits of oil originating from the valve seal above. It would appear that the fuel washes off these darker deposits on all sides of the valve, with the exception of the reverse side. This agrees with observations regarding the cleaning effect of fuel injection discussed in the literature review. It is not uncommon for minor oil leakage from the stem seal to occur in engines, particularly in older models. Given that older engines are

the engines most affected by IVD, it is possible that oil leakage from the valve stem seal may serve to exacerbate the existing problem of IVD. This could be an area worthy of further investigation, which this experimental rig allows for.

In the 200 ^{o}C and colder static test the deposits appear quite different to the hotter temperatures. The deposits are very dark and form further down the tulip. They are largely situated on the flat section of the valve tulip as opposed to the part where it transitions to the stem, like that seen in the higher temperature tests. The orientation is still relevant though as on the side facing the injector there is a viscous substance, possibly fuel deposits, and even though the reverse side has deposits, it is not as present.

The images show that the static and dynamic tests resulted in different deposit distributions. The static tests result in the majority of the fuel accumulating on the upper portion of the tulip at high temperatures and on the flat surface of the tulip at low temperatures. In contrast, the deposits observed in the dynamic tests exhibit a more uniform distribution across the entire surface of the tulip, displaying a darker shade and a greater concentration of deposits around the valve seat compared to the high temperature static tests and a similar shade and distribution to those found in the 200 ^{o}C static test. This is particularly evident in the dynamic test where valve 1 was maintained at 290 ^{o}C. The more uniform distribution of the deposits compared to the static tests can be attributed to the fact that the valves are closed for a large portion of the camshaft's rotation. This allows the liquid fuel to pool on the valve, which is a significant factor in the formation of deposits. This is particularly apparent when comparing the deposits on the edge of the valve seat between the dynamic and static

tests. This provides further support for Cheng's (27) theory that the majority of fuel deposits are created by liquid fuel.

The difference in distribution could also be due to the different valve temperature distribution with the dynamic tests. Due to the conductive heat loss to the Cylinder Head the valve in the dynamic tests is likely to be colder around the valve seat, and when the thermocouple was measuring 290 ^{o}C in the 9 hr dynamic test this could bring the outer perimeter of the valve seat that is in contact with the Cylinder Head closer to the critical temperature window around 210 ^{o}C. This aligns with the change in deposit distribution observed with the static tests, because as the valve temperature decreases it can be observed that the majority of the deposits move further down the valve towards the valve seat, which is also where most the deposits are in the dynamic tests. This is possibly because at high valve seat temperatures such as 370 ^{o}C the upper portion of the valve will be colder, especially where the fuel impinges, potentially close to the critical temperature of 210 ^{o}C and thus more deposits form in this location, and as the valve seat temperature decreases the lower portions of the valve enter the critical temperature window. When comparing this to results in Figure 6-27b a theory can be made that the deposit mass increases when the valve temperature distribution results in the lower portion of the valve tulip being in the critical temperature window, as it has a larger surface area for deposit formation, and is more flat and horizontal, preventing droplets of fuel from falling off, increasing fuel residency time on the valve.

The distribution of temperature and hence deposits could be slightly different with the rig compared to a real engine as the heater applies heat through conduction rather than

convection. This was mitigated by aiming to ensure that the thermocouple was in contact with the valve so its temperature could be matched to that of valves found in combustion engines, regardless of how the heat was transferred to it. The temperature distribution around the valve could be further measured by placing thermocouples on the upper side of the valve, allowing for differences between the simulations and a real engines temperature distribution to be accounted for. However, this was challenging with the dynamic movement of the valve but could be possible for future static tests. The design of the cartridge heater holder could also impact airflow around the valves as it obstructs the area between the two valves, this could then in turn impact where the fuel impinges on the valve. This design however was necessary to provide sufficient heat to the valves.

The shorter dynamic preliminary test, in which valve 2 was at 250 ^{o}C, also demonstrated the presence of dark deposits around the tulip, accompanied by the emergence of additional dust-like deposits, which were exclusively observed on the side oriented towards the injector. This suggests that although the distribution of deposits is more uniform in the dynamic tests the location of the injection still influences the deposit distribution. This can also be observed in both Figure 6-33 as well Figure 6-34. In Figure 6-33 there is an area on the reverse side to the injection which appears to be free of deposits and in Figure 6-34 the same pattern can be observed along with another pattern on the side facing the fuel injection. The pattern on the rear side is likely caused by their being more fuel pooling around the side of the valve facing the injector than the rear, leading to fewer deposits on the rear. The pattern on the front face is likely due to

the direct impact of the fuel providing some washing effect before the fuel then pools to create the deposits.

Another observation that was made was that at the lower temperatures, 250 ^{o}C and below, the deposits were much easier to remove from the valve, both with the initial soak in ethanol and the thorough cleaning with the cloth. Suggesting a different structure of the deposits at lower temperatures. To further investigate this aspect, elemental analysis could be performed on the deposits.

Further experimentation is required to conclude if it is necessary to simulate valve movement to accurately represent IVD or if results from static tests alone can replicate the behaviour of different fuels in an engine. These preliminary results have shown that dynamic valves potentially result in different IVD and temperature distributions even though the IVD mass remains similar to those found in the static tests. There is also potential for dynamic valves impacting the air flow and distribution of fuel between the valves as seen by the difference in IVD between the valves. Currently these effects seem small, so it is suggested that for preliminary investigations that a static test is sufficient. However, studies (145) (9) discussed in the literature review, found that the shape and composition of the IVD can impact airflow over the valve and fuel adsorption, resulting in poor engine performance, thus the impact that dynamic valves have on IVD shape and composition should be investigated in the latter stages of fuel and additive development to more reliably predict how they will impact IVD formation and how this could impact engine performance.

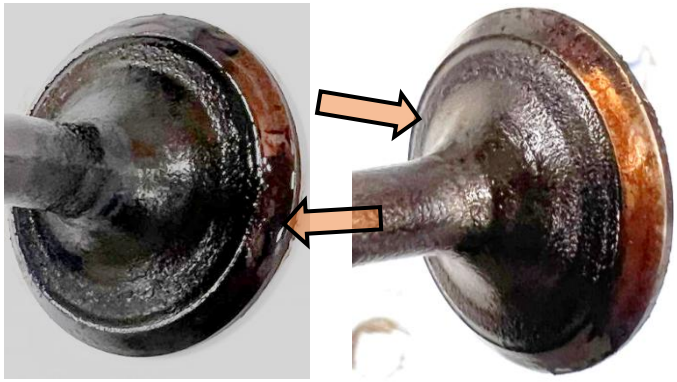


Figure 6-28: 170 ^{o}C static test images.



Figure 6-29: 210 ^{o}C static test images.

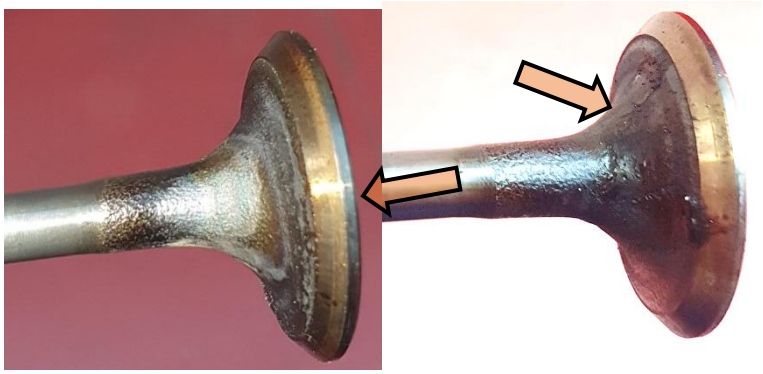


Figure 6-30: 250 ^{o}C static test images.

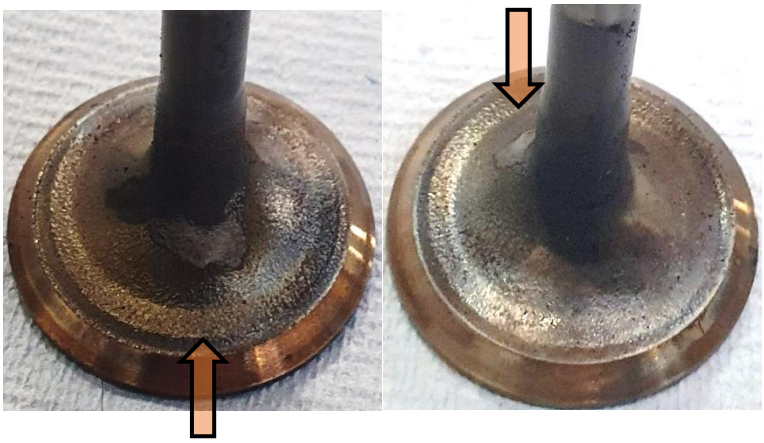


Figure 6-31: 330 ^{o}C static test images.

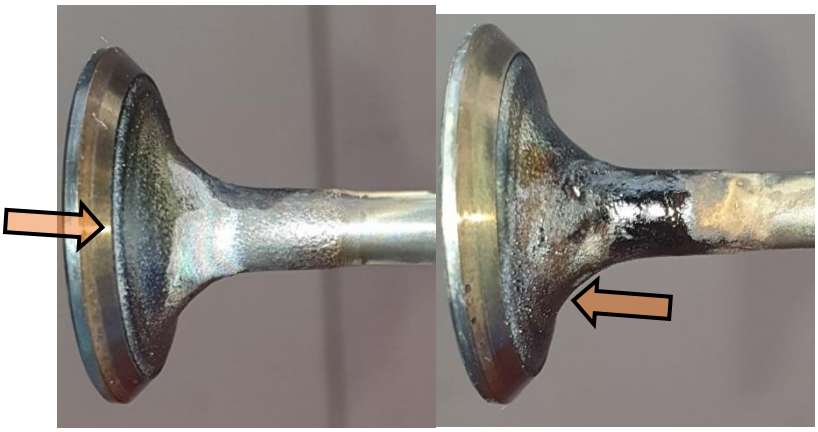


Figure 6-32: 370 ^{o}C static test images.

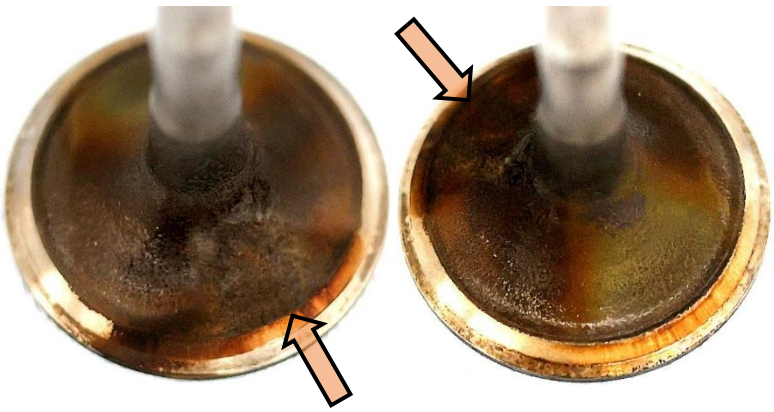


Figure 6-33: 270 ^{o}C 9 hr dynamic test images (Valve 1).



Figure 6-34: 290^{o}C 9 hr dynamic test images (Valve 2).

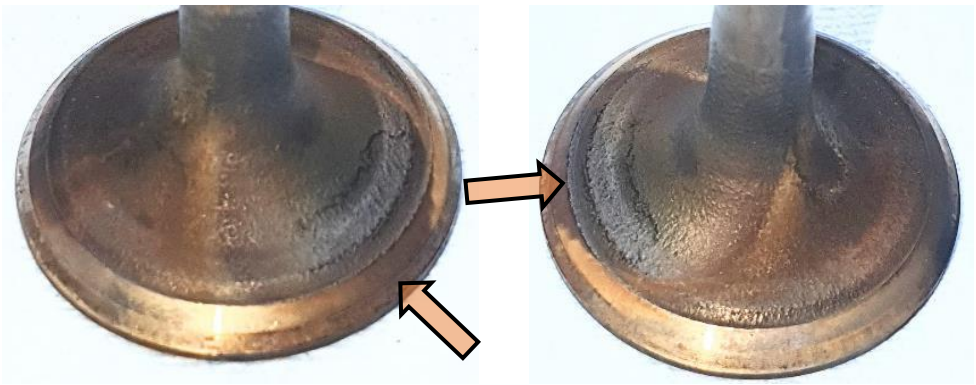


Figure 6-35: 250^{o}C 2 hr dynamic test images (Valve 2).

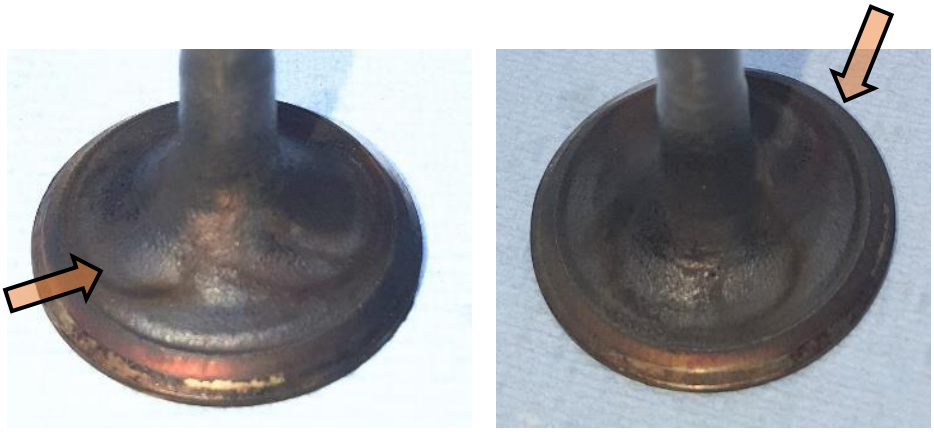


Figure 6-36: 230 ^{o}C 2 hr dynamic test images (Valve 1).

6.3.3 Control Variables

The response of the variables that were controlled by the PID controllers constructed for the experimental rig are illustrated in Figure 6-37. Figure 6-37a shows that the valve temperature response was effectively regulated, exhibiting an initial overshoot that subsequently stabilised. Then, a decline in temperature is observed due to the beginning of the fuel injection. However, the PID successfully recovers the temperature and kept it constant for the duration of the tests, with fluctuations within a confidence interval of ± 0.2 ^{o}C from the mean over a sample size of 5 min ($p < 0.05$). The sum of the small fluctuations and the measurement error of the thermocouple results in a total error of ± 2.2 ^{o}C, fulfilling the specification. In addition to accurate measurements the valve heater was found to have successfully fulfilled the specification outlined in its subsystem section, as it was observed to reach the peak temperature of 370 ^{o}C. Furthermore, the valve heater holder was able to maintain the heaters in contact with the valve without colliding with any stationary objects, despite the high valve speeds. Additionally, it was removable for the measurement of valve mass.

Figure 6-37b shows the control response of the Heat Exchanger and Cylinder Head controller. The code described in section 6.2.2.5 was successful in controlling both the systems, where initially control priority was given to Heat Exchanger during the warmup phase where the Heat Exchanger stabilised at approximately 80 ^{o}C, and remained at this temperature for approximately 20 min, to allow the heat to evenly spread throughout the oil, ensuring the oil entering the pump was at 70 ^{o}C. The pump was then engaged, rapidly increasing the Cylinder Head temperature. Control priority was then given to the

Cylinder Head where the temperature stabilised at 67 ± 3 ^{o}C (± 2 ^{o}C thermocouple measurement error plus ± 1 ^{o}C fluctuations). Whilst maintaining the Heat Exchanger temperature at ~70 ^{o}C to protect the oil pump.

67 ^{o}C was chosen as the Cylinder Head Temperature as it was the coldest temperature where the Heat Exchanger Temperature remained at ~70 ^{o}C. A relatively cold Cylinder Head Temperature was chosen, because as explained in the literature review a low intake temperature where the fuel is injected prevents the fuel vaporising, resulting in more condensed fuel, producing more deposits. The temperature control was tested up to the maximum required Cylinder Head temperature of 90 ^{o}C as well. The safety control described in section 6.2.2.5 was also checked and found to be successful. The Cylinder Head control only engaged once it was clear that the pump was working properly, i.e. the Cylinder Head temperature increased. This was important as if the pump is not functioning and the Cylinder Head thermocouple is in control, the PID will demand more heating power, but the temperature recording will not increase, thus even more power will be demanded, potentially resulting in severe overheating of the Heat Exchanger. The temporary and full shutdown procedures also acted as secondary protection mechanisms to prevent overheating and were successful as if the Heat Exchanger ever exceeded either of these shutdown thresholds the PID power demand was set to zero. The function of the Heat Exchanger was fulfilled to the PDS as it did successfully withstand temperatures of 110 ^{o}C, and its insulation also showed adequate performance as shown by the low temperature difference between the Heat Exchanger and the Cylinder Head in Figure 6-37b of <3 ^{o}C.

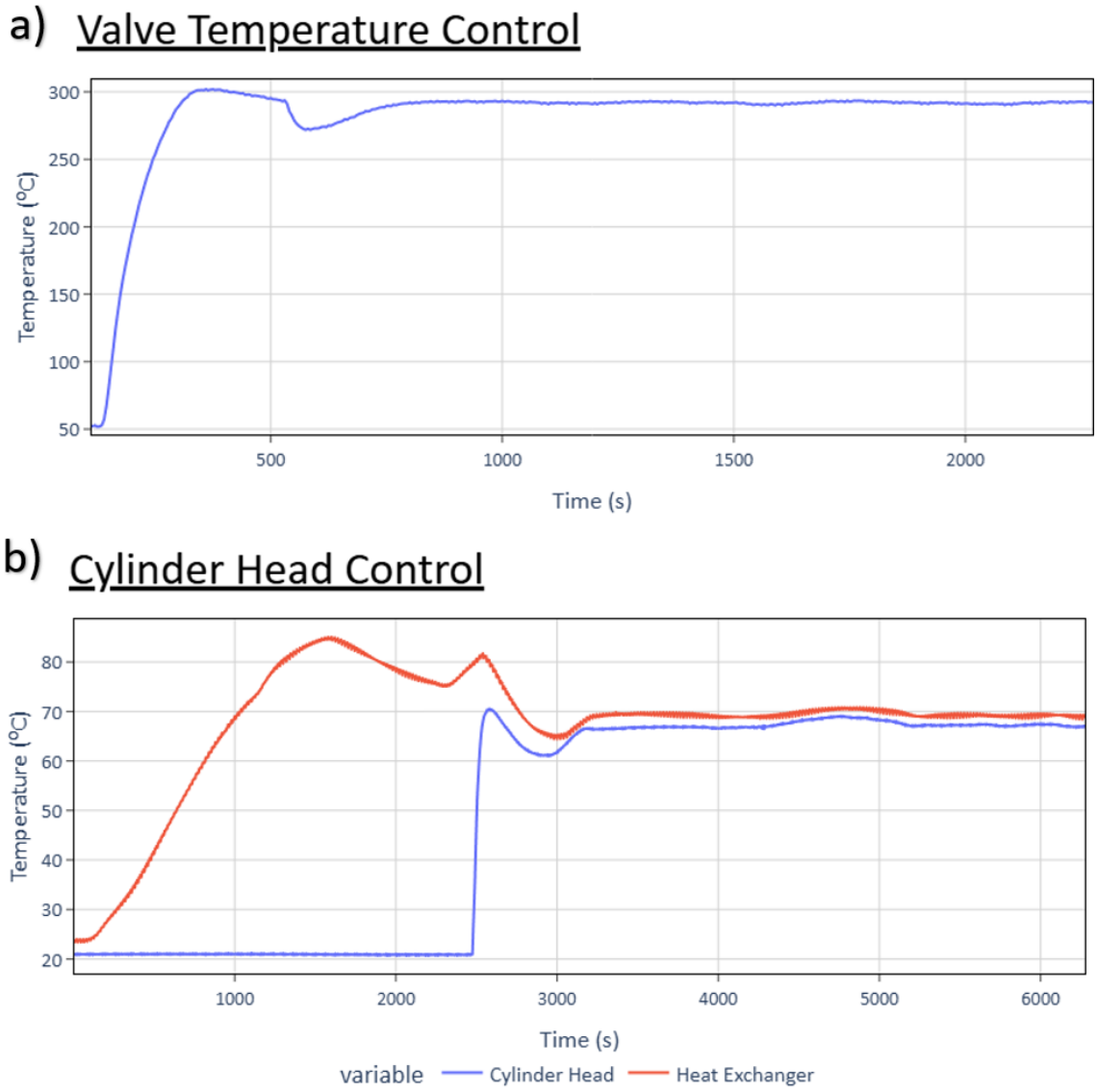


Figure 6-37: Control of temperatures a) Valve, b) Cylinder Head.

The other control parameters outlined in the PDS were also successful where the camshaft successfully actuated the valve in a realistic way, and this was tested over a 9 hr test. The motor speed was recorded by the motor inverter and was recorded to be 740 rpm, resulting in a camshaft speed of 620 rpm. This speed was chosen to be conservative for the longer duration tests, however the motor was tested to be capable of generating camshaft speeds of 1500 rpm in shorter duration tests.

The intake air mass flow rate, pressure, and temperature were tested and were successfully adjustable. The Intake air temperature was capable of temperatures up to 80 ^{O}C which exceeds those normally found in an engine's intake manifold, indicating the range of regular engine conditions is achievable. The pressure was controllable up to 6 bar which far exceeds those seen in regular intake manifolds. This allowed the mass flow rate to be controlled between 5 and 40 kg/h, representing a range of engine conditions from low speed-low load (e.g. 1200 rpm 10 Nm) to medium speed-high load (e.g. 2000 rpm 150 Nm). This was successfully measured using the volumetric flow rate displayed by the rotameter and the temperature and pressure measured before it.

The intake air coming through the non-heated valves successfully diluted the air-fuel ratio inside the extraction box. No large increase in extraction temperature was seen indicating no combustion. The fuel vapour was successfully extracted from the extraction box as the laboratory alarms did not detect any fuel vapours.

The Fuel system was also tested and found to fulfil the PDS. The fuel flow rate was adjustable by changing the injection pulse width or frequency. This was calibrated to a fuel mass flow rate as described in section 6.2.5.2. To check fuel flow consistency throughout the test, the fuel rail pressure was monitored, and the calibration was repeated after the test. The fuel flow was found to be consistent and the pressure stayed at 3 bar. The system was successfully integrated into the fuel injection system of the original Hyundai engine with no leaks and stored enough fuel for 1 hr of testing. The storage could be improved upon as currently it has to be topped up throughout the test.

6.4 Conclusions

In conclusion the IVD experimental rig successfully fulfilled the overall product design specifications, each sub system also fulfilled its own specification. The control of the parameters was demonstrated to be stable and accurate allowing for operators using the experimental rig to identify the impact of the key selected parameters that the experimental rig can control. This will allow for the investigation of fuels and additives to be carried out with a great deal of control in a more efficient way than using the traditional method of a full-scale engine on a dynamometer.

The preliminary results showed that the experimental rig can produce significant fuel derived IVD in a short period of time. The preliminary results showed insights into the impact of temperature on deposit mass and how realistic dynamic actuation of the valves potentially impacts deposit distribution differently compared to static valve tests. Dynamic and static tests both fit into the same trendline with regards to deposit mass against valve temperature, which supported existing literature on the existence of a critical temperature where deposits are formed.

This chapter provides guidance on how to create an Intake Valve Deposit Experimental Rig, with detailed descriptions of the design and manufacturing methods deployed. This allows future readers to use this as a framework to adapt to their own needs. After many design iterations this framework is a useful tool, which will help other researchers create a similar rig in fewer iterations and at less cost.

7. CONCLUSIONS AND FUTURE WORK

7.1 Conclusions

The work carried out in this thesis aimed to investigate the impact of key parameters on the formation of deposits on three engine components: fuel injectors, EGR Coolers and intake valves, and how different fuels and additives could impact the fouling. This aim was successfully fulfilled for all components as deposits were formed on all components after successfully creating a method for accelerating the formation of the deposits. In the case of the injector and EGR work, the additives were found to have a significant impact on the formation of deposits. In addition to this a Renewable fuel was found to have a different impact on the rate of deposition on injectors compared to a Base Gasoline. The Base Renewable fuel and Additivated Gasoline were found to prevent injector deposition primarily in the *Phase* immediately after transitioning from high to low load, they also successfully had a higher cleaning rate than the Base Gasoline at high load conditions. This was attributed to the cleaning properties of the Additive and the ethanol within the Renewable fuel.

Soot emissions increased linearly with Gasoline and logarithmically with the Renewable fuel, with additives improving the soot emissions with Gasoline in both the injector and EGR studies. It was concluded that this impact was observed due to a combination of high external deposits and low internal deposits with the Renewable fuel and the opposite trend was seen with the Gasoline. The EGR study also found that fuels which could prevent soot and THC emissions from increasing would prevent EGR Cooler

fouling, unlike in previous studies this was compared directly by using the EGR Cooler with multiple additives. It is therefore concluded that the increased soot emissions observed in the injector fouling study would also result in increased EGR Cooler fouling.

The analysis of the impact of fuels and key parameters on injector, EGR Cooler and IVD was possible due to the success of the methodologies that were developed in each study. The iterative approach undertaken in the injector study provides a framework for future studies to create similar methodologies. Analysis of injection duration over different *Phases* of each *Sequence* as well as its evolution over a whole *Cycle* proved an effective technique to reduce the iterations required to find a successful accelerated fouling procedure. The design and manufacturing process undertaken to construct the IVD experimental rig successfully created a product that could simulate the formation of IVD in a controlled and accelerated manner. Key parameters could be independently controlled across a range of conditions, replicating real engine behaviour. The results generated by the rig successfully replicated a common trend for deposit mass against valve temperature where a critical temperature was found, which aligned with current literature. A significant mass of deposits was generated, which was comparable to literature, and generated in a timeframe that allowed testing, measurement and analysis to be carried out daily. The mass was significant enough that it is predicted that a discernible difference will be observed when testing the rig with various fuels and additives. The description of the process provides guidance for future researchers to emulate the techniques used, helping similar experimental rigs to be built in less time, improving the efficiency of testing in this field.

The injector deposition results concluded that *Cycle* properties such as a *Sequence* that cycled between high and low loads balanced with an increased *Setpoint* duration at high and low load showed a positive correlation with accelerating injector deposit formation. The parameters that were found to have a positive correlation with the effectiveness of the Additive to reduce deposits were: sufficient time at high load for increased additive washing and sufficient time at low load-low speed to increase contact time between the Additive and the deposits. These parameters had to be balanced carefully to both show deposits and allow the effectiveness of the Additive to be investigated. The lack of difference between the final results with the Base Renewable fuel and its Additivated counterpart suggest that the parameters that work to build deposits and demonstrate additive efficacy are different for fuels with different properties, especially with regards to evaporation temperatures.

The parameters which successfully created exhaust conditions to demonstrate EGR Cooler fouling were found when cycling between various engine *Setpoints* leading to an exhaust with high HC and soot concentration as well as high temperature. The impacts of the observed EGR Cooler fouling were an increased *dP* and reduced Cooler effectiveness, especially at the high speed condition. Calculations predicted that increased *dP* would lead to reduced maximum EGR flow rate in LP and HP pre inter cooler setups and that the reduced Cooler effectiveness would lead to increased BSFC in HP post intercooler configurations. The impacts of the above varied depending on engine condition, meaning that all EGR configurations were negatively impacted during at least one engine operating condition. Signifying that EGR Cooler fouling has significant potential to limit the benefits of EGR and GDI engines such as reducing the level to which

engines can be downsized and have their compression ratios increased. The success of Fuel Additive 1 in limiting the EGR Cooler fouling was predicted to significantly mitigate the above consequences on engine performance.

The parameters that impacted IVD were pre-dominantly the valve temperature. Results suggested that the motion of the valves had an impact on the distribution of the IVD mass but not the total deposit mass. The valve temperature also impacted the distribution of the deposits with the deposits seemingly moving further down the valve as the heater temperature dropped. The coloration of the deposits and their structure also changed with temperature, with the deposits becoming darker and less solid as valve temperature decreased.

7.2 Future Work

Future work will involve conducting more controlled tests to gain a deeper understanding of how engine and *Cycle* parameters influence injector deposits, particularly with various fuel types and additives. The use of a controlled ECU will be essential to ensure precise monitoring, and the utilisation of injector temperature measurements would also increase the scope of the study. In addition, the adaptive test method could be repeated with the aim focused more on finding parameters that increase the deposits observed with the Renewable fuel, allowing for analysis of the effects of specially formulated additives designed for use with renewable fuels. This will also help to evolve the understanding of the interactions between fuel properties and engine/*Cycle* parameters that create injector deposits.

More test repetitions with a controllable ECU could be conducted to further assess the impact of deposits on emissions with greater certainty. This will also involve further investigation into the distinct *Phases* of each *Sequence* (such as *Initial* and *Post Start*) and the transitions between low and high load *Setpoints*. Multiple clean injector tests will be necessary to establish a clear baseline of how each phase typically behaves when deposit free, for comparison with "dirty" injector runs. Such experimentation will facilitate comparisons not only between different fuels but also between varying engine and *Cycle* parameters.

The predictions made regarding how EGR Cooler Fouling could impact engine performance could be tested with an engine with an EGR loop setup in the configurations studied in this work. The reduced effectiveness could be simulated by varying the EGR coolant temperature and the increased *dP* simulated via a controllable restriction valve. A similar valve setup to that used in this study could be used to ensure that changes to the EGR Cooler behaviour that happen throughout the test are controlled. To further understand real-world implications, it will be important to examine an already fouled EGR Cooler under real driving conditions, such as those seen in a drive cycle. This approach will offer valuable insights into the extent of the fouling issue across various engine operating conditions as well as EGR configurations.

Future research into IVD will involve the use of additives on the experimental rig to observe their impact across a range of simulated engine conditions. Furthermore, additional tests will be conducted to test for repeatability and to enable better comparisons between dynamic and static valves, offering a more comprehensive

understanding of their impact on deposit formation. This is an important understanding to have as it will allow future researchers to make decisions on whether or not to pay the cost and time involved with constructing a rig with a functioning camshaft system. Additionally, design of experiments (DOE) testing will be performed, incorporating all controllable variables to identify key interactions and determine the most significant factors affecting deposit formation.

The morphology and composition of all deposit types in this study could be examined in greater detail to gain insights into the micro-structure and chemical composition pf the deposits. This will provide greater understanding of the deposit formation processes and the impacts of various parameters.

8. LIST OF REFERENCES

1. Intergovernmental Panel on Climate Change (IPCC), editor. Transport. In: Climate Change 2022 - Mitigation of Climate Change: Working Group III Contribution to the Sixth Assessment Report of the Intergovernmental Panel on Climate Change [Internet]. Cambridge: Cambridge University Press; 2023 [cited 2024 Sep 24]. p. 1049–160. Available from: https://www.cambridge.org/core/books/climate-change-2022-mitigation-of-climate-change/transport/90D9E570DA9236EB0C8A2BFE38AEF454

2. Ravi SS, Osipov S, Turner JWG. Impact of Modern Vehicular Technologies and Emission Regulations on Improving Global Air Quality. Atmosphere. 2023 Jul;14(7):1164.

3. Lake T, Stokes J, Murphy R, Osborne R, Schamel A. Turbocharging concepts for downsized DI gasoline engines. SAE Paper; 2004.

4. Spicher U, Reissing J, Kech JM, Gindele J. Gasoline Direct Injection (GDI) Engines - Development Potentialities [Internet]. Warrendale, PA: SAE International; 1999 Aug [cited 2024 Feb 7]. Report No.: 1999-01–2938. Available from: https://www.sae.org/publications/technical-papers/content/1999-01-2938/

5. Maricq MM. Engine, aftertreatment, fuel quality and non-tailpipe achievements to lower gasoline vehicle PM emissions: Literature review and future prospects. Science of The Total Environment. 2023 Mar 25;866:1612–25.

6. Shuai S, Ma X, Li Y, Qi Y, Xu H. Recent Progress in Automotive Gasoline Direct Injection Engine Technology. Automot Innov. 2018 Apr 1;1(2):95–113.

7. Alkidas AC, Tahry SHE. Contributors to the Fuel Economy Advantage of DISI Engines Over PFI Engines. In SAE International; 2003 [cited 2024 Sep 23]. Available from: https://saemobilus.sae.org/papers/contributors-fuel-economy-advantage-disi-engines-pfi-engines-2003-01-3101

8. Chen L, Liang Z, Zhang X, Shuai S. Characterizing particulate matter emissions from GDI and PFI vehicles under transient and cold start conditions. Fuel. 2017 Feb 1;189:131–40.

9. Tupa RC, Koehler DE. Intake Valve Deposits - Effects of Engines, Fuels & Additives. In SAE International; 1988 [cited 2024 Sep 24]. Available from: https://saemobilus.sae.org/papers/intake-valve-deposits-effects-engines-fuels-additives-881645

10. Gail S, Nomura T, Hayashi H, Miura Y, Yoshida K, Natarajan V. An Intake Valve Deposit (IVD) Engine Test Development to Investigate Deposit Build-Up

Mechanism Using a Real Engine. SAE International Journal of Fuels and Lubricants [Internet]. 2017 Oct 8 [cited 2024 Sep 23];10(3). Available from: https://saemobilus.sae.org/articles/intake-valve-deposit-ivd-engine-test-development-investigate-deposit-build-mechanism-using-a-real-engine-2017-01-2291

11. Reid JBJ, Mulqueen S, Langley GJ, Wilmot EMJ, Vadodaria S, Castle J, et al. The Investigation of the Structure and Origins of Gasoline Direct Injection (GDI) Deposits. In SAE International; 2019 [cited 2024 Sep 22]. Available from: https://saemobilus.sae.org/papers/investigation-structure-origins-gasoline-direct-injection-gdi-deposits-2019-01-2356

12. Xu H, Wang C, Ma X, Sarangi AK, Weall A, Krueger-Venus J. Fuel injector deposits in direct-injection spark-ignition engines. Progress in Energy and Combustion Science. 2015 Oct 1;50:63–80.

13. Raza M, Chen L, Leach F, Ding S. A Review of Particulate Number (PN) Emissions from Gasoline Direct Injection (GDI) Engines and Their Control Techniques. Energies. 2018 Jun;11(6):1417.

14. Jiang C, Xu H, Srivastava D, Ma X, Dearn K, Cracknell R, et al. Effect of fuel injector deposit on spray characteristics, gaseous emissions and particulate matter in a gasoline direct injection engine. Applied Energy. 2017 Oct 1;203:390–402.

15. Slavchov RI, Mosbach S, Kraft M, Pearson R, Filip SV. An adsorption-precipitation model for the formation of injector external deposits in internal combustion engines. Applied Energy. 2018 Oct 15;228:1423–38.

16. Henkel S, Hardalupas Y, Taylor A, Conifer C, Cracknell R, Goh TK, et al. Injector Fouling and Its Impact on Engine Emissions and Spray Characteristics in Gasoline Direct Injection Engines. SAE International Journal of Fuels and Lubricants. 2017 Mar 28;10(2):287–95.

17. Abarham M, Hoard J, Assanis DN, Styles D, Curtis EW, Ramesh N, et al. Numerical Modeling and Experimental Investigations of EGR Cooler Fouling in a Diesel Engine. In: Detroit, MI, United States [Internet]. SAE International; 2009 [cited 2024 Sep 23]. Available from: https://saemobilus.sae.org/papers/numerical-modeling-experimental-investigations-egr-cooler-fouling-a-diesel-engine-2009-01-1506

18. Ismail B. The Heat Transfer and the Soot Deposition Characteristics in Diesel Engine Exhaust Gas Recirculation System Cooling Devices [PhD Thesis,]. [Hamilton, Ontario]: McMaster University; 2004.

19. Teng H, Barnard M, Teng H, Barnard M. Physicochemical Characteristics of Soot Deposits in EGR Coolers. In SAE International; 2010 [cited 2024 Sep 22]. Available

from: https://saemobilus.sae.org/papers/physicochemical-characteristics-soot-deposits-egr-coolers-2010-01-0730

20. Teng H, Regner G, Teng H, Regner G. Particulate Fouling in EGR Coolers. SAE International Journal of Commercial Vehicles. 2009 Oct 6;2(2):154–63.

21. Siokos K, Koli R, Prucka R, Schwanke J, Miersch J. Assessment of Cooled Low Pressure EGR in a Turbocharged Direct Injection Gasoline Engine. SAE International Journal of Engines. 2015 Apr 14;8(4):1535–43.

22. Fischer M, Kreutziger P, Sun Y, Kotrba A, Fischer M, Kreutziger P, et al. Clean EGR for Gasoline Engines – Innovative Approach to Efficiency Improvement and Emissions Reduction Simultaneously. In SAE International; 2017 [cited 2024 Sep 23]. Available from: https://saemobilus.sae.org/papers/clean-egr-gasoline-engines-innovative-approach-efficiency-improvement-emissions-reduction-simultaneously-2017-01-0683

23. Božić M, Vučetić A, Sjerić M, Kozarac D, Lulić Z. Experimental study on knock sources in spark ignition engine with exhaust gas recirculation. Energy Conversion and Management. 2018 Jun 1;165:35–44.

24. Szybist J. Knock Mitigation Effectiveness of EGR across the Pressure-Temperature Domain. SAE Int J Adv & Curr Prac in Mobility. 2020 Sep 15;3(1):262–75.

25. Demirci A, Doğan H, Cihan Ö, Kutlar A. The Effect of Injection Parameters on Fuel Consumption and Emissions in A PFI Small Spark Ignition Engine. ijastech. 2021 Jun 30;5(2):157–65.

26. Kalghatgi GT. Deposits in Gasoline Engines - A Literature Review. In SAE International; 1990 [cited 2024 Sep 24]. Available from: https://saemobilus.sae.org/papers/deposits-gasoline-engines-a-literature-review-902105

27. Cheng S wai S. The Physical Parameters that Influence Deposit Formation on an Intake Valve [Internet]. Warrendale, PA: SAE International; 1992 Oct [cited 2024 May 7]. Report No.: 922257. Available from: https://www.sae.org/publications/technical-papers/content/922257/

28. Ramadhas AS, Singh VP, Subramanian M, Acharya GK, Basu B, Malhotra RK. Impact of Fuel Additives on Intake Valve Deposits, Combustion Chamber Deposits and Emissions [Internet]. Warrendale, PA: SAE International; 2011 Aug [cited 2024 May 7]. Report No.: 2011-01–1980. Available from: https://www.sae.org/publications/technical-papers/content/2011-01-1980/

29. Esaki Y, Ishiguro T, Suzuki N, Nakada M. Mechanism of Intake-Valve Deposit Formation Part 1: Characterization of Deposits [Internet]. Warrendale, PA: SAE

International; 1990 Feb [cited 2024 May 6]. Report No.: 900151. Available from: https://www.sae.org/publications/technical-papers/content/900151/

30. Daneshgari P, Borgmann K, Job H. The Influence of Temperature Upon Gasoline Deposit Build-Up on the Intake Valves. SAE Transactions. 1989;98:171–8.

31. Bitting B, Gschwendtner F, Kohlhepp W, Kothe M, Testroet CJ, Ziwica KH, et al. Intake Valve Deposits — Fuel Detergency Requirements Revisited. In SAE International; 1987 [cited 2024 May 7]. Available from: https://saemobilus.sae.org/papers/intake-valve-deposits-fuel-detergency-requirements-revisited-872117

32. Chapman E, Cummings J, Conran D. Effects of Gasoline and Ethanol Fuel Corrosion Inhibitors on Powertrain Intake Valve Deposits. SAE International Journal of Fuels and Lubricants. 2013;6(1):63–79.

33. Zhang W, Ding H, Shuai S, Zheng B, Cantlay A, Natarajan V, et al. Effect of Fuel Detergent on Injector Deposit Formation and Engine Emissions in a Gasoline Direct Injection (GDI) Engine. In SAE International; 2017 [cited 2024 Sep 24]. Available from: https://saemobilus.sae.org/papers/effect-fuel-detergent-injector-deposit-formation-engine-emissions-a-gasoline-direct-injection-gdi-engine-2017-01-2247

34. Grant LJ, Mason RL. SwRI-BMW N.A. Intake Valve Deposit Test - A Statistical Review [Internet]. Warrendale, PA: SAE International; 1992 Oct [cited 2024 May 6]. Report No.: 922215. Available from: https://www.sae.org/publications/technical-papers/content/922215/

35. Gutierrez SJ, Wolff EG, Sanchez CJ. Metodo de evaluacion de depositos producidos por un combustible en los sistemas de admision de motores de encendido por chispa, [Internet]. ES2152150B1, 2001 [cited 2024 Jul 30]. Available from: https://patents.google.com/patent/ES2152150B1/es?q=(Guti%C2%B4errez+Serna%2c+Jaime)&assignee=REPSOL+PETROLEO%2c&oq=REPSOL+PETROLEO%2c+Guti%C2%B4errez+Serna%2c+Jaime

36. Pilbeam J, Weissenberger D. Characterisation of Gasoline Fuels in a DISI Engine. Afton Chemical. Bracknell, UK. SGS S.A. Vienna, Austria.; 2018.

37. Storey JME, Sluder CS, Lance MJ, Styles DJ, Simko SJ. Exhaust Gas Recirculation Cooler Fouling in Diesel Applications: Fundamental Studies of Deposit Properties and Microstructure. Heat Transfer Engineering. 2013 Jul 15;34(8–9):655–64.

38. Lacey PI, Kohl KB, Stavinoha LL, Estefan RM. A Laboratory-Scale Test to Predict Intake Valve Deposits. In SAE International; 1997 [cited 2024 Sep 24]. Available from: https://saemobilus.sae.org/papers/a-laboratory-scale-test-predict-intake-valve-deposits-972838

39. China P, Rivere JP. Development of a Direct Injection Spark Ignition Engine Test for Injector Fouling. SAE Transactions. 2003;112:1927–34.

40. US EPA O. The EPA Automotive Trends Report [Internet]. 2017 [cited 2024 Sep 22]. Available from: https://www.epa.gov/automotive-trends

41. Gasoline Direct Injection Market by Engine [Internet]. 2022 Dec. Available from: https://www.marketsandmarkets.com/Market-Reports/gdi-system-market-196131228.html

42. Ku D, Bencekri M, Kim J, Lee S, Lee S. Review of European Low Emission Zone Policy. Chemical Engineering Transactions. 2020 Apr 11;78:78, 241–6.

43. Huang Y, Surawski NC, Zhuang Y, Zhou JL, Hong G. Dual injection: An effective and efficient technology to use renewable fuels in spark ignition engines. Renewable and Sustainable Energy Reviews. 2021 Jun 1;143:1109–21.

44. Mundorff F, Carstensen H, Bierbaumer J. Direct Injection Internal Combustion Engines - The Automotive Industry's Contribution to Reduced CO2 Emissions. In SAE International; 1998 [cited 2024 Sep 24]. Available from: https://saemobilus.sae.org/papers/direct-injection-internal-combustion-engines-automotive-industrys-contribution-reduced-co2-emissions-982217

45. Kume T, Iwamoto Y, Iida K, Murakami M, Akishino K, Ando H. Combustion Control Technologies for Direct Injection SI Engine. In SAE International; 1996 [cited 2024 Sep 24]. Available from: https://saemobilus.sae.org/papers/combustion-control-technologies-direct-injection-si-engine-960600

46. Lee Z, Kim T, Park S, Park S. Review on spray, combustion, and emission characteristics of recent developed direct-injection spark ignition (DISI) engine system with multi-hole type injector. Fuel. 2020 Jan 1;259:1162–09.

47. Posselt A, Mai A, Leder M, Salvio R, Coletto T, Posselt A. Advanced PFI: The Economical, High-Performance Systems Approach. In SAE International; 2015 [cited 2024 Jul 31]. Available from: https://saemobilus.sae.org/papers/advanced-pfi-economical-high-performance-systems-approach-2015-36-0392

48. Kalwar A, Agarwal A. Overview, Advancements and Challenges in Gasoline Direct Injection Engine Technology. In 2020. p. 111–47.

49. Heywood JB. 7.7 Direct Fuel Injection. In: Internal Combustion Engine Fundamentals. Second edition. New York ; London: McGraw-Hill Education; 2018. p. 327–35.

50. Preussner C, Döring C, Fehler S, Kampmann S. GDI: Interaction Between Mixture Preparation, Combustion System and Injector Performance [Internet]. Warrendale, PA: SAE International; 1998 Feb [cited 2024 Feb 7]. Report No.:

980498. Available from: https://www.sae.org/publications/technical-papers/content/980498/

51. Heywood JB. 7.4 Port (Multipoint) Fuel Injection. In: Internal combustion engine fundamentals [Internet]. Second Edition. New York ; London: New York : McGraw-Hill; 2018 [cited 2024 Aug 1]. p. 270–5. Available from: http://archive.org/details/john-heywood-internal-combustion-engine-fundamentals-mc-graw-hill-science-engineering-math-1988

52. Rimpas D, Papadakis A, Samarakou M. OBD-II sensor diagnostics for monitoring vehicle operation and consumption. Energy Reports. 2020 Feb 1;6:55–63.

53. Takagi Y, Itoh T, Muranaka S, Iiyama A, Iwakiri Y, Urushihara T, et al. Simultaneous Attainment of Low Fuel Consumption High Output Power and Low Exhaust Emissions in Direct Injection SI Engines [Internet]. Warrendale, PA: SAE International; 1998 Feb [cited 2024 Feb 15]. Report No.: 980149. Available from: https://www.sae.org/publications/technical-papers/content/980149/

54. Ortmann R, Arndt S, Raimann J, Grzeszik R, Würfel G. Methods and Analysis of Fuel Injection, Mixture Preparation and Charge Stratification in Different Direct Injected SI Engines [Internet]. Warrendale, PA: SAE International; 2001 Mar [cited 2024 Feb 13]. Report No.: 2001-01–0970. Available from: https://www.sae.org/publications/technical-papers/content/2001-01-0970/

55. Hershberger J, Ozturk O, Ajayi OO, Woodford JB, Erdemir A, Fenske GR. Near-frictionless carbon coatings for spark-ignited direct-injected fuel systems. Final report, January 2002. [Internet]. Argonne National Lab., IL (US); 2002 Apr [cited 2024 Aug 1]. Report No.: ANL/ET/RP-107306. Available from: https://www.osti.gov/biblio/795901

56. Wu Y hu, Hou Z xiang, Gong H. Modeling and Simulating of Intake Pipe Fuel Film Dynamic Characteristic in Gasoline Engine Start Process. In: 2010 International Conference on Intelligent Computation Technology and Automation [Internet]. 2010 [cited 2024 Aug 1]. p. 700–4. Available from: https://ieeexplore.ieee.org/document/5522666

57. Li Y, Huang Y, Luo K. Combined experimental and numerical study on fuel deposition characteristics of an impinging PFI spray with different impingement geometries. Proceedings of the Institution of Mechanical Engineers, Part D: Journal of Automobile Engineering. 2022 Nov 21;238:095440702211353.

58. Anand TNC, Ravikrishna RV. Modelling of mixture preparation in a small engine with port fuel injection. Progress in Computational Fluid Dynamics, an International Journal [Internet]. 2012 [cited 2024 Aug 1];12(6). Available from: https://doi.org/10.1504/pcfd.2012.049810

59. Anderson W, Yang J, Brehob DD, Vallance JK, Whiteaker RM. Understanding the Thermodynamics of Direct Injection Spark Ignition (DISI) Combustion Systems: An Analytical and Experimental Investigation [Internet]. Warrendale, PA: SAE International; 1996 Oct [cited 2024 Feb 15]. Report No.: 962018. Available from: https://www.sae.org/publications/technical-papers/content/962018/

60. Iwamoto Y, Noma K, Nakayama O, Yamauchi T, Ando H. Development of Gasoline Direct Injection Engine. In SAE International; 1997 [cited 2024 Sep 24]. Available from: https://saemobilus.sae.org/papers/development-gasoline-direct-injection-engine-970541

61. VanDerWege BA, Han Z, Iyer CO, Muñoz RH, Yi J. Development and Analysis of a Spray-Guided DISI Combustion System Concept. In SAE International; 2003 [cited 2024 Sep 24]. Available from: https://saemobilus.sae.org/papers/development-analysis-a-spray-guided-disi-combustion-system-concept-2003-01-3105

62. Yang J, Anderson RW. Fuel Injection Strategies to Increase Full-Load Torque Output of a Direct-Injection SI Engine [Internet]. Warrendale, PA: SAE International; 1998 Feb [cited 2024 Feb 7]. Report No.: 980495. Available from: https://www.sae.org/publications/technical-papers/content/980495/

63. Baumgarten C. Mixture Formation in Internal Combustion Engine [Internet]. Springer Berlin Heidelberg; 2006 [cited 2024 Feb 7]. (Heat, Mass Transfer). Available from: http://link.springer.com/10.1007/3-540-30836-9

64. Knop V, Essayem E. Comparison of PFI and DI Operation in a Downsized Gasoline Engine. SAE International Journal of Engines. 2013 Apr 8;6(2):941–52.

65. Bozza F, De Bellis V, Teodosio L. Potentials of cooled EGR and water injection for knock resistance and fuel consumption improvements of gasoline engines. Applied Energy. 2016 May 1;169:112–25.

66. Hudson C, Gao X, Stone R. Knock measurement for fuel evaluation in spark ignition engines. Fuel. 2001 Feb 1;80(3):395–407.

67. Grandin B, Ångström HE. Replacing Fuel Enrichment in a Turbo Charged SI Engine: Lean Burn or Cooled EGR [Internet]. Warrendale, PA: SAE International; 1999 Oct [cited 2024 Feb 15]. Report No.: 1999-01–3505. Available from: https://www.sae.org/publications/technical-papers/content/1999-01-3505/

68. Caton JA. A Comparison of Lean Operation and Exhaust Gas Recirculation: Thermodynamic Reasons for the Increases of Efficiency [Internet]. Warrendale, PA: SAE International; 2013 Apr [cited 2024 Feb 15]. Report No.: 2013-01–0266. Available from: https://www.sae.org/publications/technical-papers/content/2013-01-0266/

69. Heywood JB. Internal combustion engine fundamentals / John B. Heywood. Second edition. New York ; London: McGraw-Hill Education; 2018.

70. Zhao FQ, Lai MC, Harrington DL. A Review of Mixture Preparation and Combustion Control Strategies for Spark-Ignited Direct-Injection Gasoline Engines. In SAE International; 1997 [cited 2024 Sep 24]. Available from: https://saemobilus.sae.org/papers/a-review-mixture-preparation-combustion-control-strategies-spark-ignited-direct-injection-gasoline-engines-970627

71. Zhao F, Lai MC, Harrington DL. Automotive spark-ignited direct-injection gasoline engines. Progress in Energy and Combustion Science. 1999 Oct 1;25(5):437–562.

72. Serras-Pereira J, Aleiferis PG, Richardson D, Wallace S. Mixture Preparation and Combustion Variability in a Spray-Guided DISI Engine. In SAE International; 2007 [cited 2024 Sep 24]. Available from: https://saemobilus.sae.org/papers/mixture-preparation-combustion-variability-a-spray-guided-disi-engine-2007-01-4033

73. Francqueville L de. Effects of Ethanol Addition in RON 95 Gasoline on GDI Stratified Combustion [Internet]. Warrendale, PA: SAE International; 2011 Sep [cited 2024 Feb 12]. Report No.: 2011-24–0055. Available from: https://www.sae.org/publications/technical-papers/content/2011-24-0055/

74. Park C, Kim S, Kim H, Moriyoshi Y. Stratified lean combustion characteristics of a spray-guided combustion system in a gasoline direct injection engine. Energy. 2012 May 1;41(1):401–7.

75. Raju TB, Hithaish D. A Review on Gasoline Direct Injection System. IJRAME. 2014;2(3):224–31.

76. Lohfink C, Baecker H, Tichy M. Experimental Investigation on Catalyst-Heating Strategies and Potential of GDI Combustion Systems [Internet]. Warrendale, PA: SAE International; 2008 Oct [cited 2024 Feb 7]. Report No.: 2008-01–2517. Available from: https://www.sae.org/publications/technical-papers/content/2008-01-2517/

77. Mittal M, Hung DLS, Zhu G, Schock H. A Study of Fuel Impingement Analysis on In-Cylinder Surfaces in a Direct-Injection Spark-Ignition Engine with Gasoline and Ethanol-Gasoline Blended Fuels [Internet]. Warrendale, PA: SAE International; 2010 Oct [cited 2024 Feb 7]. Report No.: 2010-01–2153. Available from: https://www.sae.org/publications/technical-papers/content/2010-01-2153/

78. Zhou ZF, Mohd Murad SH, Tian JM, Camm J, Stone R. Experimental investigation on heat transfer of *n*-pentane spray impingement on piston surface. Applied Thermal Engineering. 2018 Jun 25;138:197–206.

79. Karavalakis G, Short D, Vu D, Russell R, Asa-Awuku A, Durbin T. A Complete Assessment of the Emissions Performance of Ethanol Blends and Iso-Butanol

Blends from a Fleet of Nine PFI and GDI Vehicles. SAE International Journal of Fuels and Lubricants. 2015 Apr 14;8(2):374–95.

80. Kheirbek I, Haney J, Douglas S, Ito K, Matte T. The contribution of motor vehicle emissions to ambient fine particulate matter public health impacts in New York City: a health burden assessment. Environmental Health. 2016 Aug 26;15(1):89.

81. Kumar P, Morawska L, Birmili W, Paasonen P, Hu M, Kulmala M, et al. Ultrafine particles in cities. Environment International. 2014 May 1;66:1–10.

82. Commission Regulation (EU) No 459/2012 of 29 May 2012 amending Regulation (EC) No 715/2007 of the European Parliament and of the Council and Commission Regulation (EC) No 692/2008 as regards emissions from light passenger and commercial vehicles (Euro 6) Text with EEA relevance [Internet]. OJ L May 29, 2012. Available from: http://data.europa.eu/eli/reg/2012/459/oj/eng

83. Lähde T, Giechaskiel B, Pavlovic J, Suarez-Bertoa R, Valverde V, Clairotte M, et al. Solid particle number emissions of 56 light-duty Euro 5 and Euro 6 vehicles. Journal of Aerosol Science. 2022 Jan 1;159:1058–73.

84. Mamakos A, Steininger N, Martini G, Dilara P, Drossinos Y. Cost effectiveness of particulate filter installation on Direct Injection Gasoline vehicles. Atmospheric Environment. 2013 Oct 1;77:16–23.

85. Joshi A, Johnson TV. Gasoline Particulate Filters—a Review. Emiss Control Sci Technol. 2018 Dec 1;4(4):219–39.

86. Adam F, Olfert J, Wong KF, Kunert S, Richter JM. Effect of Engine-Out Soot Emissions and the Frequency of Regeneration on Gasoline Particulate Filter Efficiency. In SAE International; 2020 [cited 2024 Sep 23]. Available from: https://saemobilus.sae.org/papers/effect-engine-soot-emissions-frequency-regeneration-gasoline-particulate-filter-efficiency-2020-01-1431

87. Saito C, Nakatani T, Miyairi Y, Yuuki K, Makino M, Kurachi H, et al. New Particulate Filter Concept to Reduce Particle Number Emissions [Internet]. Warrendale, PA: SAE International; 2011 Apr [cited 2024 Feb 12]. Report No.: 2011-01–0814. Available from: https://www.sae.org/publications/technical-papers/content/2011-01-0814/

88. Achleitner E, Frenzel H, Grimm J, Maiwald O, Rösel G, Senft P, et al. System approach for a vehicle with gasoline direct injection and particulate filter for RDE [Internet]. 39th International Vienna Motor Symposium; 2018 Apr 26 [cited 2024 Feb 12]; Vienna. Available from: https://oevk.at/en/papers/070745a0-c4c5-4071-82c5-9fb2aac09c5f?returnUrl=https%253A%252F%252Fwiener-motorensymposium.at%252Fliteratursuche%252F%253Fseite%253D40&cHash=0ca277fb2774953d9c1f2c4efa8a9cfa

89. Chen JG, Crooks RM, Seefeldt LC, Bren KL, Bullock RM, Darensbourg MY, et al. Beyond fossil fuel–driven nitrogen transformations. Science [Internet]. 2018 [cited 2024 Aug 1];360(6391). Available from: https://doi.org/10.1126/science.aar6611

90. Parks JE, Prikhodko V, Partridge W, Choi JS, Norman K, Huff S, et al. Lean Gasoline Engine Reductant Chemistry During Lean NOx Trap Regeneration. SAE International Journal of Fuels and Lubricants. 2010 Oct 25;3(2):956–62.

91. Fujiwara A, Tsurunari Y, Iwashita S, Yoshida H, Ohyama J, Machida M. Surface State Changes of Pd Three-Way Catalysts under Dynamic Lean/Rich Perturbation Compared with Static Condition. The Journal of Physical Chemistry C [Internet]. 2022 [cited 2024 Aug 2];127(1). Available from: https://doi.org/10.1021/acs.jpcc.2c07428

92. Yoon S, Collins J, Thiruvengadam A, Gautam M, Herner J, Ayala A. Criteria pollutant and greenhouse gas emissions from CNG transit buses equipped with three-way catalysts compared to lean-burn engines and oxidation catalyst technologies. Journal of the Air & Waste Management Association. 2013 Aug 1;63(8):926–33.

93. Granger P, Pârvulescu VI. Catalytic NO_x Abatement Systems for Mobile Sources: From Three-Way to Lean Burn after-Treatment Technologies. Chemical Reviews [Internet]. 2011 [cited 2024 Aug 2];111(5). Available from: https://doi.org/10.1021/cr100168g

94. Hedinger R, Elbert P, Onder C. Optimal Cold-Start Control of a Gasoline Engine. Energies. 2017 Oct;10(10):1548.

95. Altin O, Eser S. Carbon deposit formation from thermal stressing of petroleum fuels. ACS Division of Fuel Chemistry, Preprints. 2004 Sep;49(2):764–6.

96. Bacho PSV, Sofianek JK, Galante-Fox JM, McMahon CJ. Engine Test for Accelerated Fuel Deposit Formation on Injectors Used in Gasoline Direct Injection Engines [Internet]. Warrendale, PA: SAE International; 2009 Apr [cited 2024 May 3]. Report No.: 2009-01–1495. Available from: https://www.sae.org/publications/technical-papers/content/2009-01-1495/

97. Medina M, Alzahrani F, Fatouraie M, Wooldridge M, Sick V. Mechanisms of fuel injector tip wetting and tip drying based on experimental measurements of engine-out particulate emissions from gasoline direct-injection engines. International Journal of Engine Research. 2021 Jun 1;22(6):2035–53.

98. Rounthwaite NJ, Williams R, McGivery C, Jiang J, Giulliani F, Britton B. A Chemical and Morphological Study of Diesel Injector Nozzle Deposits - Insights into their Formation and Growth Mechanisms. SAE International Journal of Fuels and Lubricants. 2017 Mar 28;10(1):106–14.

99. Cheng Q, Zhang ZD, Guo H, Xie NL. Simulation and analysis on electro-magnetic-thermal coupling of solenoid GDI injector. International Journal of Applied Electromagnetics and Mechanics. 2014 Jan 1;46(4):775–92.

100. Zhang X, Xiao D, Qiu S, Li T, Su J, Hung DLS, et al. Influence of Different Injector Structures on Tip Wetting by Visualization Method: Paper 362. In: International Conference on Liquid Atomization and Spray Systems (ICLASS) [Internet]. Edinburgh, UK; 2021 [cited 2024 Sep 24]. Available from: https://journals.ed.ac.uk/ICLASS_Edinburgh/article/view/6088

101. Aradi AA, Imoehl B, Avery NL, Wells PP, Grosser RW. The Effect of Fuel Composition and Engine Operating Parameters on Injector Deposits in a High-Pressure Direct Injection Gasoline (DIG) Research Engine [Internet]. Warrendale, PA: SAE International; 1999 Oct [cited 2024 May 3]. Report No.: 1999-01–3690. Available from: https://www.sae.org/publications/technical-papers/content/1999-01-3690/

102. Sarmast S, Ziabasharhagh M, Salavati-Zadeh A, Fajri HR. Numerical Study on the Effects of Fuel Injection Characteristics on the Performance of a Lean Burn SG-GDI Engine towards High Efficiency and Emissions Reduction. Journal of Applied Fluid Mechanics. 2019 May 1;12(3):763–76.

103. Wang X, Zhao H. Understanding of closely spaced split injections of an outward-opening piezoelectric gasoline injector by large eddy simulations: Paper 134. International Conference on Liquid Atomization and Spray Systems (ICLASS) [Internet]. 2021 Aug 30 [cited 2024 Sep 24];1(1). Available from: https://journals.ed.ac.uk/ICLASS_Edinburgh/article/view/5896

104. Tsai WC, Zhan TS. An Experimental Characterization for Injection Quantity of a High-pressure Injector in GDI Engines. Journal of Low Power Electronics and Applications. 2018 Dec;8(4):36.

105. Szybist JP, Youngquist AD, Barone TL, Storey JM, Moore WR, Foster M, et al. Ethanol Blends and Engine Operating Strategy Effects on Light-Duty Spark-Ignition Engine Particle Emissions. Energy Fuels. 2011 Nov 17;25(11):4977–85.

106. He X, Ratcliff MA, Zigler BT. Effects of Gasoline Direct Injection Engine Operating Parameters on Particle Number Emissions. Energy Fuels. 2012 Apr 19;26(4):2014–27.

107. Qin J, Li X, Pei Y. Effects of Combustion Parameters and Lubricating Oil on Particulate Matter Emissions from a Turbo-Charged GDI Engine Fueled with Methanol/Gasoline Blends. In SAE International; 2014 [cited 2024 Sep 24]. Available from: https://saemobilus.sae.org/papers/effects-combustion-parameters-lubricating-oil-particulate-matter-emissions-a-turbo-charged-gdi-engine-fueled-methanol-gasoline-blends-2014-01-2841

108. Li X, Li D, Liu J, Ajmal T, Aïtouche A, Mobasheri R, et al. Comparative Study on the Macroscopic Characteristics of Gasoline and Ethanol Spray from a GDI Injector under Injection Pressures of 10 and 60 MPa. ACS Omega. 2022;7(10):8864–73.

109. Kinoshita M, Saito A, Matsushita S, Shibata H, Niwa Y. A Method for Suppressing Formation of Deposits on Fuel Injector for Direct Injection Gasoline Engine. In SAE International; 1999 [cited 2024 Sep 24]. Available from: https://saemobilus.sae.org/papers/a-method-suppressing-formation-deposits-fuel-injector-direct-injection-gasoline-engine-1999-01-3656

110. Carlisle HW, Frew RW, Mills JR, Aradi AA, Avery NL. The Effect of Fuel Composition and Additive Content on Injector Deposits and Performance of an Air-Assisted Direct Injection Spark Ignition (DISI) Research Engine [Internet]. Warrendale, PA: SAE International; 2001 May [cited 2024 May 3]. Report No.: 2001-01–2030. Available from: https://www.sae.org/publications/technical-papers/content/2001-01-2030/

111. Hajbabaei M, Karavalakis G, Miller JW, Villela M, Xu KH, Durbin TD. Impact of olefin content on criteria and toxic emissions from modern gasoline vehicles. Fuel. 2013 May 1;107:671–9.

112. Fatouraie M, Frommherz M, Mosburger M, Chapman E, Li S, McCormick R, et al. Investigation of the Impact of Fuel Properties on Particulate Number Emission of a Modern Gasoline Direct Injection Engine. In SAE International; 2018 [cited 2024 Sep 23]. Available from: https://saemobilus.sae.org/papers/investigation-impact-fuel-properties-onparticulate-number-emission-a-modern-gasoline-direct-injection-engine-2018-01-0358

113. Leach F, Knorsch T, Laidig C, Wiese W. A Review of the Requirements for Injection Systems and the Effects of Fuel Quality on Particulate Emissions from GDI Engines. In SAE International; 2018 [cited 2024 Sep 24]. Available from: https://saemobilus.sae.org/papers/a-review-requirements-injection-systems-effects-fuel-quality-particulate-emissions-gdi-engines-2018-01-1710

114. Venkataraman R, Eser S. Characterization of deposits formed on diesel injectors in field test and from thermal oxidative degradation of n-hexadecane in a laboratory reactor. Chem Cent J. 2008 Dec 17;2(1):25.

115. Stępień Z, Pielecha I, Cieslik W, Szwajca F. The impact of alcohol admixture with gasoline on carbon build-up and fuel injectors performance. Eksploatacja i Niezawodność – Maintenance and Reliability. 2022 Jun 30;24(2):226–36.

116. Wang C, Xu H, Herreros JM, Wang J, Cracknell R. Impact of fuel and injection system on particle emissions from a GDI engine. Applied Energy. 2014 Nov 1;132:178–91.

117. Sandquist H, Denbratt I, Owrang F, Olsson J. Influence of Fuel Parameters on Deposit Formation and Emissions in a Direct Injection Stratified Charge SI Engine. In SAE International; 2001 [cited 2024 Sep 24]. Available from: https://saemobilus.sae.org/papers/influence-fuel-parameters-deposit-formation-emissions-a-direct-injection-stratified-charge-si-engine-2001-01-2028

118. Bertsch M, Weidenlener A, Dörnhöfer J, Koch T, Velji A. Effect of implementing large-scale charge motion, reducing hydraulic flow of the injector and increasing injection pressure on particle emissions of a GDI engine at WOT and boosted operation. International Journal of Engine Research. 2016;18(5–6):467–89.

119. Fatouraie M, Wooldridge MS, Petersen B, Wooldridge S. Effects of Ethanol on In-Cylinder and Exhaust Gas Particulate Emissions of a Gasoline Direct Injection Spark Ignition Engine. Energy &Amp; Fuels [Internet]. 2015 [cited 2024 May 3];29(5). Available from: https://doi.org/10.1021/ef502758y

120. Choi K, Kim J, Myung CL, Lee M, Kwon S, Lee Y, et al. Effect of the mixture preparation on the nanoparticle characteristics of gasoline direct-injection vehicles. Proceedings of the Institution of Mechanical Engineers, Part D: Journal of Automobile Engineering. 2012 Nov 1;226(11):1514–24.

121. Yue Z, Reitz RD. Application of an Equilibrium-Phase Spray Model to Multicomponent Gasoline Direct Injection. Energy Fuels. 2019 Apr 18;33(4):3565–75.

122. Moreira ALN, Moita AS, Panão MRO. Advances and challenges in explaining fuel spray impingement: How much of single droplet impact research is useful? Progress in Energy and Combustion Science. 2010;36(5):554–80.

123. Maiboom A, Tauzia X, Hétet JF. Experimental study of various effects of exhaust gas recirculation (EGR) on combustion and emissions of an automotive direct injection diesel engine. Energy. 2008;33(1):22–34.

124. Wei H, Zhu T, Shu G, Tan L, Wang Y. Gasoline engine exhaust gas recirculation – A review. Applied Energy. 2012 Nov 1;99:534–44.

125. Ceviz MA, Kaymaz İ. Temperature and air–fuel ratio dependent specific heat ratio functions for lean burned and unburned mixture. Energy Conversion and Management. 2005 Sep 1;46(15):2387–404.

126. Alger T, Mangold B, Roberts C, Gingrich J. The Interaction of Fuel Anti-Knock Index and Cooled EGR on Engine Performance and Efficiency. SAE International Journal of Engines. 2012 Apr 16;5(3):1229–41.

127. Szybist JP, Wagnon SW, Splitter D, Pitz WJ, Mehl M. The Reduced Effectiveness of EGR to Mitigate Knock at High Loads in Boosted SI Engines. SAE International Journal of Engines. 2017 Sep 4;10(5):2305–18.

128. Alger T, Chauvet T, Dimitrova Z, Alger T, Chauvet T, Dimitrova Z. Synergies between High EGR Operation and GDI Systems. SAE International Journal of Engines. 2008 Apr 14;1(1):101–14.

129. Hwang K, Hwang I, Lee H, Park H, Choi H, Lee K, et al. Development of New High-Efficiency Kappa 1.6L GDI Engine. In SAE International; 2016 [cited 2024 Sep 24]. Available from: https://saemobilus.sae.org/papers/development-new-high-efficiency-kappa-16l-gdi-engine-2016-01-0667

130. Hakariya M, Toda T, Sakai M. The New Toyota Inline 4-Cylinder 2.5L Gasoline Engine. In SAE International; 2017 [cited 2024 Sep 24]. Available from: https://saemobilus.sae.org/papers/new-toyota-inline-4-cylinder-25l-gasoline-engine-2017-01-1021

131. Potteau S, Lutz P, Leroux S, Moroz S, Tomas E. Cooled EGR for a Turbo SI Engine to Reduce Knocking and Fuel Consumption. In SAE International; 2007 [cited 2024 Sep 24]. Available from: https://saemobilus.sae.org/papers/cooled-egr-a-turbo-si-engine-reduce-knocking-fuel-consumption-2007-01-3978

132. Paz C, Suárez E, Vence J, Cabarcos A. Numerical Modelling of Fouling Process in EGR System: A Review. In: Environmental Issues and Sustainable Development [Internet]. IntechOpen; 2020 [cited 2024 Sep 24]. Available from: https://www.intechopen.com/chapters/72892

133. Housiadas C, Drossinos Y. Thermophoretic Deposition in Tube Flow. Aerosol Science and Technology. 2005 Apr 1;39(4):304–18.

134. Khalef MS, Soba A, Korsgren J. Study of EGR and Turbocharger Combinations and Their Influence on Diesel Engine's Efficiency and Emissions. In SAE International; 2016 [cited 2024 Sep 24]. Available from: https://saemobilus.sae.org/papers/study-egr-turbocharger-combinations-influence-diesel-engines-efficiency-emissions-2016-01-0676

135. Rogers DT, H FLJA. Mechanism of Intake Valve Underside Deposit Formation [Internet]. Warrendale, PA: SAE International; 1958 Jan [cited 2024 May 7]. Report No.: 580083. Available from: https://www.sae.org/publications/technical-papers/content/580083/

136. Lepperhoff G, Schommers J, Weber O, Leonhardt H. Mechanism of the Deposit Formation at Inlet Valves [Internet]. Warrendale, PA: SAE International; 1987 Nov [cited 2024 May 7]. Report No.: 872115. Available from: https://www.sae.org/publications/technical-papers/content/872115/

137. Mikkonen S, Niemi A, Niemi M, Niskala J. Effect of Engine Oil on Intake Valve Deposits. In SAE International; 1989 [cited 2024 Sep 24]. Available from: https://saemobilus.sae.org/papers/effect-engine-oil-intake-valve-deposits-892111

138. Stępień Z, Oleksiak S. Deposit forming tendency in sparkignition engines and evaluation of gasoline detergent additives effectiveness. Journal of KONES. 2009;16(2):421–31.

139. Nomura Y, Ohsawa K, Ishiguro T, Nakada M. Mechanism of Intake-Valve Deposit Formation Part 2: Simulation Tests. In SAE International; 1990 [cited 2024 Sep 24]. Available from: https://saemobilus.sae.org/papers/mechanism-intake-valve-deposit-formation-part-2-simulation-tests-900152

140. Ansomboon J, Wuttimongkolchai A, Pannoi S, Fukuda K. Characterization of Deposits and Effects of Detergent Additive, Olefin Content and Engine Oil on Intake Valve Deposit Formation. In SAE International; 2000 [cited 2024 May 7]. Available from: https://saemobilus.sae.org/papers/characterization-deposits-effects-detergent-additive-olefin-content-engine-oil-intake-valve-deposit-formation-2000-01-2856

141. Bennett J. 7 - Advanced fuel additives for modern internal combustion engines. In: Folkson R, editor. Alternative Fuels and Advanced Vehicle Technologies for Improved Environmental Performance [Internet]. Woodhead Publishing; 2014 [cited 2024 May 8]. p. 165–94. Available from: https://www.sciencedirect.com/science/article/pii/B9780857095220500078

142. Merola SS, Tornatore C, Sementa P. Optical investigation of the fuel injector influence in a PFI spark ignition engine for two-wheel vehicles. J Mech Sci Technol. 2012 Jan 1;26(1):223–33.

143. Daneshagari P. A Test Procedure for Identifying the Gasoline's Deposit Formation Tendency on Intake Valves. In SAE International; 1989 [cited 2024 May 7]. Available from: https://saemobilus.sae.org/papers/a-test-procedure-identifying-gasolines-deposit-formation-tendency-intake-valves-892120

144. Costa J, Sarkisov L, Seaton N, Cracknell R. Adsorption-based Structural Characterization of Intake Valve Deposits [Internet]. Warrendale, PA: SAE International; 2011 Apr [cited 2024 May 8]. Report No.: 2011-01–0901. Available from: https://www.sae.org/publications/technical-papers/content/2011-01-0901/

145. Glawar AFG, Ziman PR, Wu K, Natarajan V, Wolgast EJ, Dankers C, et al. Understanding the Adverse Effects of Inlet Valve Deposits on SI Engine Operation, through a Novel Technique to Create Surrogate Deposits. In SAE International; 2018 [cited 2024 May 8]. Available from: https://saemobilus.sae.org/papers/understanding-adverse-effects-inlet-valve-deposits-si-engine-operation-a-novel-technique-create-surrogate-deposits-2018-01-1742

146. Arters DC, Schiferl EA, Szappanos G. Effects of Gasoline Driveability Index, Ethanol and Intake Valve Deposits on Engine Performance in a Dynamometer-Based Cold Start and Warmup Procedure. In SAE International; 2002 [cited 2024 May 8].

Available from: https://saemobilus.sae.org/papers/effects-gasoline-driveability-index-ethanol-intake-valve-deposits-engine-performance-a-dynamometer-based-cold-start-warmup-procedure-2002-01-1639

147. Gething JA. Performance=Robbing Aspects of Intake Valve and Port Deposits. In SAE International; 1987 [cited 2024 May 8]. Available from: https://saemobilus.sae.org/papers/performance-robbing-aspects-intake-valve-port-deposits-872116

148. Taniguchi BY, Peyla RJ, Parsons GM, Hoekman SK, Voss DA. Injector Deposits — The Tip of Intake System Deposit Problems. In SAE International; 1986 [cited 2024 May 8]. Available from: https://saemobilus.sae.org/papers/injector-deposits-tip-intake-system-deposit-problems-861534

149. Lewis RA, Newhall HK, Peyla RJ, Voss DA, Welstand JS. A New Concept in Engine Deposit Control Additives for Unleaded Gasolines. In Society of Automotive Engineers of Japan; 1983 [cited 2024 Sep 24]. Available from: https://saemobilus.sae.org/papers/a-new-concept-engine-deposit-control-additives-unleaded-gasolines-830938

150. Price RJ, Martin DP, Dickens N, Bohr P. The Impact of Inlet Valve Deposits on PFI Gasoline SI Engines – Quantified Effects on Fuel Consumption. In SAE International; 2007 [cited 2024 May 8]. Available from: https://saemobilus.sae.org/papers/impact-inlet-valve-deposits-pfi-gasoline-si-engines-quantified-effects-fuel-consumption-2007-01-0004

151. Stępień Z, Żak G, Markowski J, Wojtasik M. Investigation into the Impact of the Composition of Ethanol Fuel Deposit Control Additives on Their Effectiveness. Energies. 2021 Jan;14(3):604.

152. Srivastava, SP, Hancsók J. Fuel Additives. In: Fuels and Fuel-Additives [Internet]. John Wiley & Sons, Ltd; 2014 [cited 2024 Sep 24]. p. 177–269. Available from: https://onlinelibrary.wiley.com/doi/abs/10.1002/9781118796214.ch5

153. Beck Á, Bubálik M, Hancsók J. Development of Multifunctional Detergent-Dispersant Additives Based on Fatty Acid Methyl Ester for Diesel and Biodiesel Fuel. In: Biodiesel - Quality, Emissions and By-Products [Internet]. IntechOpen; 2011 [cited 2024 Sep 23]. Available from: https://www.intechopen.com/chapters/23675

154. Rath HP, Lange A, Posselt D. Polyisobutenamines [Internet]. 7291681, 2007 [cited 2024 Aug 8]. Available from: https://www.freepatentsonline.com/7291681.html

155. Arters D, Daily DT, Jackson MM. Fuel additives and fuel compositions comprising said fuel additives [Internet]. EP1237945A1, 2002 [cited 2024 Aug 8]. Available from: https://patents.google.com/patent/EP1237945A1/en

156. MacDuff MGJ, Jackson MM, Arters DC, McAtee RJ. Fuel additive compositions and fuel compositions containing detergents and fluidizers [Internet]. US6458172B1, 2002 [cited 2024 Aug 8]. Available from: https://patents.google.com/patent/US6458172B1/en

157. Danilov AM. Progress in research on fuel additives (review). Pet Chem. 2015 May 1;55(3):169–79.

158. Ahmadi MR. Method for controlling engine deposits in a direct injection spark ignition gasoline engine [Internet]. US6475251B1, 2002 [cited 2024 Aug 8]. Available from: https://patents.google.com/patent/US6475251B1/en

159. Aradi AA, Colucci WJ, Scull HM, Openshaw MJ. A Study of Fuel Additives for Direct Injection Gasoline (DIG) Injector Deposit Control. In SAE International; 2000 [cited 2024 Sep 23]. Available from: https://saemobilus.sae.org/papers/a-study-fuel-additives-direct-injection-gasoline-dig-injector-deposit-control-2000-01-2020

160. Chen Z, Yuan H, Foong TM, Yang Y, Brear M. The impact of nitric oxide on knock in the octane rating engine. Fuel. 2019 Jan 1;235:495–503.

161. Bika AS, Warey A, Long D, Balestrino S, Szymkowicz P. Characterization of Soot Deposition and Particle Nucleation in Exhaust Gas Recirculation Coolers. Aerosol Science and Technology. 2012 Dec 1;46(12):1328–36.

162. Yao Y, Han Z, Tian W, He G, Wu Y, Yan Y, et al. An original nondestructive sampling method to study the effect of gravity on the deposition of micron-sized large particles in exhaust gas recirculation (EGR) cooler fouling. International Journal of Engine Research. 2024 May 1;25(5):928–39.

163. Lacey J, Kameshwaran K, Filipi Z, Fuentes-Afflick P, Cannella W. The effect of fuel composition and additive packages on deposit properties and homogeneous charge compression ignition combustion. International Journal of Engine Research. 2020 Nov 1;21(9):1631–46.

164. Martín P, Rodríguez G, León A. Additive Evaluation in Venezuelan Diesel Formulations [Internet]. Warrendale, PA: SAE International; 1999 May [cited 2024 Aug 8]. Report No.: 1999-01–1480. Available from: https://www.sae.org/publications/technical-papers/content/1999-01-1480/

165. McArragher, CONCAWE. Fuel quality, vehicle technology and their interactions / by J.S. McArragher and others. CONCAWE; 1999. (CONCAWE report).

166. Lin JJ, Ho YS, Ku WS, Shiu WJ, Lee CN. Process for manufacturing gasoline additives of ester-free polyoxyalkylene amide [Internet]. US6627775B2, 2003 [cited 2024 Aug 8]. Available from: https://patents.google.com/patent/US6627775B2/en

167. Brennan ME, Yeakey EL. Preparation of polyalkylene polyamines [Internet]. US4036881A, 1977 [cited 2024 Aug 8]. Available from: https://patents.google.com/patent/US4036881A/en

168. Williams R, Smith A, Buttery I. Formation and Removal of Injector Nozzle Deposits in Modern Diesel Cars. SAE Int J Fuels Lubr. 2013 Apr 8;6(1):230–40.

169. Barbour R, Quigley R, Browne D, Panesar A. A Comparison of Peugeot DW10 Dynamometer and Vehicle Engine Performance. In: 8th Int Colloq. 2011.

170. Stepien Z, Krasodomski W. Effect of trace zinc amounts introduced in various chemical structures in diesel fuel on coke deposits of fuel injectors of a CI engine. International Journal of Engine Research. 2020 Jun;21(5):755–65.

171. Brinklow G, Herreros JM, Zeraati Rezaei S, Tsolakis A, Oliva F. Developing an Accelerated Procedure for Assessing the Injector Fouling Abatement of Different Fuel Additives,. In: NEW CONCEPTS FOR ULTRAEFFICIENT & CLEAN ICES. Valencia: CMT–Clean Mobility & Thermofluids; 2022.

172. Stępień Z. Influence of physicochemical properties of gasoline on the formation of DISI engine fuel injector deposits. Combustion Engines. 2021 Mar 30;184(1):16–23.

173. Wen Y, Wang Y, Fu C, Deng W, Zhan Z, Tang Y, et al. The Impact of Injector Deposits on Spray and Particulate Emission of Advanced Gasoline Direct Injection Vehicle. In SAE International; 2016 [cited 2024 May 21]. Available from: https://saemobilus.sae.org/papers/impact-injector-deposits-spray-particulate-emission-advanced-gasoline-direct-injection-vehicle-2016-01-2284

174. Joedicke A, Krueger-Venus J, Bohr P, Cracknell R, Doyle D. Understanding the Effect of DISI Injector Deposits on Vehicle Performance. In SAE International; 2012 [cited 2024 Sep 24]. Available from: https://saemobilus.sae.org/papers/understanding-effect-disi-injector-deposits-vehicle-performance-2012-01-0391

175. Badawy T, Attar MA, Xu H, Ghafourian A. Assessment of gasoline direct injector fouling effects on fuel injection, engine performance and emissions. Applied Energy. 2018 Jun 15;220:351–74.

176. Abarham M, Chafekar T, Hoard JW, Salvi A, Styles DJ, Scott Sluder C, et al. In-situ visualization of exhaust soot particle deposition and removal in channel flows. Chemical Engineering Science. 2013 Jan 14;87:359–70.

177. Lance MJ, Sluder CS, Wang H, Storey JME. Direct Measurement of EGR Cooler Deposit Thermal Properties for Improved Understanding of Cooler Fouling. In 2009 [cited 2024 May 21]. p. 2009-01–1461. Available from: https://www.sae.org/content/2009-01-1461/

178. Hoang AT, Le AT. A review on deposit formation in the injector of diesel engines running on biodiesel. Energy Sources, Part A: Recovery, Utilization, and Environmental Effects. 2019 Mar 4;41(5):584–99.

179. Stępień Z. The reasons and adverse effect of internal diesel injector deposits formation. Combustion Engines. 2014 Feb 1;156(1):20–9.

180. Abarham M, Hoard J, Assanis DN, Styles D, Curtis EW, Ramesh N, et al. Modeling of Thermophoretic Soot Deposition and Hydrocarbon Condensation in EGR Coolers. SAE International Journal of Fuels and Lubricants. 2009 Jun 15;2(1):921–31.

181. Aradi AA, Evans J, Miller K, Hotchkiss A. Direct Injection Gasoline (DIG) Injector Deposit Control with Additives. In SAE International; 2003 [cited 2024 Sep 23]. Available from: https://saemobilus.sae.org/papers/direct-injection-gasoline-dig-injector-deposit-control-additives-2003-01-2024

182. Berndorfer A, Breuer S, Piock W, Bacho PV. Diffusion Combustion Phenomena in GDi Engines caused by Injection Process. In SAE International; 2013 [cited 2024 Sep 23]. Available from: https://saemobilus.sae.org/papers/diffusion-combustion-phenomena-gdi-engines-caused-injection-process-2013-01-0261

183. Grandin B, Ångström HE, Stålhammar P, Olofsson E, Grandin B. Knock Suppression in a Turbocharged SI Engine by Using Cooled EGR. In SAE International; 1998 [cited 2024 Sep 23]. Available from: https://saemobilus.sae.org/papers/knock-suppression-a-turbocharged-si-engine-using-cooled-egr-982476

184. Su J, Xu M, Li T, Gao Y, Wang J. Combined effects of cooled EGR and a higher geometric compression ratio on thermal efficiency improvement of a downsized boosted spark-ignition direct-injection engine. Energy Conversion and Management. 2014 Feb 1;78:65–73.

185. Lee S, Park S, Hwang C, Lee S, Park S, Hwang C. Optimal Development of an Intake Throttle LP EGR Valve for Passenger Car Diesel Engines. In SAE International; 2016 [cited 2025 Feb 4]. Available from: https://saemobilus.sae.org/papers/optimal-development-intake-throttle-lp-egr-valve-passenger-car-diesel-engines-2016-01-1071

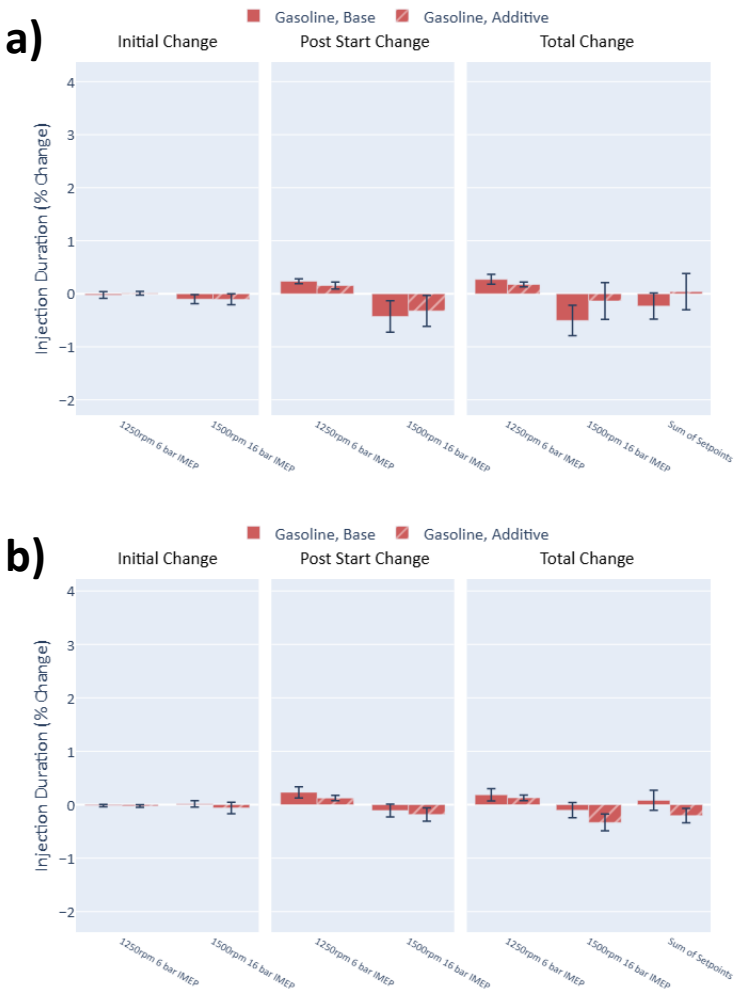
186. Cerdoun M, Khalfallah S, Beniaiche A, Carcasci C. Investigations on the heat transfer within intake and exhaust valves at various engine speeds. International Journal of Heat and Mass Transfer. 2020 Feb 1;147:119005.

187. Dritsas G, Nikolakopoulos P, Papadopoulos C. Design Evaluation of a Follower Cam With Variable Valve Lift Mechanism. International Journal of Structural Integrity. 2013 Mar 1;4:7–22.

9. APPENDICES

APPENDIX A

Segmented Phase Analysis Results from each third of the Cycle



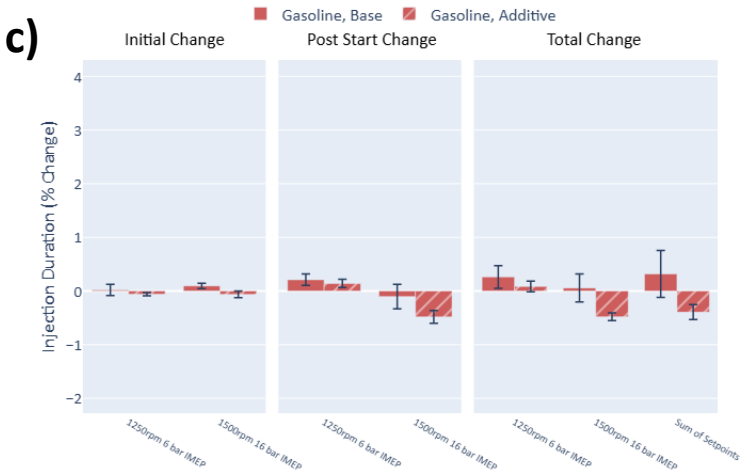
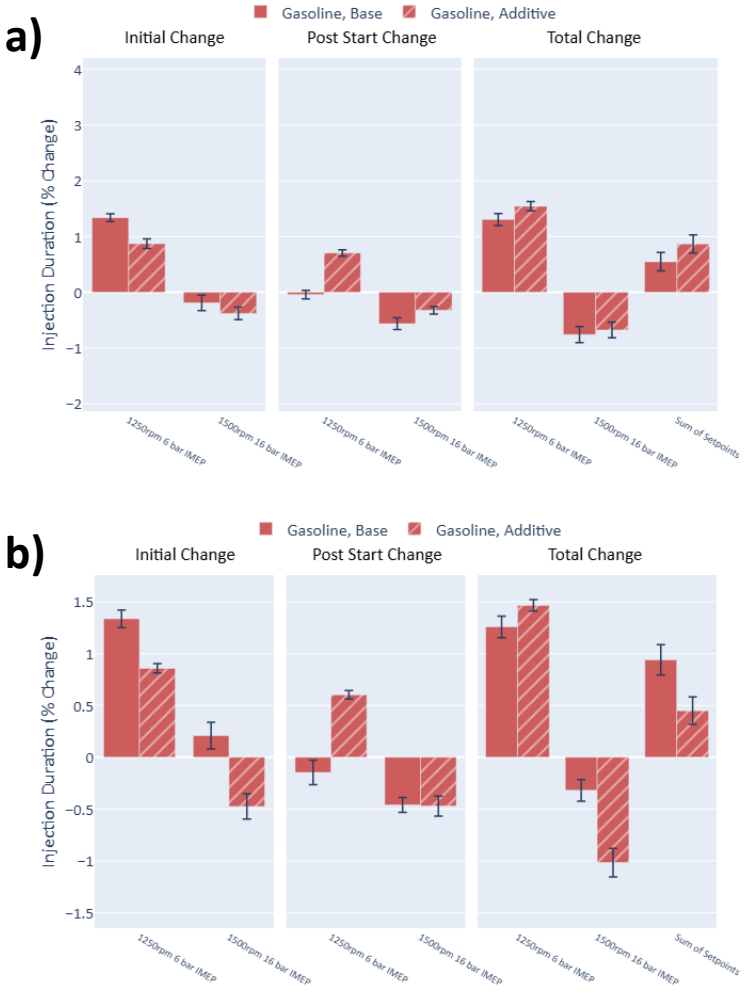


Figure A – 1 : Cycle 7, a) first segment, b) second segment, c) third segment.



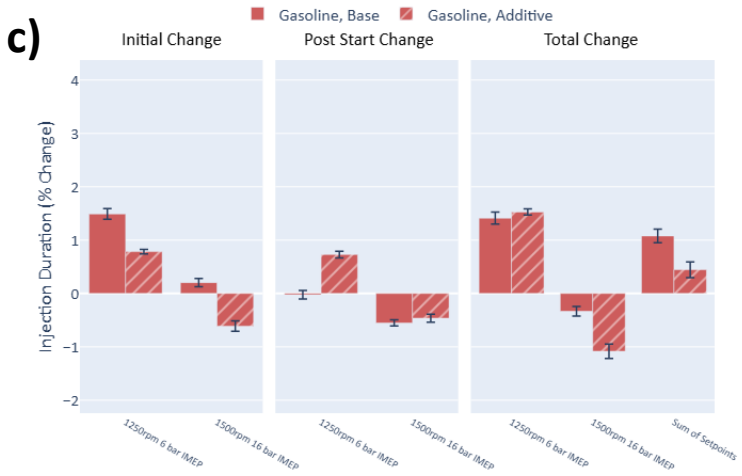
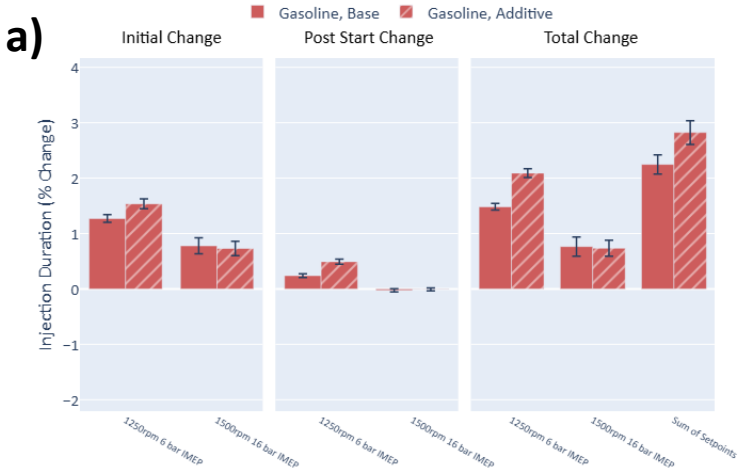
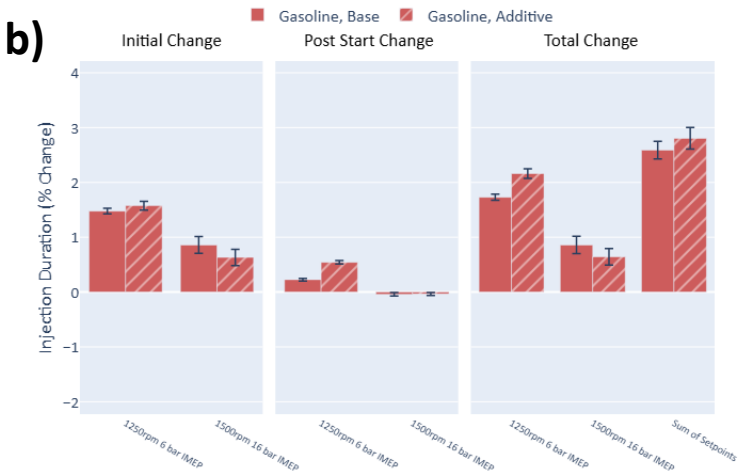


Figure A – 2 : Cycle 10, a) first segment, b) second segment, c) third segment.





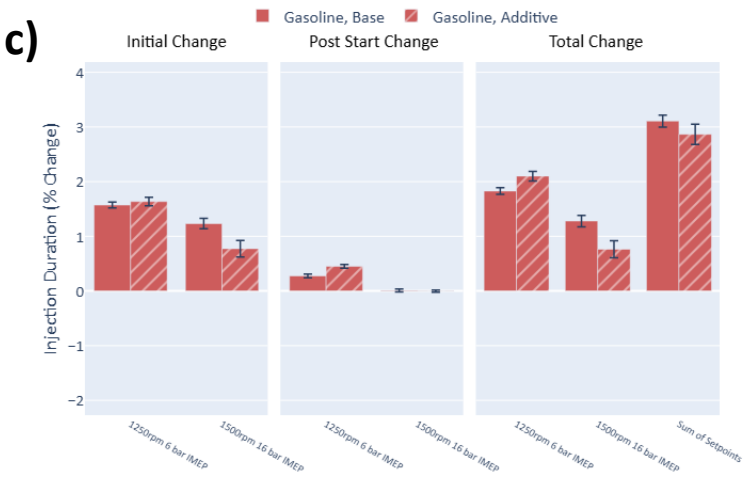
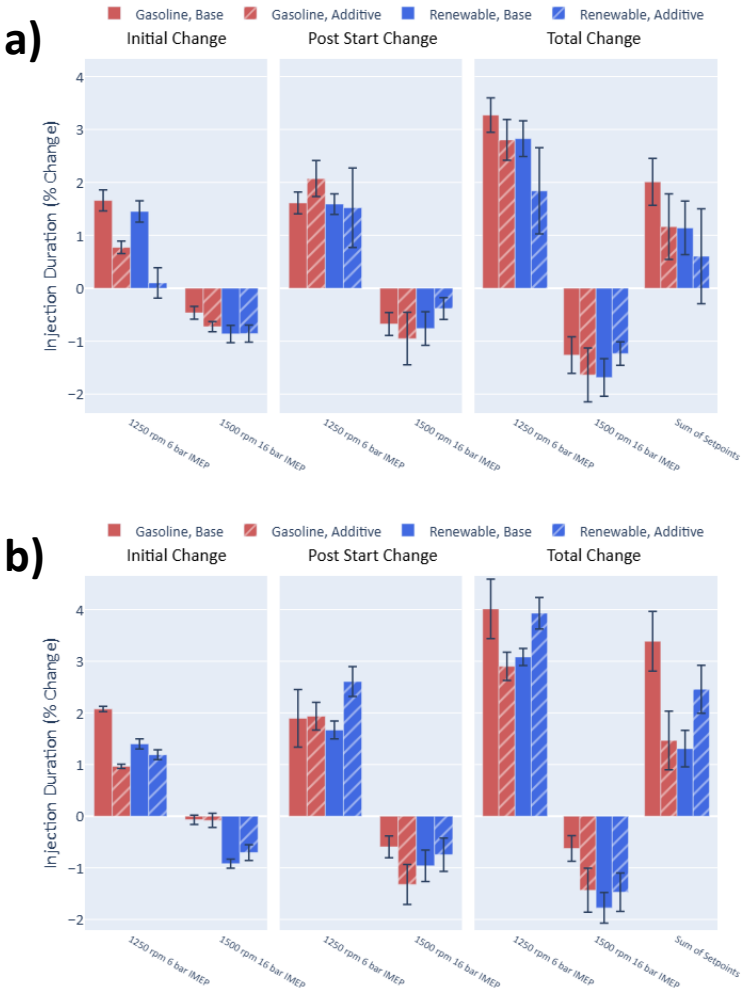


Figure A – 3 : Cycle 11, a) first segment, b) second segment, c) third segment.



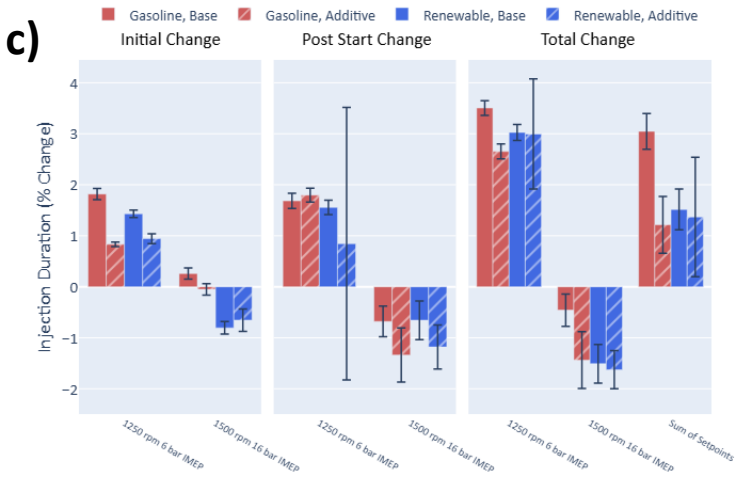


Figure A – 4 : Cycle 12, a) first segment, b) second segment, c) third segment.

APPENDIX B

Heater PID Controller Code

```
/////// libraries and parameters for OLED screen setup/////
#include <EEPROM.h>
#include <SPI.h>
#include <Wire.h>
#include <avr/pgmspace.h>
#include <Adafruit_GFX.h>
#include <Adafruit_SSD1306.h>
#define OLED_RESET 5
#define SCREEN_WIDTH 48 // OLED display width, in pixels
#define SCREEN_HEIGHT 32 // OLED display height, in pixels
Adafruit_SSD1306 display(OLED_RESET);
////// libraries needed to use thermocouple amplifiers//////
#include "max6675.h"
#include "Adafruit_MAX31855.h"
// defining thermocouple amplifier pins
#define MAXDO   12
#define MAXCS_head   10
#define MAXCS_box 9
#define MAXCLK  13
// These 2 lines below define the 2 functions that the code will use to
measure the thermocouple
// there is one used to access the head thermocouple and one for the box
Adafruit_MAX31855 thermocouple_head(MAXCLK, MAXCS_head, MAXDO);
Adafruit_MAX31855 thermocouple_box(MAXCLK, MAXCS_box, MAXDO);
//Arduino Pins
#define SSR_PIN  11
int pump_SSR_pin=3;
#define but_green  5
#define but_red  6
#define led  4
///// SAFETY VARIABLES /////
float switch_to_head_percent=0.7;//percentage of desired final
temperature when the controller will start controlling via the head TC
float box_setpoint=80; // the temperature the box is controlled to until
control is switched to the head
float box_safety_T=110;// Temperature which will trigger the PID loop
temporarily turning off and switching the SSR out to 0
float head_safety_T=92;
float box_emergency_shutdown_T=115;// temperature at which the whole
thing will shutdown triggering a warning to be displayed on OLED asking
for user to restart
float head_emergency_shutdown_T=96
```

```
float safety_check_on_percent=0.94; //percentage of the safety_T that
needs to be reached to start safety checks
float pump_on_T=70;
float pump_off_T=65;
////// PID constants //////
// kp values
float kp_normal=3;
float kp_when_pump_off=2;
// ki values
float ki_normal=0.09;
float ki_when_pump_off=0.02;
float PID_i_saturation_w_pump_off=25; //maximum number PID_i can be
float PID_i_saturation_normal=35;
// kd values
float kd=60000;
// refresh rates
int refresh_rate_normal =5000; //PID loop time in ms
int refresh_rate_startup=100;
int refresh_rate = refresh_rate_startup;
//// MOVING AVERAGE VARIABLES /////
float alpha=0.2, alpha_safety=0.7; // used to calculate the moving
average of the temperature, must be between 0 and 1, the smaller the
number the more the data is averaged.
// defines the absolute max PID that the heater will output at any time
float PID_absolute_max = 120;
float PID_absolute_max_w_pump_off = 120;
float PID_absolute_max_normal=120;
/////////////// OTHER VARIABLES ////////////////////
// other PID variables
float PID_i_saturation=PID_i_saturation_w_pump_off;
float kp = kp_when_pump_off, ki=ki_when_pump_off;
float PID_p, PID_i, PID_d, PID_total;
float now_pid_error, prev_pid_error;
float PID_i_check=0;
// Serial print variables
int box_control_flag, head_control_flag;
int numVars;
// counting variables
int on, time, start_time, restart; //variables used to calculate time in
main loop
int pump_on_time, pump_off_time, pump_switch_time, pump_on_delay=0,
pump_on_1_time=millis(), pump_on_count=0; // pump timing variables
int nan_count_out=0, nan_count=0, nan_count_interval = 30; //nan count
variables

int elapsedTime, prev_time;        //Variables for time control
```

```
int temp_shutdown_count=0;
int off_time=0, off_timer=0; // off timers
int screen_time_prev, screen_refresh_rate=500;
// buttons and potentiometer variables
float pot =0;
float Dial =0;
float Setpoint = 0;
uint8_t state = 0;
bool  D5_state = 1,D6_state = 1; //button states
float prev_isr_timeD4, prev_isr_timeD5, prev_isr_timeD6;
// LED
bool LED_State = LOW;
// temperature variables
float real_temp_in=0, real_temp_out, temp_avg_out, real_temp,
box_temp_avg_prev=0, box_temp_avg,
head_temp_avg_safety=10,head_temp_avg_safety_prev=10,box_temp_avg_safety=
10,box_temp_avg_safety_prev=10;
float
real_box_temp=0,real_head_temp=0,head_temp_avg=0,head_temp_avg_prev=0,
real_temp_control=0, real_temp_control_avg=0,
real_head_temp_raw,real_box_temp_raw;
// triggers and flags

bool pump_trigger=0, pump_flag=0, control_TC=0,
temporary_shutdown=0,shutdown=0;
// Serial print input setup
const char time_label[] PROGMEM = "Time=";
const char box_in_control_flag_label[] PROGMEM= "Box Ctrl=";
const char head_in_control_flag_label[] PROGMEM= "Head Ctrl=";
const char pump_status_label[] PROGMEM= "Pump trig=";
const char pump_flag_label[] PROGMEM= "Pump on=";
const char box_temp_avg_label[] PROGMEM= "Box T Avg=";
const char head_temp_avg_label[] PROGMEM= "Head T Avg=";
const char pid_out_label[] PROGMEM= "PID Out=";
const char setpoint_label[] PROGMEM= "Setpoint=";
const char p_label[] PROGMEM= "P=";
const char i_label[] PROGMEM= "I=";
const char d_label[] PROGMEM= "D=";
const char pid_error_label[] PROGMEM= "PID Err=";
const char nan_count_label[] PROGMEM= "Nan Count=";
const char temp_shutdown_label[] PROGMEM= "Temp Shutdwn=";
const char temp_shutdown_count_label[] PROGMEM= "Temp Shutdwn Count=";
const char pump_on_delay_label[] PROGMEM= "Pump On Delay=";
const char off_timer_label[] PROGMEM= "Off time=";
// Create an array of pointers to these string literals to send to
Serial_print function when called
```

```
const char* const labels_PID[] PROGMEM = {
  time_label,  box_in_control_flag_label,head_in_control_flag_label,
pump_status_label, pump_flag_label,box_temp_avg_label,
head_temp_avg_label,pid_out_label,
   setpoint_label, p_label, i_label, d_label,pid_error_label,
nan_count_label,temp_shutdown_label,
temp_shutdown_count_label,pump_on_delay_label,off_timer_label
};
// create an array of variables that will be filled later on in the code
float Variables_Serial_PID[] = {time, box_control_flag,head_control_flag,
pump_trigger, pump_flag,box_temp_avg, head_temp_avg, PID_total, Setpoint,
    PID_p, PID_i, PID_d, now_pid_error, nan_count,temporary_shutdown,
temp_shutdown_count, pump_on_delay,off_timer
};
////////////////////////////////////////////////
void setup() {
  cli();
  sei();

  Serial.begin(9600); //sets up the serial monitor and baud rate
  numVars=18; //number of serial variables sent
  pinMode(SSR_PIN, OUTPUT);  // defines SSR_pin as output pin
  digitalWrite(SSR_PIN, LOW);    // initialises SSR_pin to start at 0
  pinMode(led, OUTPUT);  //defines led as an output
  digitalWrite(led, LOW); // sets led to 0
  // defines real_head_temp as the output of the function readCelsius,
the inputs used for the function are defined by "thermocouple_head" which
was defined above
  real_head_temp = thermocouple_head.readCelsius();
  real_box_temp= thermocouple_box.readCelsius();
  start_time=0;
  restart=0;

  TCCR2B = TCCR2B & B11111000 | B00000111;    // D11 now set to 30 Hz
  pinMode(but_green, INPUT_PULLUP); // defines button pins as input pins
  pinMode(but_red, INPUT_PULLUP);
  PCICR |= B00000100;      // uses the PCICR register to activate
interrupts on pins D0 to D7, this is defined by the bit B00000100
  PCMSK2 |= B01100000;     //PCINT20, CINT21, CINT22 enabled -> location
of "1" in B01100000 indicates which pins from D0-D7 have been activated.
D5, D6 will trigger interrupt

  //starts the OLED screen display
  display.begin(SSD1306_SWITCHCAPVCC, 0x3C);
  delay(100);
  display.clearDisplay();
```

```
  display.setTextSize(1);
  display.setTextColor(WHITE,BLACK);
  display.display();
  delay(100);
  Setpoint=0; // sets the Setpoint to be 0 at the beginning
}
//////////////////// Main Loop ////////////////////////////
void loop() {  // this loop is looping constantly so anything that needs
to be constantly monitored is in this loop
  elapsedTime=millis()-screen_time_prev; // checks time since last screen
loop
  ////////////// SERIAL PRINT /////////////
  if (elapsedTime>screen_refresh_rate){  //only prints at the defined
refresh rate, this is defined in the variables at the top
// create an array of variables that will be filled later on in the code
    float Variables_Serial_PID[] = {time,
box_control_flag,head_control_flag, pump_trigger, pump_flag,box_temp_avg,
head_temp_avg, PID_total, Setpoint,
        PID_p, PID_i, PID_d, now_pid_error, nan_count,temporary_shutdown,
temp_shutdown_count, pump_on_delay,off_timer
    };

    Serial_print(labels_PID, Variables_Serial_PID, numVars);
    delay(300);
  screen_time_prev=millis();
  }
  ////////////// STATE CHECK /////////////
  if (state == 0){ // PID control loop is only active if state=0 // state
depends on which button is pressed or if a shutdown has been tripped
    PID_control();
  }
  else{ //if state is not 0 or 1 then cooldown mode is entered the
Setpoint is reset to 0
    Setpoint=0;
    cool_down();
  }
  ////////////// POTENTIOMETER / DIAL SETUP /////////////
  pot=analogRead(A3); // the signal reading from the potentiometer is
defined as pin A3
 // the variable Dial which is used later to change the setpoint using
the potentiometer
  Dial=map(pot,0,1023,0,110);// map function converts the input voltage
from the pot signal to a number between 0 and 110, which represents the
min and max control temperatures
  ////////////// NAN CHECK LOOP /////////////
```

```
  if (time>nan_count_interval){   // checks how many nan values are
picked up by the nan counter in the PID control section
    nan_count_interval=nan_count_interval+30; // when the time gets
bigger than the nan_count_interval then 30s are added to the nan_count
interval
// so every 30 seconds this if statement is triggered
      if (nan_count>3){ // if nan count is greater than 15 then state =
2, sending the box into cool down mode
        state=2;
      }
    nan_count=0; // nan_count resets to 0 after the check
  }
  refresh_rate=refresh_rate_startup;
  if (time>10){ // wait for 10 seconds to start these checks whilst the
thermocouples stabilise
    refresh_rate=refresh_rate_normal;
    ////////////////////// CONTROL CHECKS ///////////////////////
// see functions at the bottom of page for more detail on the functions
    control_TC=Control_TC_Check(box_temp_avg,head_temp_avg,pump_off_T,pum
p_on_T,switch_to_head_percent,Setpoint); //variable that dictates which
Thermocouple is in control
    pump_trigger=pump_trigger_check(box_temp_avg,head_temp_avg,pump_off_T
,pump_on_T,switch_to_head_percent,Setpoint);// trigger that indicates if
the conditions are correct for the pump to be turned on
    pump_flag=pump_switch_check(pump_trigger,pump_on_count,pump_off_time,
pump_on_time,pump_SSR_pin);//this flag indicates that the pump has been
turned on after the trigger above was checked
    ////////////////////// SAFETY CHECKS ////////////////////////

      // see functions at the bottom of page for more detail on the
functions
    temporary_shutdown=temporary_shutdown_check(box_temp_avg_safety,box_s
afety_T,head_temp_avg_safety,head_safety_T); //variable that triggers a
temporary shutdown
    shutdown=emergency_shutdown_check(box_temp_avg_safety,
box_emergency_shutdown_T,head_temp_avg_safety,head_emergency_shutdown_T);
// variable that triggers a full shutdown
  }
}
////////////////////////////// PID CONTROL ////////////////////////////
void PID_control(void){ //Main PID compute and execute function
  /////////// RESTART CHECK  ////////////////////////////////
  if (restart==1){  // restart will equal 1 if the red button was pressed
or if a temporary shutdown occurred
    start_time=millis();// resets the start time after a restart
  }
```

```
  restart=0; // stops start_time being overwritten until next restart
  /////////////// restart check ////////////////////////
  elapsedTime = millis() - prev_time;
  on=1;
  /////////////// CONTROL LOOP ////////////////////////
  if(elapsedTime > refresh_rate){ // only enters PID loop at the refresh
rate , this is defined in the variables at the top

    if (shutdown==1){ // checks if shutdown variable has been triggered,
this comes from the "CONTROL CHECKS" section
      state=2; //goes to cool_down loop
    }
    ////////////// TEMPORARY SHUTDOWN //////////////////
    if (temporary_shutdown==1){ // checks if temporary shutdown variable
has been triggered, this comes from the "CONTROL CHECKS" section
      if ((head_temp_avg_safety<(head_safety_T)) &&
(box_temp_avg_safety<(box_safety_T)) ) { // checks if temporary shutdown
can end
        temporary_shutdown=0; //resets temporary shutdown trigger so the
loop ends
      }
      PID_total=0;
      analogWrite(SSR_PIN,PID_total); //in temporary shutdown the SSR pin
is deactivated with a LOW PWM output
      digitalWrite(led,LOW); // same as above
      time=(millis()/1000)-(start_time/1000);//continues counting time,
this is used in several checks, filters and is outputted via the serial
monitor for measurement and troubleshooting

      ////////////// raw temperature readings ////////////////////////
      real_head_temp_raw=thermocouple_head.readCelsius();
      real_box_temp_raw=thermocouple_box.readCelsius();
      ////////////// NAN FILTER  ////////////////////////
      // see functions at the bottom of the code for detail on how they
work
      nan_count=nan_counter(real_head_temp_raw,nan_count); // counts the
number of "nan" values read by the thermocouple and is outputted from
here to the "nan_check" in the MAIN LOOP section
      nan_count=nan_counter(real_box_temp_raw,nan_count); // same as
above but for box thermocouple
      real_head_temp=Temperature_filter(real_head_temp_raw,real_head_temp
); // submits raw temperature reading through a filter that omits "nan"
values
      real_box_temp=Temperature_filter(real_box_temp_raw,real_box_temp);
// same as above but for box
      ////////// Safety Temperature averaging ///////////////
```

```
      box_temp_avg_safety=avg_temperature_readings(real_box_temp,
box_temp_avg_safety, alpha_safety);
      head_temp_avg_safety=avg_temperature_readings(real_head_temp,
head_temp_avg_safety, alpha_safety);
      box_temp_avg=box_temp_avg_safety;
      head_temp_avg=head_temp_avg_safety;
      ///////////////// OLED DISPLAY  ////////////////////
      OLED_display_temp_shutdown(box_temp_avg_safety,head_temp_avg_safety
); // outputs variables to the OLED display via the OLED function at the
base of the code
    }
    ////////////////// MAIN PID LOOP ////////////////////////////////
    if ((temporary_shutdown==0) && (shutdown==0)) { // only enters PID
loop if both shutdowns are not triggered
      time=(millis()/1000)-(start_time/1000); //continues counting time,
this is used in several checks, filters and is outputted via the serial
monitor for measurement and troubleshooting
      //////// RAW TEMPERATURE READINGS /////////////
      real_box_temp_raw=thermocouple_box.readCelsius();
      real_head_temp_raw=thermocouple_head.readCelsius();
      ////////////// NAN FILTER /////////////////
      nan_count=nan_counter(real_head_temp_raw,nan_count); // same as
that found in the section TEMPORARY SHUTDOWN
      nan_count=nan_counter(real_box_temp_raw,nan_count);
      real_head_temp=Temperature_filter(real_head_temp_raw,real_head_temp
);
      real_box_temp=Temperature_filter(real_box_temp_raw,real_box_temp);
      /////// TEMPERATURE AVERAGING /////////////////
      box_temp_avg_safety=avg_temperature_readings(real_box_temp,
box_temp_avg_safety, alpha_safety); // same as that found in the section
TEMPORARY SHUTDOWN
      head_temp_avg_safety=avg_temperature_readings(real_head_temp,
head_temp_avg_safety, alpha_safety);
      box_temp_avg=avg_temperature_readings(real_box_temp, box_temp_avg,
alpha); // uses a different alpha value than the safety averages so it is
more stable but less responsive
      head_temp_avg=avg_temperature_readings(real_head_temp,
head_temp_avg, alpha);
      ///// SETTING CONTROL TC /////////////////
      if (control_TC==0){
        real_temp_control=real_box_temp; //sets the thermocouple that is
in control
        real_temp_control_avg=box_temp_avg; // sets the average
temperature to be used by the PID calcualtions below
        box_control_flag=1; // this flag is sent to the serial monitor
for troubleshooting purposes
```

```
        head_control_flag=0; // this flag is sent to the serial monitor
for troubleshooting purposes
      }
      if (control_TC==1){ //same as above but for the head temperature
        real_temp_control=real_head_temp;
        real_temp_control_avg=head_temp_avg;
        box_control_flag=0;
        head_control_flag=1;
      }
      ////////////// PID TARGET CHECK ////////////////////
      now_pid_error = Setpoint - real_temp_control_avg; //sets the error
value for the PID calcualtions with respect to the average control
temperature defined in "SETTING CONTROL TC"
      if (control_TC==0 && Setpoint>5){ // whilst the box thermocouple is
in control and a Setpoint has been chosen then PID error is calculated
with respect to a fixed box setpoint
        now_pid_error=box_setpoint - real_temp_control_avg; //
"box_setpoint" is defined in the safety variables and is set above the
pump operating temperature of 70
      }
      ////////////// PID VALUES , PUMP ON/OFF FILTER ///////////////
      if (pump_flag==0){ // activated if the pump is off
      kp=kp_when_pump_off; // a series of different PID constants are
used when the pump is off due to the lower heat loss
      ki=ki_when_pump_off;
      PID_absolute_max=PID_absolute_max_w_pump_off;
      PID_i_saturation=PID_i_saturation_w_pump_off;
      }
      else{ // activated when pump is on
      kp = kp_normal;
      ki=ki_normal;
      PID_absolute_max = PID_absolute_max_normal;
      PID_i_saturation=PID_i_saturation_normal;
      }
      ///////////////// PID OUTPUT CALCULATION ///////////////////////
      PID_p = kp * now_pid_error; // calculation of Proportional
component
      PID_d = kd*((now_pid_error - prev_pid_error)/refresh_rate); //
calculation of differential component, uses the refresh rate as dt and
change in error as dE
      if(-40 < now_pid_error && now_pid_error < 40){ //Integral component
is only increased when 40 degrees away from the Setpoint, this prevents
it building up too much during the long warmup time and prevents
overheating
        PID_i_check = PID_i + (ki * now_pid_error); // variable to check
what the next Integral component will be, this is necessary as once over
```

```
the saturation limit PID_i will always be over as it cannot enter the if
statement below
        if (PID_i_check< PID_i_saturation){ // only activated if the
check is lower than saturation
          PID_i = PID_i + (ki * now_pid_error);
        }
        else {PID_i =PID_i_saturation;} // limits Integral at the
saturation limit
        }
      else{PID_i = 0;}

      PID_total = PID_p + PID_i + PID_d;  //Calculate and map total PID
value
      PID_total = map(PID_total, 0, 150, 0, 255);

      if(PID_total < 0){PID_total = 0;} // minimum PID value of 0
      if (PID_total > PID_absolute_max) {PID_total = PID_absolute_max; }
// maximum PID limit defined in PID variables
      if (time<5){PID_total=0;} // restricts PID output for first 5
seconds whilst the thermocouples stabilise
      analogWrite(SSR_PIN, PID_total);//Write PWM signal to the SSR
      ///////////////// OLED DISPLAY ////////////////////////////////////
      OLED_display_PID(Dial,Setpoint,
box_temp_avg,head_temp_avg,PID_total); // same as previous OLED_display
but with modified function
      // saves values for next loop
      prev_time = millis();
      prev_pid_error = now_pid_error;
      ////////////////// LED ////////////////////////////////////
      LED_function(PID_total); // activates LED if PID total > 0, see
function
    }
  }
}
////////////////////////// COOL DOWN ///////////////////////
void cool_down(void){ //
  PID_total=0;
  digitalWrite(SSR_PIN, PID_total);    //SSR is turned OFF as is LED
  digitalWrite(led, LOW);
  elapsedTime = millis() - prev_time; // elapsed time still used in this
loop for the refresh rate of thermocouple measurements
  restart=1; // restart set to 1 so the if statement in the PID loop
"RESTART CHECK" is triggered
  control_TC=0; // control thermocouple reset to box in the event of a
restart
  time=0; // time is reset
```

```
  if (on==1){ // on=1 only during PID loop so will enter this after
exiting PID
    off_time=millis()/1000; //records off time
    on=0; //sets on=0 so the off_time is not overwritten
  }
  if(elapsedTime > refresh_rate){ // only records temperatures and writes
to OLED and Serial at the refresh rate
    off_timer=(millis()/1000)-off_time; //records off time
    ///// RAW TEMPERATURE /////////
    real_box_temp_raw=thermocouple_box.readCelsius();
    real_head_temp_raw=thermocouple_head.readCelsius();
    ///////// NAN FILTER ////////////
    nan_count=nan_counter(real_head_temp_raw,nan_count); // same as
previous "NAN FILTER" in PID LOOP
    nan_count=nan_counter(real_box_temp_raw,nan_count);
    real_head_temp=Temperature_filter(real_head_temp_raw,real_head_temp);
    real_box_temp=Temperature_filter(real_box_temp_raw,real_box_temp);
    ///////// TEMPERATURE AVERAGING ////////////////
    box_temp_avg=avg_temperature_readings(real_box_temp, box_temp_avg,
alpha); // same as previous "TEMPERATURE AVERAGING" in PID LOOP
    head_temp_avg=avg_temperature_readings(real_head_temp, head_temp_avg,
alpha);

    ////////////////// TURN PUMP OFF TIMER //////////////////
    if
((real_box_temp<pump_on_T)||(real_head_temp<pump_on_T)||(off_timer>180)){
// waits for the off_timer to reach 180 seconds or the temperatures to be
low before turning off, this prevents overheating from sudden stagnation
of the oil
      analogWrite(pump_SSR_pin,LOW);
    }
    ////////////////////////// BOX OFF DISPLAY
//////////////////////////////////
    if (shutdown==0){
      OLED_display_cooldown(box_temp_avg,head_temp_avg); // same as other
OLED_dispalys with a modified function that displays temperatures and
says "off"
      prev_time = millis();
    }
    ////////////// SHUTDOWN DISPLAY ////////////////////////////////
    if (shutdown==1){ // this loop is activated if a shutdown is
triggered via the "CONTROL CHECKS"
      OLED_display_shutdown(box_temp_avg,head_temp_avg); // adds a
message to cool down loop if shutdown is initiated
```

```
      prev_time = millis(); // shutdown is never reset to 0 once this
loop is ended, forcing the user to manually reset the box so they must
see the warning sign
    }
  }
}
////////////////////// BUTTONS /////////////////////////////
ISR (PCINT2_vect) { // activated if an interrupt is triggered on the
previously defined interrupt pins D4 and D5 (see setup for details)
  cli();  // disables further interrupts whilst in this loop
  //// GREEN BUTTON ///////
  if(PIND & B00100000){ // PIND is the status register of the PD port
pins, this loop will activate if the defined PB port pins D0-D7 are high
and this pin is D5 (B00100000), saves on program speed compared to
digitalRead()
    if(D5_state == 0){
      D5_state = 1; // if D5 pin is high d5 state goes to 1 and the time
is recorded
      prev_isr_timeD5 = millis();
    }
  }
  else if (D5_state == 1 && (millis() - prev_isr_timeD5 > 2)){ // if
D5_state is 1 (should be after pressing button) and it has been 2ms since
it was pressed then this if statement is activated
    Setpoint=Dial; // The PID setpoint is set to the number on the dial
(potentiometer)
    int st = Setpoint;
    EEPROM.write(0, st); // saves this value in the Arduino memory, so it
will remember it for next time even after a reset of power
    D5_state = 0; // resets button states back to 0
  }
  ///// RED BUTTON ///////////
  if(PIND & B01000000){ // same as for green button but with pin D4
    if(D6_state == 0){
      D6_state = 1;
      prev_isr_timeD6 = millis();
    }
  }
  else if (D6_state == 1 && (millis() - prev_isr_timeD6 > 2)){
    if(state == 0 || state == 1){
      state = 2; // this will trigger the cooldown loop
    }
    else if (state == 2){
      state = 0; // if already in cooldown loop set back to PID loop
    }
    D6_state = 0;
```

```
  }
  sei(); // re-enables interrupts
}
//////////////////////////// FUNCTIONS ///////////////////////
float Control_TC_Check(float box_temp_avg,float head_temp_avg, float
pump_off_T, float pump_on_T, float switch_to_head_percent, float
Setpoint){
  float control_TC;
  control_TC=0; // always resets control_TC to 0 before going through
checks, it will then change to 1 if the below conditions are met
    // Check 1
    if ((box_temp_avg >pump_off_T) &&
(head_temp_avg>(switch_to_head_percent*Setpoint))) {// checks to see if
the head temp is above the threshold declared in the setup
      control_TC=1; //then changes control_TC to 1 which means the
head_TC is now what the controller uses
    }
    else{
      control_TC=0;
    }
    if (Setpoint<5){ // Setpoint being less than 5 indicates the user has
not selected a target yet
      // Check 2
      control_TC=0; // Control_TC is reset to 0 if there is no Setpoint
selected yet.
    }
  return control_TC;
}
float pump_trigger_check(float box_temp_avg,float head_temp_avg, float
pump_off_T, float pump_on_T, float switch_to_head_percent, float
Setpoint){
  float pump_trigger;
  // checks to see if the head temperature is above the threshold
declared in the setup
    if (Setpoint<5){// Setpoint being less than 5 indicates the user has
not selected a target yet
      if ((box_temp_avg<pump_off_T)||(head_temp_avg<pump_off_T)){ // only
sends trigger for pump_trigger to off if either temperature is too low
        pump_trigger=0;
      }
      if ((box_temp_avg>pump_on_T) && (head_temp_avg>pump_on_T)){ //
keeps the pump on if both temperatures are above the pump on temperature
to prevent overheating from sudden stagnation of oil
        pump_trigger=1;
      }
    }
```

```
    if (Setpoint>5){ // Setpoint being more than 5 indicates the user has
selected a target
      if (box_temp_avg<pump_off_T) { // sets pump_trigger to off if
temperature is too low
        pump_trigger=0;
      }
      if ((box_temp_avg>pump_on_T) || (head_temp_avg>50)){ // sets
pump_trigger to on if temperature is above pump operation temperature
        pump_trigger=1;
      }
    }
return pump_trigger;
}
float pump_switch_check(int pump_trigger,int pump_on_count, int
pump_off_time, int pump_on_time, int pump_SSR_pin){
  float pump_flag;
  #define pump_SSR_pin pump_SSR_pin // defines pump_ssr_pin
  pump_flag=0;
  //checks that the pump has not been triggered to switch on or off more
than once in a short period of time, this stops the pump from repeatedly
turning on and off when near the pump_off and pump_on temperatures
  if (pump_trigger==1){ // if pump trigger has been activated (see
pump_trigger_check) do the following
    pump_on_count=pump_on_count+1; //makes a count every time the loop is
repeated
    pump_on_time=millis()/1000;  // records time every loop
    pump_switch_time=pump_on_time-pump_off_time; // calculates the time
since the last time the pump was off
    if (pump_on_count==1){
      pump_on_1_time=millis()/1000; // marks the time of the first count
    }
    pump_on_delay=(millis()/1000)-pump_on_1_time;// records the time
since the pump first got triggered

    if (pump_switch_time>30 && pump_on_delay>1200){ // turns the pump on
only after 1200s (20min) from the  first time it was switched on and if
its been 30 seconds since the pump trigger was last off
    analogWrite(pump_SSR_pin,255);
    pump_flag=1; //this is printed to the serial monitor for
troubleshooting
    }
  }
  if (pump_trigger==0){ // opposite of above
    pump_on_count=0;
    pump_off_time=millis()/1000;
    pump_switch_time=pump_off_time-pump_on_time;
```

```
    if (pump_switch_time>30){
    analogWrite(pump_SSR_pin,LOW);
    }
  }
return pump_flag;
}
int temporary_shutdown_check (float box_temp_avg_safety,float
box_safety_T,float head_temp_avg_safety,float head_safety_T){
    int temporary_shutdown;
    if ((box_temp_avg_safety>box_safety_T) ||
(head_temp_avg_safety>head_safety_T)){   //checks to see if TC is over
temp shutdown threshold
    temporary_shutdown=1; //activates shutdown if statement in the PID
loop
    }
    if ((box_temp_avg_safety<box_safety_T) &&
(head_temp_avg_safety<head_safety_T)){   //checks to see if TC is below
temp shutdown threshold
      temporary_shutdown=0; //activates shutdown if statement in the PID
loop
    }
  return temporary_shutdown;
}
int emergency_shutdown_check(float box_temp_avg_safety, float
box_emergency_shutdown_T, float head_temp_avg_safety, float
head_emergency_shutdown_T){
    if ((box_temp_avg_safety>box_emergency_shutdown_T) ||
(head_temp_avg_safety>head_emergency_shutdown_T)){//checks to see if temp
is over emergency shutdown threshold
      shutdown=1 ;// activates shutdown if statement in the PID loop
    }
}
int nan_counter(float real_temp_raw,int nan_count_in){
  int nan_count_out;
  // nan_count is outputted from here and goes to the "nan_check" in the
loop section
  if (isnan(real_temp_raw)){
    nan_count_out=nan_count_in+1; // if the reading is a nan then the nan
count goes up, if this nan count gets too high it will be detected in the
"nan_check" then the box will shutdown
  }
  else{
    nan_count_out=nan_count_in;
  }
return nan_count_out;
}
```

```
float Temperature_filter(float real_temp_raw,float real_temp_in){
  float real_temp_out;
  // outputs temperature only if it is not a "nan" value
  if (!isnan(real_temp_raw)){
    real_temp_out=real_temp_raw; // converts the measurement to the real
temperature only if the reading is NOT a nan
  }
  else{
    real_temp_out=real_temp_in;
  }
  return real_temp_out;
}
float  avg_temperature_readings(float real_temp, float temp_avg_in, float
alpha){
  float temp_avg_prev=temp_avg_in;
  // outputs average temperatures
  temp_avg_out=(real_temp*alpha)+(temp_avg_prev*(1-alpha)); // uses
moving average formula, alpha is defined in the variables section
  return temp_avg_out;
}
/////////////// OLED FUNCTIONS ////////////////
void OLED_display_temp_shutdown(float box_temp, float head_temp) {

  display.clearDisplay(); // clear display
  display.setCursor(0,0);
  //line 1
  display.println(F("Temp off, will auto")); // strings printed using F()
so that flash memory is used to save on dynamic memory
  //line 2
  display.println(F("reset when T drops"));
  //line 3
  display.print(F("Box T: "));
  display.print(box_temp_avg_safety,1);
  display.print(F(" "));
  display.print((char)247); // degrees symbol
  display.println(F("C"));
  // line 4
  display.print(F("Head T: "));
  display.print(head_temp_avg_safety,1);
  display.print(F(" "));
  display.print((char)247);
  display.println(F("C"));
  display.display();//Finally display the created image
}
void OLED_display_PID(int Dial, int Setpoint, float box_temp, float
head_temp, int PID_out) {
```

```
    display.clearDisplay(); // clear display

    display.setCursor(0,0);
    //line 1, displays value from potentiometer, and confirmed target
    display.print(F("Dial:")); // strings printed using F() so that flash
memory is used to save on dynamic memory
    display.print(Dial);
    display.print(F(", Target:"));
    display.println(Setpoint);
    //line 2, shows box temperature
    display.print(F("Box T: "));
    display.print(box_temp,1);
    display.print(F(" "));
    display.print((char)247); // degrees symbol
    display.println(F("C"));
    //line 3, shows head temperature
    display.print(F("Head T: "));
    display.print(head_temp,1);
    display.print(F(" "));
    display.print((char)247);  // degrees symbol
    display.println(F("C"));
    //line 4, shows PID output
    display.print(F("PID Output: "));
    display.print(((PID_total*100)/255),0); // converts PID output to a
percentage
    display.println(F(" %"));
    display.display();//Finally display the created image
}
//Function to display variables on the screen
void OLED_display_cooldown(float box_temp, float head_temp) {

      display.clearDisplay();
      display.setCursor(0,0);
      // line 1, shows box temperature
      display.print(F("Box T: "));
      display.print(box_temp,1);
      display.print(F(" "));
      display.print((char)247); // degrees symbol
      display.println(F("C"));
      //line 2, shows head temperature
      display.print(F("Head T: "));
      display.print(head_temp,1);
      display.print(F(" "));
      display.print((char)247);  // degrees symbol
      display.println(F("C"));
      //line 3
```

```
      display.print(F("Off"));
      display.display();//Finally display the created image
}
void OLED_display_shutdown(float box_temp, float head_temp) {

      display.clearDisplay();
      display.setCursor(0,0);
      //line 1, displays warning message
      display.print(F("HOT OIL| "));
      display.print(F("Box:"));
      display.print(box_temp,1);
      display.print((char)247);
      display.println(F("C"));
      //line 2, displays second part of warning message
      display.print(F("Head:"));
      display.print(head_temp,1);
      display.print((char)247);  // degrees symbol
      display.println(F("C"));
      //line 3, displays instructions for user
      display.println(F("reset at wall when"));
      //line 4, displays instructions for user
      display.println(F("head T<95 & box <110"));
      display.display();//Finally display the created image
}
void Serial_print(const char* const labels[], float vars[], int numVars)
{
  for (int i = 0; i < numVars; i++) { // starts a for loop that iterates
through the number of variables
    char buffer[30]; // Buffer to hold the string from flash memory
    strcpy_P(buffer, (PGM_P)pgm_read_word(&(labels[i]))); // reads buffer
and converts to string
    Serial.print(buffer); // prints buffer
    Serial.print("\t"); //prints a tab
    Serial.print(vars[i]); // prints variable
    Serial.print("\t");
  }
  Serial.println();//makes a new line
}
void LED_function(float PID_total){
        // turns LED on if PID_total > 0
        if (PID_total==0){
          digitalWrite(led,LOW);
        }
        else {
          digitalWrite(led,HIGH);
      }
```

```
}
```